PhD Thesis of Cristian Colombini 879654

Influence of Obstacles on High-Pressure Jets

Department of Chemical, Material and Chemical Engineering “Giulio Natta”

PhD in Industrial Chemistry and Chemical Engineering

XXXII cycle

2020 – 2021

Head of PhD course: Prof. Alessio Frassoldati

Tutor: Prof. Selena Sironi

Supervisor: Prof. Valentina Busini

INDEX

INDEX I

CHAPTER 1: EXECUTIVE SUMMARY 1

Chapter 2.1: *Ground Influence on High-Pressure Methane Jets: Practical Tools for Risk Assessment* 9

Chapter 2.2: Ground Interaction on High-Pressure Jets: Effect on Different Substances 12

Chapter 3: Unignited High-Pressure Methane Jet Impinging a Pipe Rack: Practical Tools for Risk Assessment 14

Chapter 4: Safety Evaluations on Unignited High-Pressure Methane Jets Impacting a Spherical Obstacle 18

Chapter 5.1: Obstacle Influence on High-Pressure Jets based on Computational Fluid Dynamics Simulations 21

Chapter 5.2: High-Pressure Methane Jet: Analysis of the Jet-Obstacle Interaction 24

References 27

CHAPTER 2: GROUND EFFECT ON HIGH-PRESSURE JETS DEVELOPMENT 32

CHAPTER 2.1: GROUND INFLUENCE ON HIGH-PRESSURE METHANE JETS: PRACTICAL TOOLS FOR RISK ASSESSMENT 33

Abstract 35

Acronyms 36

Nomenclature 37

Introduction 38

Material and Methods 41

Results and Discussion 42

BASE CASE SCENARIO 42

CFD MODEL DEFINITION 42

ANALYSIS OF THE RESULTS 47

PROPOSED CRITERION AND ANALYTICAL CORRELATION 49

SCENARIO SENSITIVITY ANALYSIS 51

ME FREEJET ESTIMATION 58

Conclusions 60

References 62

CHAPTER 2.2: GROUND INTERACTION ON HIGH-PRESSURE JETS: EFFECT ON DIFFERENT SUBSTANCES 67

Abstract 69

Acronyms 70

Nomenclature 71

Introduction 72

Material and Methods 74

Results and Discussion 75
Conclusions 79
References 80
CHAPTER 3: UNIGNITED HIGH-PRESSURE METHANE JET IMPINGING A PIPE RACK: PRACTICAL TOOLS FOR RISK ASSESSMENT 82
Abstract 84
Acronyms 85
Nomenclature 86
Introduction 88
Material and Methods 90
Scenario Description 91
Results and Discussion 97
Conclusions 105
References 107
CHAPTER 4: SAFETY EVALUATIONS ON UNIGNITED HIGH-PRESSURE METHANE JETS IMPACTING A SPHERICAL OBSTACLE 111
Abstract 113
Acronyms 114
Nomenclature 115
Introduction 117
Scenario and CFD Model Specifics 120
Quantitative Results and Discussion 125
Qualitative Results and Discussion 130
Conclusions 134
References 136
CHAPTER 5: CYLINDRICAL TANKS EFFECT ON HORIZONTAL HIGH-PRESSURE METHANE JETS DEVELOPMENT COUPLED WITH THE TERRAIN EFFECT 141
CHAPTER 5.1: OBSTACLE INFLUENCE ON HIGH-PRESSURE JETS BASED ON COMPUTATIONAL FLUID DYNAMICS SIMULATIONS 143
Abstract 145
Acronyms 146
Nomenclature 147
Introduction 148
Material and Methods 149
Results and Discussion 149
Conclusions 155
References 157

CHAPTER 5.2: HIGH-PRESSURE METHANE JET: ANALYSIS OF THE JET-OBSTACLE INTERACTION 160
Abstract 162
Acronyms 163
Nomenclature 164
Introduction 165
General Aspects of the CFD model 166
Validation Case 167
Case Study 168
Sensitivity Analysis 172
OBSTACLE SIZE 172
OBSTACLE SHAPE 174
Conclusions 180
References 181
CHAPTER 6: CONCLUSIONS 184
ANNEX A 187
Table A1 188
Figure A1 189
Figure A2 191
ANNEX B 192
Table B1 193
Figure B1 194
Figure B2 195
ANNEX C 196
Table C1 197
Table C2 201
Figure C1 202

CHAPTER 1: EXECUTIVE SUMMARY

Although transporting and storing of chemicals under liquefied conditions (obtained through compression or cooling) is widespread, many of them are still handled in gaseous form (Kim et al., 2013; Bariha et al., 2017; Deng et al., 2018; Baalisampang et al., 2019; Lim et al., 2019; Stewart, 2019).

Therefore, from the industrial safety point of view, the risk assessment of accidental toxic or flammable high-pressure gaseous releases (i.e., High-Pressure jets, HP jets) is a critical challenge, especially for Quantitative Risk Analysis (QRA) and in the hazardous area classification framework (Pontiggia et al., 2014; Liao et al., 2018).

Concerning the flammable case this leads to several safety implications, related to both the high-pressure at which the gas is stored and to its flammability (Palazzi et al., 2016a). In particular, in case of late ignition the release scenario can evolve in a Flash Fire (FF), whose hazardous distance is usually quantified as the Lower Flammability Limit (LFL) distance of the unignited cloud. Therefore, to predict how severe may be the consequences of a FF, the extension of the unignited flammable cloud needs to be estimated (Souza et al., 2019b). Commonly, in the risk analysis framework, for the case of a leakage of a flammable substance such evaluation traduces in the prediction of the Maximum axially-oriented Extent (ME) of the cloud (Tchouvelev et al., 2007; Houf et al., 2010; Pontiggia et al., 2014).

Thus, the damage area estimation becomes a crucial information to be predicted (Souza et al., 2019b). It is, therefore, quite evident the importance to have available predictive computational methods by which it is possible to assess the magnitude of the unignited accidental release (Palazzi et al., 2016b). Broadly speaking, two different situations of HP gaseous release can be identified: the free jet (intended as a release occurring in an unconfined environment (Dey et al., 2017) and the impinging jet (intended as a release interacting with structures or facilities in the surroundings (i.e., obstacles) (Schefer et al., 2009).

For the latter, which can be expected to be the most probable accidental scenario in an industrial environment (Xu et al., 2011), it has been shown that, in some cases, with respect to the free jet situation an increase of the hazardous area (i.e., the ME of the jet cloud) can occur (Kotchourko et al., 2014; Hall et al., 2017).

Despite this, in the past a large amount of the research in the process safety framework has been focused on the free jet situation (e.g., Lockwood and Moneig (1980), Chen and Rodi (1980), Birch et al. (1984), Schefer and Dibble (1986), Birch et al. (1987), Becker et al. (1988), Pitts (1991), TNO (1997), Holt and Witlox (1999) and SHELL (2004) just to mention some), while, for what concerns

impinging jets, only recently some works have been performed with the aim of understanding how an obstacle can influence the jet behavior.

Concerning the numerical methods that can be used to provide this safety assessment, these have to be reliable even when modeling the depicted realistic accidental scenario.

As widely reported in literature, the many analytical correlations (Becker et al., 1965; Thring and Newby, 1952; Chen and Rodi, 1980) and the well-known integral models (such as DEGADIS, SLAB, ALOHA and UDM) (Brook et al., 2003; Bernatik and Libisova, 2004; EPA, 2011; Pandya et al., 2012) developed within the industrial safety framework are reliable when analyzing the free jet scenario (intended as a release occurring in an unconfined environment (Dey et al., 2017)), showing they limits when dealing with a situation in which a HP jet interacts with an obstacle (Cameron and Raman, 2005; Derudi et al., 2013; Pontiggia et al., 2014; Schelder et al., 2015; Gerbec et al., 2017; Uggenti et al., 2017; Dasgotra et al., 2018).

Regarding integral models, the main reason why this kind of numerical tool usually fails to reproduce accidental releases in complex geometries is that they account for some physical phenomena through semi empirical correlations having parameters that have been fitted to some field test data (Derudi et al., 2014). Their accuracy is therefore strictly related to the experimental tests used to tune the model parameters. Given that obstacles are not usually present in such field trials, it is easy to understand how the integral models give reliable predictions only for free jet scenarios.

From the literature analysis, although improvements have been made in recent years concerning low-computational-cost tools in the framework of accidental releases risk assessment, the previously highlighted limits of the integral models in reproducing complex geometry situations are still present.

Computational Fluid Dynamics (CFD) is the numerical approach traditionally employed to face such industrial safety issue (Deng et al., 2018; Souza et al., 2019a; Tolias et al., 2019). Since it is a numerical tool that can thoroughly account for the flow field with a high-level detail, the CFD allows to address for any geometrical complexity (Efthimiou et al., 2017; Gerbec et al., 2017; Luo et al., 2018; Jiang et al., 2020).

Although the high computational costs and the user knowledge demanded (Zuliani et al., 2016), the quite spread literature available about unignited HP jets impacting an obstacle confirms that, to date, CFD is the only trustworthy numerical tool. In the following, the literature review is reported. From this, we can note that almost all the works used CFD-based models.

In 2007 Benard and co-workers numerically investigated the influence of vertical and horizontal flat surfaces parallel to unignited vertical and horizontal hydrogen and methane HP jets. The results showed that in spite of the high-momentum of the releases, the ME of hydrogen jets is strongly influenced by the buoyancy effect, while the ME of methane jets is not. Tchouvelev et al. (2007) combined the commercial CFD software PHOENICS with two analytical models, one for the time-dependent source variables (pressure, density and flow rate) and the other accounting for a real equation of state describing the gas density. The focus has been on the quantitative prediction of the extent of the lower flammability limit cloud of a HP unignited hydrogen release impingement against a protective wall. In 2009 Desilets et al. performed an experimental campaign aiming to characterize the shape of the plume of different unignited hydrogen jets when influenced by a nearby horizontal flat surface. For comparison purposes, CFD numerical simulations have been further performed. Hourri et al. (2009) extended the analysis of Benard et al. (2007) adding two distances of the jet source from the surface. As Hourri et al. in 2009, in the same year Benard et al. considered more orifice diameters, storage pressures and distances from the flat surface. Houf et al. (2010) conducted a numerical evaluation of barrier walls for the mitigation of hydrogen releases, both ignited and unignited. Middha et al. (2010) performed a small scale experimental campaign on ignited HP hydrogen jets interacting with an obstacle with the purpose of validating the commercial CFD software FLACS for this specific scenario. In 2011, Hourri et al. and Angers et al. further extended the analysis of Hourri et al. (2009) considering several higher pressures and a different jet orientation, respectively. Kim et al. (2013) investigated experimentally the self-ignition near an obstacle of high-pressure hydrogen jets. Pontiggia et al. (2014) compared the results of an integral model (PHAST) to the ones of a CFD model (FLUENT) for the case of an unignited HP methane jet impacting a cylindrical obstacle. The aim has been to show that, in this scenario, integral models become unreliable. Tolias and Venetsanos (2015) investigated how to model an accidental impinging hydrogen jet through CFD models with the aim of giving best practices guidelines for hydrogen impinging jet simulations. With CFD code FLACS, Benard et al. (2016) investigated how a vertically or horizontally oriented flat surface influences the maximum extent of the lower flammability limit cloud of both hydrogen and methane unignited HP jets. They derived engineering correlations able to substitute the use of more computationally expensive CFD software. However, their useful results have been verified for only one orifice diameter of the source, one wind condition, one concentration level observed (i.e., the LFL) and using one Equivalent Diameter Model. In 2017, Gerbec et al. analyzed the case of a vertical unignited propane jet impacting against

the roof of a refueling station, comparing the results computed with a CFD software (FLUENT) and an integral model (UDM). They shown differences in predicting the damage area extension when using the two kinds of model. Of the same year is the work of Hall et al. (2017), where they investigated how two horizontal surfaces (namely, the ground and a ceiling) influence unignited HP hydrogen clouds at different concentrations. Starting from the state of the art regarding CFD modeling for risk assessment of offshore installations, Uggenti et al. (2017) proposed a new hybrid approach, combining a semi-empirical model with a CFD one. In 2018, Hu et al. accounted for the problem of unignited HP hydrogen jets impacting a vertical obstacle with the novelty of using a specific equation of state (EoS) (e.g., Abel-Noble (Johnston, 2005)) to model hydrogen density.

Despite, on one hand, the extensive use of the CFD in this specific framework of risk assessment and, on the other one, the technological improvements of the computing resources, as already discussed, CFD is not yet drawbacks-free (Pontiggia et al., 2014; Hu et al., 2018). For this reason, to date, CFD use is still limited in daily risk analysts' activities.

Therefore, the availability of quick as well as simple tools (such as engineering correlations) allowing the estimation of the damage area of unignited impinging accidental releases it is of primary interest.

From the analysis of the literature survey reported, the following can be pointed out:

- High pressure jet impacting a realistic industrial obstacle is a credible scenario, however little studied in literature;
- Dealing with high pressure jets impacting an obstacle, CFD is the only reliable numerical method (the only one able to proper account for any kind of geometrical complexity);
- To date, CFD still presents some drawbacks for its use in daily risk assessment activities

Based on the above, it results of primary interest the development of risk assessment tools that allow to obtain reliable results (as CFD does), however with less time/efforts demanding.
Accordingly, the development of simple as well as reliable simplified models and correlations predicting the effect of a realistic obstacle on the behavior of unignited high-pressure jet is the main objective of this thesis.
In order to tackle this goal, an extensive CFD-based analysis was carried out. Such analysis entailed the development of a dedicated numerical strategy to model the specific scenario considered which resulted in a non-trivial task given the harsh problems encountered when considering high velocity flows interacting with solid surfaces and, the need of limiting computational costs when considering large computational domain coupled with high mesh resolution needed in correspondence of that zones characterized by a large gradients variation (*i.e.*, in the vicinity of the jet orifice). Such models have been implemented in the Ansys Workbench platform.
In the following, some key methodological aspects considered for the simulations performed within the present PhD research activity are presented. These are general aspects, so that shared by all the CFD models used to simulate the different scenarios considered. Details of the scenarios are given in the following Chapters.
Ansys Workbench (Ansys Workbench, 2017) was used as platform tool collecting all the needed specific software. The computational domain was created with Ansys DesignModeler, the grid was built using Ansys Meshing and the computations were performed with the numerical solver Ansys Fluent (Ansys DesignModeler User Guide, 2017; Ansys Meshing User Guide, 2017; Ansys Fluent User Guide, 2017).
In case of a large pressure difference between a reservoir and the environment (such as in all the scenarios analyzed in this project), a supersonic jet is expected, leading to a high demand of computational resources (Colombini et al., 2020a). However, since the focus of the analysis is on the so-called farfield zone of the jet (*i.e.,* far from the jet source), the commonly adopted way of using empirical relationships to model the supersonic release source was followed (Hess et al., 1973;

Sposato et al., 2003; Pontiggia et al., 2014; Benard et al., 2007; Houf et al., 2007; Stewart et al., 2019; Tolias et al., 2019). Named, by way of example, Equivalent Diameter Model (EDM), in literature many of these are available (Franquet et al., 2015). All these models use a fictitious jet source that, placed immediately downstream the actual one, and based on the upstream characteristics, has the primary specificity to obtain the fluid released as incompressible, which permits to save computational costs keeping the reliability of the results within an acceptable range (Novembre et al., 2006). To perform the present CFD analysis, the model developed by Birch et al. (1984) was chosen. This meant that, the hole diameter to be considered in the geometry definition was based on the EDM (and the upstream conditions).

As computational domain, a rectangular box was used. For each scenario considered, domain extents were sized based on specific preliminary tests. When available, specific guidelines on domain sizing for single obstacle problem were also followed. Moreover, a key aspect in the geometry definition is the use of vertical planar symmetry in correspondence of the jet axis, when applicable. The strategy used for the domain discretization is detailed in Colombini et al. (2020a). An optimized grid was obtained: a finer mesh surrounding the jet axis (which is the computationally critical zone), and a coarser one close to the domain boundaries (where demanding physical phenomena are not expected). The inflation mesh feature was used for a specific grid definition of the cells surrounding, when present, the tank surface (Ansys Meshing User Guide, 2017). In general, the grid obtained was tetrahedral, fully unstructured.

As it pertains to numerical settings, the Reynolds-averaged approach was used for the governing Navier-Stokes equations (RANS approach) and coupled with the two-equation eddy-viscosity k-ω SST turbulence closure model (Menter, 1993). The simulations were performed in steady state conditions and the pressure-based solver was chosen, since the EDM used (allowing the flow to be treated as incompressible). To account for the multi-species problem (hydrocarbon release in ambient air), the species transport model was selected and the ideal gas Equation of State was used to model the fluid mixture density. The COUPLED pressure-velocity scheme was adopted while the second order upwind spatial-discretization scheme was used for all the convective terms. The effect of gravity was always included.

In the following, a summary of the main results achieved during the PhD research activity is given, divided into four main Chapters.

The first three Chapters detail the analysis of the effect that a single realistic obstacle has on unignited high-pressure jets of flammable substances, proposing engineering correlations as alternative tool to CFD computations that, giving reliable results with practical precision, become more suitable for daily tasks in risk assessment field. While the last Chapter presents the results of two preliminary analysis, each of them involving two realistic obstacles impinged by the jet at the same time. In this work, useful semi-quantitative results were obtained.

Please note that Chapters of the present PhD thesis have been published, or have been submitted and are currently under review in peer reviewed international journals and conference proceedings. Only the visual appearance has been revised, maintaining the original information content. For the reader's convenience, reference to the published contributions is given.

- **Chapter 2**: Ground effect on horizontal high-pressure jets development; this Chapter is divided into two sections, depending on the gases considered;
  - **Chapter** 2.1: methane (Colombini et al., 2020a)
  - **Chapter** 2.2: methane, hydrogen and propane (Colombini et al., 2020b)
- **Chapter 3**: Pipe rack effect on horizontal high-pressure methane jets development (Colombini et al., 2021a);
- **Chapter 4**: Spherical obstacle effect on horizontal high-pressure methane jets development (Colombini et al., 2021b);
- **Chapter 5**: Cylindrical tanks effect on horizontal high-pressure methane jets development coupled with the terrain effect; this Chapter is divided into two sections, depending on the tank orientation;
  - **Chapter** 5.1: Horizontal (Colombini and Busini, 2019a)
  - **Chapter** 5.2: Horizontal and vertical (Colombini and Busini, 2019b)

CHAPTER 2.1: *GROUND INFLUENCE ON HIGH-PRESSURE METHANE JETS: PRACTICAL TOOLS FOR RISK ASSESSMENT*

When dealing with high-pressure jets as potential accidental loss of containment, in risk assessment the damage area of the jet cloud (in particular, the hazardous distance reached by the LFL concentration value) is recognised as the characteristic distance of interest. To estimate the maximum axially-oriented extent of the flammable cloud, in their daily activities loss prevention specialists use quick and well-established numerical tools such as integral models (*e.g.*, PHAST (DNV, 2020)). However, the presence of an obstacle in the flow field of the jet is a more realistic situation to deal with. Therefore, the main aim of this Chapter is to investigate how an industrial ground surface (*i.e.*, made of concrete) can influence the LFL cloud size of a horizontal high-pressure methane jet through an extensive CFD analysis performed with Ansys Fluent 19.0. The main innovative aspect is a quick procedure making it possible to i) determine the minimum height from which the ground begins to influence the hazardous distance; since below this height the predictions of standard simulation tools are not reliable and a simple tool allowing practitioners to know whether or not a given accidental scenario can be simulated with standard modelling tools is of paramount practical importance, and ii) estimate how much the hazardous distance increases when the ground influence makes the predictions of the standard simulation tools unreliable. To study the effect of the ground on a horizontally oriented high-pressure release of methane, the analysis was carried out varying the height of the source above ground (h) and observing how the maximum extent of the LFL jet cloud varies consequently. From the results analysis, it was observed that i) over a specific critical height of the jet above ground (h*), the maximum extent of the jet is not influenced by the ground presence (*i.e.*, the ME is equal to the free jet one); ii) once the ground influence is noticed, it enhances the ME of the jet; iii) the overall increase of ME presents an almost inverse linear proportionality to h. Since nearly 250 cases of jets interacting with the ground (differing in terms of upstream pressure, upstream temperature, orifice diameter, wind conditions and equivalent diameter model considered) were investigated, in order to collect them and providing a meaningful comparison, a specific plane was properly defined. In Figure 1.1 below, the x axis corresponds to the ratio between h and the equivalent diameter calculated for each specific case (d_{PS}), whereas the y axis corresponds to the ratio between the maximum extent ME and the ME of the free jet of each of the specific case considered (ME_{FJ}). Firstly, the analysis focused on a limited number of cases in order to derive an analytical correlation. Then, adding the results of all

the rest of the cases analysed, the findings were consolidated. *Figure 1.1* shows the results obtained on the defined plane using all the cases analysed.

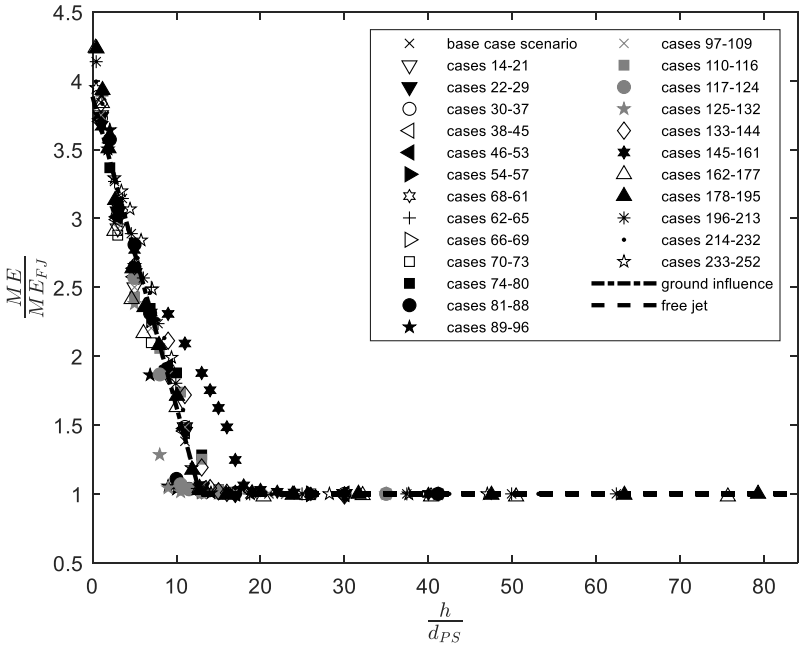

Figure 1.1: Dimensionless ME vs. dimensionless height of the source above ground for all the 252 cases investigated.

From *Figure 1.1* we can see that almost all the results overlap well with each other, sharing a threshold value indicating the limit of the ground influence. Only the results obtained using the pseudo-source model of Yuceil and Otugen (2002) (cases 145-161) are slightly different. From what is shown in *Figure 1.1*, it was possible to derive a simple four-steps procedure that can be done by hand, enabling safety analysts to estimate the hazardous distance, based on known information of the scenario.

The derived procedure is reported in the following.

1. From the accidental release characteristics, estimate the d_{PS} value using the Birch et al. (1984) model:

$$d_{PS} = d\sqrt{C_D\left(\frac{p}{p_{amb}}\right)\left(\frac{2}{\gamma+1}\right)^{\frac{(\gamma+1)}{2(\gamma-1)}}}$$

2. Estimate the ME_{FJ} value using the Chen and Rodi (1980) model:

$$ME_{FJ} = \frac{k d_{PS}}{LFL}\left(\frac{\rho_a}{\rho_g}\right)^{\frac{1}{2}}$$

3. If $h/d_{PS} > 13$, ME_{FJ} provides directly the order of magnitude of ME
4. If $h/d_{PS} < 13$, the order of magnitude of ME can be estimated as

$$ME = ME_{FJ}\left(3.89 - 0.22\frac{h}{d_{PS}}\right)$$

CHAPTER 2.2: GROUND INTERACTION ON HIGH-PRESSURE JETS: EFFECT ON DIFFERENT SUBSTANCES

As in Chapter 2.1, here the ground influence was investigated in terms of how the flammable area extent of a high-pressure jet increases (in terms of Maximum axially-oriented Extent (ME) of the LFL cloud) as a function of the height of the source above ground. In particular, the aim was to compare how three widely used flammable substances (namely methane, propane and hydrogen) behave when their release is modified by the presence of a horizontal surface. All three gases were considered at their typical handling conditions. For methane and propane, the numerical outcomes were computed by using the in-house developed CFD model, whereas for hydrogen, data were taken from the work of Benard et al. (2016). As stated, the objective is to compare how the ground affects high-pressure jets of three different substances. However, performing such a comparison highlighting only the effect of considering different substances is not as immediate as it seems. In fact, other aspects change when changing the substance:

- considering the correspondent LFL value implies different observed concentrations
- considering typical handling conditions means, at least, different source pressures

Therefore, to fruitfully show which is the dependency of the ME upon only the substance change, it was needed to define a proper space that allows to offset both the different concentrations observed, and the different source pressures considered. As done by Colombini et al., (2020a), to investigate the influence of the ground on the jet, the height of the source above the ground (h) was systematically varied. To offset the effect of the stagnation pressure, for each data set, the y axis was normalized by the corresponding ME of the free jet (ME_{FJ}), while the x axis was divided by the correspondent equivalent source diameter (d_{PS}); this normalization works because both the ME_{FJ} and the d_{PS} depend on the upstream pressure (but also temperature and actual orifice diameter) (Colombini et al., 2020a). To offset the effect of the observed concentration level, only the x axis required a further manipulation since both ME and ME_{FJ} already depend on the concentration considered. In particular, the ratio LFL/LFL_{REF}, where LFL is the concentration value observed for each substance considered while LFL_{REF} a reference concentration arbitrarily chosen (preferably among the ones considered; in this case, the methane LFL), was used to perform the scaling. *Figure 1.2* shows the results collected on the dimensionless space just defined.

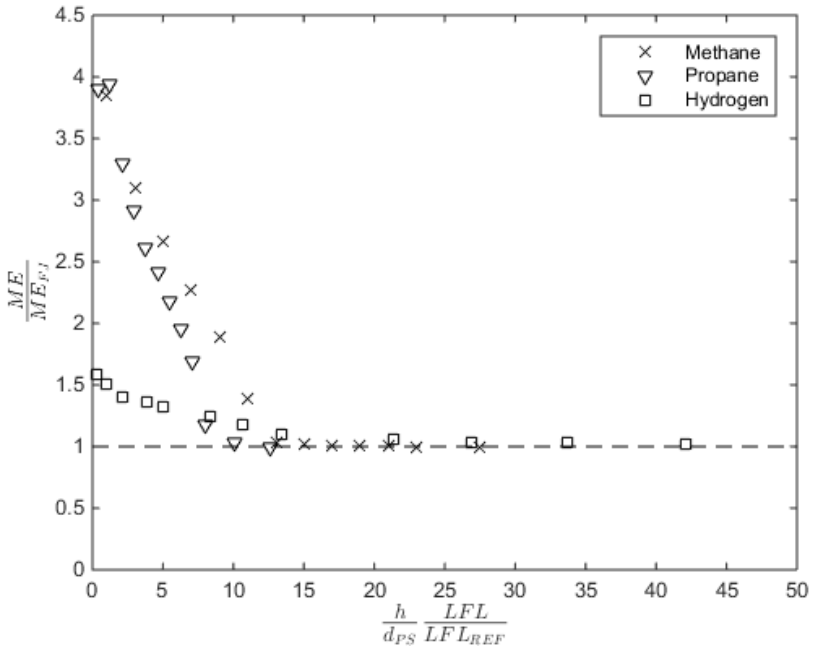

Figure 1.2: Results are reported in the dimensionless space defined to offset both different stagnation conditions and different concentrations.

When considering substances heavier than, or similar to, air (it is the case for propane and methane) the behavior of the jet (and thus the ground influence) appears to be significantly less different than that of considering a much lighter one (*i.e.,* hydrogen). In particular, the heavier the gas is, the steeper the curve is. This leads to the conclusion that the ground affects significantly more high momentum releases of heavy compounds. This can be explained by buoyancy: hydrogen jets have a tendency to lift up, whereas methane and propane jets tend to stay parallel to the ground.

CHAPTER 3: UNIGNITED HIGH-PRESSURE METHANE JET IMPINGING A PIPE RACK: PRACTICAL TOOLS FOR RISK ASSESSMENT

Going beyond the study of the simple interaction between a high-pressure jet and a single well-shaped obstacle, in this Chapter was investigated how a typical industrial structure (*i.e.*, a pipe rack) can influence the development of a high-pressure methane jet in terms of maximum axial extent of the flammable cloud. Through an extensive CFD-based analysis performed with Ansys Fluent 19.1 (Ansys Fluent User Guide, 2017), the main geometrical parameters on which the impinging jet behavior depends have been identified, allowing for the development of a simple analytical relationship that roughly predicts the influence of the pipe rack without the need of performing complex CFD simulations. Moreover, a simple criterion capable of identifying the situations where the pipe rack does not influence the high-pressure methane jet behavior has been developed, providing a means to identify the scenarios where simpler models (*e.g.,* analytical correlations able to estimate the maximum axial extent of a free jet) can be used. Both these outcomes can be quite valuable for practitioners daily involved in industrial safety assessments. Several parameters (related to both the jet source and the obstacle) have been considered, namely: upstream methane pressure (p); actual orifice diameter of the jet source (d); rack pipes diameter (d_p); number of shelves (n_s); number of pipes per shelf (n_{PS}); rack distance from the jet source (D); pipe rack horizontal rotation with respect to the jet axis (α). Moreover, also the target concentration considered in relation to the maximum axial extent of the jet (c) was varied in order to see how the jet development modifies when different concentrations are of interest. The following equations define three dimensionless parameters used to summarize the high-pressure jet-rack interactions:

$$VBR = \frac{n_{PS} \cdot n_S \cdot \frac{\pi \cdot d_P^2}{4} + 2 \cdot (n_S + 1) \cdot s \cdot h}{H \cdot W}$$

$$ABR = \frac{h \cdot (n_S + 1) + d_P \cdot n_S}{H}$$

$$VFP = \frac{d_{FJ}(D)}{H}$$

where s is the pipe rack leg's width, h is the pipe rack shelves height, H is the height of the pipe rack case and W is the width of the pipe rack case. All the parameters involved in these equations are related to only geometrical aspects of the pipe rack (see Figure 4.1), except for $d_{FJ}(D)$ that is the free jet diameter evaluated in correspondence of the pipe rack position. VBR (which stands for Volume

Blockage Ratio, that is the ratio between occupied rack case volume and full rack case volume) indicates how the volume within the rack case is occupied by pipes and structural beams (Figure 4.3); ABR (which stands for Area Blockage Ratio, that is the ratio between occupied rack case frontal area and full rack case frontal area) indicates how the frontal area of the rack case is hindered by pipes and structural beams (Figure 4.3); VFP (which stands for Vertical FootPrint, that is the hypothetical free jet footprint on the pipe rack) indicates whether the free jet cloud radial extent (at the considered concentration level) is larger than (or smaller) the height of the rack case (Figure 4.5). Upon variation of the scenario parameters identified to be characteristic of this jet-obstacle scenario, several cases were simulated (130 in total). The main findings of this Chapter are shown in *Figure 1.3*.

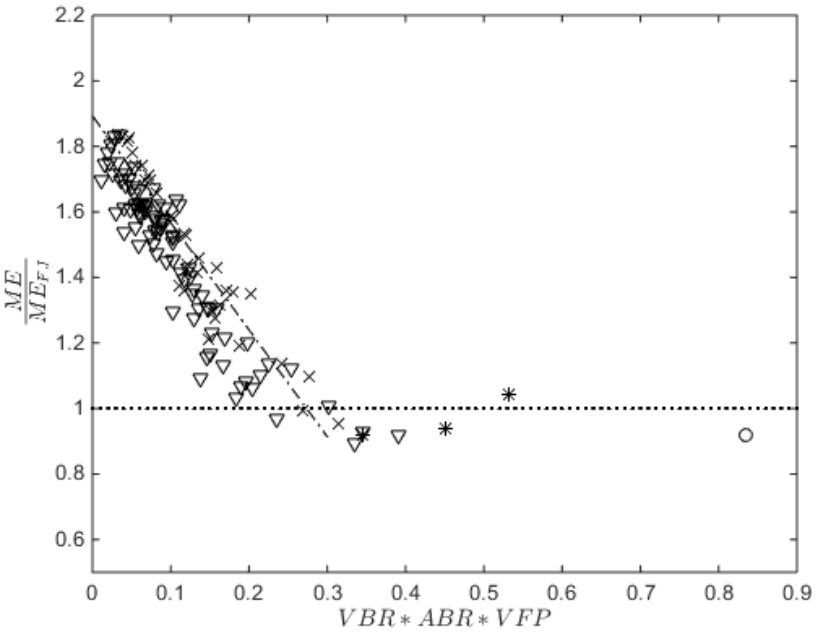

Figure 1.3: Results of the 130 runs are shown of the dimensionless space specifically defined. Different markers refer to different scenario characteristics that was varied (details of each set of the results are reported in the work of Colombini et al. (2021a). The dotted line is the dimensionless maximum axial extent correspondent to the free jet case, while the dashed-dotted line is the linear fitting of the achieved results.

From this Figure we can see a clear trend showing how the rack influences the jet development: maximum axial extent of the LFL jet cloud is always larger than (or almost equal to) the free jet one. This means that the rack is never able to reduce the LFL jet maximum extent; in the worst case, the maximum extent of the free jet is almost doubled by the presence of the rack. Moreover, the following linear interpolation of the results provides a reasonable fitting when pipe rack influence is notified.

$$\frac{ME}{MF_{FJ}} = 1.89 - 3.26 \cdot (VBR \cdot ABR \cdot VFP)$$

Considering the 130 scenarios analyzed it is possible to see that only a few of them present a value of VBR·ABR·VFP greater than 0.3 and they show a value of ME/ME_{FJ} around one. This leads to the inference that for values of VBR·ABR·VFP larger than 0.3 the obstacle expires its influence on the jet development.

Based on the above considerations, the following procedure was defined, which allows estimating the ME of a methane flammable cloud without any demanding (in terms of both time and analyst skill) CFD-based computation.

1. From both the obstacle and source characteristics, estimate VBR, ABR, and VFP values:

$$VBR = \frac{n_{PS} \cdot n_S \cdot \frac{\pi \cdot d_P^2}{4} + 2 \cdot (n_S + 1) \cdot s \cdot h}{H \cdot W}$$

$$ABR = \frac{h \cdot (n_S + 1) + d_P \cdot n_S}{H}$$

$$VFP = \frac{d_{FJ}(D)}{H}$$

2. to analytically estimate $d_{FJ}(D)$, the following equations need to be used:

$$d_{FJ}(D) = 2 \cdot \sqrt{-\frac{D^2}{50} \cdot \ln\left(\frac{LFL}{c_{ax}(D)}\right)}$$ Cushman-Roisin (2020)

$$c_{ax}(D) = \frac{k d_{PS}}{D}\left(\frac{\rho_{amb}}{\rho_{PS}}\right)^{\frac{1}{2}}$$ Chen and Rodi (1980)

where D is the pipe rack distance from the jet source, LFL (5.3 %) is the specific methane concentration in air considered, $c_{ax}(D)$ is the methane concentration along the free jet axis computed at a distance D from the jet source, k is the axial decay constant (4.4 (Birch et al. (1984)), d_{PS} is the pseudo-source orifice diameter (computed with the model of Birch et al. (1984)), ρ_{amb} is the air density (computed at the ambient conditions), ρ_{PS} is the methane density at pseudo-source conditions.

3. From the source characteristics, estimate the ME_{FJ} value using the Chen and Rodi (1980) concentration decay model:

$$ME_{FJ} = \frac{kd_{PS}}{LFL}\left(\frac{\rho_{amb}}{\rho_{PS}}\right)^{\frac{1}{2}}$$

   Notice that, the Chen and Rodi (1980) model reliability in estimating ME_{FJ} is discussed in detail in the work of Colombini et al. (2020a).

4. If VBR·ABR·VFP > 0.3, ME_{FJ} provides the order of magnitude of ME
5. If VBR·ABR·VFP < 0.3, the order of magnitude of ME can be estimated as

$$\frac{ME}{MF_{FJ}} = 1.89 - 3.26 \cdot (VBR \cdot ABR \cdot VFP)$$

CHAPTER 4: SAFETY EVALUATIONS ON UNIGNITED HIGH-PRESSURE METHANE JETS IMPACTING A SPHERICAL OBSTACLE

As a matter of fact, the methane high-pressure gaseous release is a relevant safety-related problem that needs attention. The reason of its importance is related to the severe consequences of the subsequent domino effect that may take place if ignition occurs, either immediately (jet fire) or with a delay (flash fire). In risk assessment the size of the damage area is the characteristic distance of interest. To perform this evaluation, quick and well-established numerical tools, such as integral models (e.g., PHAST (DNV, 2020)), are widely used. However, the presence of an obstacle in the flow field is a more realistic situation to deal with, and for which the aforementioned tools can provide unreliable results. In this context, this Chapter proposes a way to overcome this drawback (*i.e.,* unreliability of integral models when facing problems involving obstacles presence), by providing useful quick tools for daily activities in risk assessment field. Considering as realistic accidental situation the case of an unignited high-pressure methane jet impacting a spherical obstacle, varying the distance between the release source and the obstacle as well as obstacle diameter, storage pressure and concentration level observed, we investigated several possible configurations of this scenario. For such configurations, two useful quick tools as potential alternative to CFD were derived. By these, it is possible to predict: i) when the obstacle influence on the interacting jet extent expires (thus allowing the use of well-established analytical correlations for the modeling of the free jet case) and, ii) when present, how, by order of magnitude, the obstacle influence can be predicted. To study the influence of the obstacle on the jet development, several parameters (both of jet source and obstacle) were varied: upstream methane pressure (p), obstacle diameter (D_T), distance between jet source and obstacle (D_{NT}) and the methane concentration in air (c). Aiming to show intuitively the influence of all the aforementioned parameters on the jet development, the results of all the runs simulated were streamlined thanks to a plane whose axes were defined as shown in *Figure 1.4*, where, ME_{FJ} is the cloud ME computed for the correspondent free jet and $d_{FJ}(D)$ is the free jet diameter evaluated in correspondence of the spherical obstacle centre position. Note that both ME_{FJ} and $d_{FJ}(D)$ can be easily estimated using analytical correlations (Colombini et al., 2021a). The main findings of this Chapter are shown in *Figure 1.4*.

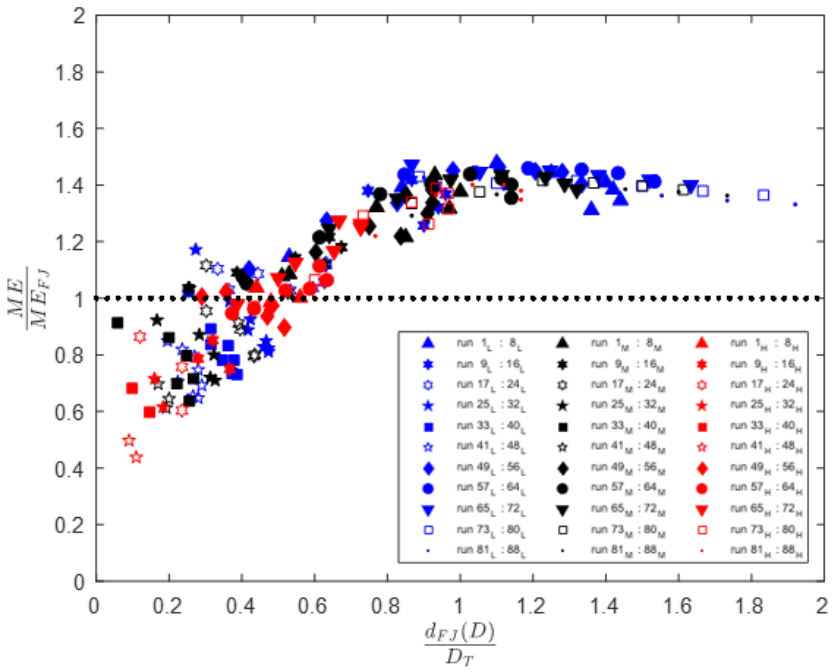

Figure 1.4: Results of the 264 runs are shown of the dimensionless space specifically defined. Marker colours show the methane concentration levels observed: blue is c = 3.5 % (low), red corresponds to 5.3 % (midrange) and black is for 10 % (high). In the Figure, the dotted line identifies when the jet cloud ME is equal to the ME of the correspondent free jet.

From the Figure we can see a clear trend showing how the spherical obstacle influences the jet development:

- up to $d_{FJ}(D)/D_T \approx 0.5$, ME of the jet cloud is lower than (or equal to) the ME_{FJ} (considering a 10 % margin around $ME/ ME_{FJ} = 1$);
- for $d_{FJ}(D)/D_T$ comprised between about 0.5 and about 1, ME of the jet cloud linearly increases up to be 1.5 times greater than the ME_{FJ};
- over $d_{FJ}(D)/D_T \approx 1$, ME/ME_{FJ} of the jet cloud slightly decreases

Therefore, independently on the scenario specifics, the spherical obstacle has two main effects:

- when the obstacle diameter is, at least, two times the free jet width (evaluated in correspondence of the tank centre position), the obstacle reduces the cloud ME with respect to the correspondent free jet, leading to a smaller damage area;
- when the free jet width (evaluated in correspondence of the tank centre position) is, at least, half of the obstacle diameter, the jet cloud ME is increased with respect to the correspondent free jet, leading to a larger damage area; in the worst case, the ME of the free jet is almost 1.5 times increased by the presence of the obstacle.

As a result, the simple as well as quick tool proposed to estimate ME of a jet impinging a spherical obstacle, that is based on only by hand calculations, can be summarized as in the following.

1. From the source characteristics, estimate the ME_{FJ} value using the Chen and Rodi (1980) concentration decay model:

$$ME_{FJ} = \frac{kd_{PS}}{\bar{c}}\left(\frac{\rho_{amb}}{\rho_{PS}}\right)^{\frac{1}{2}}$$

   Where $\bar{c}$ is the specific methane concentration in air considered, k is the axial decay constant (4.4 (Birch et al. (1984)), d_{PS} is the pseudo-source orifice diameter (computed with the model of Birch et al. (1984)), ρ_{amb} is the air density (computed at the ambient conditions) and ρ_{PS} is the methane density at pseudo-source conditions. Notice that, the Chen and Rodi (1980) model reliability in estimating ME_{FJ} is discussed in detail in the work of Colombini et al. (2020a)

2. From the source characteristics, estimate $d_{FJ}(D)$ exploiting the following models:

$$d_{FJ}(D) = 2 \cdot \sqrt{-\frac{D^2}{50} \cdot \ln\left(\frac{\bar{c}}{c_{ax}(D)}\right)}$$ Cushman-Roisin (2020)

$$c_{ax}(D) = \frac{kd_{PS}}{D}\left(\frac{\rho_{amb}}{\rho_{PS}}\right)^{\frac{1}{2}}$$ Chen and Rodi (1980)

   where D is the distance of the spherical obstacle centre from the jet source, $c_{ax}(D)$ is the methane concentration along the free jet axis computed in correspondence of the spherical obstacle centre position. Notice that, the Cushman-Roisin (2020) model reliability in estimating $d_{FJ}(D)$ is discussed in detail in the work of Colombini et al. (2021a)

3. If $d_{FJ}(D) / DT < 0.5$, ME_{FJ} provides the order of magnitude of ME
4. If $d_{FJ}(D) / DT \geq 0.5$, the order of magnitude of ME can be estimated as $1.5 \cdot ME_{FJ}$

CHAPTER 5.1: OBSTACLE INFLUENCE ON HIGH-PRESSURE JETS BASED ON COMPUTATIONAL FLUID DYNAMICS SIMULATIONS

From the physical point of view, the presence of an obstacle affects significantly the behaviour of jets (Hall et al., 2017) through increased turbulence and eddy generation. It can also greatly affect their momentum. In particular, the mixing with fresh air can be enhanced or reduced (Pontiggia et al., 2014), influencing the extent of the flammable region with respect to the one expected from the free jet (Kotchourko et al., 2014).

As previously reported, some efforts have been spent in the past on this topic: most of the studies has investigated the influence of obstacles on high momentum jet releases (more precisely, to determine the extent of the flammable/toxic clouds) only for specific cases. However, none of this literature works explicitly investigated the influence of a real 3D obstacle on the flammable area extent of a high-pressure jet with respect to the free jet case. Therefore, in this section, the influence of obstacles was investigated by varying some of the key geometrical parameters of both obstacle and orifice. More specifically, a realistic case-study of industrial interest was considered. It involves a high-pressure methane jet impinging a horizontal cylindrical tank positioned in front of the jet release.

The aims are:

- to define the geometrical parameters significant for this scenario;
- to quantify these parameters' influence on the jet-obstacle interaction, with respect to the free jet case;
- to define which of them are the most influential.

The effect of the cylindrical tank on the Lower Flammability Limit area extent is systematically studied using CFD simulations, performed with ANSYS Fluent v. 18.2.

Assuming a release from a large storage tank (or a pipeline) of methane gas, the leakage can be considered as a steady state scenario. A pressure of 65 bara and a temperature of 5 °C were assumed inside the storage unit, while a diameter of 1 inch was adopted as a realistic accidental hole on the facility (Pontiggia et al., 2014). The obstacle was modelled as a horizontal cylinder of 5 m in length and 1.7 m in diameter. Notice that the domain dimensions were chosen such that the prescription for the domain extension for CFD analysis of urban environment were fulfilled (Franke et al., 2007). The free jet scenario, (defined as a jet with no wall conditions - no ground nor obstacle), was performed with the aim of obtaining a reference result for comparison purposes. As geometric key

parameters, the distance of the obstacle from the jet orifice (D), the height of the orifice above ground (H), the rotation (α) and the lateral displacement (S) of the tank with respect to the jet axis were chosen. Therefore, an array of simulation was conducted varying one (or in some cases two) per time the geometric parameters. A way to show most information of the simulation results is to graph them into a 3D plot (Figure 2 in Colombini et al. (2019a)), where a dimensionless area A is plotted over two dimensionless spatial coordinates: in detail, the dimensionless A is defined as the ratio $A_{sim\#}/A_{free\ jet}$, where $A_{sim\#}$ is the product of the LFL maximum extent in x ($X_{sim\#}$) times the LFL maximum extent in z ($Z_{sim\#}$) (that is to say the lateral maximum extent), and the same goes for $A_{free\ jet}$ in the free jet case. The dimensionless X is the ratio $X_{sim\#}/X_{free\ jet}$ and Z is $Z_{sim\#}/Z_{free\ jet}$, where $X_{free\ jet}$ is the LFL maximum extent in x and $Z_{free\ jet}$ in z for the free jet case. For the sake of clarity, Figure 1.5 in the following reports two of the three orthogonal views.

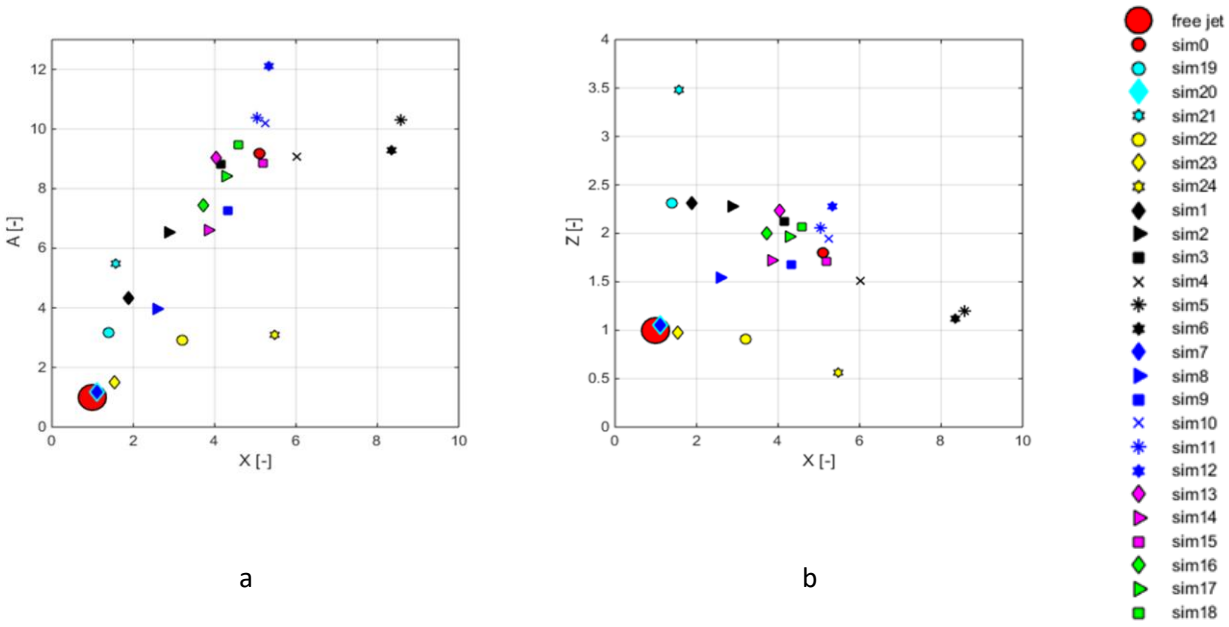

a b

Figure 1.5: a) Side view of the 3D plot; b) Top view of the 3D plot.

From Figure 1.5 it is possible to observe that, except for sim7 and sim20, for all the other cases an influence of the obstacle and/or the ground is noticeable. This is correct since, in sim7 and 20, the distance of the obstacle and the height of the orifice are such that practically no influence occurs. Paying attention to the maximum extents, from Figure 1.5b it is appreciable that the maximum axial extent is 3.5 times the free jet one (sim21), while the lateral maximum extent is about 8.5 times the free jet case (sim5). Furthermore, it becomes clear that more the jet is crosswise extended, less it is axially, and vice versa (Figure 1.5b). In terms of area A, it appears to be larger when the jet is extended in X rather than when extended in Z. In particular, the largest influence with respect to

the free jet is obtained for sim12 (see Figure 1.5a). It is also possible to see that about the 60 % of the results are grouped into a small region of the plane X, Z, ranging from 2 to 6 and from 1.5 to 2.5 in X and Z, respectively (Figure 1.5b). Lastly, sim1 to sim6 and sim7 to sim12 seems to be aligned each other. Moreover, in terms of A, such an alignment follows an ascending order.

Considering the results achieved it was possible to point out that:

- with respect to the free jet case, the ground evidently affects more the axial extent rather than the transverse one
- the prevalent obstacle effect is the enhancement of the crosswise extension with respect to the free jet
- the more the jet is crosswise extended, the less it is axially, and vice versa

Therefore, it was possible to observe that this kind of obstacle has the effect of reducing the hazardous axial distance reached by the jet, while the ground enhances it.

CHAPTER 5.2: HIGH-PRESSURE METHANE JET: ANALYSIS OF THE JET-OBSTACLE INTERACTION

This Chapter examines an unignited high-pressure methane jet interacting with a realistic obstacle placed along its axis. Similarly to Colombini et al. (2019a), the aim was to assess, with respect to the distance between obstacle and jet orifice, the influence of such an obstacle on the jet behavior (*i.e.*, in terms of Lower Flammability Limit area extent). In this section, the scenario investigated in section 5.1 is expanded to consider both horizontal and vertical cylindrical tanks as realistic obstacle. Also, as part of the analysis, the effect of the obstacle size was studied. This works seeks to address two issues: i) when does the obstacle most influences the jet cloud extents and, ii) when the influence of the obstacle expires. A realistic industrial gas source and a realistic industrial obstacle were selected to perform the first part of the analysis: a stationary 65 bara unignited methane jet outflowing from a one-inch diameter hole and a medium-size horizontal cylindrical tank were considered. The tank was cylindrical, its length was 2.5 m and its diameter was 1.7 m. The tank was located 1 m above ground. A sensitivity analysis on the size and shape of the obstacle was conducted. To this effect, we examined the effect of a vertical cylindrical tank (with the same dimensions) and a larger horizontal cylindrical tank on the flow properties.

In general, to study the effect of the obstacle on the horizontally oriented high-pressure release, the analysis was carried out by varying the distance of the obstacle from the release source (D) and observing how the maximum extent of the LFL jet cloud (ME) varies consequently. Combining the results achieved for different values of the distance, the sensitivity of the obstacle shape and size on the jet became manifest.

As it pertains to the effect of the size of the obstacle, we noticed that:

- the results related to the case study Horizontal Cylindrical Tank (HCT_{CS}) and the larger one considered for the sensitivity analysis (HCT_{SA}) present a similar behavior
- in both cases, the results present a clear point (in terms of distance of the tank from the source) where the obstacle expires its influence on ME

While, about the shape effect it was possible to point out that:

- the results of the Vertical Cylindrical Tank used for the sensitivity analysis (VCT_{SA}) are similar to the ones of HCT_{CS}
- similar to the results obtained with the HCT_{SA}, the results present a clear point (in terms of distance of the tank from the source) where the obstacle expires its influence on ME

To profitably analyze the results all at once, a specific space was defined. In *Figure 1.6*, all the results are indeed collected and plotted in terms of ΔME over δ. The parameter δ is defined as the percentage variation with respect to D^0, such as $D = D^0+(\delta/100)\cdot D^0$ for each case (where D^0 is the distance at which the obstacle was placed at first instance, serving as guessing point for the analysis), while $\Delta ME = (ME^{ref}-ME)/ME^{ref}$, where ME^{ref} is the cloud Maximum Extent obtained in sim^{ref} while ME is the cloud Maximum Extent obtained in each of the simulations performed. sim^{ref} corresponds at the simulation in which the Maximum Extent (ME in general, ME^{ref} in this case) of the LFL cloud was measured for the scenario wherein the obstacle was not placed in the domain (*i.e.,* the jet interacts only with the ground). As well as the simulations results, in Figure 1.6, a dashed line is also shown corresponding to ΔME = 5 %. This set threshold can be acceptable, for all the scenarios here addressed, since it corresponds to a little absolute jet ME variation with respect to ME^{ref}.

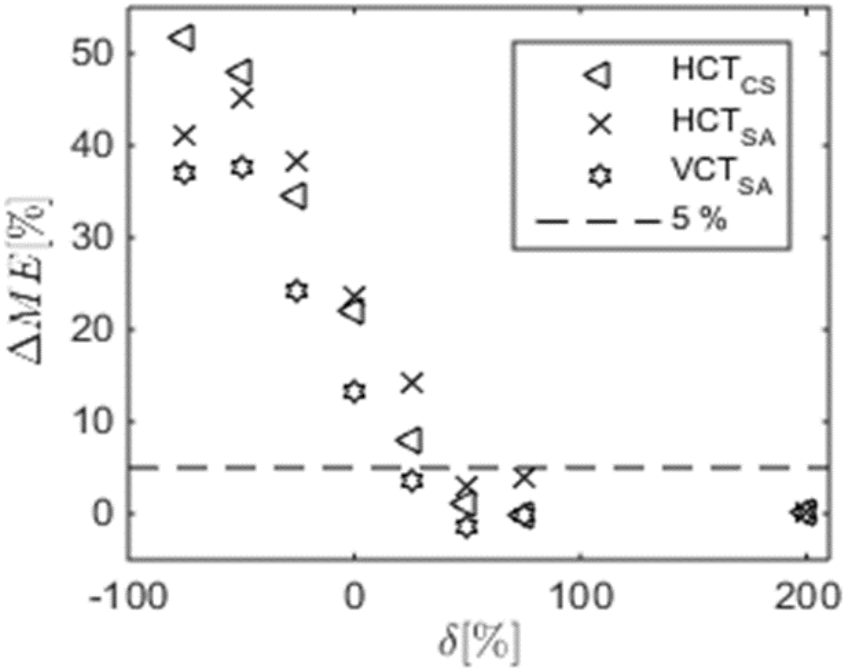

Figure 1.6: Comparison of the ME obtained varying both size and obstacle shape: ΔME over δ trend.

Concerning *Figure 1.6*, it was possible to state that:

- in a qualitatively perspective, all the results present a similar behavior
- the results compose two straight sections in which ΔME decreases constantly or remains practically constant
- for all the findings, the slope change takes place at δ = +50 %
- the results of the HCT_{CS} and HCT_{SA} show similar ΔME, while the ones of VCT_{SA} are, for δ < +50 %, always lower than the others. The cause can be mainly attributed to the larger height of

the source above ground in the VCT_{SA} scenario with respect to the one in both HCT_{CS} and HCT_{CS} scenarios (leading to a different involvement of the ground).

Based on the above, for δ = + 50 %, ME = ME^{ref}, meaning that, for greater distances of the obstacle from the source, the only interaction that the jet still has is with the ground. Therefore, for scenarios where δ > 50 %, the procedure developed by Colombini et al. (2020a) can be deployed to predict the ME of the jet.

REFERENCES

Angers, B., Hourri, A., Benard, P., Tchouvelev, A., 2011. Numerical investigation of a vertical surface on the flammable extent of hydrogen and methane vertical jets. *Int. J. Hydrogen Energy* 36, 2567-72.

Ansys DesignModeler User's Guide, 2017. Release 19.0. ANSYS, Inc.

Ansys Fluent User's Guide, 2017. Release 19.0. ANSYS, Inc.

Ansys Meshing User's Guide, 2017. Release 19.0. ANSYS, Inc.

Ansys Workbench User's Guide, 2017. Release 19.0. ANSYS, Inc.

Baalisampang, T., Abbassi, R., Garaniya, V., Khan, F., Dadashzadeh, M., 2019. Accidental release of Liquefied Natural Gas in a processing facility: Effect of equipment congestion level on dispersion behaviour of the flammable vapour. *J. Loss Prev. Process Ind.* 61, 237–248. https://doi.org/10.1016/j.jlp.2019.07.001.

Bariha, N., Srivastava, V.C., Mishra, I.M., 2017. Theoretical and experimental stuDies on hazard analysis of LPG/LNG release: A review. *Rev. Chem. Eng.* 33, 387–432. https://doi.org/10.1515/revce-2016-0006.

Becker, H.A., Cho, S.H., Ozum, B., Tsujikawa, H., 1988. Turbulent mixing in the impingement zone of dual opposed free jets and of the normal wallimpinging jet. *Chem. Eng. Commun*. 67, 291-313. http://dx.doi.org/10.1080/00986448808940390

Bernatik, A., Libisova, M., 2004. Loss prevention in heavy industry: Risk assessment of large gasholders. J. loss Prev. Process Ind. 17 (4), 271.

Birch, A.D., Brown, D.R., Dodson, M.G., Swaffield, F., 1984. The structure and concentration decay of high pressure jets of natural gas. *Combust. Sci. Technol.* 36, 249–261. https://doi.org/10.1080/00102208408923739.

Birch, A.D., Hughes, D.J., Swaffield, F., 1987. Velocity decay of high pressure jets. *Combust. Sci. Technol.* 52, 161-171. http://dx.doi.org/10.1080/00102208708952575

Bénard, P., Tchouvelev, A., Hourri, A., Chen, Z., Angers, B., 2007. High pressure hydrogen jets in the presence of a surface. *Int. Conf. Hydrog. Saf.* 40.

Bénard, P., Hourri, A., Angers, B., Tchouvelev, A., Agranat, V., 2009. Effects of surface on the flammable extent of hydrogen jets. *Int. Conf. Hydrog. Saf*.

Bénard, P., Hourri, A., Angers, B., Tchouvelev, A., 2016. Adjacent surface effect on the flammable cloud of hydrogen and methane jets: Numerical investigation and engineering correlations. *Int. J. Hydrogen Energy* 41, 18654–18662. https://doi.org/10.1016/j.ijhydene.2016.08.173.

Brook, D. R., Felton, N. V., Clem, C. M., Strickland, D. C. H., Griffiths, I. H., Kingdon, R. D., 2003. Validation of the urban dispersion model (UDM). Int. J. Environ. Pollut. 20 (1−6), 11.

Cameron, I., Raman, R., 2005. Process System Risk Management, first ed. Elsevier Amsterdam.

Chen, C.J., Rodi, W., 1980. Vertical Turbulent Buoyant Jets – A review of Experimental Data, First ed. Pergamon Press Vol. 4.

Colombini, C. and Busini, V., 2019a. Obstacle Influence on High-Pressure Jets based on Computational Fluid Dynamics Simulations. *Chem. Eng. Trans.* 77. DOI: 10.3303/CET1977136.

Colombini, C. and Busini, V., 2019b. High-Pressure Methane Jet: Analysis of the Jet-Obstacle Interaction. Proceedings of the European Safety and Reliability Conference (ESREL), Hannover, Germany, 22-26 September 2019.

Colombini, C., Martani, A., Rota, R., Busini, V., 2020a. Ground influence on high-pressure methane jets: Practical tools for risk assessment. *J. Loss Prevent. Proc*. 67, 104240. https://doi.org/10.1016/j.jlp.2020.104240

Colombini, C., Carlini, L., Rota, R., Busini, V., 2020b. Ground Interaction on High-Pressure Jets: Effect on Different Substances. *Chem. Eng. Trans*. 82. https://doi.org/10.3303/CET2082062

Colombini, C., Maugeri G., Zanon, G., Rota, R., Busini, V., 2021a. Unignited High-Pressure Methane Jet Impinging a Pipe Rack: Practical Tools For Risk Assessment. *J. Loss Prevent. Proc.* 69, 104378. https://doi.org/10.1016/j.jlp.2020.104378

Colombini, C., Carminati, E., Parisi, A., Rota, R., Busini, V., 2021b. Safety Evaluations on Unignited High-Pressure Methane Jets Impacting a Spherical Obstacle. *J. Loss Prevent. Proc*. Under Review.

Cushman-Roisin, B., Environmental Fluid Mechanics – John Wiley & Sons, Book in preparation. Last online access: August 2020. http://www.dartmouth.edu/~cushman/books/EFM/chap9.pdf

Dasgotra, A., Varun Teja, G. V.V., Sharma, A., Mishra, K.B., 2018. CFD modeling of large-scale flammable cloud dispersion using FLACS. *J. Loss Prev. Process Ind.* 56, 531–536. https://doi.org/10.1016/j.jlp.2018.01.001.

Deng, Y., Hu, H., Yu, B., Sun, D., Hou, L., Liang, Y., 2018. A method for simulating the release of natural gas from the rupture of high-pressure pipelines in any terrain. *J. Hazard. Mater.* 342, 418–428. https://doi.org/10.1016/j.jhazmat.2017.08.053.

Derudi, M., Bovolenta, D., Busini, V., Rota, R., 2014. Heavy gas dispersion in presence of large obstacles: Selection of modeling tools. *Ind. Eng. Chem. Res.* 53, 9303–9310. https://doi.org/10.1021/ie4034895.

Desilets, S., Cote, S., Nadau, G., Benard, P., Tchouvelev, A., 2009. Experimental results and comparison with simulated data of a low pressure hydrogen jet. *Int. Conf. Hydrog. Saf*.

Dey, S., Kishore, G.R., Castro-Orgaz, O., Ali, S.Z., 2017. Hydrodynamics of submerged turbulent plane offset jets. *Phys. Fluids* 29. https://doi.org/10.1063/1.4989559.

DNV, *PHAST - Process Hazard Analysis Software Tool,* DNV Software, last access: 27/03/2020. https://www.dnvgl.com/services/process-hazard-analysis-software-phast-1675

Efthimiou, G.C., Andronopoulos, S., Tavares, R., Bartzis, J.G., 2017. CFD-RANS prediction of the dispersion of a hazardous airborne material released during a real accident in an industrial environment. *J. Loss Prev. Process Ind.* 46, 23–36. https://doi.org/10.1016/j.jlp.2017.01.015

EPA 2011. Computer Aided management of emergency operations (CAMEO), ALOHA v5.4.1

Franquet, E., Perrier, V., Gibout, S., Bruel, P., 2015. Free underexpanded jets in a quiescent medium: A review. *Prog. Aerosp. Sci.* 77, 25–53. https://doi.org/10.1016/j.paerosci.2015.06.006.

Gerbec, M., Pontiggia, M., Antonioni, G., Tugnoli, a., Cozzani, V., Sbaouni, M., Lelong, R., 2017. Comparison of UDM and CFD simulations of a time varying release of LPG in geometrical complex environment. *J. Loss Prev. Process Ind.* 45, 56–68. https://doi.org/10.1016/j.jlp.2016.11.020.

Hall, J.E., Hooker, P., O'Sullivan, L., Angers, B., Hourri, A., Benard, P., 2017. Flammability profiles associated with high-pressure hydrogen jets released in close proximity to surfaces. *Int. J. Hydrogen Energy* 42, 7413–7421. https://doi.org/10.1016/j.ijhydene.2016.05.113.

Hess, K., Leukel, W., Stoeckel, A., 1973. Formation of explosive clouds on overhead release and preventive measure. *Chemie-Ingenieur-Technik* 45, 5.

Houf, W., Schefer, R., Evans, G., Merilo, E., Groethe, M., 2010. Evaluation of barrier walls for mitigation of unintended releases of hydrogen. *Int. J. Hydrogen Energy* 35, 4758–4775. https://doi.org/10.1016/j.ijhydene.2010.02.086.

Hourri, A., Angers, B., Bénard, P., 2009. Surface effects on flammable extent of hydrogen and methane jets. *Int. J. Hydrogen Energy* 34, 1569–1577. https://doi.org/10.1016/j.ijhydene.2008.11.088.

Hourri, A., Angers, B., Bénard, P., Tchouvelev, A., Agranat, V., 2011. Numerical investigation of the flammable extent of semi-confined hydrogen and methane jets. *Int. J. Hydrogen Energy* 36, 2567–2572. https://doi.org/10.1016/j.ijhydene.2010.04.121.

Jhonston, I.A., 2005. The Noble-Abel Equation of State: Thermodynamic Derivations for Ballistics Modelling. *Weapons Systems Division Defence Science and Technology Organisation*. DSTO-TN-0670.

Jiang, Y., Xu, Z., Wei, J., Teng, G., 2020. Fused CFD-interpolation model for real-time prediction of hazardous gas dispersion in emergency rescue. *J. Loss Prev. Process Ind.* 63, 103988. https://doi.org/10.1016/j.jlp.2019.103988.

Kim, S., Lee, H.J., Park, J.H., Jeung, I.S., 2013. Effects of a wall on the self-ignition patterns and flame propagation of high-pressure hydrogen release through a tube. *Proc. Combust. Inst.* 34, 2049–2056. https://doi.org/10.1016/j.proci.2012.09.001.

Lim, J.W., Baalisampang, T., Garaniya, V., Abbassi, R., Khan, F., Ji, J., 2019. Numerical analysis of performances of passive fire protections in processing facilities. *J. Loss Prev. Process Ind.* 62, 103970. https://doi.org/10.1016/j.jlp.2019.103970.

Liao, N., Huang, K., Chen, L., Wang, Z, Wu, J., Zhang, F., 2018. Numerical simulation of gas dispersion during cold venting of natural gas pipelines. *Adv. Mech. Eng.* 10, 1–14. https://doi.org/10.1177/1687814018755244.

Lockwood, F. C., Moneib, H. A., 1980. Fluctuating Temperature Measurements in a Heated Round Free Jet. *Combust. Sci. Technol.* 22, 63-81. https://doi.org/10.1080/00102208008952372

Luo, T., Yu, C., Liu, R., Li, M., Zhang, J., Qu, S., 2018. Numerical simulation of LNG release and dispersion using a multiphase CFD model. *J. Loss Prev. Process Ind.* 56, 316–327. https://doi.org/10.1016/j.jlp.2018.08.001.

Menter, F.R., 1993. Zonal Two Equation kω Turbulence Models for Aerodynamic Flows. *24th Fluid Dynamics Conference*.

Middha, P., Hansen, O.R., Grune, J., Kotchourko, A., 2010. CFD calculations of gas leak dispersion and subsequent gas explosions: Validation against ignited impinging hydrogen jet experiments. *J. Hazard. Mater.* 179, 84–94. https://doi.org/10.1016/j.jhazmat.2010.02.061

Novembre, N., Podenzani, F., Colombo, E., 2006. Numerical study for accidental gas releases from high pressure pipelines. *European Conference on Fluid Dynamics (ECCOMAS CFD).*

Palazzi, E., Curro', F., Lunghi, E., Fabiano, B., 2016a. A novel index based framework for assessing hazards of toxic and flammable gaseous releases in the process industry. *Chem. Eng. Trans.* 48, 121-126 DOI:10.3303/CET1648021

Palazzi, E., Curro', F., Lunghi, E., Fabiano, B., 2016b. An analytical model of carbon dioxide jet from pressurized systems for safety distance evaluation, *Chem. Eng. Trans.* 53, 301-306 DOI: 10.3303/CET1653051

Pandya, N., Gabas, N., Marsden, E., 2012. Sensitivity analysis of Phast's atmospheric dispersion model for three toxic materials (nitric oxide, ammonia, chlorine). J. Loss Prev. Process Ind., 25 (1), 20.

Pitss, W.M., 1991. Effects of global density ratio on the centerline mixing behavior of axisymmetric turbulent jets. *Exp. Fluids* 11, 125-134.

Pontiggia, M., Busini, V., Ronzoni, M., Uguccioni, G., Rota, R., 2014. Effect of large obstacles on high momentum jets dispersion. *Chem. Eng. Trans.* 36, 523–528. https://doi.org/10.1016/j.jhazmat.2009.06.064.

Kotchourko, A., Baraldi, D., Bénard, P., Eisenreich, N., Jordan, T., Keller, J., Kessler, A., LaChance, J., Molkov, V., Steen, M., Tchouvelev, A., 2014. State of the Art and Research Priorities in Hydrogen Safety. Joint Research Centre of the European Commission (JRC), Honolulu, Hawaii.

Schefer, R., Groethe, M., Houf, W.G., Evans, G., 2009. Experimental Evaluation of Barrier Walls for Risk Reduction of Unintended Hydrogen Releases, *Int. J. Hydrogen Energ.* 34, 1590-1606. https://doi.org/10.1016/j.ijhydene.2008.11.044

Schefer, R.W., Dibble, R.W., 1986. Mixture fraction measuremetns in a turbulent nonreacting propane jet. AIAA paper, 86-0278.

Schleder, A.M., Pastor, E., Planas, E., Martins, M.R., 2015. Experimental data and CFD performance for cloud dispersion analysis: The USP-UPC project. *J. Loss Prev. Process Ind.* 38, 125-138.

Shell, 2004. FRED – Fire, Release, Explosion and Dispersion, Shell Global Solutions. http://www.shellglobalsolutions.com/hse/software/fred.html. Last access: 15/07/2020.

Souza, A. O., Luiz, A. M., Neto A. T. P., Araujo A. C. B., Silva H. B., Silva A. K., Alves J. J. N, 2019b. CFD predictions for hazardous area classification. *Chinese J. Chem. Eng.* 27, 21–31. https://doi.org/10.1016/j.cjche.2018.06.002

Sposato, C., Tamanini, F., Rogers, W.J., Sam Mannan, M., 2003. Effects of Plate Impingement on the Flammable Volume of Fuel Jet Releases. *Process Saf. Prog.* 22, 4. https://doi.org/10.1002/prs.680220406

Stewart, J.R., 2019. CFD modelling of underexpanded hydrogen jets exiting rectangular shaped openings. *Inst. Chem. Eng. Symp. Ser.* 2019-May.

Tchouvelev, A.V., Cheng, Z., Agranat, V.M., Zhubrin, S.V., 2007. Effectiveness of small barriers as means to reduce clearance distances. *Int. J. Hydrogen Energy* 32, 1409–1415. https://doi.org/10.1016/j.ijhydene.2006.10.020.

Thring, M.W. and Newby, M. P., 1952. Combustion length of enclosed turbulent jet flames. 4th international symposium on combustion, 789.

Tolias, I. C., Giannissi, S.G., Venetsanos, A.G., Keenan, J., Shentsov, V., Makarov, D., Coldrick, S., Kotchourko, A., Ren, K., Jedicke, O., Melideo, D., Baraldi, D., Slater, S., Duclos, A., Verbecke, F., Molkov, V., 2019. Best practice guidelines in numerical simulations and CFD benchmarking for hydrogen safety applications. *Int. J. Hydrogen Energy* 44, 9050–9062. https://doi.org/10.1016/j.ijhydene.2018.06.005.

Tolias, I.C., Venetsanos, A.G., Comparison of convective schemes in hydrogen impinging jet cfd simulation, 2015. 6th International conference on hydrogen safety (ICHS2015).

Uggenti, A.C., Carpignano, A., Savoldi, L., Zanino, R., 2017. Perspective and criticalities of CFD modelling for the analysis of oil and gas offshore accident scenarios. *Risk, Reliability and Safety: Innovating Theory and Practice: Proceedings of ESREL 2016.*

Van den Bosch, C.J.H., Weterings, R.A.P.M., Duijim, N.J., Bakkum, E.A., Mercx, W.P.M., Engelhard, W.F.J.M., Van den Berg, A.C., Van den Doormaal, J.C.A.M., van wees, R.M.M., 1997. Methods for the calculation of physical effects "Yellow book". The hague.

Witlox, H.W.M., Holt, A., 1999. A unified model for jet, heavy and passive dispersion including droplet rainout and re-evaporation. CCPS international conference& workshop on modeling the consequences of accidental releases of hazardous materials.

Xu, B.P., Wen, J.X., Tam, V.H.Y., 2011. The effect of an obstacle plate on the spontaneous ignition in pressurized hydrogen release: A numerical study. *Int. J. Hydrogen Energy* 36, 2637–2644. https://doi.org/10.1016/j.ijhydene.2010.03.143.

Yüceil, K.B., Ötügen, M.V., 2002. Scaling parameters for underexpanded supersonic jets. *Phys. Fluids* 14, 4206–4215. https://doi.org/10.1063/1.1513796.

Zuliani C., De Lorenzi C., Ditali S., 2016. Application of CFD Simulation to Safety Problems – Challenges and Experience Including a Comparative Analysis of Hot Plume Dispersion from a Ground Flare, Chemical Engineering Transactions, 53, 79-84. DOI: 10.3303/CET1653014.

CHAPTER 2: GROUND EFFECT ON HIGH-PRESSURE JETS DEVELOPMENT

CHAPTER 2.1: GROUND INFLUENCE ON HIGH-PRESSURE METHANE JETS: PRACTICAL TOOLS FOR RISK ASSESSMENT

Journal of Loss Prevention in the Process Industries 67 (2020) 104240

Contents lists available at ScienceDirect

Journal of Loss Prevention in the Process Industries

journal homepage: http://www.elsevier.com/locate/jlp

Ground influence on high-pressure methane jets: Practical tools for risk assessment

Cristian Colombini, Andrea Martani, Renato Rota, Valentina Busini *

Politecnico di Milano, Department of Chemistry, Materials and Chemical Engineering "Giulio Natta", Piazza Leonardo da Vinci 32, 20133, Milano, Italy

ABSTRACT

High-pressure gaseous methane release is a relevant safety-related problem mainly in the Oil and Gas industry. As well documented, the reason for these safety concerns is connected with the severe consequences of the domino effect subsequent to the possible ignition. In risk assessment activities, estimation of the damage area is of primary importance in order to draw up proper safety guidelines. To do this, loss prevention specialists use quick and well-established numerical tools (i.e., integral models) in their daily activities. However, the presence of an obstacle in the flow field of the jet (e.g., the ground) is a more probable situation to deal with. It is known that integral models fail in this kind of scenario, leading to unreliable predictions. Hence, the present analysis investigates how an industrial ground surface influences the LFL cloud size of a horizontal high-pressure methane jet. An innovative quick procedure is proposed allowing to determine the height below which the ground begins to influence the LFL cloud size and the extent of such influence. Therefore, this procedure allows practitioners to establish when integral models can be used and when not to use them, and also provides a simple and reliable alternative to their use. These analytical instruments are derived from an extensive computational fluid dynamics analysis performed with Ansys Fluent 19.0.

ACRONYMS

CFD Computational Fluid Dynamics

HPJ High Pressure Jet

LFL Lower Flammability Limit

ME Maximum Extent

QRA Quantitative Risk Analysis

UDF User Defined Function

NOMENCLATURE

a: virtual orifice displacement

C_D: discharge coefficient

d: actual orifice diameter

d_{PS}: pseudo-source orifice diameter

h: height of the source above ground

h*: critical height of the source above ground

k: axial decay constant

ME: LFL cloud maximum extent in direction of the jet axis

ME_{FJ}: free jet LFL cloud maximum extent in direction of the jet axis

ME_X: maximum lateral extent of the LFL jet cloud

p: storage pressure

p_{amb}: environmental pressure

T: storage temperature

T_{amb}: environmental static temperature

v_Z: wind velocity component parallel to the jet axis

z: downstream distance

Δ: percentage variation of ME with respect to ME of the free jet

γ: specific heat ratio

η: axial mole fraction

ρ_a: air density

ρ_g: methane density

INTRODUCTION

Although transporting and storing of chemicals under liquefied conditions (obtained through compression or cooling) is widespread, many of them are still handled in gaseous form (Kim et al., 2013; Bariha et al., 2017; Deng et al., 2018; Baalisampang et al., 2019; Lim et al., 2019; Stewart, 2019).

Therefore, from the industrial safety point of view, the risk assessment of accidental toxic or flammable high-pressure gaseous releases (*i.e.*, High-Pressure Jets, HPJ) is a critical challenge, especially for Quantitative Risk Analysis (QRA) and in the hazardous area classification framework (Pontiggia et al., 2014; Liao et al., 2018).

Regardless of the kind of substance involved, generally the safety evaluation mainly involves estimation of the hazardous area connected (Souza et al., 2019).

Concerning the flammable case, if an ignition takes place, the possible consequences of a leak can be considerable (Bariha et al., 2017; Kong et al., 2019; Pu et al., 2019; Tolias et al., 2019; Yang et al., 2020): due to the domino effect, flash fires and jet fires are among the most hazardous accidents (Benard et al., 2009; Casal et al, 2012; Zhou et al., 2018).

In general, the safety evaluation related to the accidental discharge of flammable materials can be performed by determining the Maximum axially-oriented Extent (ME) of the flammable cloud (Tchouvelev et al., 2007; Houf et al., 2010; Pontiggia et al., 2014; Colombini and Busini, 2019a; Colombini and Busini, 2019b).

Thinking of a realistic industrial situation where a high-pressure flammable jet may occur, it is quite evident that the flammable cloud may interact with equipment or structures (Xu et al., 2011).

In this case the jet development can be influenced by interaction with an obstacle (Tchouvelev et al., 2007; Benard et al., 2009; Middha et al., 2010; Kotchourko et al., 2014): in principle, the enhanced turbulence effects on one hand (that increases the entrainment of fresh air, leading to a faster dilution of the hazardous substance) and the reduction of momentum on the other hand (inducing a lower turbulence level that can lead to an increase in the critical area involved) suggest that from the industrial safety point of view the obstacle could affect the jet behaviour either positively or negatively. Therefore, with respect to the free jet scenario (intended as a release occurring in an unconfined environment (Dey et al., 2017)), which is the most common situation considered in the industrial safety practice (Dasgotra et al., 2018), in some cases the effect can be an increase in the hazardous area involved, *i.e.*, the ME of the jet cloud is larger than that of a free jet, while in other cases it can be lower (Kotchourko et al., 2014; Hall et al., 2017).

As for accidental scenarios involving low momentum spills of hazardous gases (*e.g.,* cloud dispersions from liquid pools), in the presence of any kind of obstacle, integral models can give unreliable results (Cameron and Raman, 2005; Schelder et al., 2015; Gerbec et al., 2017; Uggenti et al., 2017; Dasgotra et al., 2018).

The main reason why this kind of numerical model usually fails to reproduce accidental releases in complex geometries is that integral models account for some physical phenomena through semi empirical correlations having parameters that have been fitted to some field test data (Derudi et al., 2014). Their accuracy is therefore strictly related to the experimental tests used to tune the model parameters. Given that obstacles are not usually present in such field trials, it is easy to understand how the integral models give reliable predictions only for free jet scenarios.

To the best of Authors' knowledge, although improvements have been made in recent years concerning low-computational-cost tools in the framework of accidental releases risk assessment, the previously highlighted limits of the integral models in reproducing complex geometry situations are still present.

Therefore, simulation models developed in the frame of Computational Fluid Dynamics (CFD) need to be used (Batt et al., 2016; Alves et al., 2019). The reason is that only a distributed parameter model can address a problem at any level of geometrical complexity (Efthimiou et al., 2017; Gerbec et al., 2017; Luo et al., 2018; Jiang et al., 2020), providing the user with detailed qualitative and quantitative information on the flow field (Cameron and Raman, 2005; Deng et al., 2018; Luo et al., 2018; Tolias et al., 2019). However, this approach is not yet free of drawbacks: the amount of resources needed, both in terms of computational costs and analyst skills required, still limits its use (Jiang et al., 2020).

Falling under the general definition of an obstacle, flat surfaces close to the jet source, such as the ground or vertical walls, are of particular interest in the industrial safety field since they can induce an enlargement of the hazardous area (Benard et al., 2007; Benard et al., 2009; Desilets et al., 2009; Hourri et al., 2009; Hourri et al., 2011; Angers et al., 2011; Kotchourko et al., 2014; Benard et al., 2016; Hall et al., 2017).

In particular, in 2007 Benard and co-workers numerically investigated the influence of vertical and horizontal flat surfaces parallel to unignited vertical and horizontal hydrogen and methane HPJ. They performed the study considering a single reservoir pressure value (284 bar), a specific orifice dimension (8.5 mm) and a fixed distance of the jet source from the surface (1 m). The results showed that in spite of the high-momentum of the releases, the ME of hydrogen jets is strongly influenced

by the buoyancy effect, while the ME of methane jets is not. Starting from this work, Hourri et al. (2009) included two more distances of the jet source from the surface (0.5 and 2 m). Benard et al. (2009) considered horizontal releases occurring from an orifice with a different diameter (6.35 mm), from two different storage pressure values (100 and 700 barg) and several distances from the surface (from 0.1 to 10 m). Hourri et al. (2011) investigated different storage pressures (250, 400 and 550 barg), while, Angers et al. (2011) extended the analysis done by Hourri et al. (2011) to the case of vertical jets. Benard et al. (2016) combined the results of some of these works establishing engineering correlations to quantify the flammable extent of both hydrogen and methane jet releases.

Limited to hydrogen releases, some empirical information is also available: Desilets et al. (2009) performed a series of laboratory experiments on the LFL cloud extension considering two storage pressures (6.6 and 16.3 bar), two orifice diameters (1.6 and 0.79 mm), and several distances from the horizontal adjacent surface (1-30 cm), Hall et al. (2017) reported empirical data for two storage pressure values (150 and 425 barg) through nozzles with a diameter of 0.64 and 1.06 mm, respectively. The focus was on understanding how horizontal surfaces influence the releases of both unignited and ignited hydrogen.

As a matter of fact, the methane high-pressure gaseous release is a relevant safety-related problem mainly in the Oil and Gas (O&G) industry. The reason for its importance is related to the severe consequences of the subsequent domino effect that may take place if ignition of the release occurs, either immediately (jet fire) or with a delay (flash fire). In risk assessment the damage area of the jet cloud (in particular, the hazardous distance reached by the LFL concentration value) is recognised as the characteristic distance of interest in the risk analysis process. To estimate the maximum axially-oriented extent of the flammable cloud, in their daily activities loss prevention specialists use quick and well-established numerical tools such as integral models (*e.g.*, PHAST (DNV, 2020)). However, the presence of an obstacle in the flow field of the jet is a more realistic situation to deal with. Therefore, the main aim of the present work is to investigate how an industrial ground surface (*i.e.*, made of concrete) can influence the LFL cloud size of a horizontal high-pressure methane jet through an extensive CFD analysis performed with Ansys Fluent 19.0. The main innovative result of this work is a quick procedure making it possible to i) determine the minimum height from which the ground begins to influence the hazardous distance; since below this height the predictions of standard simulation tools are not reliable and a simple tool allowing practitioners to know whether or not a given accidental scenario can be simulated with standard modelling tools is of paramount

practical importance, and ii) estimate how much the hazardous distance increases when the ground influence makes the predictions of the standard simulation tools unreliable.

The paper outline is the following: at first, key methodological aspects of the CFD model developed are discussed; then, referring to a selected case among the various analysed, the proposed criterion and the derived analytical correlation are discussed in detail. Therefore, the reliability of the proposed approach is investigated by comparison with the CFD results of many realistic scenarios (nearly 250 cases). Finally, a simple way to use the proposed methodology independently from any CFD computation is suggested and compared with the previous results. In the conclusions, an overall simple procedure is presented that allows safety analysts to estimate by hand the hazardous distance.

MATERIAL AND METHODS

Thanks to the capabilities of bring-together and easy-to-use design, to perform the present CFD numerical analysis the Ansys Workbench suite (v. 19.0) was used. A particular aspect that has to be highlighted about this software suite is the possibility of easy design and parametric analysis study. The geometry domain was created with Ansys DesignModeler software, the grid was built using Ansys Meshing and the computations were undertaken with the numerical solver Ansys Fluent. Description of the Workbench platform and the three specific software used is extensively reported in the corresponding owner User Guides (Ansys DesignModeler User Guide, 2017; Ansys Meshing User Guide, 2017; Ansys Fluent User Guide, 2017). Reasons, kinds and values of all the CFD analysis settings are reported and described in detail in the next Section.

With the aim of avoiding the need to simulate the early stage of the jet development (*i.e.*, the so-called nearfield zone of the jet), the use of a fictitious jet source makes it possible to save computational costs keeping the reliability of the results within an acceptable range (in particular, if the farfield zone of the jet is of primary interest). Named in several ways, such as equivalent diameter, notional nozzle, pseudo-source or fictional nozzle (Franquet et al., 2015), this widely adopted kind of approach was used to model the jet source term as discussed in the following Section.

RESULTS AND DISCUSSION

Further below the base case scenario analysis is discussed with particular reference to the definition of the physical scenario, the setup of the CFD analysis in each of its steps and the results of the analysis. Then the parametric analysis conducted is outlined and the main results are discussed. As a last step, with the double aim of further validating the CFD model and making the analytical tools proposed more usable for on-field assessments, a comparison with the results obtained exploiting a simpler tool than CFD is presented for the free jet situation.

BASE CASE SCENARIO

The base case scenario was a realistic situation of industrial interest involving an accidental horizontally oriented high-pressure release of methane adjacent to the ground. Assuming a release from a storage tank (or a pipeline) sufficiently large, the loss of containment can be treated as stationary. Referring to the scenario considered in the work of Colombini and Busini (2019a), a pressure of 65 bara and a temperature of 278 K were considered as upstream gas conditions. A one-inch diameter hole was assumed as a possible accidental orifice (Hendrickson et al., 2015). Since the scenario is outdoors, and the purpose of this work is risk-assessment oriented, the analysis was conducted considering the 5D atmospheric stability class (*i.e.*, a wind intensity of 5 m/s at 10 m from the ground and a Pasquill stability class of D) (Pontiggia et al., 2009). In particular, the worst case situation of wind blowing alongside and in the same direction of the jet was taken as reference and adopted in all the simulations. As regards the flat surface adjacent to the release, a concrete ground surface was assumed as the kind of terrain that can be more often found in an industrial plant.
Hence the base case scenario was set as an array of situations defined by different heights of the source above ground (namely 13 cases, from 14.5 cm to 4.3 m).

CFD MODEL DEFINITION

As described in Section *MATERIAL AND METHODS* of this Chapter, the jet source term was modelled through the use of an equivalent diameter model instead of considering the actual source term. In defining the geometry this meant that the hole diameter to be considered was based on the equivalent diameter model adopted (and the upstream conditions). In the present work the model developed by Birch et al. (1984) was chosen, leading to a pseudo-source diameter of 14.58 cm (*i.e.*,

almost 6 times the actual one). It is worth mentioning that because the farfield zone of the jet is of primary interest in this work and according to the work of Crist et al. (1966), the axial displacement of the pseudo-source from the actual one, a, was neglected.

The computational domain extents were sized similarly to the work of Hourri et al. (2009). Since the ground can only increase the ME of the jet cloud, to avoid any boundary interference on the jet cloud development the domain extents were sized considering the worst-case scenario (*i.e.*, the lower h) (Tolias et al., 2019). Thus the computational domain was a rectangular box of 100 m length, 25 m height and 10 m wide (when a symmetry plane is adopted, while 20 m when the full 3D geometry is considered).

The domain was discretised using five virtual line bodies splitting the jet axis which served as geometrical base for the Ansys Meshing body of influence feature. As a result, cells thickening within a volume surrounding the jet axis was achieved and less expensive coarse mesh far from the "critical" zone of the domain (*i.e.*, where gradients are expected to be less relevant) was obtained. In Table 2.1, all the specifics about the body of influence feature for each of the five line bodies are listed; length and cell size are expressed with respect to the equivalent diameter value allowing to maintain proportionality of the grid specifics when the scenario characteristics, which affect the d_{PS} value, vary. While, Figure 2.1 shows the computational domain considered for one of the source heights investigated in the base case. In particular, the five line bodies are highlighted in the Figure (core in green, far1 in orange, far2 in light blue, far3 in magenta and far4 in blue). Another constraint on the grid generation was imposed at the jet exit. In particular, the same cell dimension along the jet axis used for the ''core'' line body was adopted.

In this way the fluid domain was discretised using a fully unstructured tetrahedral grid. Figure 2.2 shows how the whole resulting mesh appears (a) and its detail in proximity to the jet orifice (b). Depending on the height of the source from the ground, the cell count ranged between 7.3 and 7.8 million of elements. Quality requirements in terms of skewness and orthogonal quality were always satisfied. With respect to the independence of the results from the grid, it was checked for a reference case by repeating the simulation twice: with respect to the values reported in Table 2.1, the elements size of the body of influence features were halved and doubled, respectively. Both qualitatively (in terms of cloud shape) and quantitatively (in terms of concentration decay along the jet centreline), good matching was achieved. Figure A1 in the supplementary material shows the comparison of the sensitivity analysis results in terms of methane mole fraction contours.

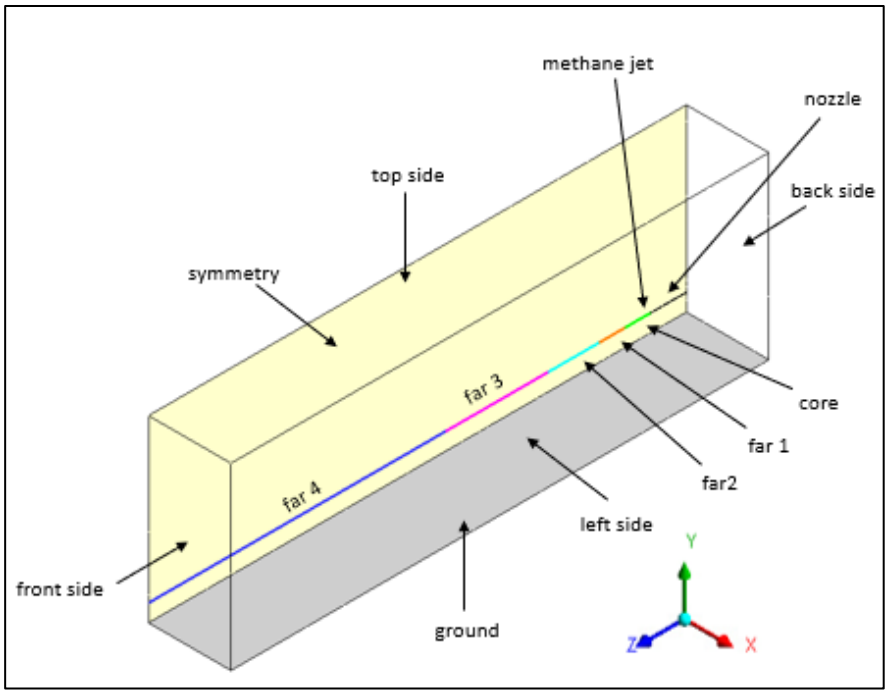

Figure 2.1: Sketch of the computational domain for h = 4.374 m.

Table 2.1: Geometrical and mesh specifics of the five body of influence features used in the base case scenario simulations (Legend as in Figure 2.1).

	Core	**Far1**	**Far2**	**Far3**	**Far4**
$\frac{Length}{d_{PS}}$ [-]	35	35	70	140	391
$\frac{d_{PS}}{Cell\ size}$ [-]	73	18	10	3	1
Growth rate	1.075	1.1	1.15	1.175	1.2

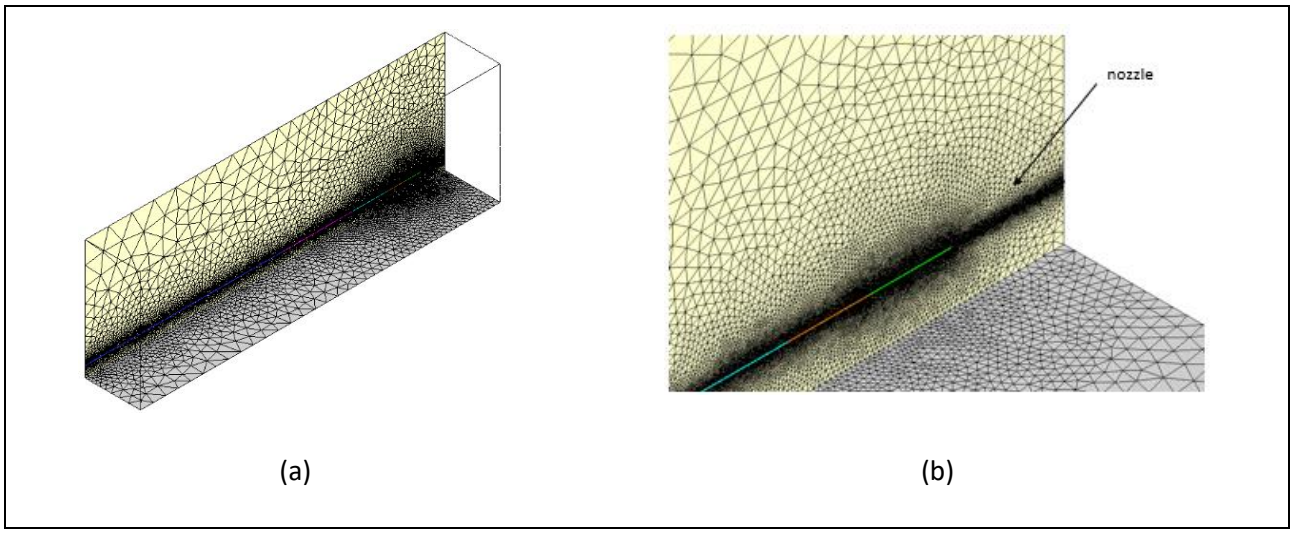

Figure 2.2: Whole grid appearance around the jet centreline (a) and a detail in the surrounding of the orifice (b) for the case of h = 4.374 m.

All the simulations of the base case scenario discussed here (and all those of the sensitivity cases presented later on) were performed in steady state conditions and the pressure-based solver was chosen thanks to the equivalent diameter model deployment (allowing the flow to be treated as incompressible). The Reynolds-averaged approach was employed for the governing Navier-Stokes equations (RANS approach). The two-equation eddy-viscosity k-ω SST turbulence closure model (Menter, 1993) was chosen to account for the turbulence on the flow field avoiding, on the other hand, the need to simulate the boundary layer region precisely next to the ground. To account for the multi-species problem (methane release in ambient air), the species transport model without any kind of reaction was selected and the ideal gas equation of state was used to model the fluid mixture density. The COUPLED pressure-velocity coupling scheme was adopted while the second order upwind spatial-discretisation scheme was considered for all the convective terms. Table A1 in the supplemental information lists the model equations together with the definition of the main parameters.

Table 2.2 reports all the characteristics of the methane pseudo-source inlet boundary condition according to the Birch et al. (1984) approach. *Table 2.3* lists all the other boundary conditions together with their specifics, while, *Figure 2.1* shows also their correspondent position in the computational domain. Notice that to properly model the realistic wind conditions of an open field scenario, a velocity profile reproducing the atmospheric class 5*D* was provided through an *ad hoc* User Defined Function (UDF). Gravity acceleration was always included perpendicularly to the ground surface.

Table 2.2: Pseudo-source characteristics as calculated by the model of Birch et al. (1984) for the base case scenario.

Characteristic	Value
Equivalent diameter	0.145 m
Velocity	440.9 m/s
Mass flow rate	5.184 kg/s
Total temperature	343.8 K
Pressure	101325 Pa

Table 2.3: Boundary conditions assignments used for the simulations.

Boundary name	Type	Specifics
Back side	Velocity inlet	air, v_z = UDF velocity profile, T = 300 K
Top side	Velocity inlet	air, v_z = 5.5 m/s, T = 300 K
Left side	Velocity inlet	air, v_z = UDF velocity profile, T = 300 K
Ground	Wall	0.01 m roughness height, adiabatic
Symmetry	Symmetry	-
Front side	Pressure outlet	air, $T_{BACKFLOW}$ = 300 K
Nozzle	Wall	0.001 m roughness height, adiabatic
Methane jet	Mass flow inlet	See Table 2.2

ANALYSIS OF THE RESULTS

To study the effect of the ground on the ME of a horizontally oriented high-pressure release of methane, an analysis varying the height of the jet exit above the ground was performed. The entire set of leak orifice heights simulated (from 1 pseudo diameter up to 30 pseudo diameters above ground) together with the corresponding me values computed and their percentage variation with respect to the free jet one (δ_z), are reported in Table 2.4. Moreover, to remark quantitatively on the significant difference between the parallel and the normal to the jet axis maximum extent of the LFL jet cloud, the last row of Table 2.4 lists the maximum lateral extent of the LFL jet cloud (ME_x). Notice that the lateral dimensions are related to the symmetry case (i.e., the full lateral extent of the cloud is twice such values). For comparison purposes, the last column (case 13 in the Table) lists the characteristics of the free jet situation. Figure 2.3 shows the LFL contours for some representative scenarios. Moreover, Figure A2 in the supplemental information shows, for the same cases, contours of temperature, velocity and turbulent kinetic energy.

Table 2.4: computed values of ME and their percentage variations with respect to the ME of the free jet case for the base case scenario. Last row lists the corresponding MEx of the LFL envelopes.

Case	**1**	**2**	**3**	**4**	**5**	**6**	**7**	**8**	**9**	**10**	**11**	**12**	**13**
h [m]	0.145	0.437	0.729	1.026	1.312	1.604	1.895	2.187	2.479	2.77	3.061	3.353	4.374
h/d_{PS} [-]	1	3	5	7	9	11	13	15	17	19	21	23	30
ME [m]	63.4	51	43.8	37.4	31	22.8	17.05	16.7	16.6	16.5	16.5	16.45	16.45
Δ_z [%]	+285	+210	+166	+127	+88	+38	+3.6	+1.5	+0.9	+0.3	+0.3	+0	+0
ME_X [m]	1.68	1.65	1.63	1.45	1.15	1.08	1.07	1.07	1.07	1.05	1.07	1.05	1.05

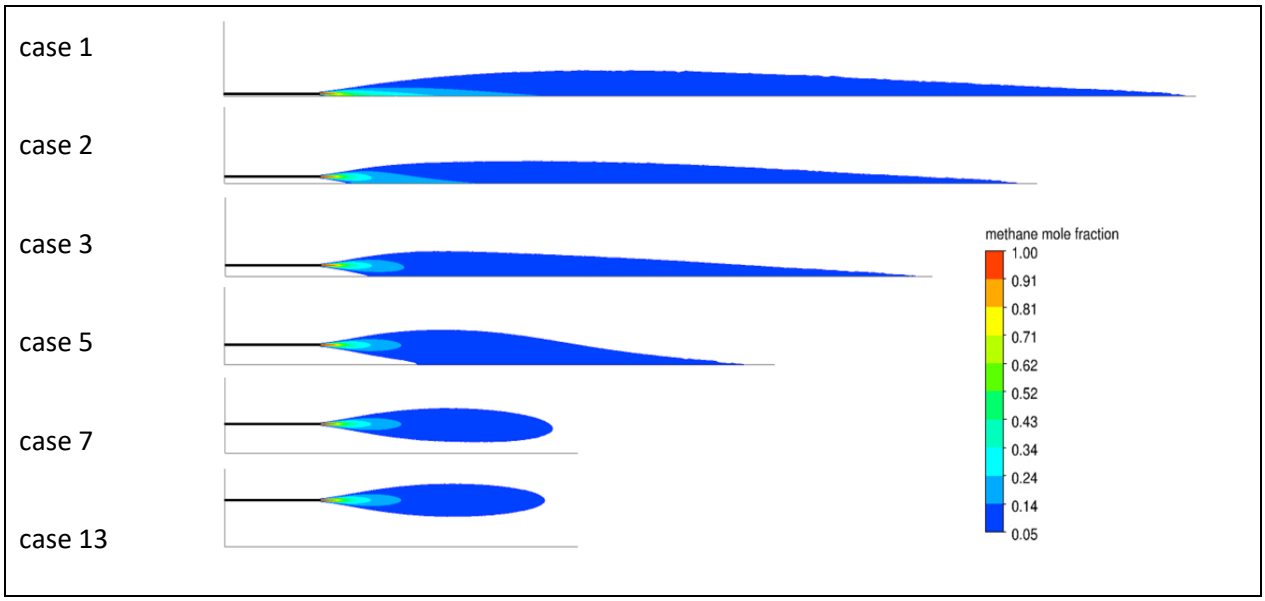

Figure 2.3: LFL mole fraction contours of methane in air for some of the heights considered.

From both *Figure 2.3* and *Table 2.4*, it can be noted that more the jet exit is close to the ground, the longer the ME is. The fact that for small heights (i.e., in the order of the pseudo-source diameter) the resulting ME of the jet is almost four times the ME of the correspondent free jet underlines the need for the ground presence in safety risk assessments analysis to be carefully accounted for.

From the results shown in *Figure 2.3* we can see that methane jets are momentum dominated. For the various situations investigated, no significant buoyancy effects can be noticed. Moreover, the Coanda effect deviates the jet development towards the ground (Miozzi et al., 2010). This occurs because the ground limits the entrainment of surrounding air causing, with respect to the upper side of the jet, a lower pressure that attracts the jet.

Figure 2.4 shows how ME varies as a function of the source height above the ground (h). This plot clearly depicts some findings: i) over a specific critical height of the jet above ground (h*), the jet is not influenced by the ground presence (*i.e.*, the ME is equal to the free jet one); ii) once the ground influence is noticed, it acts enhancing the ME of the jet; iii) the overall increase of ME presents an almost inverse linear proportionality to h.

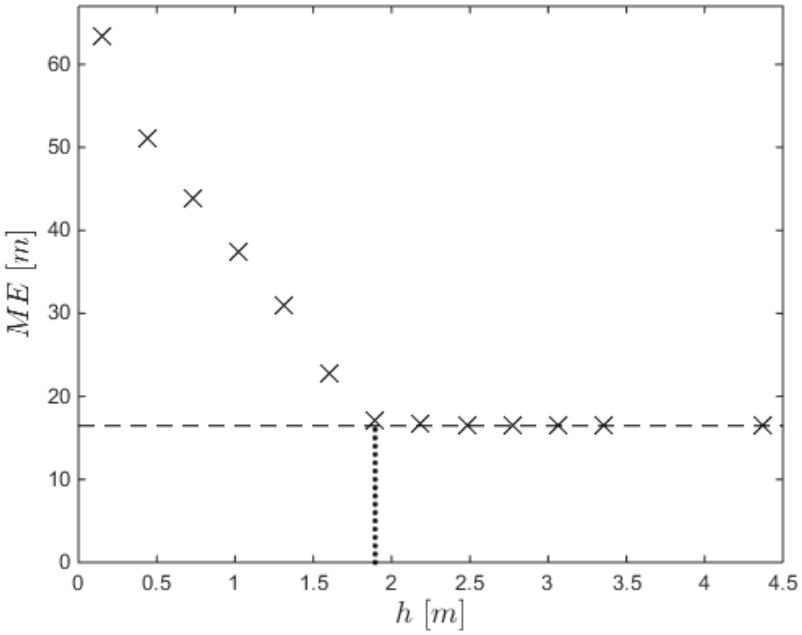

Figure 2.4: LFL ME plotted against h for all the cases considered in the base case scenario. In the Figure, the dashed line and the dotted line represent the ME of the free jet case (MEFJ = 16.45 m) and the critical height of the jet above ground (h = 1.895 m), respectively*.

PROPOSED CRITERION AND ANALYTICAL CORRELATION

Although the results previously shown can be expected to be qualitatively valid for different scenarios, they could lack general application for three main reasons:

1. varying the storage pressure, the results might be different in terms of ME
2. a variation of the actual orifice diameter will affect the jet characteristics in some way and therefore even the ME will also be influenced. In fact the orifice diameter directly influences the pseudo-source diameter, as shown by the following equation (Birch et al., 1984):

$$d_{PS} = d\sqrt{C_D\left(\frac{p}{p_{amb}}\right)\left(\frac{2}{\gamma+1}\right)^{\frac{(\gamma+1)}{2(\gamma-1)}}} \tag{2.1}$$

   where d_{ps} is the resulting diameter of the pseudo-source, d is the actual orifice diameter, C_D is the discharge coefficient, p is the storage pressure, p_{amb} is the environmental pressure and γ is the specific heat ratio
3. Since there are several equivalent diameter models available in literature (Franquet et al., 2015), the choice of a particular model can affect the jet characteristics

To generalise the results reported in *Figure 2.4*, they were made dimensionless using the ME value of the free jet case (ME_{FJ}) and the pseudo-source diameter (d_{PS}) as shown in *Figure 2.5*. This graph

shows how the ME (obtained in each of the cases) varies with respect to ME_{FJ} as function of the height above ground of the jet orifice (h) expressed as the number of pseudo-source diameters (d_{PS}).

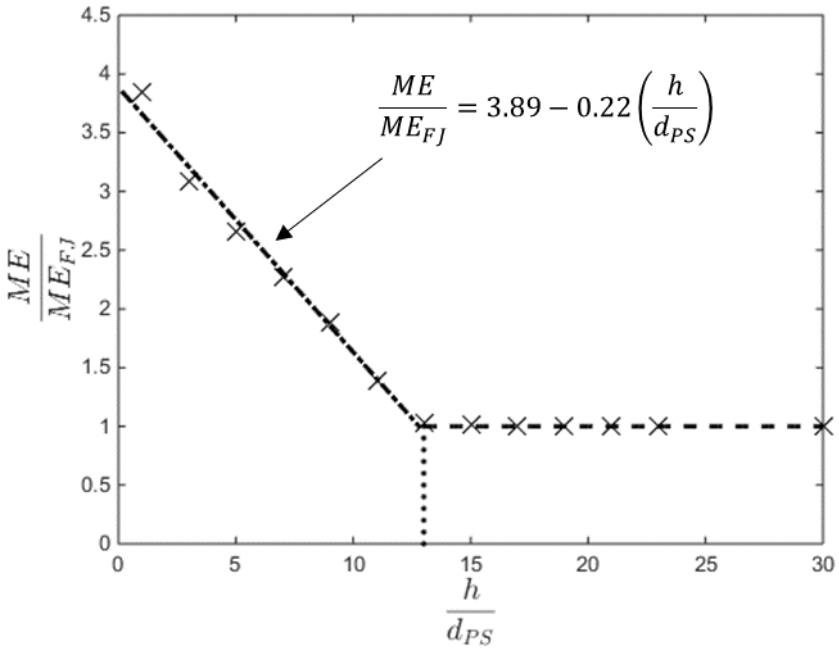

Figure 2.5: Dimensionless ME over the dimensionless height of the source above ground for all the cases of the base case scenario. In the Figure, the dashed-dotted line represents the linear fitting of the computed results influenced by the ground, the dashed line represents the linear fitting of the ones not influenced by the ground and, the dotted line represents the critical dimensionless height of the jet above ground ($h/d_{PS}^* = 13$).

From *Figure 2.5* it is possible to: i) determine a threshold value that, in terms of h/d_{PS}, acts as a criterion establishing when the ground effect starts to be noticeable and ii) derive an analytical correlation that makes it possible to assess the increase of the LFL cloud extent due to the ground effect.

With respect to the first point, the h/d_{PS} threshold limit is equal to about 13 while, the first-order polynomial function that best fits the numerical outcomes for $h/d_{PS} < 13$ (with a coefficient of determination equal to 0.988) is

$$\frac{ME}{ME_{FJ}} = 3.89 - 0.22\frac{h}{d_{PS}} \tag{2.2}$$

SCENARIO SENSITIVITY ANALYSIS

To investigate the validity of both the threshold criterion and the correlation discussed in the previous Section, a sensitivity analysis considering several realistic scenarios (nearly 250 cases) was performed. First, various source conditions (in terms of storage pressure and actual orifice diameter) were analysed. Second, three other wind intensities were considered as possible open field conditions in which the jet can occur. Third, two other pseudo-source models were used to determine the source characteristics for the incompressible simulations. Finally, when coherent with the present analysis, the numerical results of Benard et al. (2016) were included.

The full set of the analysed scenarios is reported in Table 2.5, while the computed results, in terms of ME as a function of the height above ground of the jet source, are shown in Figure 2.6. When required, domain size and cell dimensions of the bodies of influence features were properly resized to contain the whole LFL envelopes in the domain.

Concerning the ME sensitivity dependent on the storage pressure, the minimum value to obtain critical conditions (cases 14-21), halving the value used in the base case scenario (cases 22-29) and doubling it (cases 30-37), was used. From Figure 2.6a it is possible to observe that at the same value of h, the higher the storage pressure is, the larger the ME is. This is expected since an increase in the storage pressure leads to an increase in the corresponding equivalent orifice diameter (see Eq. 2.1) which at constant velocity implies a larger mass flow rate. For the same reason the influence of the terrain starts at different heights; the lower the storage pressure is, the lower the threshold value h* is. However, regardless of the storage pressure value, once the ground influence starts it deviates the jet in the same way. This is why the slope of the ME vs. h curve is practically the same for all the four pressures investigated.

Cases 38-53 in Table 2.5 refer to a variation of the orifice diameter (namely, halving the base case scenario value (cases 38-45) and increasing it 1.5 times (cases 46-53)), while cases 54-73 involve a variation of both the storage pressure and the orifice diameter. From the corresponding plots (*Figure 2.6*b and 2.6c, respectively), we can see that the trends are similar to the ones found when varying the storage pressure (*Figure 2.6*a). In particular, considering the same value of h, the larger the pressure or the orifice diameter are, the larger ME is. Therefore, the previous comments on the results in *Figure 2.6*a hold true also for the ones in *Figure 2.6*b and 2.6c. Considering cases 74-96, in *Figure 2.6*d the results show the effect that different constant wind conditions have on the ME of the jet cloud for each wind profile used in the base case scenario. From this figure it is possible to observe how the wind intensity and shape modify the jet-ground interaction rather than the free

jet characteristics. In fact, in terms of ME_{FJ}, all the results are within about 10% of the base case scenario, while in terms of h*, the range in which the results vary is equal to about 50% of the base case scenario. In particular, the larger the wind velocity is, the smaller the h* is. Looking at the results influenced by the ground, two wind effects were identified: i) the lifting effect and ii) the stretching effect. The former acts by limiting the jet development toward the ground allowing greater air entrainment that leads to a reduction of the jet cloud's extent. The latter acts by increasing the extent of the jet in the axial direction because of the velocity of the flow field surrounding the jet. Two distinct situations can be highlighted: i) when the jet is close to the ground, the jet attaches quickly to it excluding the lifting effect. In this case only the contribution of the stretching effect is noticeable (the larger the wind velocity is, the larger the corresponding ME is); ii) when the jet is quite high over the ground, but still within the ground influence region, both effects are present.

For the purposes of comparison, in cases 97-132 the same constant wind conditions of tests 74-96 were considered together with a lower storage pressure.

With regard to cases 133-161, in which the influence of the pseudo-source was tested, *Figure 2.6*f shows some dependence on the pseudo-source model. Since the same mass flow rate was used, the model of Yuceil and Otugen (2002), which predicts a smaller (nearly 2 times) equivalent diameter, leads to a much higher exit velocity and therefore to larger differences compared to the base case scenario. On the other hand, the pseudo-source model of Ewan and Moodie (1986) predicts almost the same equivalent diameter, leading to results that practically overlap the ones of the base case scenario. The results of this sensitivity are noticeably coherent with the findings reported by Franquet et al. (2015).

Table 2.5: Specifics and simulations settings.

case	p [bara]	T [K]	d [m]	d_{PS} model	v_z [m/s]	T_{amb} [K]	h [m]	
14-21	2.5	278	0.0254	Birch et al. (1984)	profile	300	0.028, 0.085, 0.143, 0.257, 0.314, 0.371, 0.486, 0.858	Figure 2.6a
22-29	32.5	278	0.0254	Birch et al. (1984)	profile	300	0.103, 0.309, 0.515, 0.927, 1.134, 1.340, 1.752, 3.09	
30-37	130	278	0.0254	Birch et al. (1984)	profile	300	0.206, 0.618, 1.03, 1.855, 2.268, 2.680, 3.505, 6.186	
38-45	65	278	0.0127	Birch et al. (1984)	profile	300	0.073, 0.218, 0.364, 0.656, 0.802, 0.947, 1.239, 2.187	Figure 2.6b
46-53	65	278	0.0381	Birch et al. (1984)	profile	300	0.218, 0.656, 1.093, 1.968, 2.405, 2.843, 3.717, 6.56	
54-57	20	278	0.0381	Birch et al. (1984)	profile	300	0.363, 0.849, 1.576, 3.153	Figure 2.6c
58-61	30	278	0.01907	Birch et al. (1984)	profile	300	0.223, 0.520, 0.967, 1.934	
62-65	85	278	0.0127	Birch et al. (1984)	profile	300	0.250, 0.583, 1.084, 2.168	
66-69	120	278	0.0127	Birch et al. (1984)	profile	300	0.297, 0.693, 1.288, 2.576	
70-73	120	278	0.0381	Birch et al. (1984)	profile	300	0.891, 2.080, 3.863, 7.727	
74-80	65	278	0.0254	Birch et al. (1984)	1	300	0.3, 0.729, 1, 1.458, 1.895, 2.187	Figure 2.6d
81-88	65	278	0.0254	Birch et al. (1984)	10	300	0.3, 0.729, 1, 1.458, 1.676, 1.895, 2.187, 6	
89-96	65	278	0.0254	Birch et al. (1984)	20	300	0.3, 0.729, 1, 1.312, 1.458, 1.895, 2.187, 6	
97-109	2.5	278	0.0254	Birch et al. (1984)	profile	300	0.028, 0.085, 0.143, 0.200, 0.257, 0.314, 0.371, 0.429, 0.486, 0.553, 0.6, 0.657, 0.858	Figure 2.6e
110-116	2.5	278	0.0254	Birch et al. (1984)	1	300	0.143, 0.228, 0.3, 0.371, 0.429, 1, 6	
117-124	2.5	278	0.0254	Birch et al. (1984)	10	300	0.143, 0.228, 0.3, 0.328, 0.371, 0.429, 1, 6	
125-132	2.5	278	0.0254	Birch et al. (1984)	20	300	0.143, 0.228 0.257, 0.3, 0.371, 0.429, 1, 6	
133-144	65	278	0.0254	Ewan and Moodie (1986)	profile	300	0.137, 0.412, 0.687, 1.236, 1.511, 1.786, 1.923, 2.061, 2.198, 2.335, 4.122	Figure 2.6f
145-161	65	278	0.0254	Yuceil and Otugen (2002)	profile	300	0.085, 0.255, 0.425, 0.765 , 0.935, 1.105, 1.19, 1.275, 1.36, 1.445, 1.53, 1.615, 1.7, 1.87, 2.04, 2.55, 3.4	
162-177	101	293	0.00635	FLACS embedded model	Not specified	293	0.029, 0.088, 0.206, 0.368, 0.481, 0.794, 1.011, 1.615, 2.032, 2.551, 3.197, 4, 6, 8, 10, free jet	From Benard et al. (2016)
178-195	251	293	0.00635	FLACS embedded model	Not specified	293	0.048, 0.143, 0.238, 0.333, 0.591, 0.769, 0.989, 1.263, 1.603, 2.025, 2.548, 3.197, 4, 5, 6, 8, 10, free jet	
196-213	401	293	0.00635	FLACS embedded model	Not specified	293	0.059, 0.176, 0.294, 0.412, 0.559, 0.74, 0.964, 1.242, 1.586, 2.012, 2.539, 3.191, 4, 5, 6, 8, 10, free jet	
214-232	551	293	0.00635	FLACS embedded model	Not specified	293	0.069, 0.207, 0.345, 0.483, 0.621, 0.795, 1.011, 1.28, 1.614, 2.031, 2.549, 3.195, 4, 5, 6, 7, 8, 10, free jet	
233-252	701	293	0.00635	FLACS embedded model	Not specified	293	0.077, 0.231, 0.385, 0.538, 0.72, 0.949, 1.231, 1.58, 2.01, 2.54, 3.195, 4, 5, 6, 7, 8, 9, 10, 11, free jet	

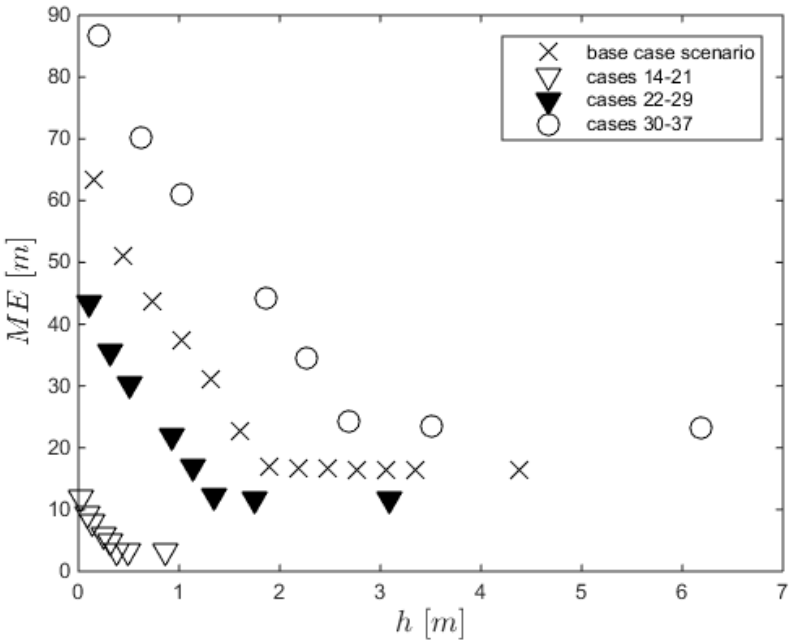
base case scenario
cases 14-21
cases 22-29
cases 30-37
$ME\ [m]$
$h\ [m]$

a

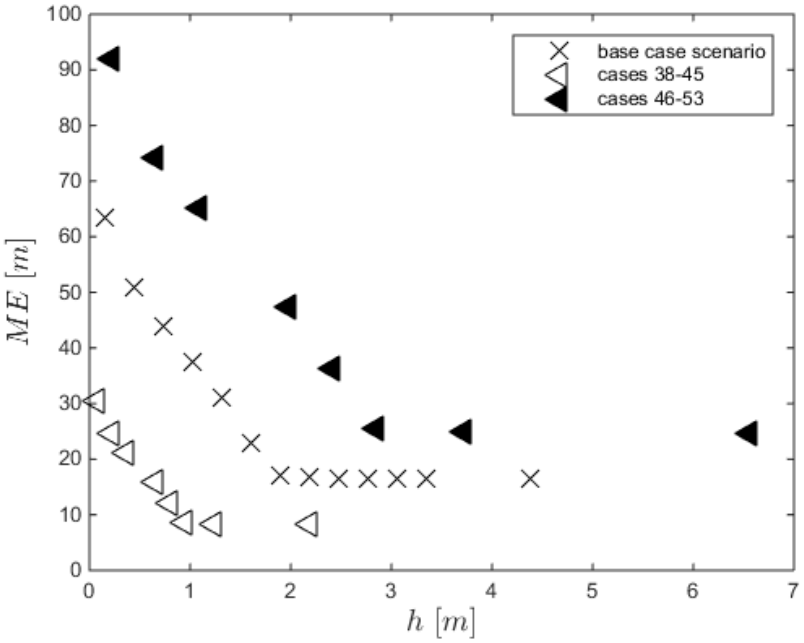
base case scenario
cases 38-45
cases 46-53
$ME\ [m]$
$h\ [m]$

b

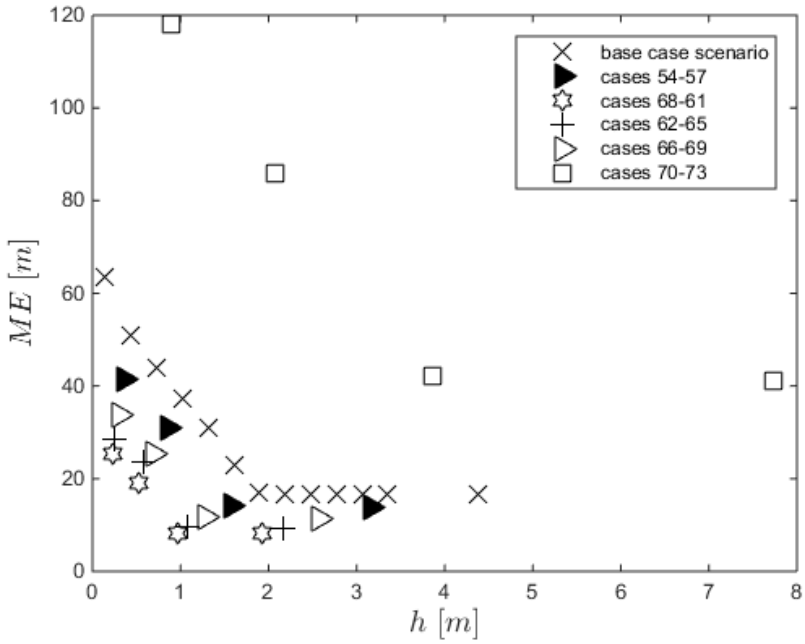
base case scenario
cases 54-57
cases 68-61
cases 62-65
cases 66-69
cases 70-73
ME [m]
h [m]

c

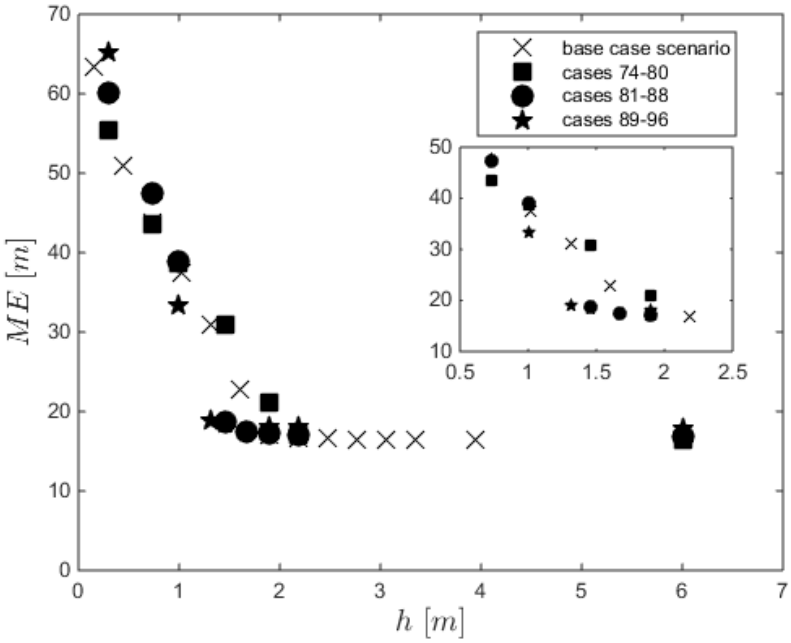
base case scenario
cases 74-80
cases 81-88
cases 89-96
ME [m]
h [m]

d

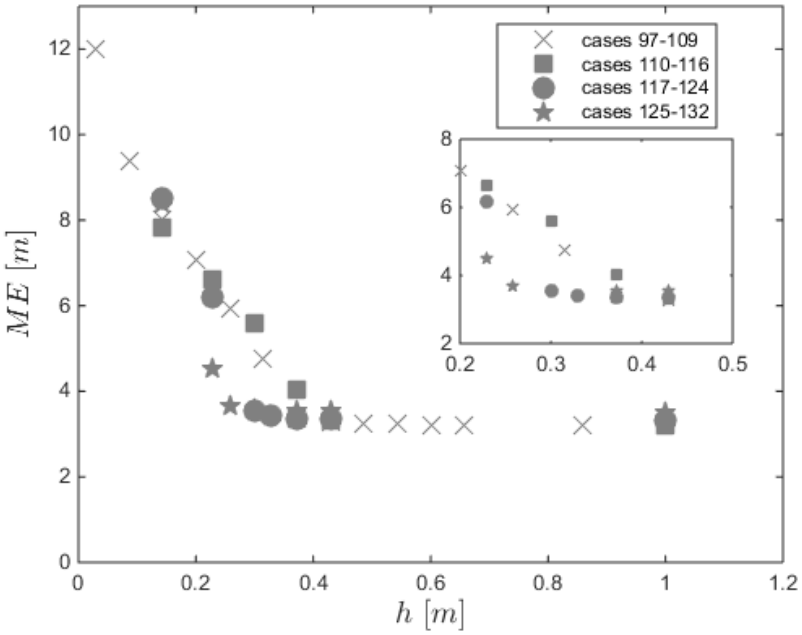

e

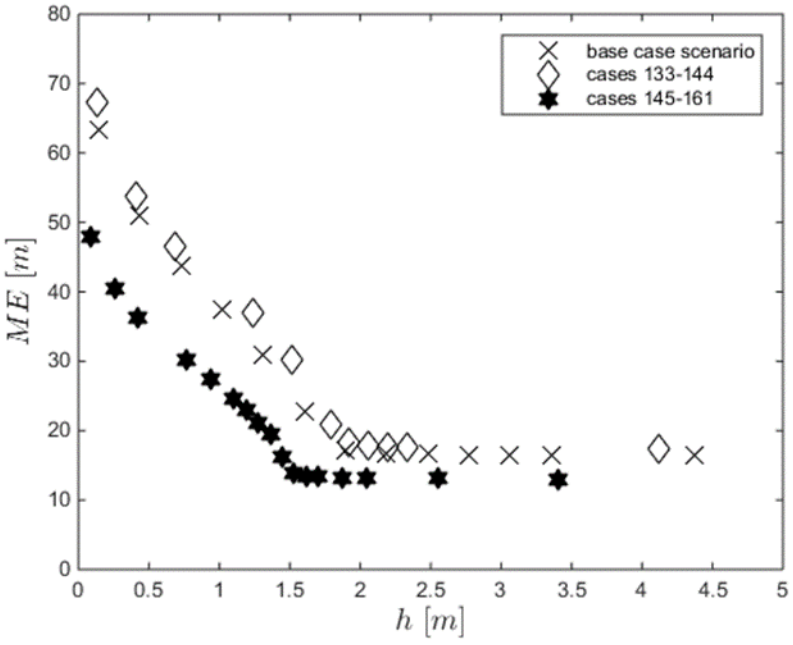

f

Figure 2.6: ME vs. h for the base case scenario compared to those of the sensitivity analysis on (a) storage pressure, (b) actual orifice diameter, (c) storage pressure together with actual orifice diameter, (d) open field wind conditions, (e) open field wind conditions for a lower storage pressure (i.e., 2.5 bara) and, (f) pseudo-source model.

*Figure 2.6*a-f clearly show a substantial variability among the collected results. However, when replotted on the dimensionless space of *Figure 2.5*, all the results collapse on the same two lines (i.e., the one due to the ground influence and the one of free jet behaviour) as shown in *Figure 2.7* that, for the purposes of comparison, also reports some data from Benard et al. (2016) (cases 162-252 in Table 2.5).

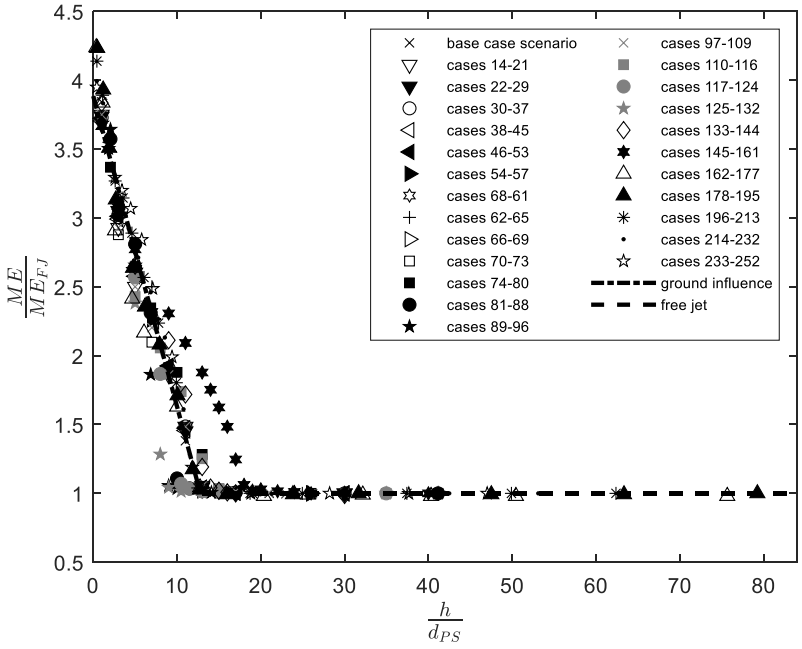

Figure 2.7: Dimensionless ME vs. dimensionless height of the source above ground for all the cases investigated in the sensitivity analysis.

From this Figure, we can see that almost all the results overlap well the analytical correlation that models the ground influence and match the threshold value that limits its influence. Only the results obtained using the pseudo-source model of Yuceil and Otugen (2002) are underestimated by the analytical correlation for the ground influence when h/d_{PS} approaches $(h/d_{PS})^*$. For values of $h/d_{PS} < 13$, the proposed correlation estimates the CFD results with a percentage error, defined as $\epsilon = \frac{\sum_{i=1}^{n}\left(\frac{|y_i - y|}{y_i}\right)}{n} \cdot 100$ (where y_i is the ratio between ME and ME_{FJ} computed for each run, y the ratio between ME and ME_{FJ} computed with Equation 2.2 and n = 252 is the number of runs), equal to 9 %. Due to the evident difference between the predictions provided by Birch et al. (1984) and Yuceil and Otugen (2002) EDMs, and thus to avoid a meaningless assessment, results computed with this last pseudo-source model are not included in the computation of the aforementioned percentage error. 60 % of CFD results are overestimated by the proposed correlation, thus leading to safe predictions for 60 % of the scenarios investigated.

ME FREEJET ESTIMATION

The wide range validity of both the criterion and correlation proposed was verified through an extensive sensitivity analysis. To achieve such a validity extent, the ME_{FJ} estimation is one of the key parameters needed. For each of the scenarios considered, the ME of the free jet was computed by means of CFD simulation. However, ME_{FJ} can be also evaluated in a simpler way, such as using the analytical correlation developed by Chen and Rodi (1980) with d_{PS} substituted for the actual orifice diameter, d:

$$\eta = \frac{k d_{PS}}{z + a}\left(\frac{\rho_a}{\rho_g}\right)^{\frac{1}{2}} \tag{2.3}$$

Where η is the mean axial mole fraction, d_{ps} is the pseudo-source diameter, a is the virtual orifice displacement, k is the axial decay constant, z is the downstream distance, and ρ_a and ρ_g are the air and methane density, respectively. *Figure 2.8* compares the mole fraction axial decay predicted using this analytical correlation and the CFD model.

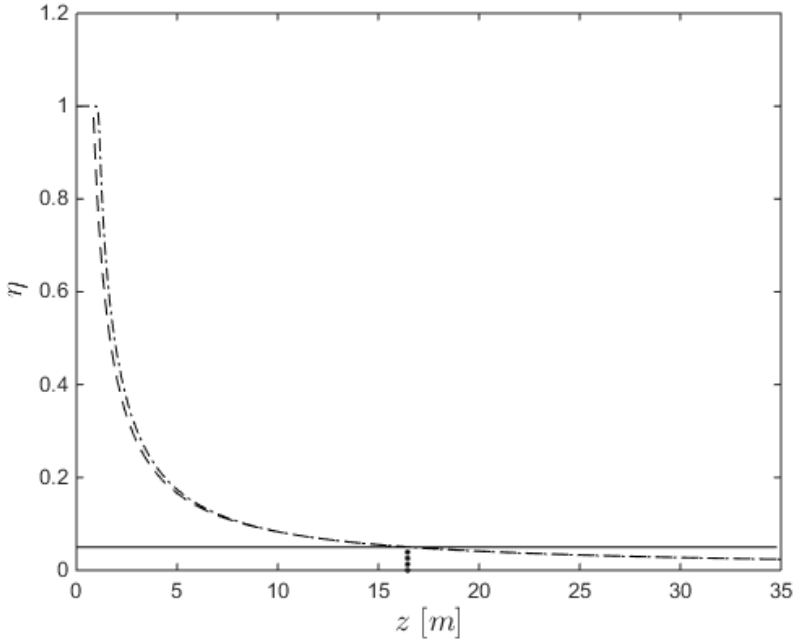

Figure 2.8: Comparison of the methane mole fraction axial decay computed with the CFD model (dashed-dotted line) and the Chen and Rodi (1980) analytical model (dashed line), for the base case scenario. The solid line represents the mole fraction equal to the LFL (0.05) and the dotted line the corresponding ME_{FJ} (16.45 m) computed using the CFD model.

We can see that the models show no remarkable differences; at the LFL, the ME_{FJ} predicted by the CFD model is equal to 16.45 m, while the one given by the analytical model (considering an axial decay constant value of 4.4) is 0.8 % shorter.

Using the values of ME_{FJ} computed with Eq. 2.3, the results summarised in *Figure 2.7* were plotted again in *Figure 2.9*. As shown in previous Section, different pseudo-source models predict different pseudo-source diameter values, and consequently different ME_{FJ} values are computed. Therefore, *Figure 2.9* includes the results having d_{PS} and ME_{FJ} values computed using the pseudo-source model of Birch et al. (1984). As expected, no significant differences compared to *Figure 2.7* are evident, therefore allowing the use of Eq. 2.3 for estimating the ME_{FJ} value.

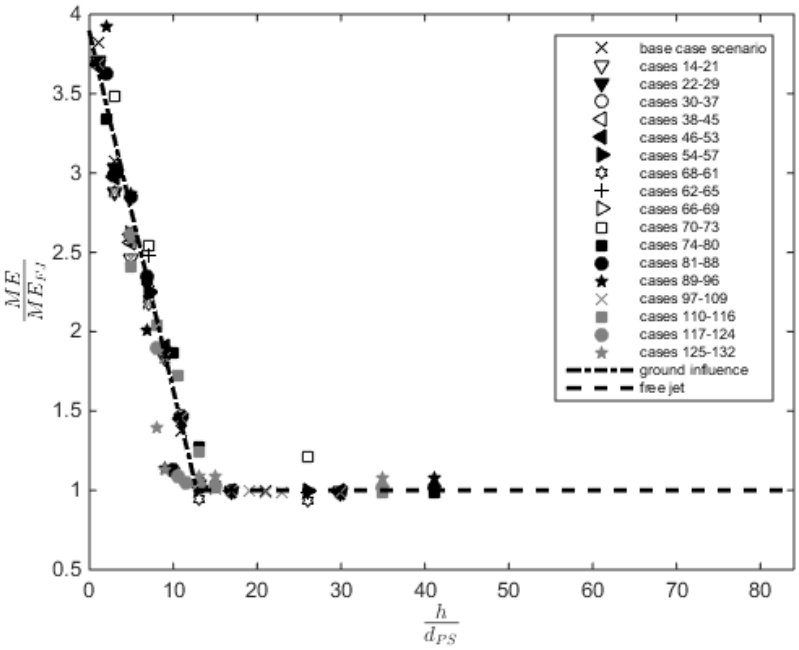

Figure 2.9: Dimensionless ME vs. dimensionless height of the source above ground for all the cases investigated in the sensitivity analysis.

However, we can see that results computed for cases 70-73 do not follow the predicted behaviour as do the other results. There are two reasons for this: i) in these cases the LFL free jet cloud is substantially larger than that of the others (see Figure 2.6c) and, ii) by Figure 2.8, for large distances from the jet source a high sensitivity of the ME_{FJ} on the model used is expected (the larger the distance from the jet source is, the closer the behaviour of the predicted mole fraction decay to the asymptotic value is).

CONCLUSIONS

As a matter of fact, the methane high-pressure gaseous release is a relevant safety-related problem mainly in the Oil and Gas (O&G) industry. In risk assessment, the damage area of the jet cloud (in particular, the hazardous distance reached by the LFL concentration value when the released compound is a flammable) is usually assumed as the hazardous distance to be estimated.

To estimate the maximum axially-oriented extent of the flammable cloud, the availability of reliable as well as simple, fast and easy-to-use tools for use in daily work is of primary importance. Focusing on the scenario of a high-pressure unignited methane jet outflowing from an accidental loss of containment close to the ground, the present work proposes a simple procedure that can be done by hand and enables safety analysts to estimate the hazardous distance.

The procedure can be summarised in the following steps:

1. From the accidental release characteristics, estimate the d_{PS} value using the Birch et al. (1984) model:

$$d_{PS} = d\sqrt{C_D\left(\frac{p}{p_{amb}}\right)\left(\frac{2}{\gamma+1}\right)^{\frac{(\gamma+1)}{2(\gamma-1)}}}$$

2. Estimate the ME_{FJ} value using the Chen and Rodi (1980) model:

$$ME_{FJ} = \frac{kd_{PS}}{LFL}\left(\frac{\rho_a}{\rho_g}\right)^{\frac{1}{2}}$$

3. If $h/d_{PS} > 13$, ME_{FJ} provides directly the order of magnitude of ME
4. If $h/d_{PS} < 13$, the order of magnitude of ME can be estimated as

$$ME = ME_{FJ}\left(3.89 - 0.22\frac{h}{d_{PS}}\right)$$

Finally, it should be stressed that this procedure is expected to provide a reasonable, and in most of the cases conservative, estimation as an order of magnitude of ME only inside the parameter window investigated (*i.e.*, for methane only, for upstream pressures between 2.5 and 700 bar, for upstream temperatures between 278 and 293 K, for orifice diameters between 0.0063 and 0.038 m, for methane concentration equal to 5.3 % (LFL) and for wind intensities between 1 and 20 m/s blowing parallelly the jet). The use of detailed CFD simulations should be always considered both

for confirming the estimated values, and for obtaining more reliable estimation in highly sensitive scenarios.

REFERENCES

Ansys DesignModeler User's Guide, 2017. Release 19.0. ANSYS, Inc.

Ansys Fluent User's Guide, 2017. Release 19.0. ANSYS, Inc.

Ansys Meshing User's Guide, 2017. Release 19.0. ANSYS, Inc.

Alves, J.J.N., Neto, A.T.P., Araújo, A.C.B., Silva, H.B., Silva, S.K., Nascimento, C.A., Luiz, A.M., 2019. Overview and Experimental Verification of Models to Classify Hazardous Areas. *Process Saf. Environ. Prot.* 122, 102–17. https://doi.org/10.1016/j.psep.2018.11.021.

Angers, B., Hourri, A., Benard, P., Tchouvelev, A., 2011. Numerical investigation of a vertical surface on the flammable extent of hydrogen and methane vertical jets. *Int. J. Hydrogen Energy* 36, 2567-72.

Baalisampang, T., Abbassi, R., Garaniya, V., Khan, F., Dadashzadeh, M., 2019. Accidental release of Liquefied Natural Gas in a processing facility: Effect of equipment congestion level on dispersion behaviour of the flammable vapour. *J. Loss Prev. Process Ind.* 61, 237–248. https://doi.org/10.1016/j.jlp.2019.07.001.

Bariha, N., Srivastava, V.C., Mishra, I.M., 2017. Theoretical and experimental stuDies on hazard analysis of LPG/LNG release: A review. *Rev. Chem. Eng.* 33, 387–432. https://doi.org/10.1515/revce-2016-0006.

Batt, R., Gant, S.E., Lacome, J.M., Truchot, B., 2016. Modelling of stably-stratified atmospheric boundary layers with commercial CFD software for use in risk assessment. *Chem. Eng. Trans.* 48, 61–66. https://doi.org/10.3303/CET1648011.

Bénard, P., Tchouvelev, A., Hourri, A., Chen, Z., Angers, B., 2007. High pressure hydrogen jets in the presence of a surface. *Int. Conf. Hydrog. Saf.* 40.

Bénard, P., Hourri, A., Angers, B., Tchouvelev, A., Agranat, V., 2009. Effects of surface on the flammable extent of hydrogen jets. *Int. Conf. Hydrog. Saf*.

Bénard, P., Hourri, A., Angers, B., Tchouvelev, A., 2016. Adjacent surface effect on the flammable cloud of hydrogen and methane jets: Numerical investigation and engineering correlations. *Int. J. Hydrogen Energy* 41, 18654–18662. https://doi.org/10.1016/j.ijhydene.2016.08.173.

Birch, A.D., Brown, D.R., Dodson, M.G., Swaffield, F., 1984. The structure and concentration decay of high pressure jets of natural gas. *Combust. Sci. Technol.* 36, 249–261. https://doi.org/10.1080/00102208408923739.

Cameron, I., Raman, R., 2005. Process System Risk Management, first ed. Elsevier Amsterdam.

Casal, J., Gómez-Mares, M., Muñoz, M., Palacios, A., 2012. Jet fires: A 'minor' fire hazard? *Chem. Eng. Trans.* 26, 13–20. https://doi.org/10.3303/CET1226003.

Chen, C.J., Rodi, W., 1980. Vertical Turbulent Buoyant Jets – A review of Experimental Data, First ed. Pergamon Press Vol. 4.

Colombini, C., Busini, V., 2019a. Obstacle Influence on High-Pressure Jets based on Computational Fluid Dynamics Simulations. *Chem. Eng. Trans.* 77, 811–816. https://doi.org/10.3303/CET1977136.

Colombini, C., Busini, V., 2019b. High-Pressure Methane Jet: Analysis of the Jet-Obstcle Interaction. *Proceeding of the 29th European Safety and Reliability Conference.*

Crist, S., Sherman, P.M., Glass, D.R., 1966. Study of the highly underexpanded sonic jet. *AIAA J.* 4, 68–71. https://doi.org/10.2514/3.3386.

Dasgotra, A., Varun Teja, G. V.V., Sharma, A., Mishra, K.B., 2018. CFD modeling of large-scale flammable cloud dispersion using FLACS. *J. Loss Prev. Process Ind.* 56, 531–536. https://doi.org/10.1016/j.jlp.2018.01.001.

Deng, Y., Hu, H., Yu, B., Sun, D., Hou, L., Liang, Y., 2018. A method for simulating the release of natural gas from the rupture of high-pressure pipelines in any terrain. *J. Hazard. Mater.* 342, 418–428. https://doi.org/10.1016/j.jhazmat.2017.08.053.

Derudi, M., Bovolenta, D., Busini, V., Rota, R., 2014. Heavy gas dispersion in presence of large obstacles: Selection of modeling tools. *Ind. Eng. Chem. Res.* 53, 9303–9310. https://doi.org/10.1021/ie4034895.

Desilets, S., Cote, S., Nadau, G., Benard, P., Tchouvelev, A., 2009. Experimental results and comparison with simulated data of a low pressure hydrogen jet. *Int. Conf. Hydrog. Saf*.

Dey, S., Kishore, G.R., Castro-Orgaz, O., Ali, S.Z., 2017. Hydrodynamics of submerged turbulent plane offset jets. *Phys. Fluids* 29. https://doi.org/10.1063/1.4989559.

DNV, *PHAST - Process Hazard Analysis Software Tool,* DNV Software, last access: 27/03/2020. https://www.dnvgl.com/services/process-hazard-analysis-software-phast-1675

Efthimiou, G.C., Andronopoulos, S., Tavares, R., Bartzis, J.G., 2017. CFD-RANS prediction of the dispersion of a hazardous airborne material released during a real accident in an industrial environment. *J. Loss Prev. Process Ind.* 46, 23–36. https://doi.org/10.1016/j.jlp.2017.01.015.

Ewan, B.C., Moodie, K., 1986. Combustion Science and Technology Structure and Velocity Measurements in Underexpanded Jets Structure and Velocity Measurements in Undenexpanded Jets. *Combust. Sci. Tech* 4586, 275–288. https://doi.org/10.1080/00102208608923857.

Franquet, E., Perrier, V., Gibout, S., Bruel, P., 2015. Free underexpanded jets in a quiescent medium: A review. *Prog. Aerosp. Sci.* 77, 25–53. https://doi.org/10.1016/j.paerosci.2015.06.006.

Gerbec, M., Pontiggia, M., Antonioni, G., Tugnoli, a., Cozzani, V., Sbaouni, M., Lelong, R., 2017. Comparison of UDM and CFD simulations of a time varying release of LPG in geometrical complex environment. *J. Loss Prev. Process Ind.* 45, 56–68. https://doi.org/10.1016/j.jlp.2016.11.020.

Hall, J.E., Hooker, P., O'Sullivan, L., Angers, B., Hourri, A., Benard, P., 2017. Flammability profiles associated with high-pressure hydrogen jets released in close proximity to surfaces. *Int. J. Hydrogen Energy* 42, 7413–7421. https://doi.org/10.1016/j.ijhydene.2016.05.113.

Hendrickson, B., Marsegan, C., Gavelli, F., 2016. Where to begin – A parametric study for vapor barriers at LNG export facilities. *J. Loss Prev. Process Ind.* 44, 573–582. https://doi.org/10.1016/j.jlp.2016.07.031.

Houf, W., Schefer, R., Evans, G., Merilo, E., Groethe, M., 2010. Evaluation of barrier walls for mitigation of unintended releases of hydrogen. *Int. J. Hydrogen Energy* 35, 4758–4775. https://doi.org/10.1016/j.ijhydene.2010.02.086.

Hourri, A., Angers, B., Bénard, P., 2009. Surface effects on flammable extent of hydrogen and methane jets. *Int. J. Hydrogen Energy* 34, 1569–1577. https://doi.org/10.1016/j.ijhydene.2008.11.088.

Hourri, A., Angers, B., Bénard, P., Tchouvelev, A., Agranat, V., 2011. Numerical investigation of the flammable extent of semi-confined hydrogen and methane jets. *Int. J. Hydrogen Energy* 36, 2567–2572. https://doi.org/10.1016/j.ijhydene.2010.04.121.

Jiang, Y., Xu, Z., Wei, J., Teng, G., 2020. Fused CFD-interpolation model for real-time prediction of hazardous gas dispersion in emergency rescue. *J. Loss Prev. Process Ind.* 63, 103988. https://doi.org/10.1016/j.jlp.2019.103988.

Kim, S., Lee, H.J., Park, J.H., Jeung, I.S., 2013. Effects of a wall on the self-ignition patterns and flame propagation of high-pressure hydrogen release through a tube. *Proc. Combust. Inst.* 34, 2049–2056. https://doi.org/10.1016/j.proci.2012.09.001.

Kong, X.X., Wang, X.S., Cong, H.Y., Liu, Y.P., Zhu, J.P., 2019. Temperature profile and flame extension length of a ceiling impinging round jet fire in an inclined tunnel. *Int. J. Therm. Sci.* 137, 526–533. https://doi.org/10.1016/j.ijthermalsci.2018.12.023.

Kotchourko, A., Baraldi, D., Bénard, P., Eisenreich, N., Jordan, T., Keller, J., Kessler, A., LaChance, J., Molkov, V., Steen, M., Tchouvelev, A., 2014. State of the Art and Research Priorities in Hydrogen Safety. Joint Research Centre of the European Commission (JRC), Honolulu, Hawaii.

Liao, N., Huang, K., Chen, L., Wang, Z, Wu, J., Zhang, F., 2018. Numerical simulation of gas dispersion during cold venting of natural gas pipelines. *Adv. Mech. Eng.* 10, 1–14. https://doi.org/10.1177/1687814018755244.

Lim, J.W., Baalisampang, T., Garaniya, V., Abbassi, R., Khan, F., Ji, J., 2019. Numerical analysis of performances of passive fire protections in processing facilities. *J. Loss Prev. Process Ind.* 62, 103970. https://doi.org/10.1016/j.jlp.2019.103970.

Luo, T., Yu, C., Liu, R., Li, M., Zhang, J., Qu, S., 2018. Numerical simulation of LNG release and dispersion using a multiphase CFD model. *J. Loss Prev. Process Ind.* 56, 316–327. https://doi.org/10.1016/j.jlp.2018.08.001.

Menter, F.R., 1993. Zonal Two Equation kω Turbulence Models for Aerodynamic Flows. *24th Fluid Dynamics Conference*.

Middha, P., Hansen, O.R., Grune, J., Kotchourko, A., 2010. CFD calculations of gas leak dispersion and subsequent gas explosions: Validation against ignited impinging hydrogen jet experiments. *J. Hazard. Mater.* 179, 84–94. https://doi.org/10.1016/j.jhazmat.2010.02.061.

Miozzi, M., Lalli, F., Romano, G.P., 2010. Experimental investigation of a free-surface turbulent jet with Coanda effect. *Exp. Fluids* 49, 341–353. https://doi.org/10.1007/s00348-010-0885-1.

Pontiggia, M., Derudi, M., Busini, V., Rota, R., 2009. Hazardous gas dispersion: A CFD model accounting for atmospheric stability classes. *J. Hazard. Mater.* 171, 739–747. https://doi.org/10.3303/CET1436088.

Pontiggia, M., Busini, V., Ronzoni, M., Uguccioni, G., Rota, R., 2014. Effect of large obstacles on high momentum jets dispersion. *Chem. Eng. Trans.* 36, 523–528. https://doi.org/10.1016/j.jhazmat.2009.06.064.

Pu, L., Tang, X., Shao, X., Lei, G., Li, Y., 2019. Numerical investigation on the difference of dispersion behavior between cryogenic liquid hydrogen and methane, *Int. J. Hydrogen Energy* 44, 22368-22379.

Schleder, A.M., Pastor, E., Planas, E., Martins, M.R., 2015. Experimental data and CFD performance for cloud dispersion analysis: The USP-UPC project. *J. Loss Prev. Process Ind.* 38, 125-138.

Souza, A. O. *et al.* A new correlation for hazardous area classification based on experiments and CFD predictions. *Process Saf. Prog.* 38, 21–26 (2019). https://doi.org/10.1002/prs.11974.

Stewart, J.R., 2019. CFD modelling of underexpanded hydrogen jets exiting rectangular shaped openings. *Inst. Chem. Eng. Symp. Ser.* 2019-May.

Tchouvelev, A.V., Cheng, Z., Agranat, V.M., Zhubrin, S.V., 2007. Effectiveness of small barriers as means to reduce clearance distances. *Int. J. Hydrogen Energy* 32, 1409–1415. https://doi.org/10.1016/j.ijhydene.2006.10.020.

Tolias, I. C., Giannissi, S.G., Venetsanos, A.G., Keenan, J., Shentsov, V., Makarov, D., Coldrick, S., Kotchourko, A., Ren, K., Jedicke, O., Melideo, D., Baraldi, D., Slater, S., Duclos, A., Verbecke, F., Molkov, V., 2019. Best practice guidelines in numerical simulations and CFD benchmarking for hydrogen safety applications. *Int. J. Hydrogen Energy* 44, 9050–9062. https://doi.org/10.1016/j.ijhydene.2018.06.005.

Uggenti, A.C., Carpignano, A., Savoldi, L., Zanino, R., 2017. Perspective and criticalities of CFD modelling for the analysis of oil and gas offshore accident scenarios. *Risk, Reliability and Safety: Innovating Theory and Practice: Proceedings of ESREL 2016.*

Xu, B.P., Wen, J.X., Tam, V.H.Y., 2011. The effect of an obstacle plate on the spontaneous ignition in pressurized

hydrogen release: A numerical study. *Int. J. Hydrogen Energy* 36, 2637–2644. https://doi.org/10.1016/j.ijhydene.2010.03.143.

Yang, R., Khan, F., Taleb-Berrouane, M., Kong, D., 2020. A time-dependent probabilistic model for fire accident analysis. *Fire Saf. J.* 111, 102891. https://doi.org/10.1016/j.firesaf.2019.102891.

Yüceil, K.B., Ötügen, M.V., 2002. Scaling parameters for underexpanded supersonic jets. *Phys. Fluids* 14, 4206–4215. https://doi.org/10.1063/1.1513796.

Zhou, K., Wang, X., Liu, M., Liu, J., 2018. A theoretical framework for calculating full-scale jet fires induced by high-pressure hydrogen/natural gas transient leakage. *Int. J. Hydrogen Energy* 43, 22765–22775. https://doi.org/10.1016/j.ijhydene.2018.10.122.

CHAPTER 2.2: GROUND INTERACTION ON HIGH-PRESSURE JETS: EFFECT ON DIFFERENT SUBSTANCES

CHEMICAL ENGINEERING TRANSACTIONS
VOL. 82, 2020
A publication of AIDIC
The Italian Association of Chemical Engineering
Online at www.cetjournal.it
Guest Editors: Bruno Fabiano, Valerio Cozzani, Genserik Reniers

ISBN 978-88-95608-80-8; **ISSN** 2283-9216
DOI: 10.3303/CET2082062

Ground Interaction on High-Pressure Jets: Effect on Different Substances

Cristian Colombini[a,b], Luca Carlini[a], Renato Rota[a], Valentina Busini[a,*]

[a] Politecnico di Milano - Department of Chemistry, Materials and Chemical Engineering "Giulio Natta", Via Mancinelli 7, 20131, Milano, Italy
[b] Presently at RINA Consulting S.p.A. – EOGRS Group, Via Cecchi 6, 16129, Genova, Italy
valentina.busini@polimi.it

ABSTRACT

Due to the severity of their consequences, accidental high-pressure flammable gas releases are relevant hazards in the process safety. In the recent decades, several are the efforts spent on the study of high-pressure jets in open field (i.e., free jets). In particular, easy-to-use mathematical models have been developed. These, by hand calculations, allow to quickly assess various physical variables that are of paramount importance in safety evaluations.

However, it is easily as possible that, in a realistic accidental scenario, the unwanted leak may involve either the ground or an equipment placed in its vicinity. As demonstrated by recent works, when a jet interacts with an obstacle, its behavior can significantly change. Hence, in the safety assessment of this situation, the mathematical models derived for the free jet scenario can lead to incorrect predictions. Focusing on the scenario of an accidental high-pressure unignited flammable jet, this work shows how the proximity to the ground can influence the lower flammability limit cloud extent of different substances. Varying the height above the ground of the source term, the effect of the ground was systematically studied through a Computational Fluid Dynamics analysis considering high-pressure unignited methane, propane and hydrogen jets. The main achievement is the demonstration that releases of compounds with similar or larger molecular weight than that of air are similarly affected by the ground while, releases of compounds lighter than air interact with the ground in a sensibly different way.

ACRONYMS

CFD Computational Fluid Dynamics

EDM Equivalent Diameter Model

LFL Lower Flammability Limit

ME Maximum Extent

RANS Reynolds Averaged Navier-Stokes

UDF User Defined Function

NOMENCLATURE

d: actual orifice diameter

d_{PS}: pseudo-source orifice diameter

h: height of the source above ground

h*: critical height of the source above ground

LFL: compound concentration equal to LFL

$\dot{m}$: mass flow rate

ME: LFL cloud maximum extent in direction of the jet axis

ME_{FJ}: free jet LFL cloud maximum extent in direction of the jet axis

p: storage pressure

T: storage temperature

T_{TOT}: release total temperature at pseudo-source conditions

INTRODUCTION

the safety implications to be considered, accidental high-pressure releases are relevant hazards in the process safety (Liao et al., 2018). In the case that a flammable substance is involved, if immediate or delayed ignition occurs, the consequences can be relevant: as reported by Casal et al. (2012), a jet or flash fire (whose hazardous distance can be roughly estimated as the maximum distance reached by Lower Flammability Limit (LFL) concentration value) can be intended as a major accident initiator.

Among the works available in literature focusing on such a critical scenario, in the recent decades several have been the efforts spent on the study of high-pressure releases as free jets (intended as a release occurring in an unconfined environment). Thanks to these works, as reported by Franquet et al. (2015), nowadays the overall structure of a high-pressure jet is very well known. In particular, a result of such a deep gathered comprehension has been the development of easy-to-use mathematical models that, by hand calculations, allow the quick estimation of various important physical variables characterizing the free jet. Therefore, for this kind of process safety issue, the risk analysis can be performed exploiting practical tools.

However, it is easily as possible that, in a more realistic situation (with respect to the free jet one), the accidental leak may involve either the ground or an equipment placed in its vicinity. It is in this more lifelike problem that, troubles using the aforementioned tools start to rise: as will be shown in this work (and in accordance with the literature (Colombini and Busini, 2019), when a jet interacts with an obstacle, its behavior significantly changes. Hence, to describe this accidental scenario, the useful mathematical models derived for the free jet situation fail, leading to incorrect predictions (Pontiggia et al., 2014).

Therefore, to properly simulate this kind of accidental scenario, only a Computational Fluid Dynamics (CFD) analysis can be feasible and reliable. This because CFD models are the only numerical tool able to account for the influence of obstacles or, more in general, of a complex geometry on the jet release (Batt et al., 2016). However, shortcomings are present: the computational demand and the required user knowledge limit the CFD use in the daily risk assessment and consequences analysis activities (Zuliani et al., 2016).

The ground can be counted among the industrial obstacles. The main reason is that its effect on the jet development is the increase of the damage area involved (Hall et al., 2017). With regards to this accidental scenario, in the past some works have been carried out. In particular, flat surface influence, which can be either horizontally or vertically oriented, has been analyzed varying some

scenario parameters (such as source-surface distance, upstream pressure, orifice diameter) both numerically (Benard et al., 2007; Hourri et al., 2009; Angers et al., 2011; Benard et al., 2016) and experimentally (Desilets et al., 2009; Hall et al., 2017).

However, none of these literature works investigated what happens if different substances are involved.

In the present analysis, the ground influence was investigated in terms of how the flammable area extent of a high-pressure jet is enlarged (in terms of Maximum axially-oriented Extent (ME) of the LFL cloud) varying the height of the source above the ground.

In particular, the aim was to compare how three widely used flammable substances (namely methane, propane and hydrogen) behave when their release is modified by the ground presence. All the three were considered at their typical handling conditions. For methane and propane, the numerical outcomes were computed by using the developed CFD model, while, for the hydrogen case, data were taken from the work of Benard et al. (2016).

As stated, the aim is to compare how the ground affects high-pressure jets of three different substances.

However, perform such a comparison highlighting only the effect of considering different substances is not as immediate as it seems. In fact, other aspects change when changing the substance:

- considering the correspondent LFL value means different observed concentrations
- considering typical handling conditions means different source pressures

Therefore, to fruitfully show which is the dependency of the ME upon only the substance change, it was needed to define a proper space that allowed to offset both the different concentrations observed, and the different source pressures considered.

MATERIAL AND METHODS

For all the three fluids considered in the present analysis, an upstream pressure greater than the critical threshold to achieve chocked conditions is noticed (Cameron and Raman, 2005). In this case, supercritical releases are expected to occur. By the numerical point of view, this implies a computationally expensive problem to face. The reason lies in the need of simulating complex phenomena such as shock waves formation and Mach disk establishment downstream to the jet orifice (Franquet et al., 2015). Since in the present work the far field zone of the jet is of primary interest, a way to overcome the aforementioned phenomena simulation is to model them exploiting well established analytical correlations (Tolias et al., 2019). Named as Equivalent Diameter Models (EDM), among the various approaches to model the jet source term available in literature, the widely adopted model of Birch et al. (1984) was chosen.

Given the outdoor location of the accidental scenario investigated, particular attention was paid to model realistic wind conditions. To consider the atmospheric conditions of an open field scenario, a velocity profile in accordance with the atmospheric class 5D of the Pasquill's categories was supplied to the solver through a User Defined Function (UDF) (Pontiggia et al., 2014).

To perform the CFD analysis, Ansys Workbench (release 19.1) was used and, Fluent was deployed to numerically solve the flow governing equations.

By the numerical resolution point of view, to obtain a good quality representation of the flow field as well as a time-saving tool, the Reynolds's Average of the governing equations (i.e, the RANS approach) was used. To avoid the need of resolve the boundary layer of the ground, among the possible turbulence models available, the k-ω SST was chosen.

RESULTS AND DISCUSSION

Guessing a spill from a storage tank (or a pipeline), for all the three substances released, the leakage was considered to be constant in time (i.e., steady state condition). Details of the actual source term (namely, stagnation pressure (p), temperature (T) and actual orifice diameter (d)) together with the correspondent equivalent conditions computed with the Birch et al. (1984) EDM (namely, mass flow rate ($\dot{m}$), total temperature (T_{TOT}) and equivalent source diameter (d_{PS})) are reported in Table 3.1. The ground was modeled as an adiabatic wall surface, with a roughness height equal to 0.01 m, simulating a concrete forecourt. While, as described in previous Section, the wind inlet and the lateral and top boundaries were set according to the aim of providing realistic wind conditions. An environmental temperature equal to 300 K was considered. For the simulations carried out in the present work, Table 3.2 reports how the boundary conditions were set.

Computational domain dimensions were properly sized in order to avoid any interference with the boundaries but, at the same time, avoiding a useless waste of computational resources. To this aim, the work of Hourri et al. (2009) was taken as reference. A rectangular box of 90x10x10 m was built for each of the simulations performed. Notice that, a vertical planar symmetry in correspondence of the jet axis was used. For what concerns the fluid volume discretization, a full unstructured tetrahedral grid was made. Ranging between 7.3 and 7.8 million of elements, the prescribed quality criteria were always fulfilled. Moreover, also the grid independence of the results was positively achieved.

Table 3.1: Actual and equivalent source term characteristics for the methane and the propane releases.

Characteristic	Methane (Colombini et al., 2020)	Propane (this work)	Hydrogen (Benard et al., 2016)
p [bar]	65	8	101
T [K]	278	278	293
d [m]	0.0254	0.0254	0.00635
$\dot{m}$ [kg/s]	5.18	0.9548	0.1987
T_{TOT} [K]	343	318	Not reported
d_{PS} [m]	0.1458	0.0518	Not reported

Table 3.2: Boundary conditions used in all the simulation.

Boundary	Type
Ground	Wall
Jet inlet	Mass flow inlet
Symmetry	Symmetry
Lateral boundary	Velocity inlet
Top boundary	Velocity inlet
Wind inlet	Velocity inlet
Wind outlet	Pressure outlet
Nozzle	Wall

To investigate the influence that the ground has on the jet behavior, the height of the source above the ground (h) was systematically varied. Figure 3.1 shows, qualitatively, the effect that this parameter variation has on the jet development of both methane and propane releases. Same figure can be found in the work of Benard et al. (2016) about the hydrogen one. While, quantitatively, *Figure 3.2* shows how the ME of each of the LFL clouds varies as a function of h.

For all the three compounds, it is noticeable that: i) there is an h threshold value (h*) after that the ground does not influence anymore the jets; such value changes based on the considered compound. ii) When h<h*, the ground influence increase ME. These results are in accordance with the physics that characterizes the jet development (i.e., the Coanda effect (Miozzi et al., 2010)).

Then, to effectively show which is the dependency of the ME upon only the substance change, it was needed to define a proper space that allowed to offset both the different LFL concentrations observed, and the different source pressures considered. To offset the stagnation pressure effect, for each data set, the y axis was normalized by dividing for the correspondent ME of the free jet (ME_{FJ}), while, the x axis was divided by the correspondent equivalent source diameter (d_{PS}); this normalization works because both the ME_{FJ} and the d_{PS} depend on the pressure (Colombini et al., 2020). To offset the effect of the observed concentration level, only the x axis required a further manipulation since both ME and ME_{FJ} already depend on the concentration considered. In particular, the ratio LFL/LFL_{REF}, where LFL is the concentration value observed for each substance considered while LFL_{REF} a reference concentration arbitrarily chosen (preferably among the ones considered; in this case, the methane LFL), was used to perform the scaling. In *Figure 3.3*, the layout

of the results appears to be very similar to the one seen in the dimensional space (*Figure 3.2*). From this plot, it is possible to remark that different substances are differently influenced by the ground.

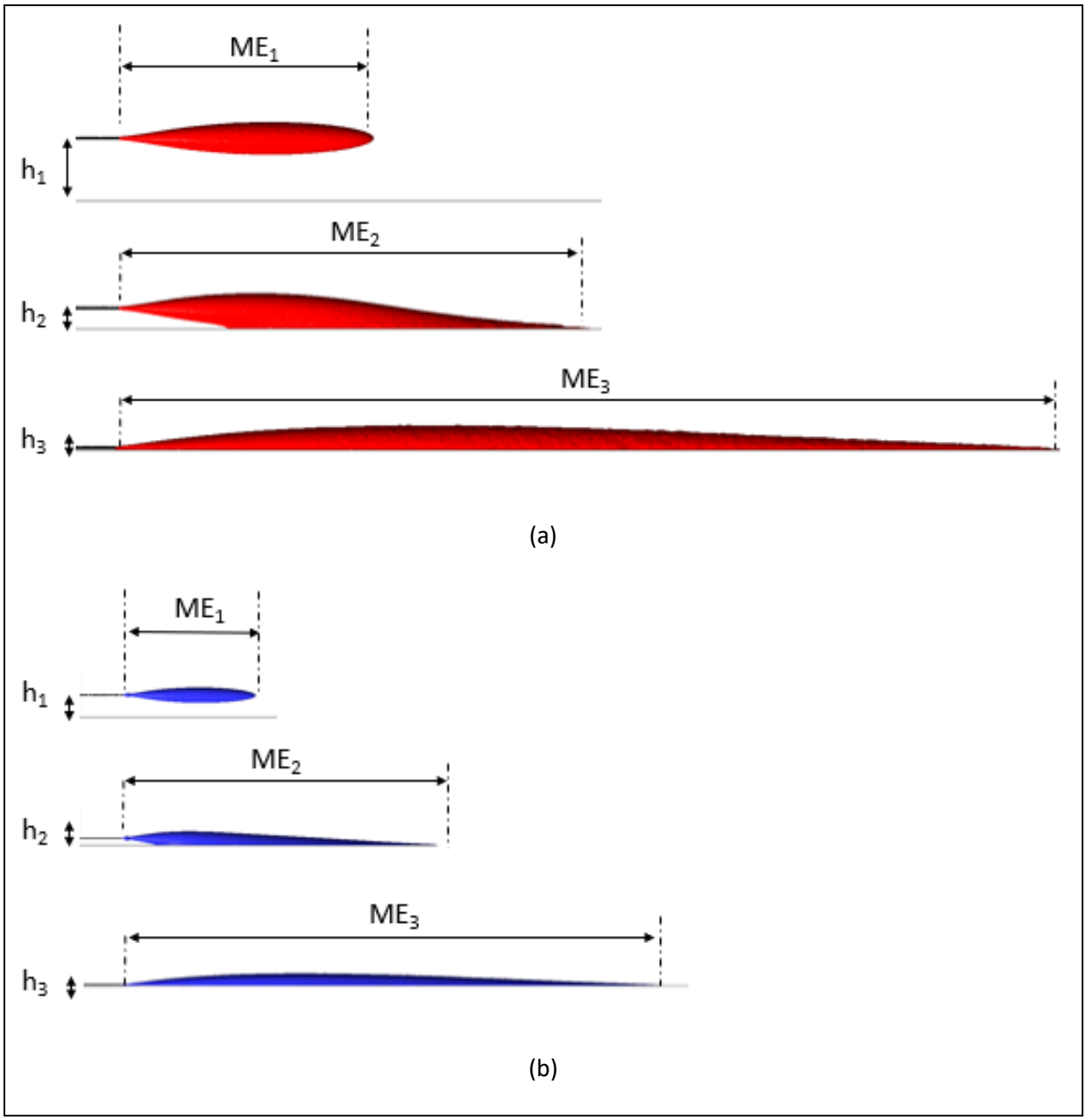

Figure 3.1: Effect of the h variation on the (a) methane and (b) propane LFL clouds.

However, when considering substances heavier than, or similar to, air (it is the case for propane and methane) the behavior of the jet (and thus the ground influence) appears to be way less different than that of considering a much lighter one (*i.e.*, hydrogen). In particular, the heavier the gas is, the steeper the curve is. This leads to remark that the ground affects much more high momentum releases of heavy compounds. The reason can be explained by the different buoyancy effect: hydrogen jets driving up, while methane and propane jets stay parallel to the ground (and thus resulting much more affected by it). Meaning that the high momentum of the flow prevails on the

buoyancy effects, this also justifies why methane and propane ME increases up to 4 times with respect to ME_{FJ} while hydrogen ME of only 1.5.

Contrarily to what seen for the ground influence, Figure 3.3 shows that the dimensionless h* value, about 13, is practically shared by all three compounds.

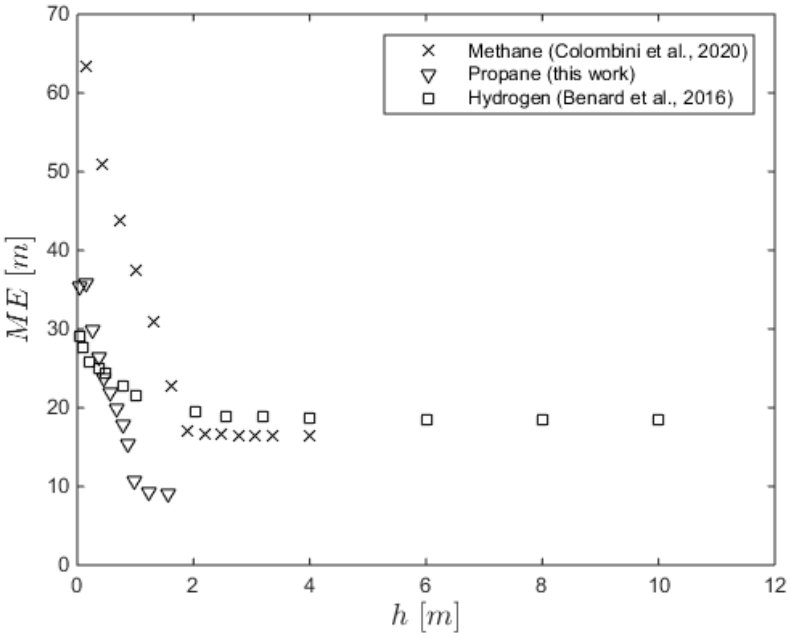

Figure 3.2: ME over h for the three considered substances, where $LFL_{Methane}$ = 5, $LFL_{Propane}$ = 2.1, $LFL_{Hydrogen}$ = 4 expressed in % of vol_{SUB}/vol_{AIR}.

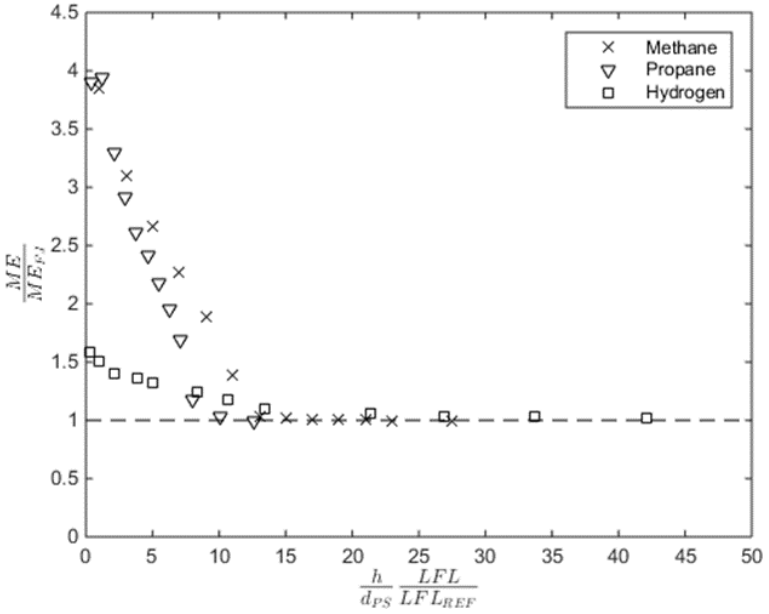

Figure 3.3: Dimensionless space defined to offset both different stagnation pressures and different concentrations.

CONCLUSIONS

In this work, the scenario of a high-pressure jet parallel to the ground, and interacting with it, was investigated. Varying the height of the source above the ground, the influence that such kind of obstacle has on the jet was analysed for three widely used process substances, namely methane, propane and hydrogen.

With regards to the preliminary results shown, it is possible to conclude that:

- the dimensionless space defined appears to be adequate to provide a direct comparison among results obtained when considering different storage conditions as well as different concentrations observed;
- both qualitatively and quantitatively, the ground influence appears to be similar when considering high-pressure jets of compounds heavier than, or similar to, air;
- both qualitatively and quantitatively, the ground influence appears to be different when considering a released compound much lighter than air;
- by order of magnitude, the dimensionless height that defines when the ground effect starts, it appears to be comparable for all the three compounds.

Broadly speaking, the ground effect is to increase the damage area. The results of the present analysis indicate that for compounds heavier than, or similar to, air a larger increase of the hazardous distance should be expected with respect to the case of considering lighter compounds

REFERENCES

Angers, B., Hourri, A., Benard, P., Tchouvelev, A., 2011. Numerical investigation of a vertical surface on the flammable extent of hydrogen and methane vertical jets. *Int. J. Hydrogen Energy* 36, 2567-72.

Batt, R., Gant, S.E., Lacome, J.M., Truchot, B., 2016. Modelling of stably-stratified atmospheric boundary layers with commercial CFD software for use in risk assessment. *Chem. Eng. Trans.* 48, 61–66. https://doi.org/10.3303/CET1648011.

Bénard, P., Tchouvelev, A., Hourri, A., Chen, Z., Angers, B., 2007. High pressure hydrogen jets in the presence of a surface. *Int. Conf. Hydrog. Saf.* 40.

Bénard, P., Hourri, A., Angers, B., Tchouvelev, A., 2016. Adjacent surface effect on the flammable cloud of hydrogen and methane jets: Numerical investigation and engineering correlations. *Int. J. Hydrogen Energy* 41, 18654–18662. https://doi.org/10.1016/j.ijhydene.2016.08.173.

Birch, A.D., Brown, D.R., Dodson, M.G., Swaffield, F., 1984. The structure and concentration decay of high pressure jets of natural gas. *Combust. Sci. Technol.* 36, 249–261. https://doi.org/10.1080/00102208408923739

Cameron, I., Raman, R., 2005. Process System Risk Management, first ed. Elsevier Amsterdam., The Netherlands.

Casal, J., Gómez-Mares, M., Muñoz, M., Palacios, A., 2012. Jet fires: A 'minor' fire hazard? *Chem. Eng. Trans.* 26, 13–20. https://doi.org/10.3303/CET1226003.

Colombini, C., Busini, V., 2019a. Obstacle Influence on High-Pressure Jets based on Computational Fluid Dynamics Simulations. *Chem. Eng. Trans.* 77, 811–816. https://doi.org/10.3303/CET1977136.

Colombini, C., Martani, A., Rota, R., Busini, V., 2020. Ground influence on high-pressure methane jets: Practical tools for risk assessment. *J. Loss Prevent. Proc.* 67, 104240. https://doi.org/10.1016/j.jlp.2020.104240

Desilets, S., Cote, S., Nadau, G., Benard, P., Tchouvelev, A., 2009. Experimental results and comparison with simulated data of a low pressure hydrogen jet. *Int. Conf. Hydrog. Saf*.

Franquet, E., Perrier, V., Gibout, S., Bruel, P., 2015. Free underexpanded jets in a quiescent medium: A review. *Prog. Aerosp. Sci.* 77, 25–53. https://doi.org/10.1016/j.paerosci.2015.06.006.

Hall, J.E., Hooker, P., O'Sullivan, L., Angers, B., Hourri, A., Benard, P., 2017. Flammability profiles associated with high-pressure hydrogen jets released in close proximity to surfaces. *Int. J. Hydrogen Energy* 42, 7413–7421. https://doi.org/10.1016/j.ijhydene.2016.05.113.

Hourri, A., Angers, B., Bénard, P., 2009. Surface effects on flammable extent of hydrogen and methane jets. *Int. J. Hydrogen Energy* 34, 1569–1577. https://doi.org/10.1016/j.ijhydene.2008.11.088.

Liao, N., Huang, K., Chen, L., Wang, Z, Wu, J., Zhang, F., 2018. Numerical simulation of gas dispersion during cold venting of natural gas pipelines. Adv. Mech. Eng. 10, 1–14. https://doi.org/10.1177/1687814018755244

Miozzi, M., Lalli, F., Romano, G.P., 2010. Experimental investigation of a free-surface turbulent jet with Coanda effect. *Exp. Fluids* 49, 341–353. https://doi.org/10.1007/s00348-010-0885-1.

Pontiggia, M., Busini, V., Ronzoni, M., Uguccioni, G., Rota, R., 2014. Effect of large obstacles on high momentum jets dispersion. *Chem. Eng. Trans.* 36, 523–528. https://doi.org/10.1016/j.jhazmat.2009.06.064.

Tolias, I. C., Giannissi, S.G., Venetsanos, A.G., Keenan, J., Shentsov, V., Makarov, D., Coldrick, S., Kotchourko, A., Ren, K., Jedicke, O., Melideo, D., Baraldi, D., Slater, S., Duclos, A., Verbecke, F., Molkov, V., 2019. Best practice guidelines in numerical simulations and CFD benchmarking for hydrogen safety applications. *Int. J. Hydrogen Energy* 44, 9050–9062. https://doi.org/10.1016/j.ijhydene.2018.06.005.

CHAPTER 3: UNIGNITED HIGH-PRESSURE METHANE JET IMPINGING A PIPE RACK: PRACTICAL TOOLS FOR RISK ASSESSMENT

Journal of Loss Prevention in the Process Industries 69 (2021) 104378

Contents lists available at ScienceDirect

Journal of Loss Prevention in the Process Industries

journal homepage: http://www.elsevier.com/locate/jlp

Unignited High-Pressure Methane Jet Impinging a Pipe Rack: Practical Tools for Risk Assessment

Cristian Colombini, Giuliana Maugeri, Gianluca Zanon, Renato Rota, Valentina Busini *

Politecnico di Milano - Department of Chemistry, Materials and Chemical Engineering "Giulio Natta", Piazza Leonardo da Vinci 32, 20133, Milano, Italy

ABSTRACT

Although the diffusion of its storage and transport under liquefied conditions, nowadays it is common to have methane in gaseous form in several industrial applications. This leads to safety implications to be considered: hazards are linked to both the high-pressure at which the gas is kept and to its flammability. Scenarios where flammable jets impact an obstacle are of paramount importance because of their possible occurrence. Following a numerical approach, literature shows up that their assessment can be reliably performed by means of only Computational Fluid Dynamics tools. However, despite the improvements of computing power, Computational Fluid Dynamics costs still limit its use in daily risk analysts' activities. Therefore, considering an accidental jet-obstacle scenario of industrial interest, the present work investigates how a pipe rack can influence the development of a high-pressure methane jet. Based on a Computational Fluid Dynamics analysis, main achievements of this analysis are a simple criterion able to identify the situations where the pipe rack does not influence the high-pressure methane jet behavior, therefore allowing to identify the scenarios where simpler models can be used (*i.e.*, analytical correlations known for the free jet situation), and, if present, a simple analytical relationship that roughly predicts the influence of the pipe rack without the need of performing complex Computational Fluid Dynamics simulations.

ACRONYMS

CFD Computational fluid Dynamics

EDM Equivalent Diameter Model

FF Flash Fire

HP High-Pressure

LFL Lower Flammability Limit

ME Maximum Extent

NG Natural Gas

RANS Reynolds Averaged Navier-Stokes

UDF User Defined Function

NOMENCLATURE

ABR: Area Blockage Ratio

A_{ps}: pseudo-source area extension

c: methane concentration in air

c_{ax}: methane concentration along the free jet axis

C_D: discharge coefficient

C_p: methane heat capacity

d: actual orifice diameter

D: pipe rack distance from the jet source

d_{FJ}: free jet diameter

d_P: rack pipes diameter

d_{ps}: pseudo-source orifice diameter

h: pipe rack case transversal beam height

H: pipe rack case height

H_L: pipe rack legs height

k: axial decay constant

L: pipe rack module extent

$\dot{m}_{ps}$: pseudo-source mass flow rate

ME: jet axial maximum extent

ME_{FJ}: free jet LFL cloud maximum extent in direction of the jet axis

n_S: shelves number

n_{PS}: number of pipes per shelf

p: upstream methane pressure

p_{amb}: environmental pressure

s: pipe rack case transversal beam width

T: upstream methane temperature

T_{ps}: methane static temperature at pseudo-source conditions

$T_{TOT,ps}$: methane total temperature at pseudo-source conditions

VBR: Volume Blockage Ratio

VFP: Vertical FootPrint

v_{ps}: methane velocity at pseudo-source conditions

W: pipe rack case width

α: pipe rack horizontal rotation with respect to the jet axis

γ: specific heat ratio

ρ_{ps}: methane density at pseudo-source conditions

ρ_{amb}: air density

INTRODUCTION

Although the diffusion of Natural Gas (NG, mainly constituted by methane) storage and transport under liquefied conditions, nowadays it is still common to have high pressure facilities using methane (or NG) in gaseous form in several industrial applications (Deng et al., 2018; Khraisheh et al., 2020).

This leads to several safety implications, related to both the High-Pressure (HP) at which the gas is stored and to its flammability. In particular, in case of late ignition the release scenario can evolve in a Flash Fire (FF), whose hazardous distance is usually quantified as the Lower Flammability Limit (LFL) distance of the unignited cloud. Therefore, to predict how severe may be the consequences of a FF, the extension of the unignited flammable cloud needs to be estimated (Souza et al., 2019b). Commonly, in the risk analysis framework, for the case of a leakage of a flammable substance such evaluation traduces in the prediction of the Maximum axially-oriented Extent (ME) of the cloud (Tchouvelev et al., 2007; Houf et al., 2010; Pontiggia et al., 2014; Colombini et al., 2020a).

Broadly speaking, two different situations of HP gaseous release can be identified: the free jet (intended as a release occurring in an unconfined environment (Dey et al., 2017) and the impinging jet (intended as a release interacting with structures or facilities in the surroundings (*i.e.*, obstacles) (Schefer et al., 2009).

For the latter, which can be expected to be the most probable accidental scenario in an industrial environment (Xu et al., 2011), it has been shown that, in some cases, an increase of the hazardous area (*i.e.*, the ME of the jet cloud) can occur (Kotchourko et al., 2014; Hall et al., 2017).

Despite this, in the past a large amount of the research in the process safety framework has been focused on the free jet scenario (cfr., Lockwood and Moneig (1980), Chen and Rodi (1980), Birch et al. (1984), Schefer and Dibble (1986); Birch et al. (1987), Becker et al. (1988), Pitts (1991), TNO (1997), Witlox and Holt (1999) and SHELL (2004)), while, for what concerns impinging jets, only recently some works have been performed with the aim of understanding how an obstacle can influence the jet behavior. In particular, Kim et al. (2013) investigated experimentally the self-ignition near an obstacle of HP hydrogen jets. Pontiggia et al. (2014) compared the performances of two different modeling approaches (namely, integral and Computational Fluid Dynamics (CFD) models) in predicting ME values for both impinged and non-impinged HP methane jets. Tolias and Venetsanos (2015) investigated how to model an accidental impinging hydrogen jet through CFD models with the aim of giving best practices guidelines for hydrogen impinging jet simulations. Benard et al. (2016) investigated the effect of a near surface on the ME of high-pressure horizontal

and vertical jets of both hydrogen and methane using CFD models. Gerbec et al. (2017) performed a CFD analysis of the release, and the subsequent environmental dispersion, of a vertical impinging propane jet out of an over-filled car tanker. Hall et al. (2017) investigated, both experimentally and numerically through CFD models, the ME of HP hydrogen jets impinging near surfaces. Uggenti et al. (2017) discussed the state-of-the-art of CFD models used for offshore installations risk assessments where impinging jets are usually involved. The aim was to compare the CFD benchmark case with the industrial standard. Hu et al. (2018) presented an improved version of the two-layer partitioning model based on the Abel-Noble equation of state (Johnston, 2005), which is able to predict more accurately the gas concentrations of HP under expanded hydrogen jets. The proposed model was applied to the flow of a horizontal HP hydrogen jet impacting a vertical obstacle. Colombini and Busini (2019a and 2019b) investigated, using a CFD model, the accidental scenarios of an unignited HP methane jet impacting a horizontal and a vertical cylindrical tank to quantify the influence of some geometric parameters on the ME of the impinging jet. Colombini et al. (2020a and 2020b) investigated the effect of the ground (considered as a lateral impinging obstacle) on unignited methane high-pressure jets.

We can note that almost all the aforementioned works used CFD-based models. As discussed by Batt et al. (2016), Souza et al. (2019a), and Tolias et al. (2019), this is motivated by the fact that only CFD-based numerical approaches are able to account properly for complex geometry. Therefore, although the high computational costs and the user knowledge demanded (Zuliani et al., 2016), CFD-based models are the most suitable numerical tools to model HP jet-obstacle scenarios and therefore they have been used extensively in this work to provide useful insights in the HP methane jets-obstacle interaction.

In particular, going beyond the study of the simple interaction between a HP jet and a single well-shaped obstacle, this work investigates how a typical industrial structure (*i.e.*, a pipe rack) can influence the development of a HP methane jet in terms of ME of the flammable cloud. Through an extensive CFD-based analysis performed with Ansys Fluent 19.1 (Ansys Fluent User Guide, 2017), the main geometrical parameters on which the impinging jet behavior depends have been identified allowing for developing a simple analytical relationship that roughly predicts the influence of the pipe rack without the need of performing complex CFD simulations. Moreover, a simple criterion able to identify the situations where the pipe rack does not influence the HP methane jet behavior has been developed, therefore allowing to identify the scenarios where simpler models (*e.g.*,

analytical correlations able to estimate the ME of a free jet) can be used. Both these outcomes can be quite valuable for practitioners daily involved in industrial safety assessments.

MATERIAL AND METHODS

The commercial platform Ansys Workbench v. 19.1 (Ansys Workbench User Guide, 2017) was used to model, through a CFD approach, an unignited HP methane jet impinging a pipe rack.

The computational domain was created with Ansys DesignModeler, the grid was built using Ansys Meshing and the computations were performed with the numerical solver Ansys Fluent (Ansys Workbench User Guide, 2017; Ansys DesignModeler User Guide, 2017; Ansys Meshing User Guide, 2017; Ansys Fluent User Guide, 2017).

Moreover, as usually done when modeling HP jets in the safety assessment field (*e.g.,* Hess et al., 1973; Sposato et al., 2003; Pontiggia et al., 2014; Benard et al., 2007; Houf et al., 2007; Stewart et al., 2019; Tolias et al., 2019), instead of simulating through the CFD also the early stage of the jet development (*i.e.*, the so-called nearfield zone of the jet), the Equivalent Diameter Model (EDM) approach has been used (Franquet et al., 2015); in particular, the EDM proposed by Birch et al. (1984) has been used, as discussed in the following Section.

SCENARIO DESCRIPTION

The scenario analyzed mimes an industrial situation involving a horizontally oriented high-pressure release of methane impinging a pipe rack as sketched in *Figure 4.1*, where also the relevant geometric dimensions are labelled.

The methane source was modelled as a nozzle while the pipe rack was represented by a rectangular structure housing several pipes far from the ground. The HP jet nozzle was located at 4.85 m above the ground (which corresponds to the mid-height of the pipe case). 5D atmospheric conditions (*i.e.*, a wind intensity of 5 m/s at 10 m from the ground and a Pasquill stability class of D) with the wind blowing alongside and in the same direction of the jet were considered. To properly model such wind conditions, the inlet velocity profile was provided to the numerical solver through an *ad hoc* User Defined Function (UDF).

To investigate how the HP jet development is influenced by the rack, several parameters (related to both the jet source and the obstacle) have been considered, namely: upstream methane pressure (p); actual orifice diameter of the jet source (d); rack pipes diameter (d_p); shelves number (n_s); number of pipes per shelf (n_{PS}); rack distance from the jet source (D); pipe rack horizontal rotation with respect to the jet axis (α). Moreover, also the target concentration considered in relation to the ME of the jet (c) was varied in order to see how the jet development modifies when different concentrations are of interest.

As previously mentioned, since the early stage of the jet development was modelled using the EDM approach proposed by Birch et al. (1984), to include all the physical phenomena on one hand and to avoid any unwanted interference of the boundaries on the other hand, the domain extents were defined through some preliminary tests, resulting in a rectangular box of 100 m length, 25 m height and 15 m wide. Note that 15 m is half the width of the domain, thanks to the symmetry of the geometry; in the few cases where no symmetry plane is present, a 30 m width was used.

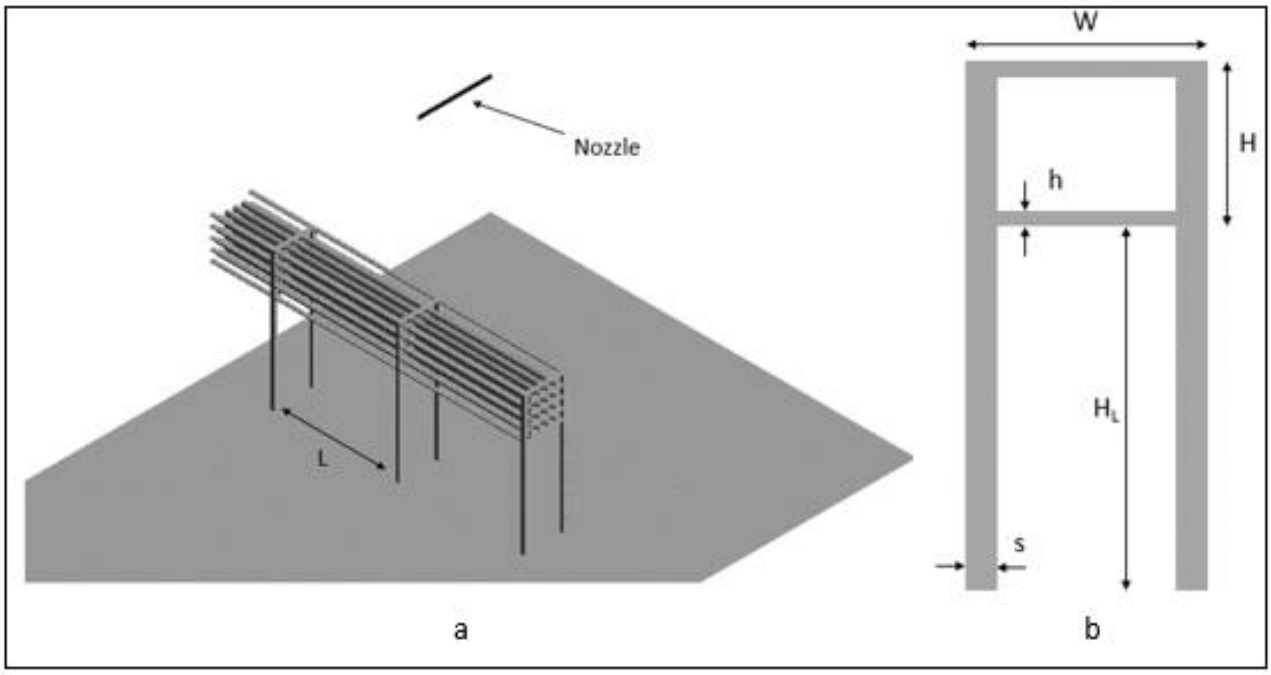

Figure 4.1: Scenario configuration: a) whole appearance, b) pipe rack structure details. Figure 4.1b reports the relevant dimensions of the rack structure that were kept the same in all the analysis: s = 0.15 m, h = 0.05 m, H = 1.7 m, H_L = 4 m, W = 1.75 m, L = 5 m. The scenario that is shown is symmetric with respect to the vertical plane crossing the jet axis.

The strategy used for the mesh deployment is discussed in detail elsewhere (Colombini et al. (2020a)). In particular, the *body of influence* feature was used to thicken the computational grid in a volume surrounding the jet axis (which is the computationally critical zone), allowing a less dense mesh close to the domain boundaries (where demanding physical phenomena are not expected). To properly model the flow-rack interaction, the *inflation* mesh feature was applied to the surfaces of the obstacle to achieve an adequate boundary layer discretization (Ansys Meshing User Guide, 2017). In the investigated conditions, the flow interacting with a solid surface cohabits with regions in which the turbulent flow does not interact with any solid surface. To correctly model both the situations and, at the same time, to limit the computational costs, the Reynolds Averaged Navier-Stokes (RANS) approach was adopted and coupled with the two-equation eddy-viscosity k-ω SST turbulence closure model (Menter, 1993). Figure 4.2 shows, for one of the cases investigated (run 12 in Table 3), the resulting full-tetrahedral mesh. Depending on the specific case considered (which is related to the values of the parameters involved) the number of cells ranged from 8 to 18 million. Quality requirements (i.e., skewness and orthogonal quality) were always verified. Moreover, for a reference case (run 12 in Table 3), the independence of the results from the grid was qualitatively

and quantitatively verified in terms of concentration and velocity decay in correspondence of the symmetry vertical plane, by halving and doubling the elements size of the body of influence features. Figure B1 in the supplementary material shows the comparison of the sensitivity analysis results in terms of methane mole fraction in air and velocity contours.

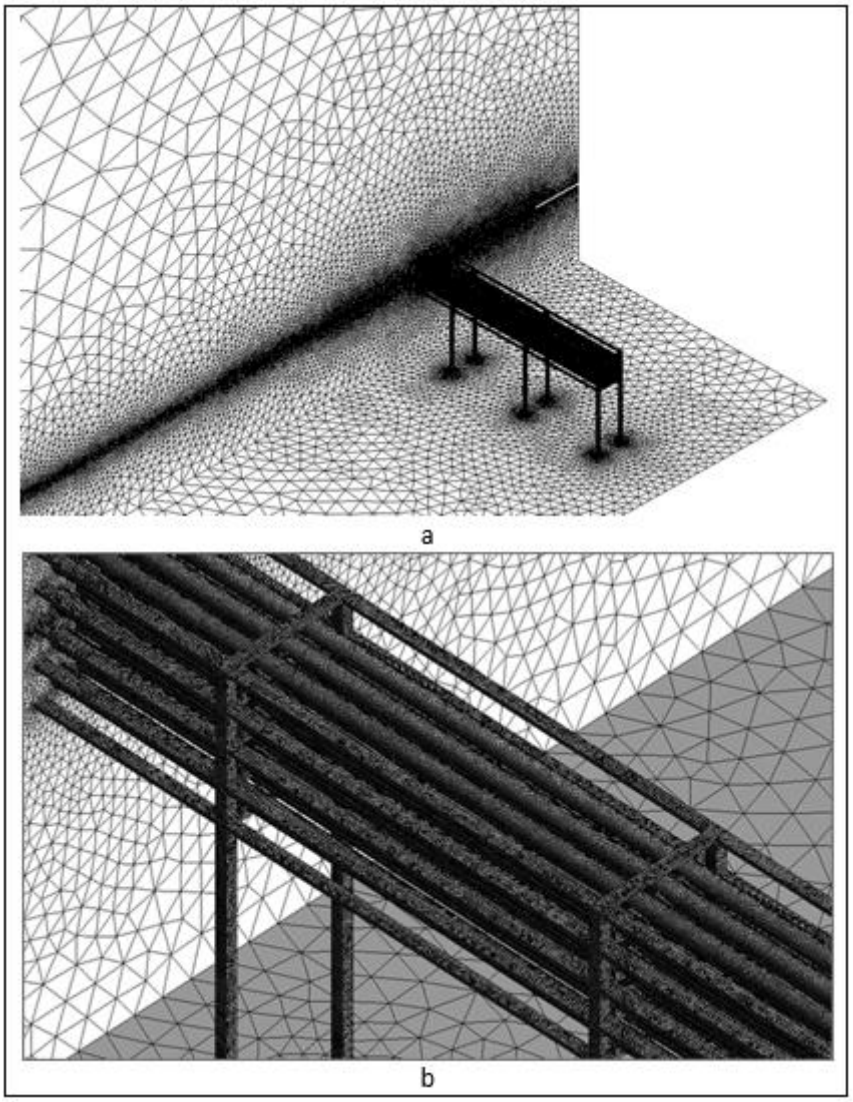

Figure 4.2: General view of the surface grid (a) and its detail in proximity to the pipe rack (b).

All the simulations were accrued out in steady-state conditions and the use of the EDM to simulate the near zone of the jet allowed the flow to be treated as incompressible. For this reason, the pressure-based solver was used. To account for the multi-species problem (methane release in ambient air), the species transport model with no reaction was selected. The fluid system was considered as an ideal gaseous mixture, and the density was modelled by means of the ideal gas Equation of State. Gravity acceleration was always included perpendicularly to the ground surface.

The second order upwind spatial-discretisation scheme was considered for all the convective terms and the COUPLED pressure-velocity coupling scheme was adopted. Table B1 in the supplemental information lists the model equations together with the definition of the main parameters.
Using the methane upstream conditions and the actual nozzle diameter considered, the equivalent jet source boundary conditions were computed, case by case, with the Birch et al. (1984) model. Table 4.1 reports the equations defining the pseudo-source characteristics used for the methane jet inlet. The other boundary conditions were kept unchanged for all the cases and they are summarized in Table 4.2.

Table 4.1: Equations of the Birch et al. (1984) model defining the pseudo-source characteristics of the methane jet inlet. In the Equations, d_{ps} is the resulting diameter of the pseudo-source, d is the actual orifice diameter, C_D is the discharge coefficient, p is the storage pressure, p_{amb} is the environmental pressure, γ is the specific heat ratio, Cp is the methane heat capacity, $\dot{m}_{ps}$, v_{ps}, ρ_{ps}, T_{ps}, $T_{TOT,ps}$ and A_{ps} are the resulting mass flow rate, velocity, density, static temperature, total temperature and area extension of the pseudo-source, respectively. Further details are provided in the work of Birch et al. (1984).

Pseudo-source characteristic	**Equation**
Equivalent diameter	$d_{ps} = d\sqrt{C_D\left(\frac{p}{p_{amb}}\right)\left(\frac{2}{\gamma+1}\right)^{\frac{(\gamma+1)}{2(\gamma-1)}}}$
Mass flow rate	$\dot{m}_{ps} = \rho_{ps} \cdot A_{ps} \cdot v_{ps}$
Total temperature	$T_{TOT,ps} = T_{ps} + \frac{v_{ps}^2}{2\,C_p}$

Table 4.2: Boundary conditions assignments.

Boundary name	Type	Specifics
Wind inlet	Velocity inlet	air, v_z = UDF velocity profile, T = 300 K
Top boundary	Velocity inlet	air, v_z = 5.5 m/s, T = 300 K
Left boundary	Velocity inlet	air, v_z = UDF velocity profile, T = 300 K
Ground	Wall	0.01 m roughness height, adiabatic
Symmetry	Symmetry	-
Wind outlet	Pressure outlet	air, $T_{BACKFLOW}$ = 300 K
Pipe nozzle	Wall	0.001 m roughness height, adiabatic
Methane jet inlet	Mass flow inlet	Computed case by case with Birch et al. (1984) model. See Table 4.1.
Pipe rack	Wall	0.001 m roughness height, adiabatic

Three dimensionless parameters have been used to summarize the HP jet-rack interaction, as detailed in the following equations as well as in *Figure 4.3*, 4.4 and 4.5:

$$VBR = \frac{n_{PS} \cdot n_S \cdot \frac{\pi \cdot d_P^2}{4} + 2 \cdot (n_S + 1) \cdot s \cdot h}{H \cdot W} \tag{4.1}$$

$$ABR = \frac{h \cdot (n_S + 1) + d_P \cdot n_S}{H} \tag{4.2}$$

$$VFP = \frac{d_{FJ}(D)}{H} \tag{4.3}$$

All the parameters involved in these equations have been already defined in *Figure 4.1* apart from $d_{FJ}(D)$ that is the free jet diameter evaluated in correspondence of the pipe rack position (see *Figure 4.5*). VBR (which stands for Volume Blockage Ratio, that is the ratio between occupied rack case volume and full rack case volume – see *Figure 4.3*) indicates how the volume within the rack case is occupied by pipes and structural beams; ABR (which stands for Area Blockage Ratio, that is the ratio between occupied rack case frontal area and full rack case frontal area – see *Figure 4.4*) indicates how the frontal area of the rack case is hindered by pipes and structural beams; VFP (which stands

for Vertical FootPrint, that is the hypothetical free jet footprint on the pipe rack - see *Figure 4.5*) indicates whether the free jet cloud radial extent (at the considered concentration level) is larger than (or smaller) the height of the rack case.

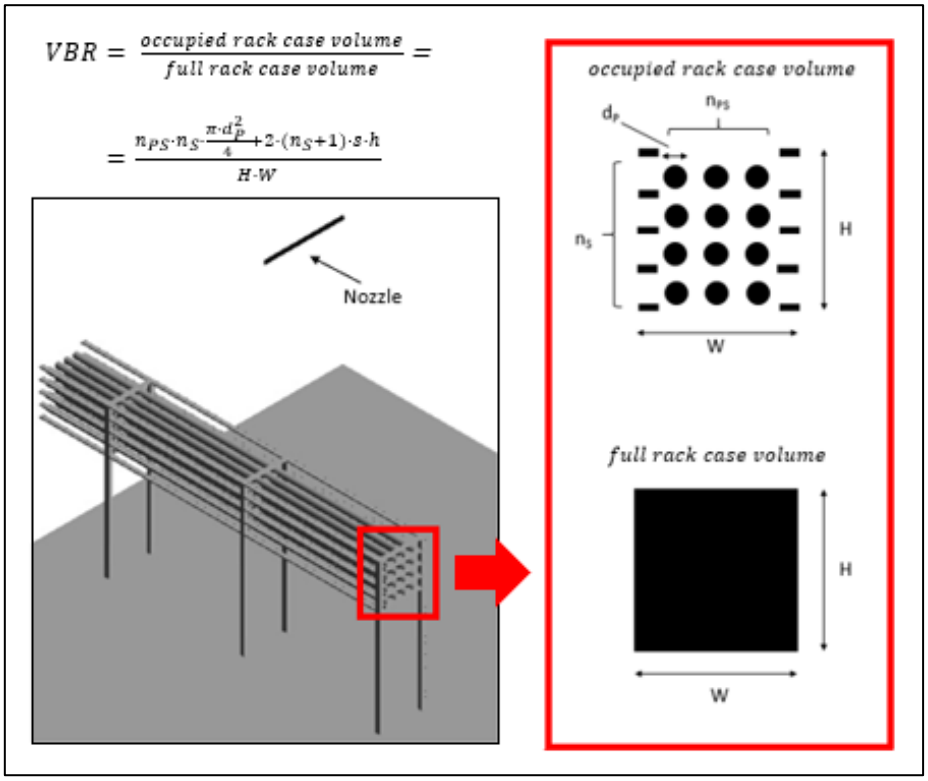

Figure 4.3: Physical meaning of VBR.

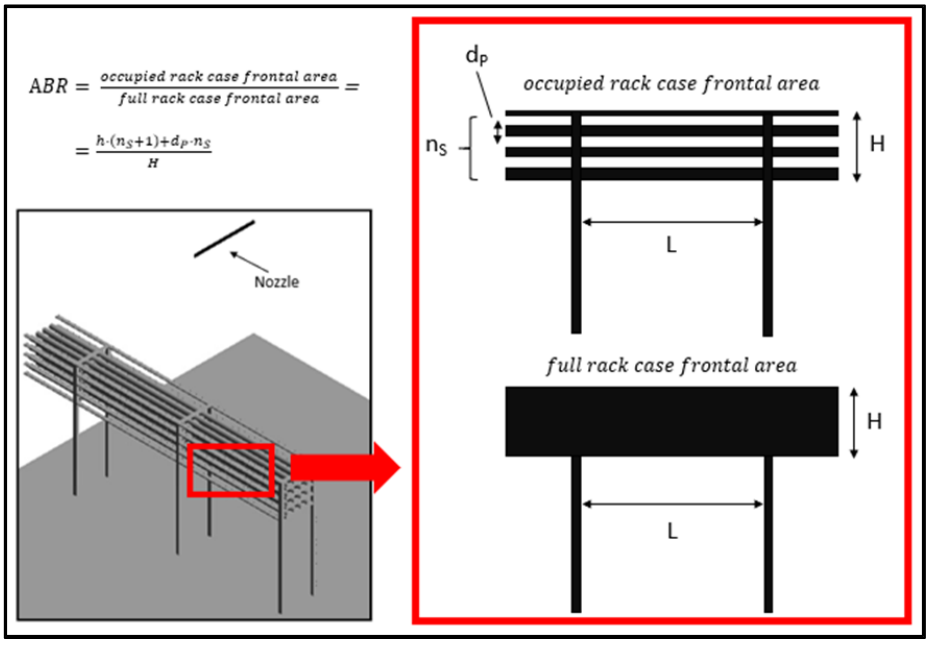

Figure 4.4: Physical meaning of ABR.

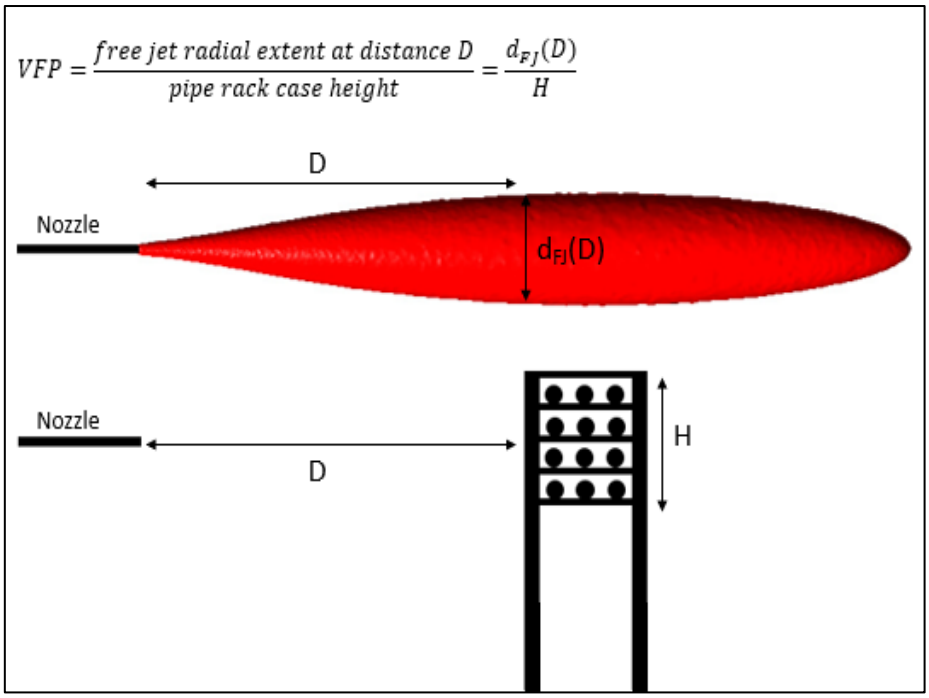

Figure 4.5: Physical meaning of VFP.

RESULTS AND DISCUSSION

At first, the geometrical characteristics of the pipe rack (namely: d_p, n_s, and n_{PS}) were changed within realistic ranges, as shown in *Table 4.3*, while the values of all the other parameters were kept unchanged: p = 65 bar, T = 278 K, d = 0.0254 m, D = 7.68 m (*i.e.*, half of ME of a free jet at methane LFL), α = 0° (that is, the pipe rack is perpendicular to the jet axis) and c = 5.3 % (methane LFL).

Table 4.3: Values of the characteristics defining the cases simulated.

Run	d_p [m]	n_{PS}	n_s	Run	d_p [m]	n_{ps}	n_s
1	15.19	2	3	**20**	25	4	3
2	21.48	2	3	**21**	26.31	4	3
3	25	2	3	**22**	15.19	5	3
4	26.31	2	3	**23**	21.48	5	3
5	30.38	2	3	**24**	25	5	3
6	33.97	2	3	**25**	15.19	3	4
7	37.21	2	3	**26**	21.48	3	4
8	15.19	3	3	**27**	25	3	4
9	17.54	3	3	**28**	15.19	4	4
10	21.48	3	3	**29**	21.48	4	4
11	24.81	3	3	**30**	28	4	4
12	25	3	3	**31**	15.19	3	5
13	26.31	3	3	**32**	21.48	3	5
14	27.74	3	3	**33**	25	3	5
15	30.38	3	3	**34**	15.19	4	5
16	15.19	4	3	**35**	21.48	4	5
17	18.61	4	3	**36**	15.19	3	6
18	21.48	4	3	**37**	21.48	3	6
19	24.02	4	3	**38**	15.19	4	6

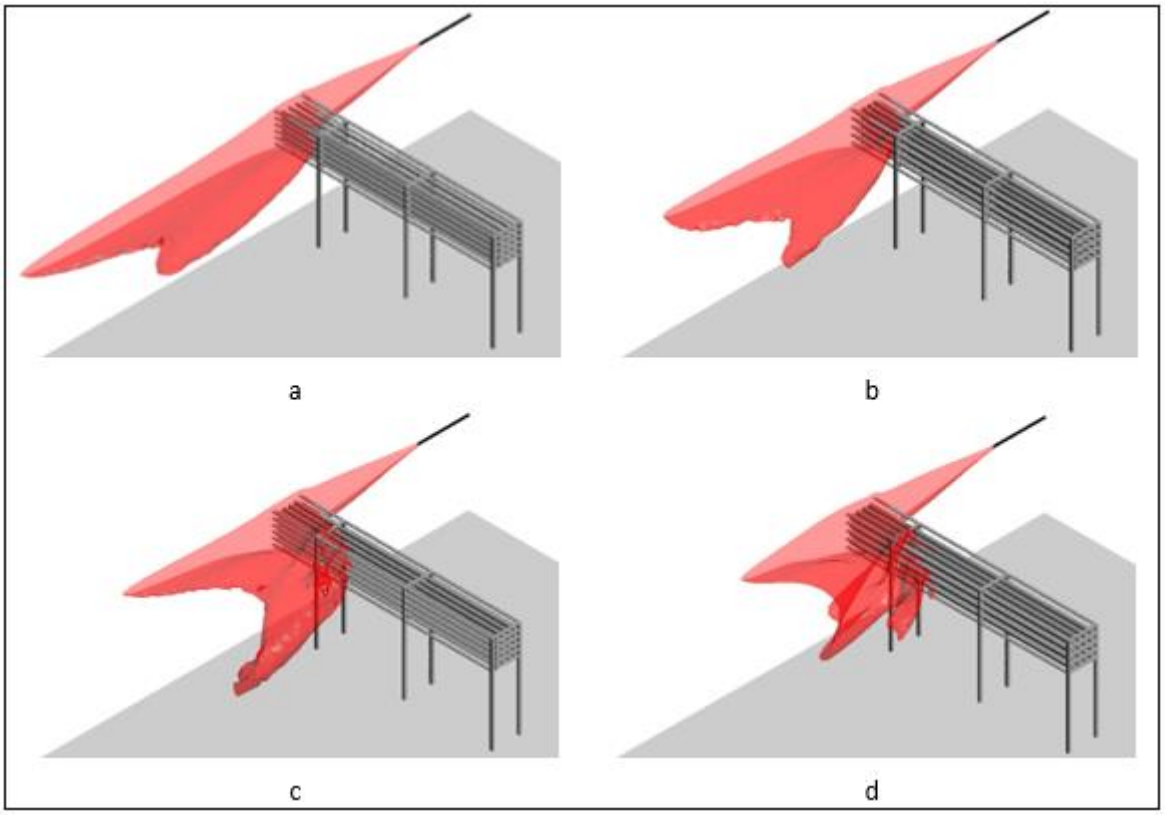

Figure 4.6: Isosurfaces of methane concentration in air equal to 5.3% for some of the runs in Table 4.2: a) run 31, b) run 29, c) run 35 and d) run 30.

Figure 4.6a-d shows the isosurfaces of some of the runs listed in *Table 4.3*. Qualitatively, we can see that, in all the cases, the jet cloud passes over the rack structure, even if the ME of the LFL is not always located along the jet axis. Comparing. Figure 4.6b and 4.6d we can see that an increase in the pipes diameter results in a reduction of the ME together with a lateral enlargement of the cloud. Comparing Figure 4.6b and 4.6c we can see that increasing the number of pipes per shelf leads to an overall ME reduction and to a more enhanced split of the jet cloud.

These behaviours can be recast in terms of VBR and ABR values considering runs 30 and 31 (which show the same VFP = 1.09 value and an VBR·ABR value about 4 times larger for run 30 than run 31) together with the free jet simulation, as shown in *Figure 4.7*.

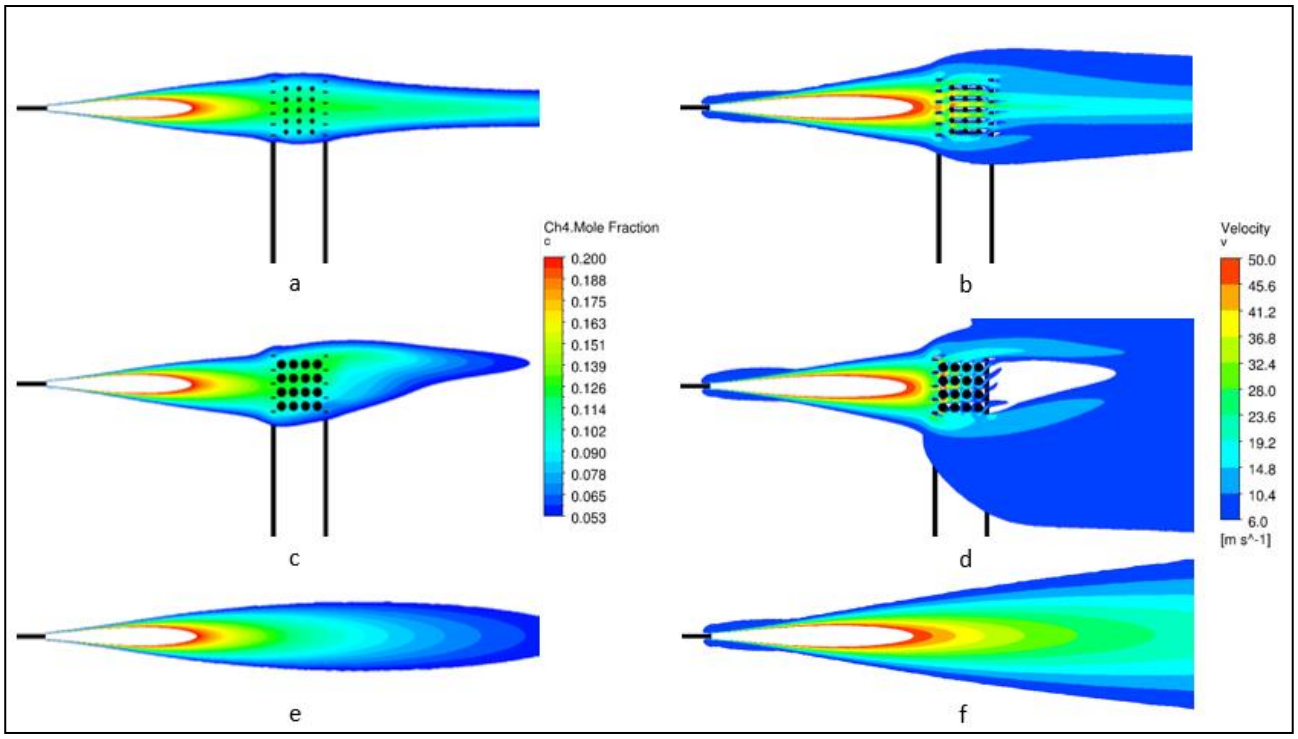

Figure 4.7: Contours of methane concentration in air and flow velocity in correspondence of the domain vertical symmetry plane for two runs of Table 4.2 (Figure 4.7a-b run 31, Figure 4.7c-d run 30) and for the free jet situation (Figure 4.7e-f). For run 31 VBR·ABR = 0.075 and ME = 23.7 m, while, for run 30 VBR·ABR = 0.287 and ME = 14.68 m.

Comparing *Figure 4.7*a and 4.7c with *Figure 4.7*e we can see that the obstacle acts as a sort of isolating structure able to reduce the jet air entrainment; as a matter of fact, the methane concentration does not decrease when the jet passes through the rack case. Moreover, the jet velocity immediately downstream the rack case is lower than that in free jet conditions, limiting the dilution effect caused by the velocity difference with the bulk fluid (see *Figure 4.7*b and 4.7d with respect to *Figure 4.7*f). The combination of these two phenomena leads to longer jet clouds. We can also see that when both the front area of the obstacle and the volume within it are less hindered by the pipes the aforementioned physical phenomena are more relevant leading to longer jet cloud when either VBR or ABR decreases. However, when VBR and ABR reduced to very low values, the pipe rack looks like more to an empty volume rather than an obstacle, therefore allowing the jet to pass through the obstacle undisturbed. In these conditions the impinging jet is expected to approximate a free jet behavior.

All these results can be rationalized as shown in *Figure 4.8*, where the ratio of the LFL cloud ME computed for all the runs in *Table 4.3* to the LFL cloud ME computed for a corresponding free jet (ME_{FJ}, that is, the LFL cloud ME computed for the same jet without any obstacle interaction) is

reported as a function of the product of the three aforementioned dimensionless parameters (note that the ME_{FJ} value can be easily estimated using well known analytical correlations, *e.g.*, Chen and Rodi (1980)).

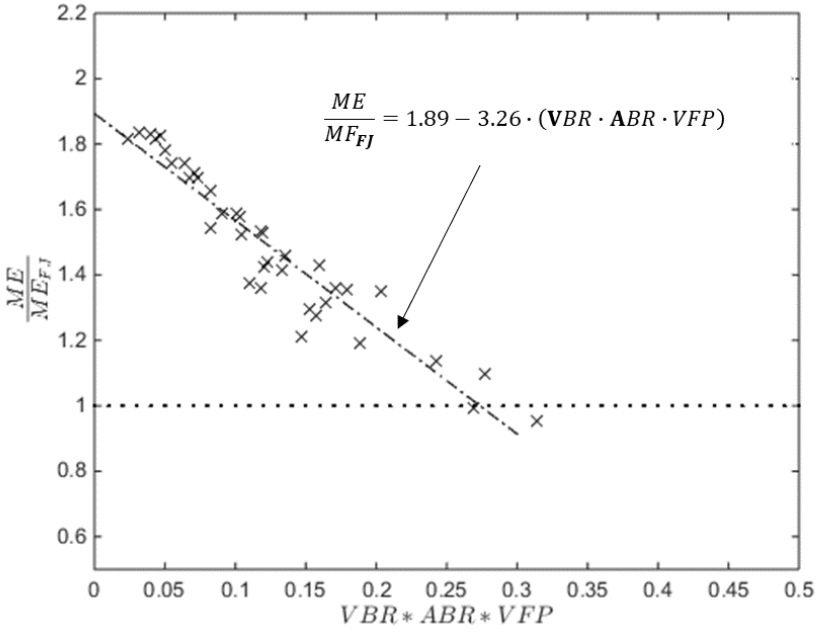

Figure 4.8: Dimensionless space defined exploiting the dimensionless parameters introduced in Section SCENARIO DESCRIPTION. X markers are the results computed for the 38 runs listed in Table 4.3, the dotted line represents ME = ME_{FJ} (MEFJ = 15.37 m) while the dashed-dotted line is the linear fitting of the computed data.

From this Figure we can see a clear trend showing how the rack influences the jet development: ME of the LFL jet cloud is always larger than (or almost equal to) ME_{FJ}. This means that the rack is never able to reduce the LFL jet ME; in the worst case, the ME of the free jet is almost doubled by the presence of the rack. Moreover, the following linear interpolation of the results provides a reasonable fitting:

$$\frac{ME}{MF_{FJ}} = 1.89 - 3.26 \cdot (VBR \cdot ABR \cdot VFP) \tag{4.4}$$

with a percentage error, defined as $\epsilon = \frac{\sum_{i=1}^{n}\left(\frac{|y_i - y|}{y_i}\right)}{n} \cdot 100$ (where y_i is the ratio between ME and ME_{FJ} computed for each run, y the ratio between ME and ME_{FJ} computed with Equation 4.4 and n=38 is the number of runs), equal to 4.4 %.

Starting from the conditions of run 12 in *Table 4.3* (that is, for the present analysis, the reference scenario in terms of pipe rack characteristics), several different scenarios were investigated, varying p, d, D, α, and c, as summarized in *Table 4.4*. Results of runs 39-126 are shown in *Figure 4.9*, where the same plan of *Figure 4.8* was used. Notice that, targeting to highlight the influence of only the observed methane concentration, runs 51-126 replicated twice the 38 runs detailed in *Table 4.3*, keeping methane source conditions of run 12 and varying the methane concentration observed (c = 2.65 % for runs 51-88 and 10 % for runs 89-126).

Table 4.4: Characteristics defining the scenarios targeting to generalize the analytical correlation.

Run	p [bar]	d [m]	D [m]	α [°]	c [%]
39	32.5	0.0254	7.68	90	5.3
40	130	0.0254	7.68	90	5.3
41	65	0.0127	7.68	90	5.3
42	65	0.0508	7.68	90	5.3
43	65	0.0254	3.84	90	5.3
44	65	0.0254	5.76	90	5.3
45	65	0.0254	9.6	90	5.3
46	65	0.0254	11.52	90	5.3
47	65	0.0254	13.44	90	5.3
48	65	0.0254	15.36	90	5.3
49	65	0.0254	7.68	112.5	5.3
50	65	0.0254	7.68	135	5.3
51-88	65	0.0254	7.68	90	2.65
89-126	65	0.0254	7.68	90	10

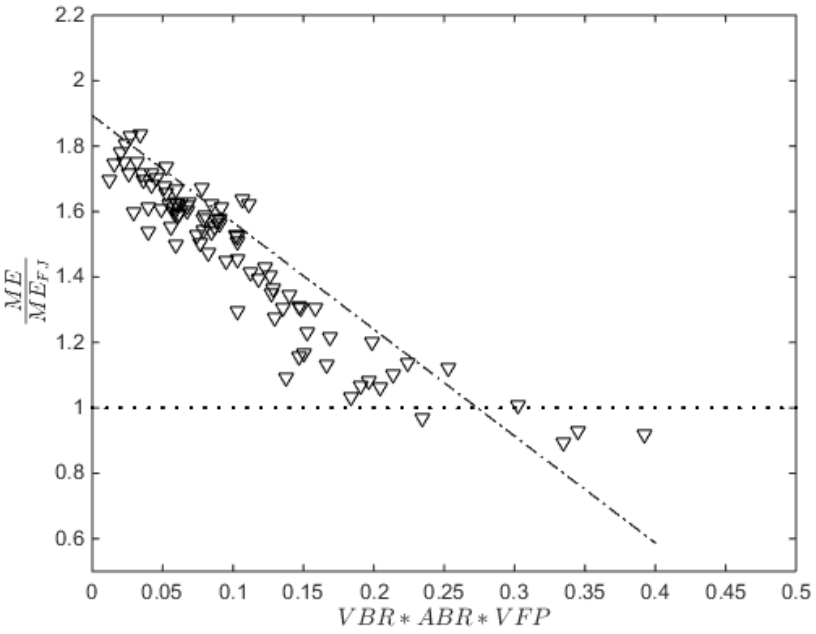

Figure 4.9: Results of runs in Table 4.4 are shown in the plan defined in Figure 4.8. The flipped triangular markers are the results computed for the 88 runs listed in Table 4.4, the dotted line represents ME = ME_{FJ} (MEFJ = 15.37 m) while the dashed-dotted line is the linear fitting of the computed data (Eq. 4.4*).*

We can see that the linear correlation deduced from the fitting of the first 38 runs (Eq. 4.4) is able to represent reasonably well also the results of the new 88 runs, with a mean percentage error equal to 7.8. This is an important evidence supporting the reliability of the proposed correlation. Moreover, the proposed correlation overestimates CFD computations nearly in 70 % of the scenarios investigated, leading to an estimated ME that is, in most of the cases, conservative from the safety point of view. Considering the 126 scenarios analysed we can see that only a few of them present a value of VBR·ABR·VFP greater than 0.3 and they show a value of ME/ME_{FJ} around one. This leads to the inference that for values of VBR·ABR·VFP larger than 0.3 the obstacle expires its influence on the jet development.

To confirm this inference four ad hoc runs were investigated, as summarized in Table 4.5. The results obtained for these four runs are summarized in Figure 4.10 together with the results of all the previous runs. Notice that, run 130 is intended to resemble a pipe rack with a high filling degree of both case volume (VBR) and front area (ABR). To do so, a horizontal cylinder with a diameter equal to the rack case height, H, and placed in the same position of the pipe rack was used as extreme situation.

Table 4.5: Characteristics defining the scenarios targeting to obtain large values of VBR·ABR·VFP.

Run	p [bar]	d [m]	D [m]	α [°]	c [%]	d_p [m]	n_{PS}	n_s	VBR [-]	ABR [-]	VFP [-]	VBR·ABR·VFP [-]
127	65	0.0254	7.68	90	5.3	21.48	4	6	0.33	0.96	1.09	0.345
128	65	0.0254	7.68	90	5.3	32	4	4	0.46	0.90	1.09	0.450
129	65	0.0254	7.68	90	5.3	22	6	6	0.50	0.98	1.09	0.532
130	65	0.0254	7.68	90	5.3	1.7	1	1	0.76	1	1.09	0.830

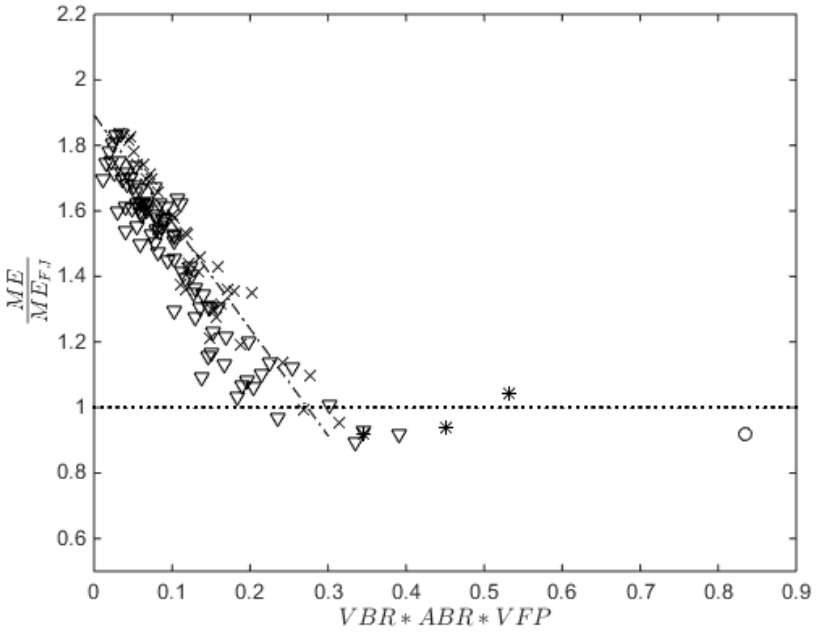

Figure 4.10: Results of runs listed in Table 4.5 are added to Figure 4.9 to show what occurs for large values of VBR·ABR·VFP. Moreover, also results in Figure 4.8 have been reported. X markers are the results computed for the 38 runs listed in Table 4.3, flipped triangular markers are the results computed for the 88 runs listed in Table 4.4, asterisk markers are the results computed for the 3 pipe rack cases listed in Table 4.5 (first three rows of the Table), circle marker is the result computed for the single horizontal cylinder case in Table 4.5 (last row of the Table), the dotted line represents ME = ME_{FJ} (ME_{FJ} = 15.37 m) while the dashed-dotted line is the linear fitting of the computed data (Eq. 4.4).

We can see that also for VBR·ABR·VFP much larger than 0.3 values of ME/ME_{FJ} around one have been obtained. The reason is that an increase in VBR or ABR results in an obstacle with a high degree of volume filled by pipes, therefore decreasing the possibility to the methane jet of passing through

it. The jet is therefore more and more forced to travel around the obstacle, leading to a ME of the jet close to that of a free jet.

CONCLUSIONS

The impinging high-pressure jet release of methane can be a relevant scenario in several industrial facilities. Among the others, the scenario involving the impingement of a pipe rack has been deeply investigated through a CFD-based model, showing that the presence of a rack either does non influence or enhance the ME of the flammable jet with respect to the free jet.
The main findings can be summarized in the following procedure, which allows estimating the ME of a methane flammable cloud without any demanding of (in terms of both time and analyst skill) CFD-based computation:

1. From both the obstacle and source characteristics, estimate VBR, ABR, and VFP values:

$$VBR = \frac{n_{PS} \cdot n_S \cdot \frac{\pi \cdot d_P^2}{4} + 2 \cdot (n_S + 1) \cdot s \cdot h}{H \cdot W}$$

$$ABR = \frac{h \cdot (n_S + 1) + d_P \cdot n_S}{H}$$

$$VFP = \frac{d_{FJ}(D)}{H}$$

to analytically estimate $d_{FJ}(D)$, the following models need to be used:

$$d_{FJ}(D) = 2 \cdot \sqrt{-\frac{D^2}{50} \cdot \ln\left(\frac{\bar{c}}{c_{ax}(D)}\right)}$$ Cushman-Roisin (2020)

$$c_{ax}(D) = \frac{k d_{ps}}{D}\left(\frac{\rho_{amb}}{\rho_{ps}}\right)^{\frac{1}{2}}$$ Chen and Rodi (1980)

Where d is the pipe rack distance from the jet source, $\bar{c}$ is the specific methane concentration in air considered, $c_{ax}(d)$ is the methane concentration along the free jet axis computed at a distance d from the jet source, k is the axial decay constant (4.4 (Birch et al. (1984)), d_{ps} is the pseudo-source orifice diameter (computed with the model of Birch et al. (1984)), ρ_{amb} is the air density (computed at the ambient conditions), ρ_{ps} is the methane density at pseudo-source conditions. To show the capability of the previous analytical models to provide a reasonable prediction of $d_{fj}(d)$, Figure B2 in the supplementary material compares the radial extent of a given free jet computed with the CFD model and the previous analytical ones.

2. From the source characteristics, estimate the ME_{FJ} value using the Chen and Rodi (1980) concentration decay model:

$$ME_{FJ} = \frac{k d_{ps}}{LFL}\left(\frac{\rho_{amb}}{\rho_{ps}}\right)^{\frac{1}{2}}$$

Notice that, the Chen and Rodi (1980) model reliability in estimating ME_{FJ} is discussed in detail in the work of Colombini et al. (2020a).

3. If VBR·ABR·VFP > 0.3, ME_{FJ} provides the order of magnitude of ME
4. If VBR·ABR·VFP < 0.3, the order of magnitude of ME can be estimated as

$$\frac{ME}{MF_{FJ}} = 1.89 - 3.26 \cdot (VBR \cdot ABR \cdot VFP)$$

Finally, it should be stressed that this procedure is expected to provide a reasonable estimation (that is, in most of the cases (70%), a safe overestimation of CFD outcomes) as an order of magnitude of ME for methane HP jets inside the parameters window investigated (*i.e.*, for methane only, for upstream pressures between 32.5 and 130 bar, for upstream temperature equal to 278 K, for orifice diameters between 1.2 and 5 cm, for shelves number between 2 and 6, for number of pipes per shelf between 2 and 6, for pipes diameter between 15 and 37 cm, for rack axis orientations with respect to jet axis between 90° and 135°, for methane concentrations level observed between 2.65 and 10 %, for pipe racks located far from the jet source between 25 and 100 % of the free jet length). The use of detailed CFD simulations should be always considered both for confirming the estimated values, as well as for obtaining more reliable estimation either in highly sensitive scenarios or in scenarios characterized by parameter values outside the investigated window.

REFERENCES

Ansys DesignModeler User's Guide, 2017. Release 19.0. ANSYS, Inc.

Ansys Fluent User's Guide, 2017. Release 19.0. ANSYS, Inc.

Ansys Meshing User's Guide, 2017. Release 19.0. ANSYS, Inc.

Ansys Workbench User's Guide, 2017. Release 19.0. ANSYS, Inc.

Batt, R., Gant, S.E., Lacome, J.M., Truchot, B., 2016. Modelling of stably-stratified atmospheric boundary layers with commercial CFD software for use in risk assessment. *Chem. Eng. Trans.* 48, 61–66. https://doi.org/10.3303/CET1648011.

Becker, H.A., Cho, S.H., Ozum, B., Tsujikawa, H., 1988. Turbulent mixing in the impingement zone of dual opposed free jets and of the normal wallimpinging jet. *Chem. Eng. Commun*. 67, 291-313. http://dx.doi.org/10.1080/00986448808940390

Bénard, P., Tchouvelev, A., Hourri, A., Chen, Z., Angers, B., 2007. High pressure hydrogen jets in the presence of a surface. *Int. Conf. Hydrog. Saf.* 40.

Bénard, P., Hourri, A., Angers, B., Tchouvelev, A., 2016. Adjacent surface effect on the flammable cloud of hydrogen and methane jets: Numerical investigation and engineering correlations. *Int. J. Hydrogen Energy* 41, 18654–18662. https://doi.org/10.1016/j.ijhydene.2016.08.173.

Birch, A.D., Brown, D.R., Dodson, M.G., Swaffield, F., 1984. The structure and concentration decay of high pressure jets of natural gas. *Combust. Sci. Technol.* 36, 249–261. https://doi.org/10.1080/00102208408923739.

Birch, A.D., Hughes, D.J., Swaffield, F., 1987. Velocity decay of high pressure jets. *Combust. Sci. Technol.* 52, 161-171. http://dx.doi.org/10.1080/00102208708952575

Chen, C.J., Rodi, W., 1980. Vertical Turbulent Buoyant Jets – A review of Experimental Data, First ed. Pergamon Press Vol. 4.

Colombini, C., Busini, V., 2019a. Obstacle Influence on High-Pressure Jets based on Computational Fluid Dynamics Simulations. *Chem. Eng. Trans.* 77, 811–816. https://doi.org/10.3303/CET1977136.

Colombini, C., Busini, V., 2019b. High-Pressure Methane Jet: Analysis of the Jet-Obstcle Interaction. *Proceeding of the 29th European Safety and Reliability Conference.*

Colombini, C., Martani, A., Rota, R., Busini, V., 2020a. Ground influence on high-pressure methane jets: Practical tools for risk assessment. *J. Loss Prevent. Proc.* 67, 104240. https://doi.org/10.1016/j.jlp.2020.104240

Colombini, C., Carlini, L., Rota, R., Busini, V., 2020b. Ground Interaction on High-Pressure Jets: Effect on Different Substances. *Chem. Eng. Trans.* 83. To be printed.

Cushman-Roisin, B., Environmental Fluid Mechanics – John Wiley & Sons, Book in preparation. Last online access: August 2020. http://www.dartmouth.edu/~cushman/books/EFM/chap9.pdf

Deng, Y., Hu, H., Yu, B., Sun, D., Hou, L., Liang, Y., 2018. A method for simulating the release of natural gas from the rupture of high-pressure pipelines in any terrain. *J. Hazard. Mater.* 342, 418–428. https://doi.org/10.1016/j.jhazmat.2017.08.053.

Dey, S., Kishore, G.R., Castro-Orgaz, O., Ali, S.Z., 2017. Hydrodynamics of submerged turbulent plane offset jets. *Phys. Fluids* 29. https://doi.org/10.1063/1.4989559.

Franquet, E., Perrier, V., Gibout, S., Bruel, P., 2015. Free underexpanded jets in a quiescent medium: A review. *Prog.*

Aerosp. Sci. 77, 25–53. https://doi.org/10.1016/j.paerosci.2015.06.006.

Gerbec, M., Pontiggia, M., Antonioni, G., Tugnoli, a., Cozzani, V., Sbaouni, M., Lelong, R., 2017. Comparison of UDM and CFD simulations of a time varying release of LPG in geometrical complex environment. *J. Loss Prev. Process Ind.* 45, 56–68. https://doi.org/10.1016/j.jlp.2016.11.020.

Hall, J.E., Hooker, P., O'Sullivan, L., Angers, B., Hourri, A., Benard, P., 2017. Flammability profiles associated with high-pressure hydrogen jets released in close proximity to surfaces. *Int. J. Hydrogen Energy* 42, 7413–7421. https://doi.org/10.1016/j.ijhydene.2016.05.113.

Hess, K., Leukel, W., Stoeckel, A., 1973. Formation of explosive clouds on overhead release and preventive measure. *Chemie-Ingenieur-Technik* 45, 5.

Houf, W., Schefer, R., 2007. Predicting Radiative Heat Flux and Flammability Envelopes from Unintended Releases of Hydrogen. *Int. J. Hydrogen Energ.* 32, 136-151. https://doi.org/10.1016/j.ijhydene.2006.04.009

Houf, W., Schefer, R., Evans, G., Merilo, E., Groethe, M., 2010. Evaluation of barrier walls for mitigation of unintended releases of hydrogen. *Int. J. Hydrogen Energy* 35, 4758–4775. https://doi.org/10.1016/j.ijhydene.2010.02.086.

Hu, J., Christopher, D.M., Li, X., 2018. Simplified partitioning model to simulate high pressure under-expanded jet flows impinging vertical obstacles. Int. J. Hydrogen Energ. 43, 13649-13658. https://doi.org/10.1016/j.ijhydene.2018.05.036

Jhonston, I.A., 2005. The Noble-Abel Equation of State: Thermodynamic Derivations for Ballistics Modelling. *Weapons Systems Division Defence Science and Technology Organisation*. DSTO-TN-0670.

Khraisheh, M., Almomani, F., Walker, G., 2020. Solid Sorbents as a Retrofit Technology for CO2 Removal from Natural Gas Under High Pressure and Temperature Conditions. *Sci. Rep.* 10, 269. https://doi.org/10.1038/s41598-019-57151-xx

Kim, S., Lee, H.J., Park, J.H., Jeung, I.S., 2013. Effects of a wall on the self-ignition patterns and flame propagation of high-pressure hydrogen release through a tube. *Proc. Combust. Inst.* 34, 2049–2056. https://doi.org/10.1016/j.proci.2012.09.001.

Kotchourko, A., Baraldi, D., Bénard, P., Eisenreich, N., Jordan, T., Keller, J., Kessler, A., LaChance, J., Molkov, V., Steen, M., Tchouvelev, A., 2014. State of the Art and Research Priorities in Hydrogen Safety. Joint Research Centre of the European Commission (JRC), Honolulu, Hawaii.

Lockwood, F. C., Moneib, H. A., 1980. Fluctuating Temperature Measurements in a Heated Round Free Jet. *Combust. Sci. Technol.* 22, 63-81. https://doi.org/10.1080/00102208008952372

Menter, F.R., 1993. Zonal Two Equation kω Turbulence Models for Aerodynamic Flows. *24th Fluid Dynamics Conference*.

Pitss, W.M., 1991. Effects of global density ratio on the centerline mixing behavior of axisymmetric turbulent jets. *Exp. Fluids* 11, 125-134.

Pontiggia, M., Busini, V., Ronzoni, M., Uguccioni, G., Rota, R., 2014. Effect of large obstacles on high momentum jets dispersion. *Chem. Eng. Trans.* 36, 523–528. https://doi.org/10.1016/j.jhazmat.2009.06.064.

Schefer, R., Groethe, M., Houf, W.G., Evans, G., 2009. Experimental Evaluation of Barrier Walls for Risk Reduction of Unintended Hydrogen Releases, *Int. J. Hydrogen Energ.* 34, 1590-1606. https://doi.org/10.1016/j.ijhydene.2008.11.044

Schefer, R.W., Dibble, R.W., 1986. Mixture fraction measuremetns in a turbulent nonreacting propane jet. AIAA paper, 86-0278.

Shell, 2004. FRED – Fire, Release, Explosion and Dispersion, Shell Global Solutions. http://www.shellglobalsolutions.com/hse/software/fred.html. Last access: 15/07/2020.

Souza, A. O., Luiz, A. M., Neto A. T. P., Araujo A. C. B., Silva H. B., Silva A. K., Alves J. J. N, 2019a. A new correlation for hazardous area classification based on experiments and CFD predictions. *Process Saf. Prog.* 38, 21–26. https://doi.org/10.1002/prs.11974.

Souza, A. O., Luiz, A. M., Neto A. T. P., Araujo A. C. B., Silva H. B., Silva A. K., Alves J. J. N, 2019b. CFD predictions for hazardous area classification. *Chinese J. Chem. Eng.* 27, 21–31. https://doi.org/10.1016/j.cjche.2018.06.002

Sposato, C., Tamanini, F., Rogers, W.J., Sam Mannan, M., 2003. Effects of Plate Impingement on the Flammable Volume of Fuel Jet Releases. *Process Saf. Prog.* 22, 4. https://doi.org/10.1002/prs.680220406

Stewart, J.R., 2019. CFD modelling of underexpanded hydrogen jets exiting rectangular shaped openings. *Inst. Chem. Eng. Symp. Ser.* 2019-May.

Tchouvelev, A.V., Cheng, Z., Agranat, V.M., Zhubrin, S.V., 2007. Effectiveness of small barriers as means to reduce clearance distances. *Int. J. Hydrogen Energy* 32, 1409–1415. https://doi.org/10.1016/j.ijhydene.2006.10.020.

Tolias, I.C., Venetsanos, A.G., Comparison of convective schemes in hydrogen impinging jet cfd simulation, 2015. 6th International conference on hydrogen safety (ICHS2015).

Tolias, I. C., Giannissi, S.G., Venetsanos, A.G., Keenan, J., Shentsov, V., Makarov, D., Coldrick, S., Kotchourko, A., Ren, K., Jedicke, O., Melideo, D., Baraldi, D., Slater, S., Duclos, A., Verbecke, F., Molkov, V., 2019. Best practice guidelines in numerical simulations and CFD benchmarking for hydrogen safety applications. *Int. J. Hydrogen Energy* 44, 9050–9062. https://doi.org/10.1016/j.ijhydene.2018.06.005.

Uggenti, A.C., Carpignano, A., Savoldi, L., Zanino, R., 2017. Perspective and criticalities of CFD modelling for the analysis of oil and gas offshore accident scenarios. *Risk, Reliability and Safety: Innovating Theory and Practice: Proceedings of ESREL 2016.*

Van den Bosch, C.J.H., Weterings, R.A.P.M., Duijim, N.J., Bakkum, E.A., Mercx, W.P.M., Engelhard, W.F.J.M., Van den Berg, A.C., Van den Doormaal, J.C.A.M., van wees, R.M.M., 1997. Methods for the calculation of physical effects "Yellow book". The hague.

Witlox, H.W.M., Holt, A., 1999. A unified model for jet, heavy and passive dispersion including droplet rainout and re-evaporation. CCPS international conference& workshop on modeling the consequences of accidental releases of hazardous materials.

Xu, B.P., Wen, J.X., Tam, V.H.Y., 2011. The effect of an obstacle plate on the spontaneous ignition in pressurized hydrogen release: A numerical study. *Int. J. Hydrogen Energy* 36, 2637–2644. https://doi.org/10.1016/j.ijhydene.2010.03.143.

Zuliani, C., De Lorenzi, C., Ditali, S., 2016. Application of CFD Simulation to Safety Problems – Challenges and Experience Including a Comparative Analysis of Hot Plume Dispersion from a Ground Flare. Chem.Eng. Trans. 53, 79-84. https://doi.org/10.3303/CET1653014

.

CHAPTER 4: SAFETY EVALUATIONS ON UNIGNITED HIGH-PRESSURE METHANE JETS IMPACTING A SPHERICAL OBSTACLE

Journal of Loss Prevention in the Process Industries

SAFETY EVALUATIONS ON UNIGNITED HIGH-PRESSURE METHANE JETS IMPACTING A SPHERICAL OBSTACLE

--Manuscript Draft--

Manuscript Number:	JLP-D-20-00478
Article Type:	Full Length Article
Keywords:	High-pressure release; methane; spherical obstacle influence; risk assessment; CFD; analytical correlation
Corresponding Author:	Valentina Busini Politecnico di Milano Dipartimento di Chimica Materiali e Ingegneria Chimica Giulio Natta Milano, MI Italy
First Author:	Cristian Colombini
Order of Authors:	Cristian Colombini
	Edoardo Carminati
	Andrea Parisi
	Renato Rota
	Valentina Busini

ABSTRACT

Nowadays methane is a fossil fuel widely used both in industries and in civil appliances. From the safety point of view, due to its flammability, its use implies hazards for people and assets. The hazardous area related to a high pressure jet of methane arising from an accidental loss of containment requires the estimation of the distance at which the methane concentration falls below the Lower Flammability limit. Such a topic is well covered in the literature when considering free jet conditions, *i.e.*, jets that do not interact with any equipment or surface. The same cannot be said for high pressure jets impacting an obstacle. In this context, the present work focuses on studying high pressure methane jets impacting spherical obstacles by means of Computational Fluid Dynamics with the aim of giving some insights about such a jet-obstacle interaction, possibly providing a brief by-hand procedure that, only based on known scenario information, allows to estimate the maximum extent of the unignited high pressure jet when interacting with a spherical obstacle.

ACRONYMS

CFD Computational fluid Dynamics

EDM Equivalent Diameter Model

FF Flash Fire

EoS Equation of State

HP High-Pressure

LFL Lower Flammability Limit

ME Maximum Extent

O&G Oil and Gas

RANS Reynolds Averaged Navier-Stokes

NOMENCLATURE

A_{ps}: pseudo-source area extension

c: methane concentration in air

c_{ax}: methane concentration along the free jet axis

C_D: discharge coefficient

C_p: methane heat capacity

d: actual orifice diameter

D: distance of the centre of the spherical obstacle from the jet source

d_{FJ}: free jet diameter

D_L: obstacle legs diameter

D_{NT}: obstacle distance from the jet source

d_{ps}: pseudo-source orifice diameter

D_T: obstacle diameter

H: jet source height

k: axial decay constant

$\dot{m}_{ps}$: pseudo-source mass flow rate

ME: jet axial maximum extent

ME_{FJ}: free jet LFL cloud maximum extent in direction of the jet axis

N_L: number of obstacle legs

p: upstream methane pressure

p_{amb}: environmental pressure

p_{ps}: methane pressure at pseudo-sourceconditions

T: upstream methane temperature

T_{ps}: methane static temperature at pseudo-source conditions

v_{ps}: methane velocity at pseudo-source conditions

α: angle between vertical direction and the points in proximity of the obstacle surface where velocity is recorded

γ: specific heat ratio

ρ_{ps}: methane density at pseudo-source conditions

ρ_{amb}: air density

INTRODUCTION

Methane is a clean and efficient hydrocarbon largely used in industry, commercial and residential sectors as well as for vehicles power (Sun, 2019; Varsegova et al., 2019; Zhu et al., 2020). Together with hydrogen, methane is expected to play a relevant role in the energy sector in the future (Zhou et al., 2018; Zhang et al., 2020). It can be handled, shipped and stored in liquefied form, keeping the fluid at very low temperatures (Zhang et al., 2020) or in gaseous form (Jafari et al., 2014) at pressures much higher than the ambient one.

In the second case, which is widely common to have, one of the safety related issues is the accidental release from a High-Pressure (HP) vessel or pipeline (Zhu et al., 2013). Considering the flammable nature of the methane jet, studies on its release characteristics and flow behavior are crucial for the risk assessment and management. This because if late ignition of the release occurs, the established Flash Fire (FF) can dramatically lead to a series of subsequent large scale events threatening people and structures. Thus, the hazardous distance estimation, which is commonly evaluated as the distance where the flammable gas concentration falls below either the Lower Flammability Limit (LFL) or LFL/2, becomes a crucial information to be predicted (Souza et al., 2019b). It is, therefore, quite evident the importance of predictive computational methods by which it is possible to assess the magnitude of the unignited accidental release (Rian et al., 2016).

It should be remarked that, thinking to an industrial accidental scenario in which a leak of methane from high-pressure conditions occurs, the situation of a congested area or, more in general, of a geometrically complex environment in which the leak can be placed (*e.g.*, in the vicinity of an obstacle), it might be considered. As widely reported in literature, the analytical correlations (c.f., Becker et al., 1967; Thring and Newby, 1952; Chen and Rodi, 1980) and the integral models (c.f., DEGADIS, SLAB, ALOHA, and UDM; Brook et al., 2003; Bernatik and Libisova, 2004; EPA, 2011; Pandya et al., 2012) developed within the industrial safety framework are reliable when analyzing a free jet scenario (intended as a release occurring in an unconfined environment, Dey et al., 2017), showing they limits when dealing with a situation in which a HP jet interacts with an obstacle (Cameron and Raman, 2005; Derudi et al., 2014; Pontiggia et al., 2014; Schelder et al., 2015; Gerbec et al., 2017; Uggenti et al., 2017; Dasgotra et al., 2018). Computational Fluid Dynamics (CFD) is the numerical approach traditionally employed to face such industrial safety issue (Deng et al., 2018; Souza et al., 2019a; Tolias et al., 2019) since it allows to address for any geometrical complexity (Efthimiou et al., 2017; Gerbec et al., 2017; Luo et al., 2018; Jiang et al., 2020).

Consequently, previous literature about unignited HP jets impacting an obstacle studied with the CFD is available, as summarized in the following. Benard et al. (2007) investigated the influence of flat surfaces parallel to unignited hydrogen and methane high-pressure jets. Tchouvelev et al. (2007) combined the commercial CFD software PHOENICS with two analytical models to investigate HP unignited hydrogen releases impinging against a protective wall. Desilets et al. (2009) performed an experimental campaign aiming to characterize the shape of the plume of different unignited hydrogen jets when influenced by a nearby horizontal flat surface. For comparison purposes, CFD numerical simulations have been also carried out. Hourri et al. (2009) extended the analysis of Benard et al. (2007) adding two distances of the jet source from the surface. Benard et al. (2009) further extended the previous analyses by considering more orifice diameters, storage pressures and distances from the flat surface. Houf et al. (2010) conducted a numerical evaluation of barrier walls for the mitigation of hydrogen releases, both ignited and unignited. Middha et al. (2010) performed a small scale experimental campaign on ignited HP hydrogen jets interacting with an obstacle with the purpose of validating the commercial CFD software FLACS for this specific scenario. Hourri et al. (2011) and Angers et al. (2011) further extended the analysis of Hourri et al. (2009) considering several higher pressures and a different jet orientation, respectively. Pontiggia et al. (2014) compared the results of an integral model (PHAST) to the ones of a CFD model (FLUENT) for the case of an unignited HP methane jet impacting a cylindrical obstacle showing that, in this scenario, integral models become unreliable. Using the CFD code FLACS, Benard et al. (2016) investigated how a vertically or horizontally oriented flat surface influences the maximum extent of the lower flammability limit cloud of both hydrogen and methane unignited HP jets. They also derived engineering correlations able to substitute the use of more computationally expensive CFD software. Gerbec et al. (2017) analyzed the case of a vertical unignited propane jet impacting against the roof of a refueling station, comparing the results computed with a CFD software (FLUENT) and an integral model (UDM). They showed differences in predicting the damage area extension when using the two kinds of model. Of the same year it is the work of Hall et al. (2017), where they investigated how two horizontal surfaces (namely, the ground and the ceiling) influence unignited HP hydrogen clouds at different concentrations. Starting from the state of the art regarding CFD modeling for risk assessment of offshore installations, Uggenti et al. (2017) proposed a new hybrid approach, combining a semi-empirical model with a CFD one. Hu et al. (2018) accounted for the problem of unignited HP hydrogen jets impacting a vertical obstacle with the novelty of using a specific equation of state (EoS) (*e.g.*, Abel-Noble (Johnston, 2005)) to model gas density. Colombini

and Busini (2019a and 2019b) studied the impingement of an unignited high-pressure methane jet on a cylindrical obstacle, both horizontally and vertically oriented. The focus has been on evaluating how a realistic obstacle influences the jet behavior, as function of the geometrical parameters of the scenario. Colombini et al. (2020a and 2020b) extensively investigated the effect of the ground on an unignited high-pressure jet of methane, hydrogen, and propane. Targeting to obtain simple relationships for risk assessment, Colombini et al. (2021) performed an extensive CFD analysis of a realistic accidental scenario involving a high-pressure unignited methane jet impacting a pipe rack.

Despite, on one hand, the extensive use of the CFD in the framework of risk assessment research and, on the other one, the technological improvements of the computing resources, the CFD is not drawbacks-free: computational costs and analyst skills required are still a limitation on its use (Zuliani et al., 2016; Jiang et al., 2020). Therefore, the availability of quick and simple engineering correlations allowing the estimation of the damage area of unignited impinging accidental releases might be useful.

Based on the depicted capabilities, the idea is that an extensive one-time-use of the CFD can be exploited as database-maker from which deriving simpler analytical relationships (Jiang et al., 2020) therefore avoiding the huge costs related to a full scale experimental approach (Wilkening and Baraldi, 2007).

In this context, the present work provides quick tools for daily activities in the risk assessment field. Considering as realistic accidental situation the case of an unignited high-pressure methane jet impacting a spherical obstacle, varying the distance between the release source and the obstacle as well as obstacle diameter, storage pressure and concentration level observed, we investigated several possible configurations of this scenario. From such configurations, we derived two instruments allowing to predict: i) when the obstacle influence expires (thus allowing the use of well-established analytical correlations for the modeling of the free jet case) and, ii) when present, how, by order of magnitude, the obstacle influence can be predicted.

SCENARIO AND CFD MODEL SPECIFICS

The scenario analyzed in this work is a horizontal high-pressure methane jet impinging a spherical obstacle. To study the influence of the obstacle on the jet development, several parameters (both of jet source and obstacle) were varied: upstream methane pressure (p); obstacle diameter (D_T); distance between jet source and obstacle (D_{NT}). Notice that, obstacle geometric characteristics were considered accordingly to ASME standards (Tarsco, 2021). The methane source was modelled as generated from a nozzle located in correspondence of the mid-height of the sphere (H): in all the analysis, it was kept constant and equal to 10 m in order to avoid any influence of the ground, therefore allowing to investigate the effect of the spherical obstacle alone. Note that the effect of the ground has been already discussed in a previous work (Colombini et al., 2020a). Figure 5.1 shows a sketch of the scenario, where the relevant geometric characteristics are also defined. Different methane concentration values in air were considered apart from 5.3%, that is the methane LFL. A constant wind of 5 m/s blowing alongside and in the same direction of the jet was considered. On the overall, 264 different conditions were investigated, as summarized in Table C1 of the Supplementary Information.

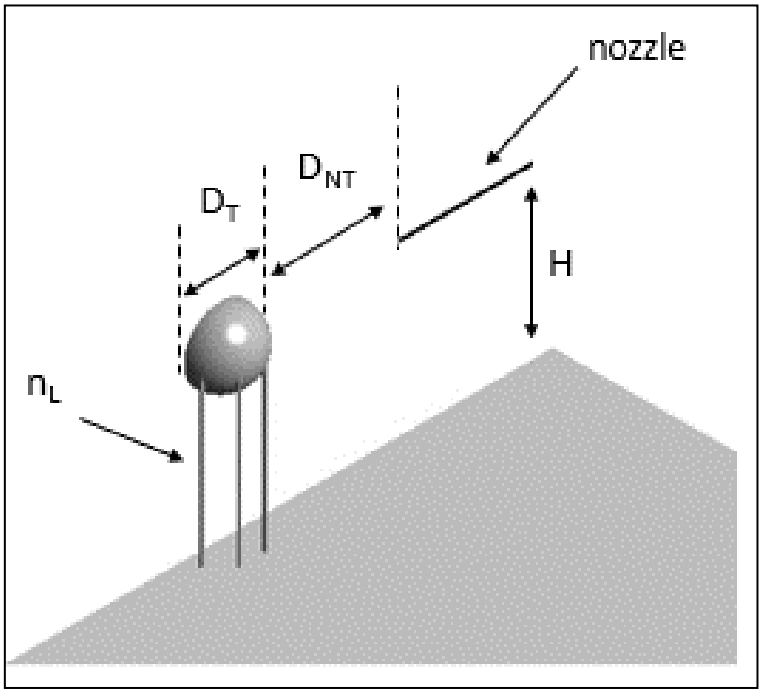

Figure 5.1: Sketch of the basic scenario, symmetric with respect to the vertical plane crossing the jet axis.

To build the CFD-computed information dataset, the commercial package Ansys Workbench v. 19.1 was used (Ansys Workbench, 2017). In particular, DesignModeler, Meshing and Fluent were the software by which realization of the computational fluid domain, fluid volume division in cells and

resolution of the fluid governing equations was performed, respectively (Ansys DesignModeler User Guide, 2017; Ansys Meshing User Guide, 2017; Ansys Fluent User Guide, 2017).

Due to a large pressure difference between the vessel/pipeline and the environment as in all the cases analyzed in this work, a supersonic jet is expected, leading to a high demand of computational resources (Colombini et al., 2020a). However, since the focus of the work is on the so-called farfield zone of the jet (*i.e.*, far from the jet source), the commonly adopted way of using empirical relationships to model the supersonic release source through the approach referred to as the Equivalent Diameter Model (EDM) has been used (Hess et al., 1973; Sposato et al., 2003; Pontiggia et al., 2014; Benard et al., 2007; Houf et al., 2007; Stewart et al., 2019; Tolias et al., 2019; Franquet et al., 2015). In particular, the model developed by Birch et al. (1984) has been used for all the computations carried out, whose equations are summarized in Table 5.1. The computational domain extents were sized following the strategy described in the work of Colombini et al. (Colombini et al., 2021) leading to a rectangular box of 120 m length, 25 m height and 15 m wide was used. Note that 15 m is half the width of the domain, thanks to the symmetry of the geometry. The strategy used for the domain discretization is discussed in detail elsewhere (Colombini et al., 2020a). In this way an optimized grid was obtained, with a finer mesh surrounding the jet axis (which is the computationally critical zone), and a less dense one close to the domain boundaries (where demanding physical phenomena are not expected). The inflation mesh feature was used for a specific grid definition of the cells surrounding the obstacle surface (Ansys Meshing User Guide, 2017). The grid obtained was tetrahedral, fully unstructured; taking run 11_M in Table C1 as example, Figure 5.2 shows how the resulting domain discretization appears. Depending on the specific case considered, which is related to the values of the involved parameters, the number of cells ranged from 3.5 to 8 million. Quality requirements in terms of skewness and orthogonal quality were always satisfied. Considering run 11_M in Table C1 as benchmark case, the grid independence of the results is summarized in Figure C1 in the Supplemental Information, which shows the comparison of the sensitivity analysis results in terms of cloud maximum axial extent (ME) variations with respect to different mesh refinements.

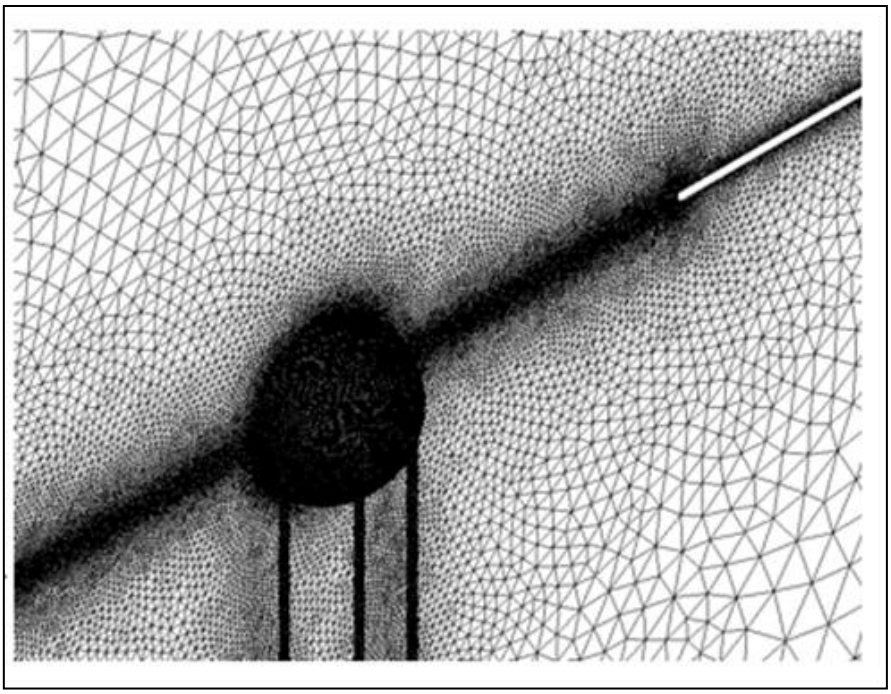

Figure 5.2: Surface grid for run 11_M.

For what concerns numerical settings, the Reynolds-averaged approach was employed for the governing Navier-Stokes equations (RANS approach) coupled with the two-equation eddy-viscosity k-ω SST turbulence closure model (Menter, 1993). All the simulations were performed in steady state conditions and the pressure-based solver was chosen thanks to the EDM approach, which allows the flow to be treated as incompressible. To account for the multi-species problem (methane release in ambient air), the species transport model was selected and the ideal gas EoS was used to model the fluid mixture density. The COUPLED pressure-velocity coupling scheme was adopted, while the second order upwind spatial-discretisation scheme was considered for all the convective terms. Table C2 in the Supplemental Information lists the model equations together with the definition of the main parameters. Gravity acceleration was always included perpendicularly to the ground surface. Table 5.1 summarizes the equations defining the methane inlet boundary condition (based on the EDM model of Birch et al., 1984), while Table 5.2 reports the other boundary conditions used.

Table 5.1: EDM equations from the Birch et al. (1984) model defining the pseudo-source of the methane jet. In the Equations, d_{ps} is the resulting diameter of the pseudo-source, d is the actual orifice diameter, C_D is the discharge coefficient, p is the storage pressure, p_{amb} is the environmental pressure, γ is the specific heat ratio, Cp is the methane heat capacity, $\dot{m}_{ps}$, v_{ps}, ρ_{ps}, T_{ps}, p_{ps} and A_{ps} are the resulting mass flow rate, velocity, density, static temperature, pressure and area extension of the pseudo-source, respectively. As indicated, methane density at the pseudo-source is computed based on the ideal gas EoS. Further details are provided in the work of Birch et al. (1984).

Pseudo-source characteristic	**Equation**
Equivalent diameter	$d_{ps} = d\sqrt{C_D\left(\frac{p}{p_{amb}}\right)\left(\frac{2}{\gamma+1}\right)^{\frac{(\gamma+1)}{2(\gamma-1)}}}$
Mass flow rate	$\dot{m}_{ps} = \rho_{ps} \cdot A_{ps} \cdot v_{ps}$
Density	$\rho_{ps} = \frac{p_{ps} \cdot MW}{R \cdot T_{ps}}$
Pressure	$p_{ps} = p_{amb}$
Static temperature	$T_{ps} = T_{amb}$

Table 5.2: Boundary conditions assignments used for all the simulations.

Boundary name	Type	Specifics
Back side	Velocity inlet	air, v_z = 5 m/s, T = 300 K
Top side	Velocity inlet	air, v_z = 5 m/s, T = 300 K
Left side	Velocity inlet	air, v_z = 5 m/s, T = 300 K
Ground	Wall	0.01 m roughness height, adiabatic
Symmetry	Symmetry	-
Front side	Pressure outlet	air, $T_{BACKFLOW}$ = 300 K
Nozzle	Wall	0.001 m roughness height, adiabatic
Methane jet	Mass flow inlet	Computed case by case according to Birch et al. (1984) model equations. See Table 5.1
Spherical obstacle	Wall	0.001 m roughness height, adiabatic

QUANTITATIVE RESULTS AND DISCUSSION

The reliability of the present CFD modeling approach has been already demonstrated elsewhere (Colombini et al., 2020a), where the CFD results have been successfully compared to results derived from experimental campaigns on HP methane free jets. Therefore, it has not been further investigated in this work.

Prior to go through the results analysis, it has to be note that, to keep the focus of the work on the spherical obstacle influence, all the scenarios considered do not include any ground effect. Therefore, in Table C1 of the Supplemental information (which collects information and results related to all the scenarios considered in this work), the cases for which the ground interference was notified were not considered. The first analysis performed was on the influence that legs (possibly coupled to a spherical obstacle to mime the usual spherical tanks configuration) have on the jet development. Considering run 10_M in Table C1, Figure 5.3 clearly shows how the legs deviate toward the ground the jet cloud, considerably reducing its axial maximum extent (ME). This can be explained by comparing the flow fields of the two situations (see *Figure 5.4*): without legs, the flow field around the sphere is completely symmetric, while with legs the flow passing under the obstacle is disturbed, leading to a reduction of its velocity with respect to the flow on the top. As a consequence of this velocity imbalance, the flow is downward deviated.

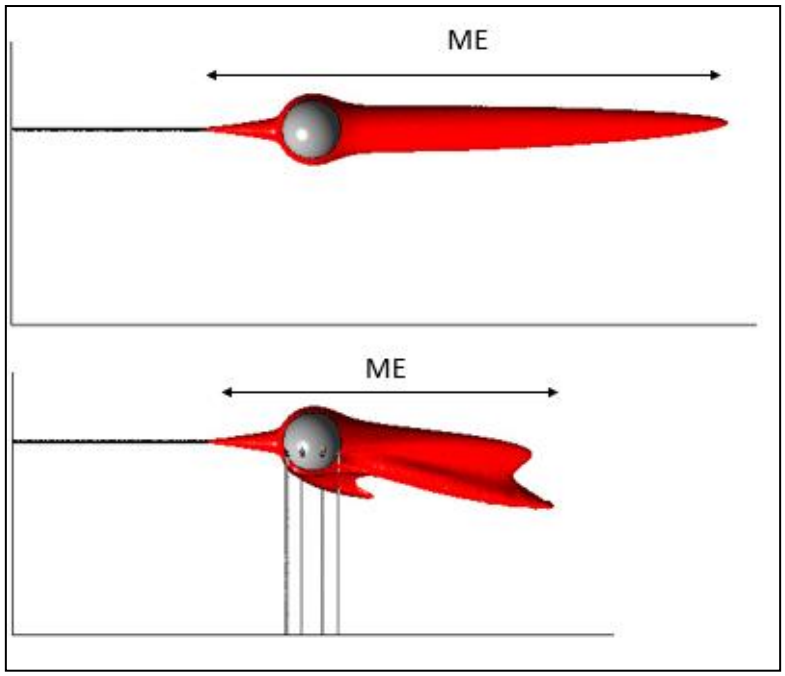

Figure 5.3: Comparison of the jet clouds around the sphere with and without legs in terms of mole fraction isosurfaces (c = 5.3 %).

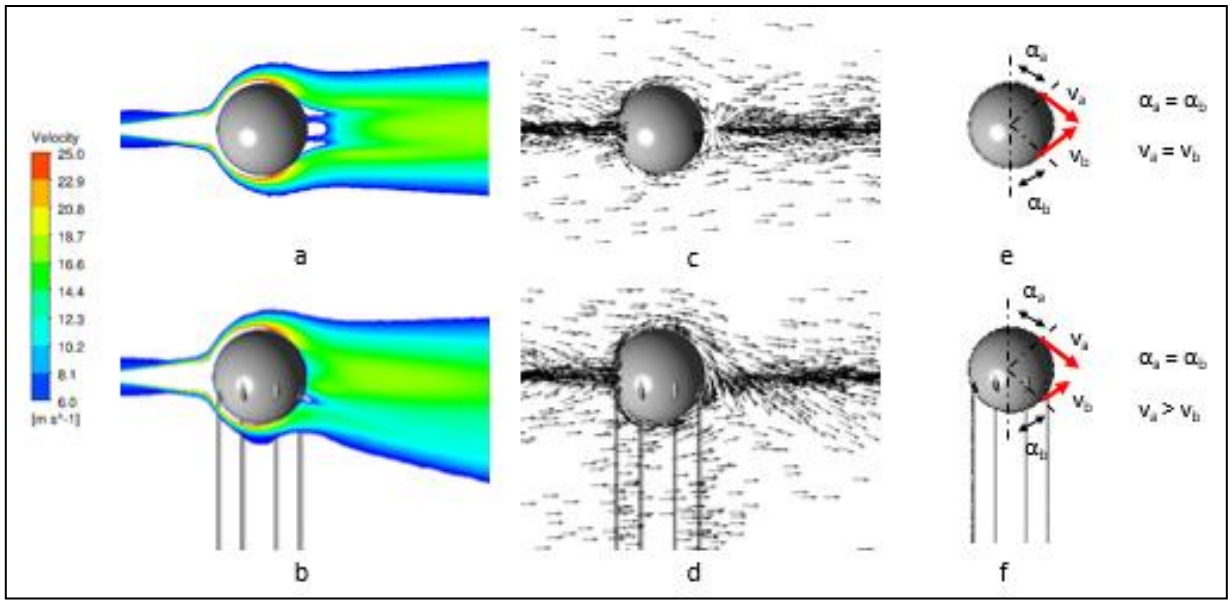

Figure 5.4: Comparison of the flow field around the obstacles in terms of velocity contours (a and b), and vectors plot along the vertical symmetry plane of the domain (c and d). Fig. e and f schematize the velocities, highlighting the difference in their intensity (α is the angle between the vertical direction and the points in proximity of the solid surfaces where velocities are recorded).

To show how any of the scenario parameters introduced in Section *SCENARIO AND CFD MODEL SPECIFICS* modifies the jet cloud development, Figure 5 reports the isosurfaces of some of the runs listed in Table C1.

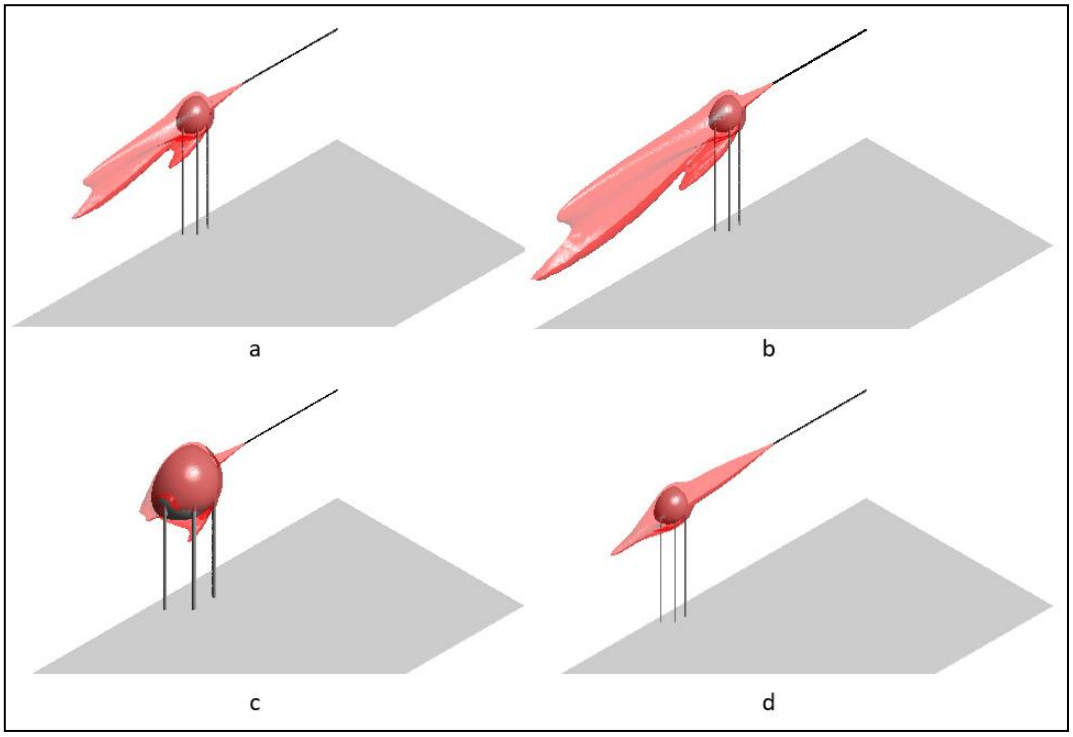

*Figure 5.5: Isosurfaces of the methane jet interacting with the spherical obstacle for some of the runs in Table C1*Table C1*: (a) run 10_M; (b) run 50_M (greater upstream pressure); (c) run 26_M (greater D_T); (d) run 13_M (greater obstacle-jet source distance).*

By way of example, considering run 10_M as reference case (Figure 5.5a), comparing the Figures shown we can say that, qualitatively: i) a greater upstream pressure (doubled) leads to a longer jet cloud (nearly 60 %) (Figure 5.5b, referred to run 50_M); ii) a greater obstacle diameter (doubled) leads to a shorter jet cloud that ends just over the obstacle (Figure 5.5c, referred to run 26_M); iii) a greater distance from the jet source (2.5 times) leads to a jet cloud practically of the same length of the one in the reference case (Figure 5.5d, referred to run 13_M). As a general observation, in all the cases shown in Figure 5.5 the jet cloud passes over the spherical obstacle. A more detailed analysis of the effect that each of the scenario parameters has on the jet cloud development is provided in Section *QUALITATIVE RESULTS AND DISCUSSION*.

The results of the runs in Table C1 have been analysed with the help of the parameters sketched in *Figure 5.6*, namely: ME_{FJ}, which is the cloud ME computed for the correspondent free jet; and $d_{FJ}(D)$, which is the free jet diameter evaluated in correspondence of the spherical obstacle centre position.

Note that both ME_{FJ} and $d_{FJ}(D)$ can be easily estimated using analytical correlations, as discussed elsewhere (Colombini et al., 2021).

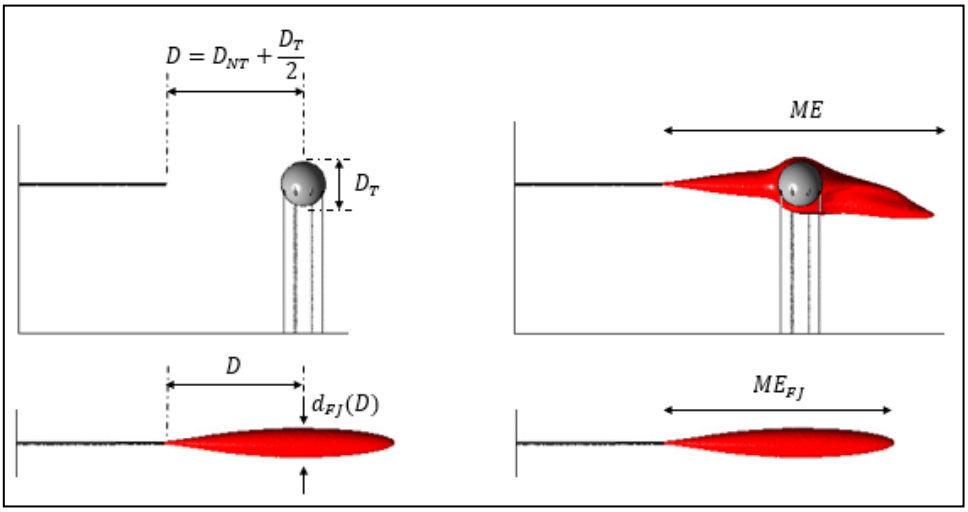

Figure 5.6: Parameters used to analyse the results of the runs in Table C1.

These two parameters have been used to define two dimensionless parameters with the physical meaning of a ratio between two characteristic dimensions (one of the free jet, the other of the sphere: $d_{FJ}(D)/D_T$) and between two ME values (one of the jet impinging the sphere, the other of the free jet: ME/ME_{FJ}).

Figure 5.7 shows the results of the simulations carried out in terms of these two dimensionless parameters. From the Figure we can see a clear trend showing how the spherical obstacle influences the jet development:

- up to $d_{FJ}(D)/D_T \approx 0.5$, ME of the jet cloud is lower than (or equal to) the ME_{FJ} (considering a 10 % safety margin around $ME/ ME_{FJ} = 1$);
- for $d_{FJ}(D)/D_T$ comprised between about 0.5 and about 1, ME of the jet cloud linearly increases up to be conservatively 1.5 times greater than the ME_{FJ};
- over $d_{FJ}(D)/D_T \approx 1$, ME/ME_{FJ} of the jet cloud becomes almost constant (and conservatively equal to 1.5).

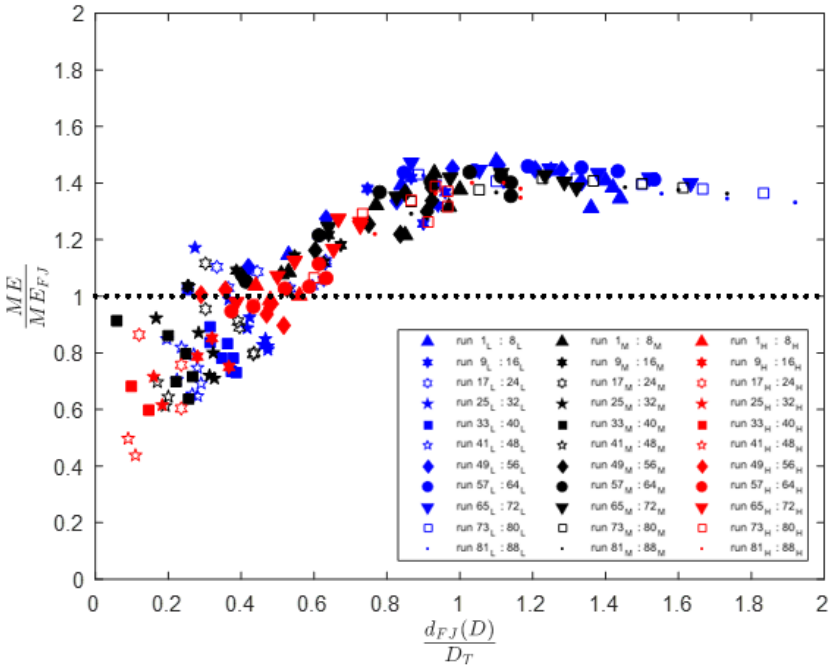

Figure 5.7: Results of runs in Table C1. Markers colour defines the methane concentration level observed: blue is for the low level (c = 3.5 %), red is for the mean level (c = 5.3 %) and black is for the high level (c = 10 %). In the Figure, the dotted line identifies when the jet cloud ME is equal to the ME of the correspondent free jet.

Therefore, independently on the scenario specifics, the spherical obstacle induces two main effects:

- when the obstacle diameter is, at least, two times the free jet width (evaluated in correspondence of the obstacle centre position), the obstacle acts more like a wall and it reduces the cloud ME with respect to the correspondent free jet, leading to a safer situation;
- when the free jet width (evaluated in correspondence of the obstacle centre position) is, at least, half of the obstacle diameter, the jet cloud ME results to be increased with respect to the correspondent free jet, leading to a less safe situation; in the worst case, the ME of the free jet is almost 1.5 times increased by the presence of the obstacle.

This can be summarized in the following conservative relations to estimate the ME of methane jet impinging a spherical obstacle:

$$\begin{cases} ME \sim ME_{FJ} & if \quad \dfrac{d_{FJ}(D)}{D_T} < 0.5 \\ ME \sim 1.5 \cdot ME_{FJ} & if \quad \dfrac{d_{FJ}(D)}{D_T} \geq 0.5 \end{cases}$$

QUALITATIVE RESULTS AND DISCUSSION

This Section provides an analysis highlighting, by a general point of view, what is the qualitative effect on the jet cloud development when some characteristic parameters of a jet impacting a spherical obstacle are alternatively varied. These parameters are both some of the ones defined in Section *SCENARIO AND CFD MODEL SPECIFCICS* (*i.e.*, p, D_T, and c) and others not previously considered, such as the number of legs and the legs diameter.

An increase of the upstream pressure value leads to an increase of the mass flow rate, resulting in a larger jet cloud, as shown in *Figure 5.8* for four runs of Table C1 (namely, run 12_M, 52_M, 68_M and 84_M). As expected from the results summarized in *Figure 5.7*, since in these cases $d_{FJ}(D)/D_T$ is always larger than 0.5 we found that the ratio ME/ME_{FJ} is always greater than one and equal to about 1.2-1.3.

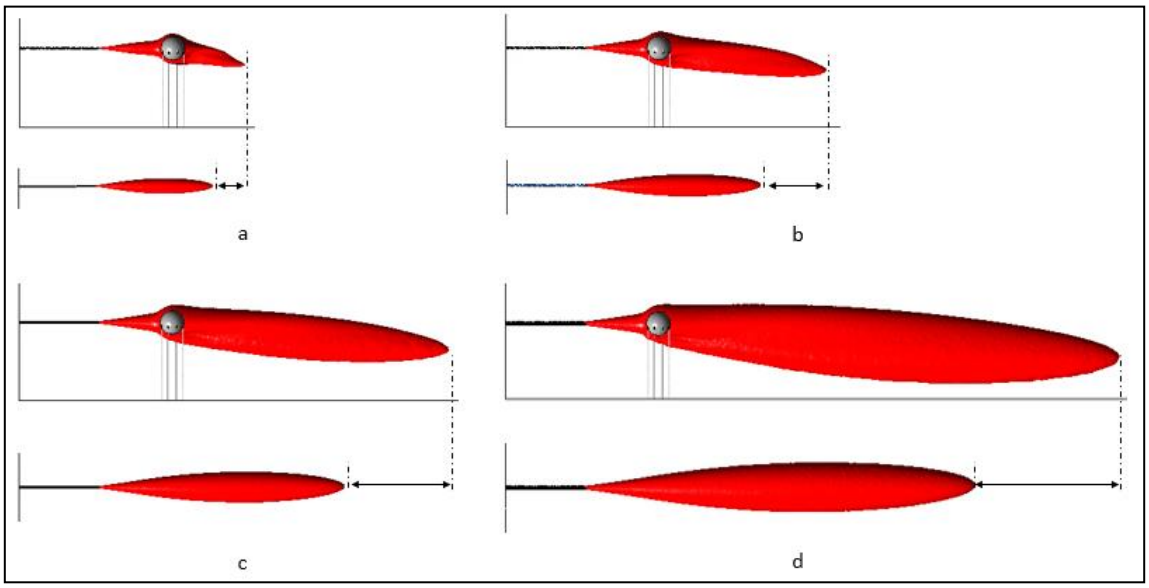

Figure 5.8: Results of the sensitivity analysis on the effect that a variation of p has on the jet cloud development, in terms of isosurfaces of methane concentration in air equal to 5.3%, when the same spherical obstacle is impinged. (a) p = 65 bar (run 12_M); (b) p = 130 bar (run 52_M); (c) p = 260 bar (run 68_M); (d) p = 650 bar (run 84_M).

Considering a variation of the obstacle diameter, the larger D_T is, the more the jet path is obstructed by the obstacle. Therefore, it can be expected that an increase of D_T will result in a decrease of the jet cloud extent. In fact, the isosurfaces of methane concentration in air (c = 5.3 %) compared in *Figure 5.9* for four selected runs of Table C1 (namely, run 9_M, 17_M, 25_M and 33_M) confirm what foreseen. About D_T variation, it is also interesting to note that the larger the D_T is, the more the

deviation of the jet cloud toward the ground is, downstream the obstacle. The reason can be explained by looking at the flow field around the spherical obstacles. The larger the D_T is, the more the velocity intensity of the jet is reduced downstream the obstacle. Coupling this effect with the legs one (i.e., that generates a velocity imbalance between the flows passing immediately above and below the obstacle), it leads to a predominance of the flow coming from the top side, resulting in a more downward deflection of the downstream flow field (see *Figure 5.10*).

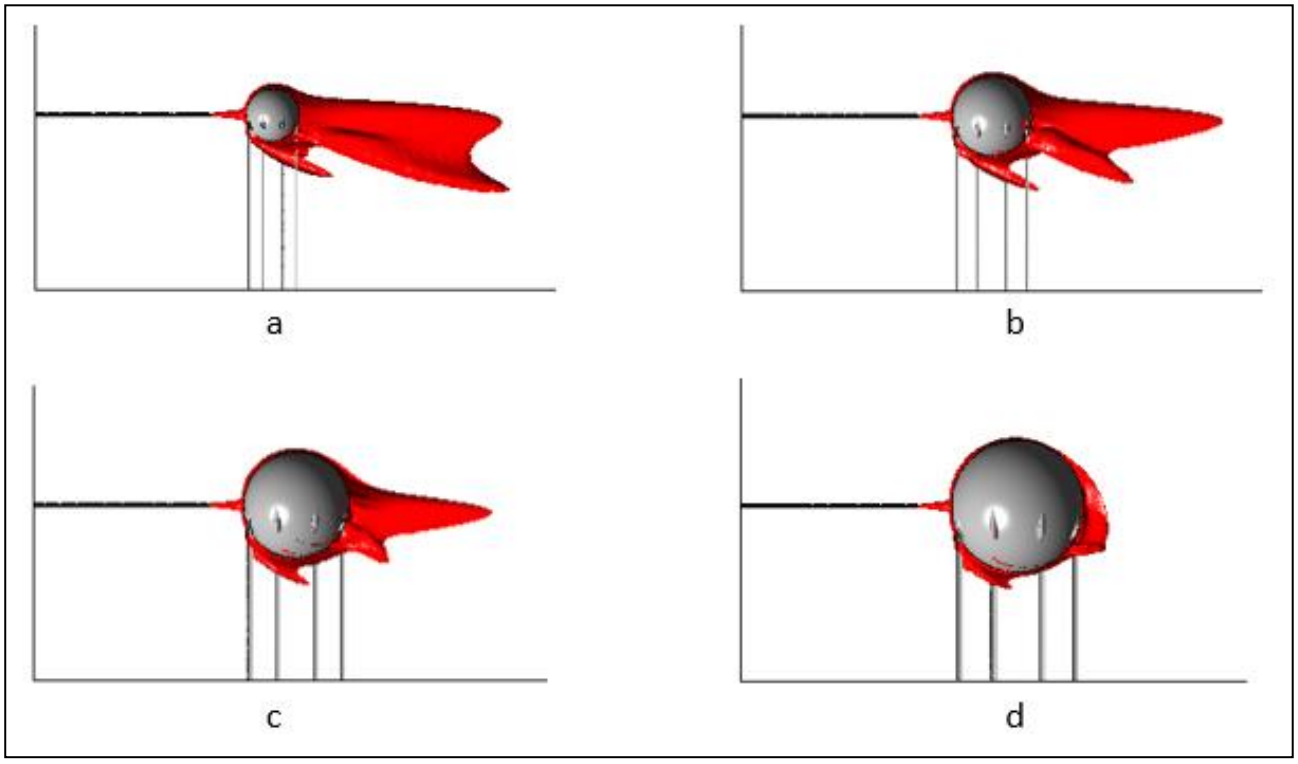

Figure 5.9: Sensitivity analysis on the effect that a variation of D_T has on the jet cloud development. Results are in terms of isosurfaces of methane concentration in air equal to 5.3%, when same jet source is considered. (a) D_T = 3 m (run 9_M); (b) D_T = 4.5 m (run 17_M); (c) D_T = 6 m (run 25_M); (d) D_T = 7.5 m (run 33_M).

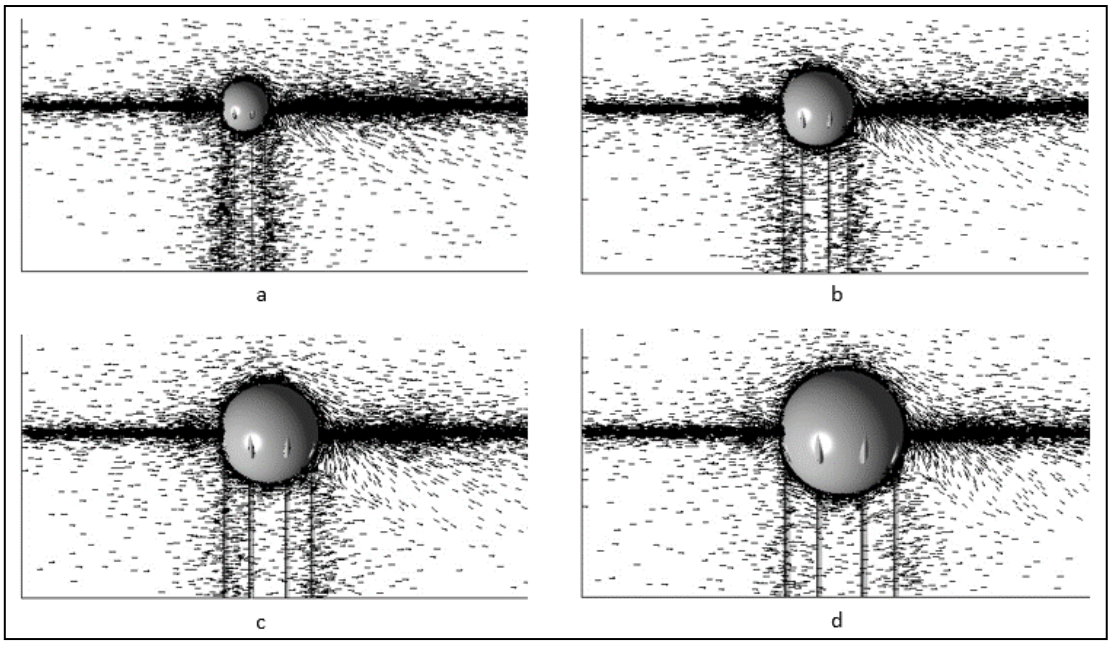

Figure 5.10: Sensitivity analysis on the effect that the variation of D_T has on the jet cloud development. Results are in terms of flow field vectors plot with same jet source considered. (a) D_T = 3 m (run 9_M); (b) D_T = 4.5 m (run 17_M); (c) D_T = 6 m (run 25_M); (d) D_T = 7.5 m (run 33_M).

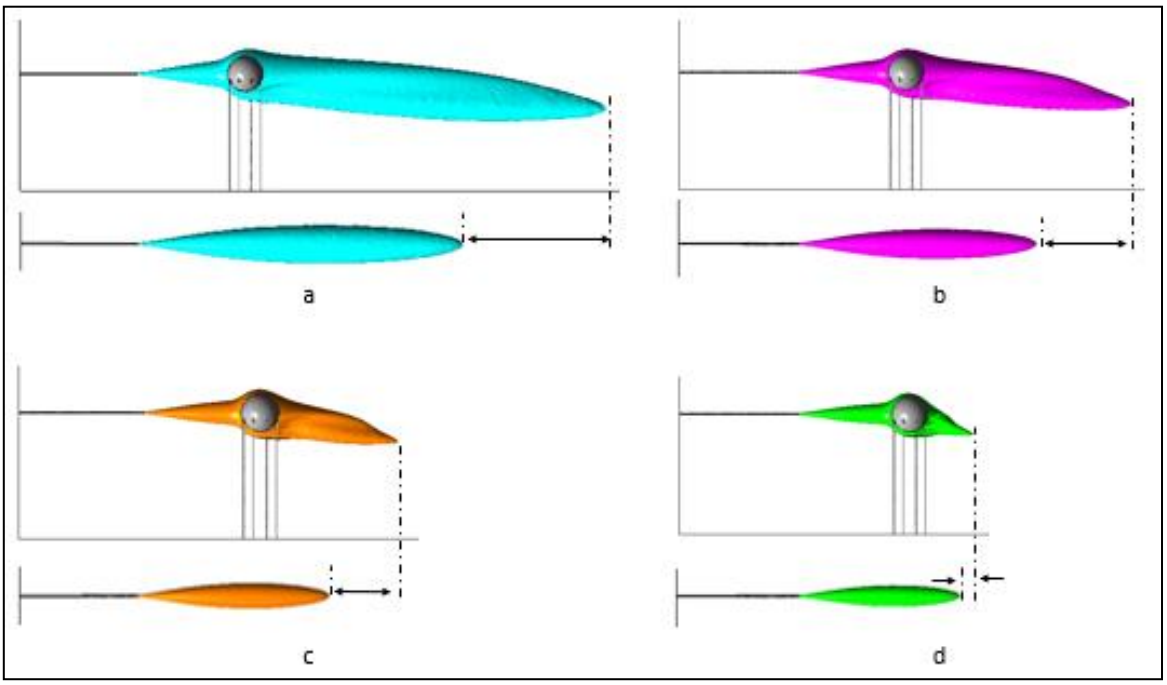

Figure 5.11: Sensitivity analysis on the effect that a variation of observed methane concentration has on the jet cloud development. Results are in terms of isosurfaces of methane concentration in air equal to: 3% (a); 4% (b); 5% (c); and 6% (d).

Lowering the observed concentration of methane in air leads to increase the cloud size. Therefore, as expected from the results summarized in Figure 5.7, the greater the size of the jet cloud is, the larger the obstacle influence on the cloud development is expected to be. Considering run 12_M of

Table C1, Figure 5.11 shows that the lower the concentration level observed is, the more the influence of the spherical obstacle on the jet cloud results to be.

Focusing on how the jet cloud may be modified only by obstacle legs characteristics, two analysis varying alternatively the number of legs and their diameter were performed. Starting from what observed in Section *QUANTITATIVE RESULTS AND DISCUSSION*, we can say that the more the number and diameter of the legs are, the more the interference on the flow field will be expected to be enhanced. Therefore, a shorter and more downward directed jet cloud would be expected for larger values of D_L or N_L. Considering run 9_M of Table C1 as benchmark case (Figure 5.12a), Figure 5.12b (where D_L was varied) and 5.12c (where N_L was varied) confirm such legs-related effect. As we can see, both an increase of N_L (Figure 5.12a with respect to Figure 5.12c) and D_L (Figure 5.12b with respect to Figure 5.12a) leads to a ME reduction together with a cloud more oriented towards the ground. From the Figures, it is noticeable that, with respect to a reasonable variation of the two legs characteristics within a realistic range (namely, new $N_L = 4$ while new $D_L = 0.353$ m), the variation of N_L largely affects the jet cloud development with respect to what a similar variation of D_L does.

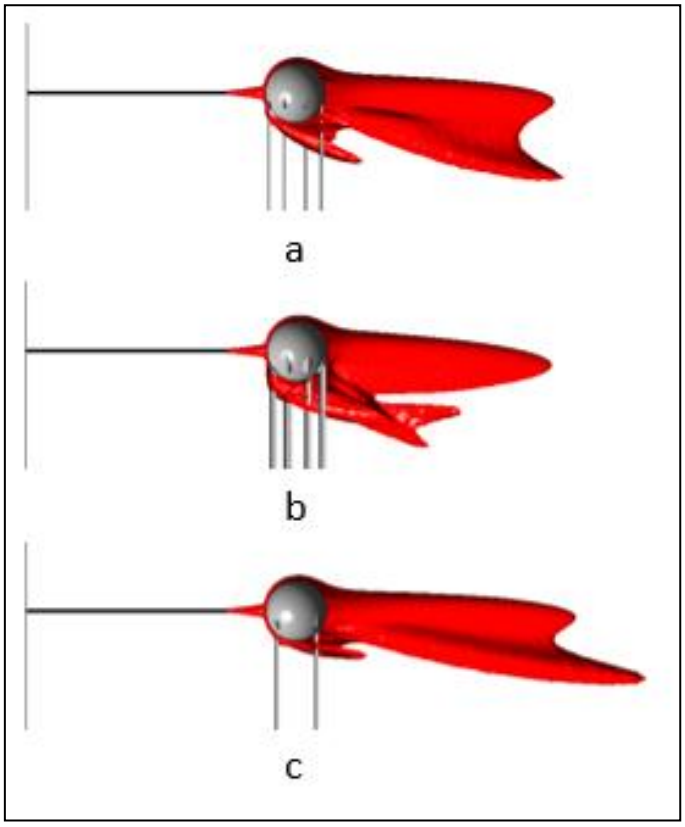

Figure 5.12: Sensitivity analysis on the effect that a variation of legs number (N_L) or legs diameter (D_L) has on the jet cloud development. (a) run 9_M; (b) double legs diameter; (c) half the legs number. Results are in terms of isosurfaces of methane concentration in air equal to 5.3 %.

CONCLUSIONS

As a matter of fact, the methane high-pressure gaseous release is a relevant safety-related problem mainly in the Oil and Gas (O&G) industry. In this work, the scenario of a spherical obstacle impinged by a methane HP jet was investigated through a CFD-based model. The analysis showed that the spherical obstacle either decreases or increases the ME of the jet cloud with respect to the free jet. However, conservative rules of thumb to estimate the influence of a spherical obstacle on the ME of an impinging jet can be summarized as follows:

1. From the source characteristics, estimate the ME_{FJ} value using the Chen and Rodi (1980) concentration decay model, whose model reliability in estimating ME_{FJ} is discussed elsewhere (Colombini et al., 2020a):

$$ME_{FJ} = \frac{k d_{ps}}{\bar{c}} \left(\frac{\rho_{amb}}{\rho_{ps}} \right)^{\frac{1}{2}}$$

Here $\bar{c}$ is the specific methane concentration in air considered, k is the axial decay constant (equal to 4.4, as suggested by Birch et al., 1984), d_{ps} is the pseudo-source orifice diameter (computed with the model of Birch et al., 1984: seeTable 5.1), ρ_{amb} is the air density, and ρ_{ps} is the methane density at pseudo-source conditions.

2. From the source characteristics, estimate $d_{FJ}(D)$ as (Cushman-Roisin, 2020; Chen and Rodi, 1980):

$$d_{FJ}(D) = 2 \cdot \sqrt{-\frac{D^2}{50} \cdot \ln\left(\frac{\bar{c}}{c_{ax}(D)} \right)}$$

$$c_{ax}(D) = \frac{k d_{ps}}{D} \left(\frac{\rho_{amb}}{\rho_{ps}} \right)^{\frac{1}{2}}$$

wherwhere D is the distance of the spherical obstacle centre from the jet source, $c_{ax}(D)$ is the methane concentration along the free jet axis computed in correspondence of the spherical obstacle centre position. Also, the Cushman-Roisin (2020) model reliability in estimating $d_{FJ}(D)$ is discussed in detail elsewhere (Colombini et al., 2021).

3. If $d_{FJ}(D) / D_T < 0.5$, ME_{FJ} provides a conservative order of magnitude of ME
4. If $d_{FJ}(D) / D_T \geq 0.5$, a conservative order of magnitude of ME can be estimated as 1.5 ME_{FJ}

Finally, it should be stressed that this procedure is expected to provide a reasonable, and conservative by the industrial safety point of view, estimation as an order of magnitude of ME only

inside the parameter window investigated (*i.e*., for methane only, for upstream pressures between 65 and 650 bar, for upstream temperature equal to 278 K, for orifice diameter equal to 0.0254, for spherical obstacle diameters between 2 and 10 m, for distances of the obstacle from the source between 25 and 100 % of the free jet length and for methane concentration levels observed between 3.5 and 10 %). In particular, the effect of the presence of more than one obstacle, as well as that of an obstacle together with the ground, have not been investigated and they deserve further investigations. Therefore, the use of detailed CFD simulations should be always considered both for confirming the estimated values, and for obtaining more reliable estimation in more complex scenarios.

REFERENCES

Angers, B., Hourri, A., Benard, P., Tchouvelev, A., 2011. Numerical investigation of a vertical surface on the flammable extent of hydrogen and methane vertical jets. *Int. J. Hydrogen Energy* 36, 2567-72.

Ansys DesignModeler User's Guide, 2017. Release 19.0. ANSYS, Inc.

Ansys Fluent User's Guide, 2017. Release 19.0. ANSYS, Inc.

Ansys Meshing User's Guide, 2017. Release 19.0. ANSYS, Inc.

Ansys Workbench User's Guide, 2017. Release 19.0. ANSYS, Inc.

Becker, H.A., Hottel, H.C., williams, G.C., 1967. The nozzle-fluid concentration of the round, turbulent free jet. *J. Fluid Mech.* 30, 285-303. https://doi.org/10.1017/S0022112067001430

Bénard, P., Tchouvelev, A., Hourri, A., Chen, Z., Angers, B., 2007. High pressure hydrogen jets in the presence of a surface. *Int. Conf. Hydrog. Saf.* 40.

Bénard, P., Hourri, A., Angers, B., Tchouvelev, A., Agranat, V., 2009. Effects of surface on the flammable extent of hydrogen jets. *Int. Conf. Hydrog. Saf*.

Bénard, P., Hourri, A., Angers, B., Tchouvelev, A., 2016. Adjacent surface effect on the flammable cloud of hydrogen and methane jets: Numerical investigation and engineering correlations. *Int. J. Hydrogen Energy* 41, 18654–18662. https://doi.org/10.1016/j.ijhydene.2016.08.173.

Bernatik, A., Libisova, M., 2004. Loss prevention in heavy industry: Risk assessment of large gasholders. *J. Loss Prev. Process Ind.* 17(4), 271.

Birch, A.D., Brown, D.R., Dodson, M.G., Swaffield, F., 1984. The structure and concentration decay of high pressure jets of natural gas. *Combust. Sci. Technol.* 36, 249–261. https://doi.org/10.1080/00102208408923739.

Brook, D. R., Felton, N. V., Clem, C. M., Strickland, D. C. H., Griffiths, I. H., Kingdon, R. D., 2003. Validation of the urban dispersion model (UDM). *Int. J. Environ. Pollut.* 20 (1−6), 11.

Cameron, I., Raman, R., 2005. Process System Risk Management, first ed. Elsevier Amsterdam.

Chen, C.J., Rodi, W., 1980. Vertical Turbulent Buoyant Jets – A review of Experimental Data, First ed. Pergamon Press Vol. 4.

Colombini, C., Busini, V., 2019a. Obstacle Influence on High-Pressure Jets based on Computational Fluid Dynamics Simulations. *Chem. Eng. Trans.* 77, 811–816. https://doi.org/10.3303/CET1977136.

Colombini, C., Busini, V., 2019b. High-Pressure Methane Jet: Analysis of the Jet-Obstcle Interaction. *Proceeding of the 29th European Safety and Reliability Conference.*

Colombini, C., Martani, A., Rota, R., Busini, V., 2020a. Ground influence on high-pressure methane jets: Practical tools for risk assessment. *J. Loss Prevent. Proc.* 67, 104240. https://doi.org/10.1016/j.jlp.2020.104240

Colombini, C., Carlini, L., Rota, R., Busini, V., 2020b. Ground Interaction on High-Pressure Jets: Effect on Different Substances. *Chem. Eng. Trans.* 82. https://doi.org/10.3303/CET2082062

Colombini, C., Maugeri G., Zanon, G., Rota, R., Busini, V., 2021. Unignited High-Pressure Methane Jet Impinging a Pipe Rack: Practical Tools For Risk Assessment. *J. Loss Prevent. Proc.* 69, 104378. https://doi.org/10.1016/j.jlp.2020.104378

Cushman-Roisin, B., Environmental Fluid Mechanics – John Wiley & Sons, Book in preparation. Last online access: August

2020. http://www.dartmouth.edu/~cushman/books/EFM/chap9.pdf

Dasgotra, A., Varun Teja, G. V.V., Sharma, A., Mishra, K.B., 2018. CFD modeling of large-scale flammable cloud dispersion using FLACS. *J. Loss Prev. Process Ind.* 56, 531–536. https://doi.org/10.1016/j.jlp.2018.01.001.

Deng, Y., Hu, H., Yu, B., Sun, D., Hou, L., Liang, Y., 2018. A method for simulating the release of natural gas from the rupture of high-pressure pipelines in any terrain. *J. Hazard. Mater.* 342, 418–428. https://doi.org/10.1016/j.jhazmat.2017.08.053.

Derudi, M., Bovolenta, D., Busini, V., Rota, R., 2014. Heavy gas dispersion in presence of large obstacles: Selection of modeling tools. *Ind. Eng. Chem. Res.* 53, 9303–9310. https://doi.org/10.1021/ie4034895.

Desilets, S., Cote, S., Nadau, G., Benard, P., Tchouvelev, A., 2009. Experimental results and comparison with simulated data of a low pressure hydrogen jet. *Int. Conf. Hydrog. Saf*.

Dey, S., Kishore, G.R., Castro-Orgaz, O., Ali, S.Z., 2017. Hydrodynamics of submerged turbulent plane offset jets. *Phys. Fluids* 29. https://doi.org/10.1063/1.4989559.

Efthimiou, G.C., Andronopoulos, S., Tavares, R., Bartzis, J.G., 2017. CFD-RANS prediction of the dispersion of a hazardous airborne material released during a real accident in an industrial environment. *J. Loss Prev. Process Ind.* 46, 23–36. https://doi.org/10.1016/j.jlp.2017.01.015.

EPA, 2011. Computer-Aided management of emergency operations (CAMEO), ALOHA v.5.4.1, http://epa.gov/ceppo/cameo/aloha.htm

Franquet, E., Perrier, V., Gibout, S., Bruel, P., 2015. Free underexpanded jets in a quiescent medium: A review. *Prog. Aerosp. Sci.* 77, 25–53. https://doi.org/10.1016/j.paerosci.2015.06.006.

Gerbec, M., Pontiggia, M., Antonioni, G., Tugnoli, a., Cozzani, V., Sbaouni, M., Lelong, R., 2017. Comparison of UDM and CFD simulations of a time varying release of LPG in geometrical complex environment. *J. Loss Prev. Process Ind.* 45, 56–68. https://doi.org/10.1016/j.jlp.2016.11.020.

Hall, J.E., Hooker, P., O'Sullivan, L., Angers, B., Hourri, A., Benard, P., 2017. Flammability profiles associated with high-pressure hydrogen jets released in close proximity to surfaces. *Int. J. Hydrogen Energy* 42, 7413–7421. https://doi.org/10.1016/j.ijhydene.2016.05.113.

Hess, K., Leukel, W., Stoeckel, A., 1973. Formation of explosive clouds on overhead release and preventive measure. *Chemie-Ingenieur-Technik* 45, 5.

Houf, W., Schefer, R., Evans, G., Merilo, E., Groethe, M., 2010. Evaluation of barrier walls for mitigation of unintended releases of hydrogen. *Int. J. Hydrogen Energy* 35, 4758–4775. https://doi.org/10.1016/j.ijhydene.2010.02.086.

Hourri, A., Angers, B., Bénard, P., 2009. Surface effects on flammable extent of hydrogen and methane jets. *Int. J. Hydrogen Energy* 34, 1569–1577. https://doi.org/10.1016/j.ijhydene.2008.11.088.

Hourri, A., Angers, B., Bénard, P., Tchouvelev, A., Agranat, V., 2011. Numerical investigation of the flammable extent of semi-confined hydrogen and methane jets. *Int. J. Hydrogen Energy* 36, 2567–2572. https://doi.org/10.1016/j.ijhydene.2010.04.121.

Hu, J., Christopher, D.M., Li, X., 2018. Simplified partitioning model to simulate high pressure under-expanded jet flows impinging vertical obstacles. *Int. J. Hydrogen Energ*. 43, 13649-13658. https://doi.org/10.1016/j.ijhydene.2018.05.036

Jafari, M., Mohammadfam, I., Zarei, I., 2014. Analysis and Simulation of Severe Accidents in a Steam Methane Reforming Plant. *Int. J. Occup. Hyg.* 6, 120-130.

Jhonston, I.A., 2005. The Noble-Abel Equation of State: Thermodynamic Derivations for Ballistics Modelling. *Weapons Systems Division Defence Science and Technology Organisation*. DSTO-TN-0670.

Jiang, Y., Xu, Z., Wei, J., Teng, G., 2020. Fused CFD-interpolation model for real-time prediction of hazardous gas dispersion in emergency rescue. *J. Loss Prev. Process Ind.* 63, 103988. https://doi.org/10.1016/j.jlp.2019.103988.

Luo, T., Yu, C., Liu, R., Li, M., Zhang, J., Qu, S., 2018. Numerical simulation of LNG release and dispersion using a multiphase CFD model. *J. Loss Prev. Process Ind.* 56, 316–327. https://doi.org/10.1016/j.jlp.2018.08.001.

Menter, F.R., 1993. Zonal Two Equation kω Turbulence Models for Aerodynamic Flows. *24th Fluid Dynamics Conference*.

Middha, P., Hansen, O.R., Grune, J., Kotchourko, A., 2010. CFD calculations of gas leak dispersion and subsequent gas explosions: Validation against ignited impinging hydrogen jet experiments. *J. Hazard. Mater.* 179, 84–94. https://doi.org/10.1016/j.jhazmat.2010.02.061.

Pandya, N., Gabas, N., Marsden, E., 2012. Sensitivity analysis of Phast's atmospheric dispersion model for three toxic materials (nitric oxide, ammonia, chlorine). *J. Loss Prev. Process Ind.* 25 (1), 20.

Pontiggia, M., Busini, V., Ronzoni, M., Uguccioni, G., Rota, R., 2014. Effect of large obstacles on high momentum jets dispersion. *Chem. Eng. Trans.* 36, 523–528. https://doi.org/10.1016/j.jhazmat.2009.06.064.

Rian, K., Evanger, T., Vembe, B., Lilleheie, N., Lakså, B., Hjertager, B., Magnussen, B., 2016. Coherent computational analysis of large-scale explosions and fires in complex geometries – from combustion science to a safer oil and gas industry. *Chem. Eng. Trans* 48, 175-180 https://doi.org/10.3303/CET1648030

Schleder, A.M., Pastor, E., Planas, E., Martins, M.R., 2015. Experimental data and CFD performance for cloud dispersion analysis: The USP-UPC project. *J. Loss Prev. Process Ind.* 38, 125-138.

Souza, A. O., Luiz, A. M., Neto A. T. P., Araujo A. C. B., Silva H. B., Silva A. K., Alves J. J. N, 2019a. A new correlation for hazardous area classification based on experiments and CFD predictions. *Process Saf. Prog.* 38, 21–26. https://doi.org/10.1002/prs.11974.

Souza, A. O., Luiz, A. M., Neto A. T. P., Araujo A. C. B., Silva H. B., Silva A. K., Alves J. J. N, 2019b. CFD predictions for hazardous area classification. *Chinese J. Chem. Eng.* 27, 21–31. https://doi.org/10.1016/j.cjche.2018.06.002

Sposato, C., Tamanini, F., Rogers, W.J., Sam Mannan, M., 2003. Effects of Plate Impingement on the Flammable Volume of Fuel Jet Releases. *Process Saf. Prog.* 22, 4. https://doi.org/10.1002/prs.680220406

Stewart, J.R., 2019. CFD modelling of underexpanded hydrogen jets exiting rectangular shaped openings. *Inst. Chem. Eng. Symp. Ser.* 2019-May.

Sun, Z.-Y., 2019. Experimental studies on the explosion indices in turbulent stoichiometric H2/CH4/air mixtures. *Int. j. hydrogen energ.* 44, 469-476 https://doi.org/10.1016/j.ijhydene.2018.02.094

Tarsco, 2021. Spheres (ASME) – Spherical shaped storage. https://tfwarren.com/tarsco/products/asme-storage-spheres. Last access: 31/01/2021.

Tchouvelev, A.V., Cheng, Z., Agranat, V.M., Zhubrin, S.V., 2007. Effectiveness of small barriers as means to reduce clearance distances. *Int. J. Hydrogen Energy* 32, 1409–1415. https://doi.org/10.1016/j.ijhydene.2006.10.020.

Thring, M.W.,Newby, M.P., Combusiton length of enclosed turbulent jet flames, 1952. 4th International symposium on combusiton, 789, williams and Wilkins, Pittsburgh, PA.

Tolias, I. C., Giannissi, S.G., Venetsanos, A.G., Keenan, J., Shentsov, V., Makarov, D., Coldrick, S., Kotchourko, A., Ren, K., Jedicke, O., Melideo, D., Baraldi, D., Slater, S., Duclos, A., Verbecke, F., Molkov, V., 2019. Best practice guidelines in numerical simulations and CFD benchmarking for hydrogen safety applications. *Int. J. Hydrogen Energy* 44, 9050–9062. https://doi.org/10.1016/j.ijhydene.2018.06.005.

Uggenti, A.C., Carpignano, A., Savoldi, L., Zanino, R., 2017. Perspective and criticalities of CFD modelling for the analysis of oil and gas offshore accident scenarios. *Risk, Reliability and Safety: Innovating Theory and Practice:*

Proceedings of ESREL 2016.

Varsegova, E., Dresvyannikova, E., Osipova, L., Sadykov, R., 2019. Damage areas during emergency depressurization of a gas pipeline. *EECE Proceedings.* 140, 06007. https://doi.org/10.1051/e3sconf/201914006007

Wilkening, H., Baraldi, D., 2007. CFD modelling of accidental hydrogen release from pipelines, *Int. J. Hydrogen Energ.,* Volume 32 (13), 2206-2215. https://doi.org/10.1016/j.ijhydene.2007.04.022

Zhang, Y., Zhu, J., Teng, L., Song, C., 2020. Experimental research of LNG accidental underwater release and combustion behavior. *J. Loss Prevent. Proc.* 64, 104036. https://doi.org/10.1016/j.jlp.2019.104036

Zhou, K., Wang, X., Liu, M., Liu, J., 2018. A theoretical framework for calculating full-scale jet fires induced by high-pressure hydrogen/natural gas transient leakage. *Int. j. hydrogen energ.* 43, 22765-775. https://doi.org/10.1016/j.ijhydene.2018.10.122

Zhu, H., Mao, Z., Wang, Q., Sun, J., 2013. The influences of key factors on the consequences following the natural gas leakage from pipeline. *Procedia Engineer.* 62, 592-601. https://doi.org/10.1016/j.proeng.2013.08.104

Zhu, Y., Wang, D., Shao, Z., Zhu, X., Xu, C., Zhang, Y., 2020. Investigation on the overpressure of methane-air mixture gas explosions in straight large-scale tunnels. *Process Saf. Environ.* 135, 101-112. https://doi.org/10.1016/j.psep.2019.12.022

Zuliani, C., De Lorenzi, C., Ditali, S., 2016. Application of CFD Simulation to Safety Problems – Challenges and Experience Including a Comparative Analysis of Hot Plume Dispersion from a Ground Flare. *Chem.Eng. Trans.* 53, 79-84. https://doi.org/10.3303/CET1653014

CHAPTER 5: CYLINDRICAL TANKS EFFECT ON HORIZONTAL HIGH-PRESSURE METHANE JETS DEVELOPMENT COUPLED WITH THE TERRAIN EFFECT

In this Chapter, a single cylindrical-shaped tank is considered and its influence, coupled with the ground effect when present, is preliminary studied. Similar methane high-pressure jet defined in previous Chapters is considered, as well as methodological aspects at the base of the analysis. However, with respect to former Chapters, this scenario was examined at a higher level, providing preliminary qualitative and semi-quantitative results and useful information regarding the effect of cylindrical tanks on high-pressure jets extent, giving suggestions on what more detailed and extensive future analysis should focus on.

In the following, a first-approach analysis is provided for the topic of cylindrical tank impinged by a high-pressure methane jet, divided into two sub-Chapters where firstly only horizontal tanks are considered and their effect on the jet extent assessed with respect to some main geometrical parameters characterizing the scenario (*i.e.*, distance from the source, tank orientation, tank height and tank lateral displacement). Limited to a narrow range of cases, from this analysis useful qualitative and semi-quantitative indications of which may be the main effects of a horizontal cylindrical tank are provided. Second sub-Chapter concerns more to an interesting although limited sensitivity analysis, with the focus of defining which can be the effect of varying both size and orientation of the cylindrical tank considered in the first sub-Chapter. Results of this further preliminary analysis on impinged cylindrical tanks revealed that, for the limited range of parameters considered, tank orientation (that is to say, horizontal or vertical) seems does not provide any substantial difference on both shape and size of the jet cloud.

Accordingly to previous Chapters, the preliminary assessments discussed in the following focus on the effect that a single obstacle (that can be entitled as a possible industrial obstacle) has on the jet cloud development, aiming to define how jet cloud size can be affected. However, because of the limited number of simulated scenarios, the provided results are limited to a narrow range of validity.

CHAPTER 5.1: OBSTACLE INFLUENCE ON HIGH-PRESSURE JETS BASED ON COMPUTATIONAL FLUID DYNAMICS SIMULATIONS

CHEMICAL ENGINEERING TRANSACTIONS
VOL. 77, 2019
A publication of AIDIC
The Italian Association of Chemical Engineering
Online at www.cetjournal.it
Guest Editors: Genserik Reniers, Bruno Fabiano

ISBN 978-88-95608-74-7; **ISSN** 2283-9216
DOI: 10.3303/CET1977136

Obstacle Influence on High-Pressure Jets based on Computational Fluid Dynamics Simulations

Cristian Colombini*, Valentina Busini

Politecnico di Milano - Department of Chemistry, Materials and Chemical Engineering "Giulio Natta", Via Mancinelli 7, 20131, Milano, Italy
cristian.colombini@polimi.it

ABSTRACT

In the industrial safety framework, high-pressure jets involving toxic or flammable substances represent one of the major risks. The presence of one or more obstacles affects the extent of the plume, normally to higher dimensions, which means that an open field modeling would not be conservative and that it is necessary to explicitly consider the obstacles effects. Thus, to study this kind of scenario, only a computational fluid dynamic model allows a complete and proper description of the obstacles influence on the jet behavior.

In this work, a realistic case-study of industrial interest which involves a high-pressure methane jet impinging a nearby cylindrical tank positioned in front of the jet release is concerned.

The aims of this work are to define the geometrical parameters of the scenario, to quantify their influence on the jet-obstacle interaction, with respect to the free jet case, and then to find which of them are the most relevant. Therefore, the effect of the cylindrical tank on the lower flammability limit area extent is systematically studied using computational fluid dynamics simulations, performed with ANSYS® FLUENT®.

ACRONYMS

CFD Computational fluid Dynamics

LFL Lower Flammability Limit

RANS Reynolds Averaged Navier-Stokes

UDF User Defined Function

NOMENCLATURE

A: dimensionless area extent of the LFL jet cloud

D: distance of the tank from the jet source

H: height of the orifice above ground

S: lateral displacement of the tank with respect to jet axis

v_i: wind velocity along the i-nth coordinates

X: dimensionless lateral extent of the LFL jet cloud

Z: dimensionless axial extent of the LFL jet cloud

α: tank rotation with respect to jet axis

INTRODUCTION

Many industrial fluids are stored and transported in gaseous form under high-pressure. For this reason, in the risk analysis framework, the modelling of high-pressure jet releases and the quantifying of their consequences play a relevant role (Busini et al., 2012). If the jet release occurs in open field, it can be considered as a free jet (Pontiggia et al., 2014) while, if an obstacle is present beside or in front of the leak, the scenario is usually known impinging jet (Schefer et al., 2009*)*. In the latter case, if the release involves a flammable material, domino effects may be relevant (Benard et al., 2009).

From the physical point of view, the presence of an obstacle affects significantly the jet behaviour (Hall et al., 2017) in terms of turbulence, producing eddies, and affecting the jet momentum. In particular, the mixing with fresh air can be enhanced or reduced (Pontiggia et al., 2014), influencing the extent of the flammable region with respect to the one expected from the free jet (Kotchourko et al., 2014). This means that, a priori, numerical models previously developed for free jets, e.g. integral models, are not suitable for the analysis of impinging flows (Brook et al., 2003. This kind of models is able to account for physical phenomena through semi-empirical relationship depending on parameters whose values are gathered from experimental data available for open field releases (Hanna, 1994). On the other hand, distributed numerical models, such as Computational Fluid Dynamic (CFD) models, are able to account for the influence of obstacles or, more generally, of a complex geometry on the jet release (Batt et al., 2016). Therefore, to properly simulate this kind of scenario, only a CFD analysis can be feasible and reliable, at the cost of possible significant computational demand and required user knowledge (Zuliani et al., 2016). Some efforts have been spent in the past on this topic: most of the studies has investigated the influence of obstacles on high momentum jet releases (more precisely, to determine the extent of the flammable/toxic clouds (Houf and Schefer 2007)) only for specific cases (Sposato et al., 2003; Tchouvelev et al., 2007; Bénard et al., 2007; Hourri et al., 2009; Bénard et al., 2009; Hourri et al., 2011; Angers et al., 2011; Bénard et al., 2016). However, none of this literature works explicitly investigates the influence of a real 3D obstacle on the flammable area extent of a high-pressure jet with respect to the free jet case.

Therefore, in this work, the obstacle influence was investigated varying some of the geometrical key parameters of both obstacle and orifice. More specifically, a realistic case-study of industrial interest was considered. It involves a high-pressure methane jet impinging a horizontal cylindrical tank positioned in front of the jet release.

The aims of this work are:

- to define the geometrical parameters significant for this scenario;
- to quantify these parameters' influence on the jet-obstacle interaction, with respect to the free jet case;
- to define which of them are the most influential.

Therefore, the effect of the cylindrical tank on the Lower Flammability Limit (LFL) area extent is systematically studied using CFD simulations, performed with ANSYS® FLUENT® v. 18.2.

Material and Methods

To obtain a good quality representation of the flow field and, at the same time, a time-saving tool, all the simulations performed are based on Reynolds Averaged Navier-Stokes (RANS) approach. To avoid the need of resolve the boundary layer of the ground and tank surface, among the possible turbulence models available, the k-ω SST was adopted (Ansys Inc., 2017). Standard boundary conditions were used for the domain's boundaries (as summarized in Table 6.1 and shown in Figure 6.1a), except for the back, left and right side boundaries, for which particular attention was payed to model realistic wind conditions. Indeed, to consider the atmospheric conditions of an open field scenario, a velocity profile in accordance with the atmospheric class 5*D* was supplied to the solver through a User Defined Function (UDF) (Pontiggia et al., 2014).

Results and Discussion

The case-study here investigated was a realistic scenario of industrial interest which involves an accidental horizontally oriented, high-pressure release of methane impinging a horizontal cylindrical tank placed in front of the leak. Guessing a spill from a huge storage tank (or a pipeline) of methane gas, the leakage can be considered as a steady state scenario. As gas conditions inside the storage, a pressure of 65 bara and a temperature of 5 °C were used, while a diameter of 1 inch was adopted as a realistic accidental hole on the facility. The methane inlet characteristics were obtained with the Birch's pseudo source model (Birch et al., 1984), whose corresponding equivalent conditions are reported in Table 6.2. The rest of the boundary conditions used are summarized in Table 6.1.

Table 6.1: Boundary conditions used for the case-study simulations.

Boundary	Type
Back side	Velocity inlet, v_x = 0 m/s, v_y = 0 m/s, v_z = velocity profile
Top side	Velocity inlet, v_x = 0 m/s, v_y = $-1e^{-9}$ m/s, v_z = 5 m/s
Left side	Velocity inlet, v_x = $-1e^{-9}$ m/s, v_y = 0 m/s, v_z = velocity profile
Ground	Adiabatic wall, 0.01 m roughness height
Central vertical plane	Symmetry (where applicable)
Right side	Velocity inlet, v_x = $1e^{-9}$ m/s, v_y = 0 m/s, v_z = velocity profile
Front side	Pressure outlet
Nozzle wall	Adiabatic wall, 0.001 m roughness height
Methane inlet	Mass flow inlet, 5.184 kg/s
Tank wall	Adiabatic wall, 0.001 m roughness height

Table 6.2: Characteristics of the methane pseudo source used in the case-study.

Characteristic	Value
Expanded diameter	0.1458 m
Velocity	440.6 m/s
Mass flow rate	5.184 kg/s
Total Temperature	70.3 °C
Pressure	101325 Pa

As done by Pontiggia and coworkers (Pontiggia et al., 2014), to take into account the surrounding of the release, i.e. the open field atmospheric conditions, a neutral stability class, namely atmospheric class D, with 5 m/s wind at 10 m from the ground was considered. The dimensions of the simulated domain were 70·10·10 (in m) while the obstacle was modelled as a horizontal cylinder of 5 m length

and 1.7 m diameter. Notice that the domain dimensions were chosen such that the prescription for the domain extension for CFD analysis of urban environment were fulfilled (Franke et al., 2007). Figure 6.1a shows a representation of the simulated domain, highlighting the boundary conditions. The free jet scenario, for which neither the ground nor the obstacle influence occurs, was performed with the aim of obtaining a reference result for comparison purposes. To be in the aforementioned situation, the nozzle was positioned at a height of 5 m and the obstacle wasn't placed (in this case, the maximum LFL extension reached is 15.54 and 1 m in z and x, respectively). The performing of the free jet scenario evidently seems of great importance to understand when and how the jet is influenced. Notice that, a grid independence analysis of the results was conducted at this stage. The initial mesh adopted ($6.08 \cdot 10^6$ cells) was tested with other two meshes, one of about $5 \cdot 10^6$ cells and the other of about $7 \cdot 10^6$ cells; all the three results were comparable. As geometric key parameters (see Figure 6.1b), the distance of the obstacle from the jet orifice (D), the height of the orifice above ground (H), the rotation (α) and the displacement (S) of the tank with respect to the jet axis were chosen. Therefore, an array of simulation was conducted varying one (or in some cases two) per time the geometric parameters.

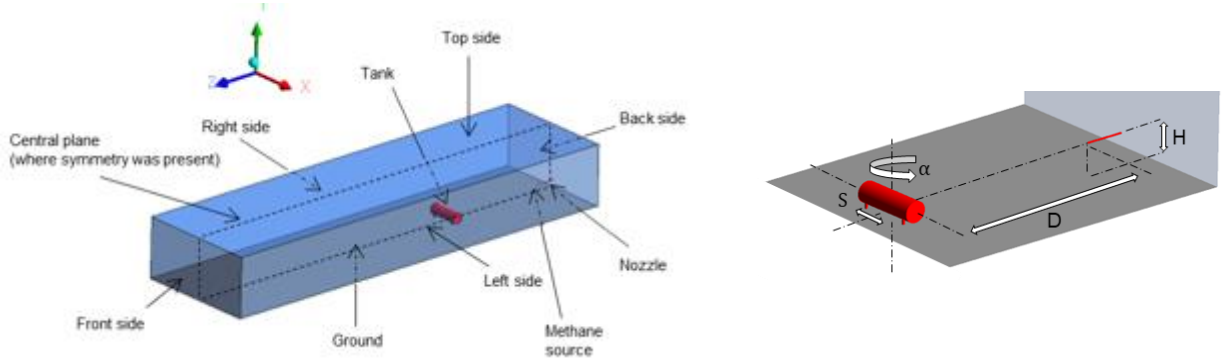

Figure 6.1: a) Computational domain represented as a full 3D; b) Geometric key parameters

Table 6.3 reports the details of all the simulation performed. As reported, each of the geometric parameters was varied of a certain amount with respect to a reference simulation which is, in most of the cases, simulation 0 (sim0). By way of example, let consider simulation 1 (sim1 in the table): the varied parameter is D, which is enhanced of the 75 % with respect to sim0. Practically, the reference simulation corresponds to the guess value of the geometric parameters, where D = 17.9 m, H = 1 m, α = 0 °, S = 0 m. The initial value of D and H were derived from the results of another preliminary simulation, in which the obstacle is not present but there is the influence of the ground

(H = 1 m): 17.9 m is the half of the LFL extent (in the z axes) obtained in this case. The guess value of the other parameters, namely α and S, was arbitrarily chosen.

Table 6.3: Details of all the simulations performed.

	Ref.	Parameter	Variation		Ref.	Parameter	Variation
sim1	sim0	D	+75 %	**sim13**	sim0	α	+75 %
sim2	sim0	D	+50 %	**sim14**	sim0	α	+50 %
sim3	sim0	D	+25 %	**sim15**	sim0	α	+25 %
sim4	sim0	D	-25 %	**sim16**	sim0	S	+75 %
sim5	sim0	D	-50 %	**sim17**	sim0	S	+50%
sim6	sim0	D	-75 %	**sim18**	sim0	S	+25 %
sim7	sim0	H	+75 %	**sim19**	sim0	D	+500 %
sim8	sim0	H	+50 %	**sim20**	sim19	H	+75 %
sim9	sim0	H	+25 %	**sim21**	sim19	H	-75 %
sim10	sim0	H	-25 %	**sim22**	free jet	D	-50 %
sim11	sim0	H	-50 %	**sim23**	sim22	D	+75 %
sim12	sim0	H	-75 %	**sim24**	sim22	D	-75 %

Notice that, in sim13 to 18 there is no symmetry of the geometry and, therefore, the computational domain has to be a full 3D one, as shown in Figure 6.1a. In all other simulations, only half domain, with a symmetry condition, was considered. In Table 6.3 there are missing simulations: these are not reported given that their results can be deduced by those of sim13 to 18 just mirroring them with respect to the jet axis. As aforementioned, some simulations (sim19 to sim24) were performed combining two parameter variations per time. These were selected to point out cases in which the obstacle or the ground influence were individually shown. In sim19 the obstacle is placed far enough such that the only ground influence is achieved, and the height of the jet corresponds to the one of sim0. sim20 and 21 were set, with respect to sim19, varying the jet height as reported in Table 6.3. While, to account only for the obstacle influence, sim22 corresponds to the situation in which the obstacle is placed in the middle of the LFL maximum extent in z of the free jet case and the height of the obstacle is 5 m, equal to the one of the orifice. As reported in Table 6.3, sim23 and 24 were then referred to sim22 instead of sim0. A way to show most information of the simulation results is to graph them into a 3D plot (Figure 6.2), where a dimensionless area A is plotted over two

dimensionless spatial coordinates: in detail, the dimensionless A is defined as the ratio $A_{sim\#}/A_{free\ jet}$, where $A_{sim\#}$ is the product of the LFL maximum extent in x ($X_{sim\#}$) times the LFL maximum extent in z ($Z_{sim\#}$), and the same goes for $A_{free\ jet}$ in the free jet case. However, to ease the results interpretation, two projections are reported in Figure 6.3a (side view) and 3b (top view). The dimensionless X is the ratio $X_{sim\#}/X_{free\ jet}$ and Z is $Z_{sim\#}/Z_{free\ jet}$, where $X_{free\ jet}$ is the LFL maximum extent in x and $Z_{free\ jet}$ in z for the free jet case.

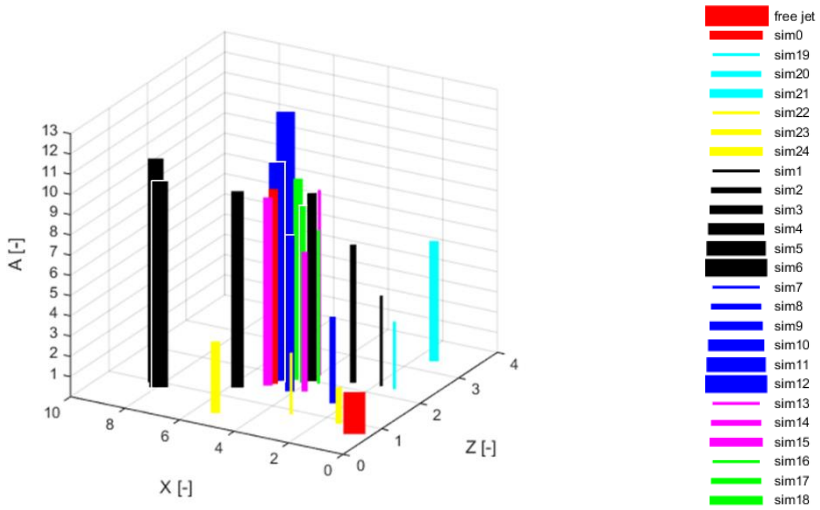

Figure 6.2: 3D plot of the simulations results

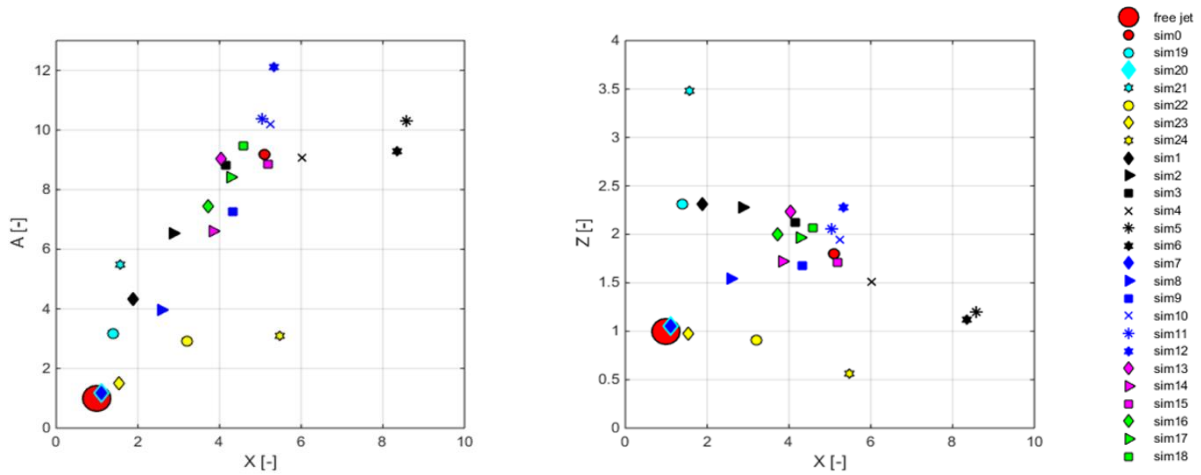

Figure 6.3: a) Side view of the 3D plot; b) Top view of the 3D plot

From Figure 6.3b it is possible to state that, except for sim7 and sim20, for all the other simulations an influence of the obstacle and/or the ground is noticeable. This is correct since, in sim7 and 20, the distance of the obstacle and the height of the orifice are such that practically no influence occurs. Paying attention to the maximum extents, from Figure 6.3b it is appreciable that the maximum axial extent is 3.5 times the free jet one (sim21), while the transverse maximum extent is

about 8.5 times the free jet case (sim5). Furthermore, it becomes clear that more the jet is crosswise extended, less it is axially, and vice versa. In terms of area A, it appears to be larger when the jet is extended in X rather than when extended in Z. In particular, the largest influence with respect to the free jet is obtained for sim12 (see Figure 6.2 and 6.3a). Both from Figure 6.2 and 6.3b, it is possible to see that about the 60 % of the results are grouped into a small region of the plane X, Z, ranging from 2 to 6 and from 1.5 to 2.5 in X and Z, respectively. Lastly, sim1 to sim6 and sim7 to sim12 seems to be aligned each other (see Figure 6.3b). Moreover, in terms of A, such an alignment follows an ascending order (see Figure 6.2 and Figure 6.3a).

CONCLUSIONS

A high-pressure release of a flammable material is considered in the present Chapter. In this case, it is known that domino effects can occur, and that they can be relevant from the safety point of view. If an obstacle is present in the area covered by the jet, it has been stated that an influence on the release behaviour appears. In particular, the main effect seems to be the enhancement, or the reduction, of the mixing with fresh air. To account for such an influence, all the geometric features present in the domain have to be taken into account and properly modelled.

In order to investigate this kind of scenario, in this paper a CFD solver was used to model a realistic high-pressure methane release impinging on a 3D realistic obstacle placed in front of the leak.

The aims of the study were fulfilled:

- the geometric key parameters of the scenario were defined: the distance of the obstacle from the jet orifice (D), the height of the orifice above ground (H), the rotation (α) and the displacement (S) of the tank with respect to the jet axis were chosen as geometric key parameters;
- with respect to the free jet case, the quantification of all the chosen geometric parameters influence was achieved in terms of Z, X and A. As shown in Figure 6.3a and 3b the ground evidently affects more the axial extent rather than the transverse one. On the other way around, the prevalent obstacle effect is the enhancement of the crosswise extension with respect to the free jet. When both the obstacle and the ground influence is present, it is noticeable that, in terms of X and Z (see Figure 6.3b), the obstacle effect is about twice the ground one. Indeed, most of the results are grouped into a small region of the plane X, Z (around the point of coordinates X = 4.5 and Z = 2). Although their opposite effect, as the obstacle and the ground influence become stronger, A increases too. Another interesting aspect deducible from the results is that an alignment of the results, in which D and H are respectively varied, can be seen. In particular, seems that: i) there is a proportional link between D and Z, ii) there is an inverse proportional link between D and X, iii) there is an inverse proportional link between H and both Z and X.
- state that one specific geometric parameter is the most relevant could be misleading. Indeed, as aforementioned, depending on which coordinate (Z, X or A) one considers, the maximum absolute influence on the free jet can be linked to a different geometric parameter: i) considering the absolute maximum Z, H is the most relevant parameter if only

the ground effect is taken into account, while H, D and α have the same effect if both ground and obstacle effects are present, ii) considering the maximum influence in terms of X, D is the most relevant parameter, iii) considering the maximum influence in terms of A, H is the most relevant parameter.

Finally, given the source conditions, the specifics of the obstacle dimensions and position and the analytical models available for the free jet case, the results achieved can be seen as the starting point for the development of a criterion that allows the user to estimate the expected damage area (and its distribution) for the jet-obstacle interaction case.

REFERENCES

Angers, B., Hourri, A., Benard, P., Tchouvelev, A., 2011. Numerical investigation of a vertical surface on the flammable extent of hydrogen and methane vertical jets. *Int. J. Hydrogen Energy* 36, 2567-72.

Ansys Fluent User's Guide, 2017. Release 18.2. ANSYS, Inc.

Baklanov A., Barmpas P., Bartzis J., Batchvarova E., Baumann-Stanzer K., Berkowicz U., Borrego C., Britter A., Brzozowski K., Burzynski J., Costa A.M, Carissimo C., Dimitrova R., Franke J., Grawe D., Goricsan I., Hellsten A., Janour Z., Karppinen A., Ketzel M., Krajcovicova J., Leitl B., Martilli A., Moussiopoulos N., Neophytou M., Olesen H., Papachristodoulou C. Papadakis M., Piringer M., Di Sabatino S., Sandberg M., Schatzmann M., Schlünzen H., Trini-Castelli S., 2007, Cost Action 732 Quality Assurance and Improvement of Microscale Meteorological Models, Brussels, Belgium

Batt, R., Gant, S.E., Lacome, J.M., Truchot, B., 2016. Modelling of stably-stratified atmospheric boundary layers with commercial CFD software for use in risk assessment. *Chem. Eng. Trans.* 48, 61–66. https://doi.org/10.3303/CET1648011.

Bénard, P., Tchouvelev, A., Hourri, A., Chen, Z., Angers, B., 2007. High pressure hydrogen jets in the presence of a surface. *Int. Conf. Hydrog. Saf.* 40.

Bénard, P., Hourri, A., Angers, B., Tchouvelev, A., Agranat, V., 2009. Effects of surface on the flammable extent of hydrogen jets. *Int. Conf. Hydrog. Saf*.

Bénard, P., Hourri, A., Angers, B., Tchouvelev, A., 2016. Adjacent surface effect on the flammable cloud of hydrogen and methane jets: Numerical investigation and engineering correlations. *Int. J. Hydrogen Energy* 41, 18654–18662. https://doi.org/10.1016/j.ijhydene.2016.08.173.

Birch, A.D., Brown, D.R., Dodson, M.G., Swaffield, F., 1984. The structure and concentration decay of high pressure jets of natural gas. *Combust. Sci. Technol.* 36, 249–261. https://doi.org/10.1080/00102208408923739

Brook, D. R., Felton, N. V., Clem, C. M., Strickland, D. C. H., Griffiths, I. H., Kingdon, R. D., 2003. Validation of the urban dispersion model (UDM). Int. J. Environ. Pollut. 20 (1−6), 11.

Busini V., Massimiliano L., Rota R., 2012, Influence of Large Obstacles and Mitigation Barriers on Heavy Gas Cloud Dispersion: A Liquefied Natural Gas Case-Study, *Industrial and Engineering Chemistry Research,* 51, 7643–50.

Hall, J.E., Hooker, P., O'Sullivan, L., Angers, B., Hourri, A., Benard, P., 2017. Flammability profiles associated with high-pressure hydrogen jets released in close proximity to surfaces. *Int. J. Hydrogen Energy* 42, 7413–7421. https://doi.org/10.1016/j.ijhydene.2016.05.113.

Hanna S. R., 1994, Hazardous Gas-Model Evaluations - Is an Equitable Comparison Possible, Journal of Loss Prevention in the Process Industries, 7, 133-138.

Houf W., Scheffer R., 2007, Predicting Radiative Heat Flux and Flammability Envelopes from Unintended Releases of Hydrogen, International Journal of Hydrogen Energy, 32, 136-151

Hourri, A., Angers, B., Bénard, P., 2009. Surface effects on flammable extent of hydrogen and methane jets. *Int. J. Hydrogen Energy* 34, 1569–1577. https://doi.org/10.1016/j.ijhydene.2008.11.088.

Hourri, A., Angers, B., Bénard, P., Tchouvelev, A., Agranat, V., 2011. Numerical investigation of the flammable extent of semi-confined hydrogen and methane jets. *Int. J. Hydrogen Energy* 36, 2567–2572. https://doi.org/10.1016/j.ijhydene.2010.04.121.

Kotchourko, A., Baraldi, D., Bénard, P., Eisenreich, N., Jordan, T., Keller, J., Kessler, A., LaChance, J., Molkov, V., Steen, M., Tchouvelev, A., 2014. State of the Art and Research Priorities in Hydrogen Safety. Joint Research Centre of the European Commission (JRC), Honolulu, Hawaii.

Pontiggia, M., Busini, V., Ronzoni, M., Uguccioni, G., Rota, R., 2014. Effect of large obstacles on high momentum jets dispersion. *Chem. Eng. Trans.* 36, 523–528. https://doi.org/10.1016/j.jhazmat.2009.06.064.

Schefer, R., Groethe, M., Houf, W.G., Evans, G., 2009. Experimental Evaluation of Barrier Walls for Risk Reduction of Unintended Hydrogen Releases, *Int. J. Hydrogen Energ.* 34, 1590-1606. https://doi.org/10.1016/j.ijhydene.2008.11.044

Sposato, C., Tamanini, F., Rogers, W.J., Sam Mannan, M., 2003. Effects of Plate Impingement on the Flammable Volume of Fuel Jet Releases. *Process Saf. Prog.* 22, 4. https://doi.org/10.1002/prs.680220406

Tchouvelev, A.V., Cheng, Z., Agranat, V.M., Zhubrin, S.V., 2007. Effectiveness of small barriers as means to reduce clearance distances. *Int. J. Hydrogen Energy* 32, 1409–1415. https://doi.org/10.1016/j.ijhydene.2006.10.020.

Zuliani C., De Lorenzi C., Ditali S., 2016. Application of CFD Simulation to Safety Problems – Challenges and Experience Including a Comparative Analysis of Hot Plume Dispersion from a Ground Flare, Chemical Engineering Transactions, 53, 79-84. DOI: 10.3303/CET1653014.

CHAPTER 5.2: HIGH-PRESSURE METHANE JET: ANALYSIS OF THE JET-OBSTACLE INTERACTION

High-Pressure Methane Jet: Analysis of the Jet-Obstacle Interaction

Cristian Colombini

Department of Chemistry, Materials and Chemical Engineering "Giulio Natta", Politecnico di Milano, Italy.
E-mail: cristian.colombini@polimi.it

Valentina Busini

Department of Chemistry, Materials and Chemical Engineering "Giulio Natta", Politecnico di Milano, Italy.
E-mail: valentina.busini@polimi.it

Proceedings of the 29th European Safety and Reliability Conference.
Edited by Michael Beer and Enrico Zio

Published by Research Publishing, Singapore.
ISBN: 978-981-11-2724-3; doi:10.3850/978-981-11-2724-3_0467-cd

ABSTRACT

The study of unplanned high-pressure gas releases is of paramount importance in the industrial safety framework because of the possible large consequences, both in case of flammable and toxic substances leakage. In addition, if an obstacle is involved in the release, it is known that the main effect on the jet behavior is the enhancement of the risk area. Pointing out the importance to consider the obstacle presence, among the various available numerical approaches, the sole reliable tool able to correctly model the scenario of a jet interacting with an obstacle seems to be the Computational Fluid Dynamics (CFD). This work lies in the context outlined through the examination of a realistic unignited high-pressure methane jet interacting with a realistic obstacle placed along its axis via CFD simulations: a stationary 65-bara unignited methane jet outflowing from a one-inch diameter hole and a medium size horizontal cylindrical tank are the building blocks of the realistic scenario. The aim is to deeply investigate how the distance between obstacle and jet orifice modifies the jet behavior. In particular, the final purposes are: i) to establish when the obstacle most influences the jet cloud extent and, ii) to assess when the obstacle influence expires. Moreover, a sensitivity analysis on the obstacle shape and size is conducted for comparison purposes.

ACRONYMS

CFD Computational fluid Dynamics

HCT Horizontal Cylindrical Tank

LFL Lower Flammability Limit

ME Maximum Extent

UDF User Defined Function

VCT Vertical Cylindrical Tank

NOMENCLATURE

D: distance of the tank from the jet source

H: height of the orifice above ground

LFL: methane concentration equal to LFL

ME: jet axial maximum extent

n: number of actual orifice diameters

S: lateral displacement of the tank with respect to jet axis

α: tank rotation with respect to jet axis

δ: percentage variation of the tank distance with respect to a reference position

η: reciprocal of the axial mole fraction

INTRODUCTION

A large part of industrial gases is normally in a compressed form. Therefore, an accidental release, which generally arises from a failure in the process or storage equipment, results in high-pressure jet yielding a wide toxic or flammable cloud. In the second case, if ignition occurs, the consequences can be relevant: as reported by Casal et al. (2012), due to the domino effect related to it, a jet fire may be among the industrial's most hazardous accidents, whose damages may involve both people, facilities and environment. It is clear, therefore, why the study of high-pressure gas releases became of great interest in the industrial and process safety framework. Examples of such an importance are given by the work of Busini et al. (2012) and Pontiggia et al. (2014), just to mention some. By referring to a common industrial plant, it is easy to find that equipments, structures or properties can be in the vicinity of a hypothetical source of a high-pressure jet: broadly speaking, it can be very common to have obstacles close to the leak. Attention should be payed, therefore, to the previous depicted scenario. In particular, the main reason that should focus the concerns is that, as reported by Hall et al. (2017), the jet behavior is significantly affected by the obstacle presence, specifically through the enhancement of the cloud extent (and so the flammable area involved) with respect to the case of no-obstacle situation (known as free jet case). In a previous work made by Colombini and Busini (2019), the non-desirable effect that a cylindrical tank, placed in the surrounding of an accidental release and acting as realistic industrial obstacle, has on the jet dimensions is clearly depicted. So, even though its prominent importance in the safety assessment, a not so spread literature is noticeable. By way of example, as regards numerical analysis, works are available focusing on the effect of lateral surfaces (Hourri et al. (2009); Benard et al. (2016)) or small front barriers (Houf et al. (2010); Middha et al. (2010); Busini and Rota (2014)). The common denominator among the cited works is that the only reliable numerical tool is the CFD. As reported by Batt et al. (2016), CFD is the sole utility able to properly account for geometry complexities, although, as stated in the work of Zuliani et al. (2016), the computational costs and the user knowledge demanded.

To the knowledge of the authors, only the previous work done by Colombini and Busini (2019) reports a follow-up about the common scenario of a 3D realistic industrial obstacle placed in the vicinity of a realistic high-pressure gaseous release.

In the framework outlined the examination of a realistic unignited high-pressure methane jet interacting with a realistic obstacle placed along its axis is preliminary performed. The aim was to assess, with respect to the distance between obstacle and jet orifice, both qualitatively and quantitatively the influence of such an obstacle on the jet behavior (*i.e.*, in terms of Lower

Flammability Limit (LFL) area extent). Two are the leading questions of the work: i) when the obstacle most influences the jet cloud extents and, ii) when the obstacle influence expires. Practically, as first, the CFD model results will be compared to experimental data found in literature for the case of a stationary unignited high-pressure methane jet without any kind of obstacle for validation purposes. Then, both a realistic industrial gas source and a realistic industrial obstacle will be selected for the analysis: a stationary 65-bara unignited methane jet outflowing from a one-inch diameter hole and a medium-size horizontal cylindrical tank will be considered. Moreover, in order to extend the knowledge acquired about the jet-obstacle interaction, a sensitivity analysis on the obstacle size and on the obstacle shape will be conducted.

General Aspects of the CFD model

As CFD software, Ansys® Fluent® release 19 was used to conduct the whole analysis. In particular, the Workbench suite was adopted due to its ease-to-use and bring-together design. The validation case, the case study and the sensitivity analysis studies share some aspects in terms of geometry, mesh and solver settings. With regard to the geometrical aspects, in all the models reported, a nozzle was used to represent the methane inlet in the domain and a symmetry vertical plane along the jet axis was adopted. As first reference, the computational domain extents were sized according to the guidelines reported in the work of Baklanov et al. (2007) that suggests proper dimensions for a CFD computational domain in the case of single building struck by the wind. The employed mesh strategy had the goal of balancing the computational costs and the results' reliability: the body of influence mesh modeler feature was found to be a good compromise. Indeed, placing virtual line bodies along the jet axis and then playing with their number, edge cells size and growth rate of the cells dimension into the fluid volume, cells thickening along the jet axis and in correspondence to the orifice was achieved, leaving a coarser mesh far from the "critical" zone of the domain. In all the models, a full tetrahedral grid was adopted. Finally, with the previously discussed solver general aspects, all simulations were performed in steady state mode and utilizing the pressure-based solver type. The Navier-Stokes equations system that describes the fluid behavior was solved in the sense of the Reynolds average. By exploiting this easier formulation, it is possible to get an acceptable trade-off between time-saving and flow field reproduction quality. The k-ω SST turbulence closure model was chosen in order to take into account the turbulence's effect on the flow field avoiding, on the other hand, the need to precisely portray the boundary layer region next to the ground and obstacle surfaces (when present). For more details about the k-ω SST turbulence model, refer to the

Ansys® Fluent® User guide (2018). To account for the multi-species problem (methane release in ambient air), the species transport model without any kind of reaction was included. The methane release was modeled as mass flow inlet boundary condition and, for the boundaries of the domain, an *ad hoc* strategy was implemented case-by-case (*i.e.*, depending on whether or not the wind presence should be considered). As pressure-velocity coupling scheme, the coupled was adopted while a 2nd order spatial-discretization scheme was considered for all the equations. Concluding, usually 1500 iterations were sufficient in all the simulations performed to obtain a converged solution.

VALIDATION CASE

As introduced in *INTRODUCTION* Section, first of all the CFD model was validated. The work of Birch et al. (1984), concerning an experimental campaign involving natural gas free jets at various pressures, was taken as reference for the results comparison. However, other than for matching purposes, this work was also relevant because it provides the so-called pseudo-diameter model: it consists in an analytical model that returns a diameter of a pseudo gas source whereby the mass flow rate is preserved but the supercritical conditions are replaced by critical conditions (i.e., easier to be treated). In their work, the authors have shown that the Chen and Rodi (1980) axial concentration decay model, which is developed for sub-critical releases, can be also valid for super-critical ones as long as the actual diameter is substituted by the pseudo-diameter one. For further details, the reader can refer to the work of Birch et al. (1984). Hence, following the general aspects depicted in Section *GENERAL ASPECTS OF THE CFD MODELS* and accordingly to the Birch's experiment conditions, the CFD model was set. Exploiting the same results visualization style as in Birch et al. (1984), wherein the reciprocal of the axial mole fraction (η) is plotted over a suitable dimensionless axial distance from the jet orifice (i.e., n, number of actual orifice diameters properly scaled), Figure 7.1 shows the fulfilling comparison achieved between CFD results and the experimental data (here reproduced through a Matlab® model that matches the Chen and Rodi (1980) axial concentration decay model with the pseudo-diameter model of Birch et al. (1984)).

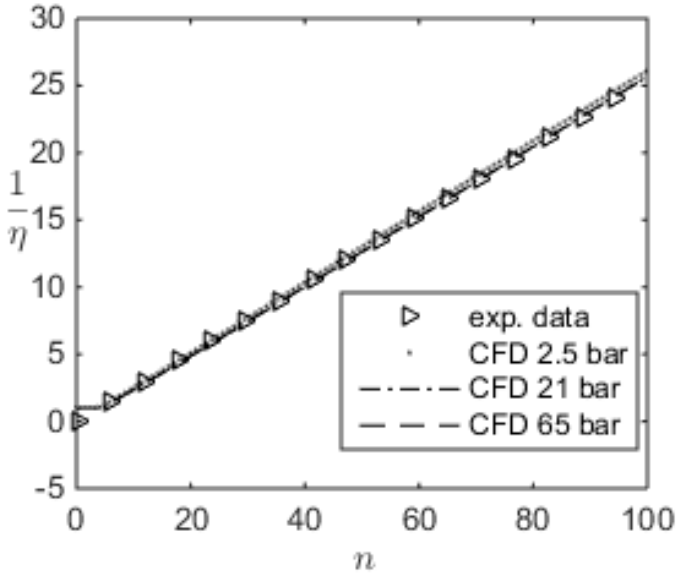

Figure 7.1: Comparison of CFD results at three different pressures (namely 2.5, 21 and 65 bar) and experimental data.

Analyzing the matching shown in Figure 7.1, in the range defined by Birch et al. (1984) in which the model should be considered valid, no scatter between experimental data and CFD can be practically seen. Therefore, it is possible to conclude that the CFD model developed for the free jet scenario can be intended as validated.

CASE STUDY

The case study, from which the analysis addressed started, was a stationary 65-bara unignited methane jet outflowing from a one-inch diameter hole impinging a medium size horizontal cylindrical tank. The realistic obstacle is 2.5 m long (in the symmetric domain), it has a diameter of 1.7 m and its longitudinal axis is 1 m high above ground. As anticipated in Section *VALIDATION CASE*, the orifice diameter was sized using the Birch's pseudo diameter model: one-inch actual diameter and 65-bara of pressure give back a virtual source diameter equal to 0.1458 m, *i.e.*, almost 6 times the actual one. While, as regards the domain dimensions, according to what mentioned in Section *GENERAL ASPECTS OF THE CFD MODELS*, the domain extents were defined fulfilling the guideline of Baklanov et al. (2007). In particular, it was 10 m high, 10 m wide (in the symmetric domain) and 70 m long. The meshes built following the strategy illustrated in Section *GENERAL ASPECTS OF THE CFD MODELS* resulted in good quality full tetrahedral grids whose elements number ranged between $4.94 \cdot 10^6$ and $5.64 \cdot 10^6$. Notice that, such a variation in the cells count is related to the obstacle

position (with respect to the jet orifice) and the interaction of the cells face size on the tank surface with the cells edge size used for the bodies of influence placed along the jet axis. In the solver settings, the methane inlet was defined as a mass flow inlet boundary condition. In detail, a flow rate of 2.5924 kg/s and a total temperature of 344.3 K were the values assigned. Furthermore, since the scenario examined in the case study is outdoor located (contrary to the validation case depicted in Section *VALIDATION CASE*, which is an indoor experiment), efforts were spent to define realistic wind conditions. In particular, a neutral atmospheric behavior with a wind intensity of 5 m/s at 10 m from the ground was considered. Therefore, to include in the solver the proper wind profile an ad hoc User Defined Function (UDF) was written. Lastly, to include the effect of an industrial ground surface on the wind field (e.g., a concrete forecourt), a roughness height of 0.01 m was specified in the ground boundary condition dialog box.

From an operational point of view, to correctly investigate the influence of the distance between orifice and obstacle (D) on the jet behavior, two simulations were previously performed: i) a simulation (sim^{rif}) in which the Maximum Extent (ME in general, ME^{rif} in this case) of the LFL cloud was measured for the scenario wherein the obstacle was not placed in the domain (i.e., the jet interacts only with the ground); ii) a simulation (sim0) in which the obstacle was placed at a distance correspondent to the half of ME^{rif}, namely D^0. Notice that, according to Colombini and Busini (2019), in addition to D there are three other geometrical key parameters which have to be set, that is to say: the height of the orifice above ground (H), the rotation (α) and the displacement (S) of the tank with respect to the jet axis. Therefore, the value issued for the four geometrical parameters used in sim^{rif} are the following: H = 1 m (H^{rif}), α = 0° (α^{rif}), S = 0 m (S^{rif}) and D = 53.7 m (D^{rif}). While, in sim0: $H = H^{rif}$ (H^0), $\alpha = \alpha^{rif}$ (α^0), $S = S^{rif}$ (S^0) and, consistently to what previously stated, D = 17.9 m (D^0). It is worth noting that H^{rif} was chosen equal to 1 m in order to have the orifice at the same height of the tank axis. Therefore, ME^{rif} is definitely linked to the height of the obstacle axis. To study the influence of D on the jet, a set of six simulations (sim1 to sim6) was performed.

Table 7.1 lists the percentage variation with respect to D^0, δ, such as $D = D^0+(\delta/100)\cdot D^0$ for each case. By way of example, let consider simulation 3 (sim3 in the table): D^3 is equal to D^0 1.25, corresponding to D^3 = 22.375 m. It is worth noting that, in these six trials, the value of H, α and S was kept equal to the one used for sim0.

Prior to go through the results achieved, it has to be mentioned that the grid sensitivity analysis on the LFL cloud was successfully concluded. Indeed, using sim0 as check case, the results obtained

with an initial mesh of about $5.54 \cdot 10^6$ elements are comparable with those produced by two other meshes of about $4 \cdot 10^6$ and $6.85 \cdot 10^6$ cells.

A qualitative way to evaluate the results is to plot the LFL isosurface. By way of example, *Figure 7.2* shows the LFL cloud outline obtained from the results of sim3. In particular, *Figure 7.2*a shows a 3D view while *Figure 7.2*b shows a side view. Mostly from *Figure 7.2*b, although the relatively small height from the ground, it is possible to appreciate that most of the gas (for molar fractions larger than the LFL) goes beyond the tank passing below it. In general, it is also appreciable the role of the ground in the enhancement of the jet cloud due to its reflection effect. On the other way around, a quantitative assessment of the influence of the medium size horizontal cylindrical tank distance on the jet cloud can be obtained plotting the ME of the LFL clouds over δ. Figure 7.3 shows these information gathered from sim^{rif}, sim0 and the six trials listed in Table 7.1. By the findings shown in Figure 7.3, what deduced from Figure 7.2 is confirmed: the ground presence increases the jet length. In particular, the more the obstacle is far from the orifice and the more the ground influence progressively dominates. This last sentence allows to state that, in such a scenario, the obstacle plays as a barrier, whose effect opposes to the ground one. Finally, referring to the results of sim2 and sim^{rif} in *Figure 7.3*, it is noticeable that ME is practically the same, meaning that, at D obtained with δ = +50 %, the tank effect on the jet cloud is expired.

Table 7.1: δ values in the six trials.

Simulation	**δ (%)**
sim1	+75
sim2	+50
sim3	+25
sim4	-25
sim5	-50
sim6	-75

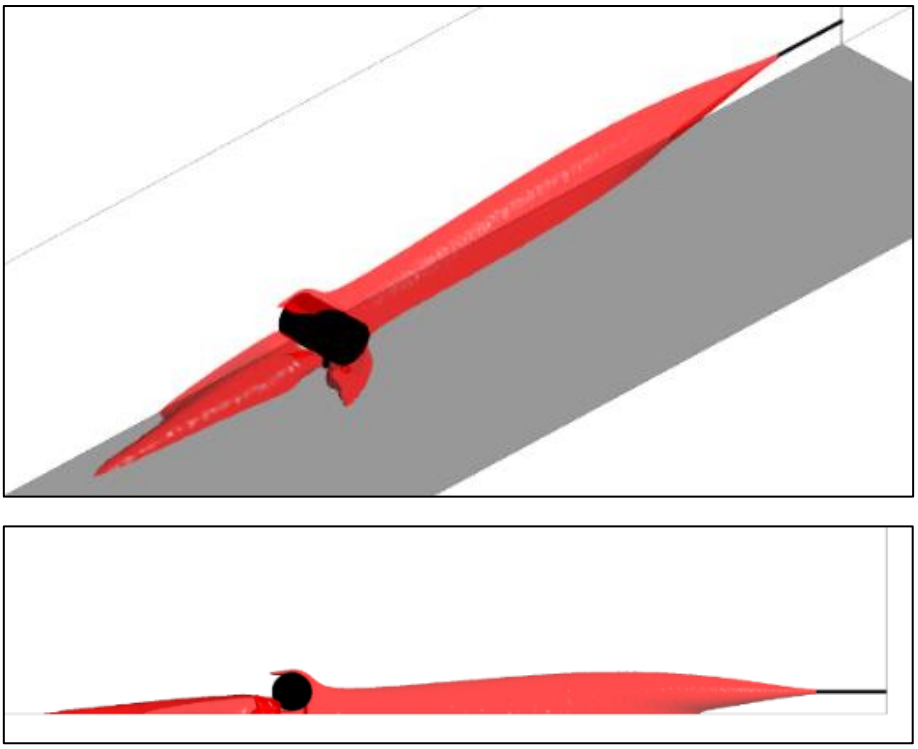

Figure 7.2: 3D view (a) and side view (b) of the LFL cloud outline obtained from the results of sim3.

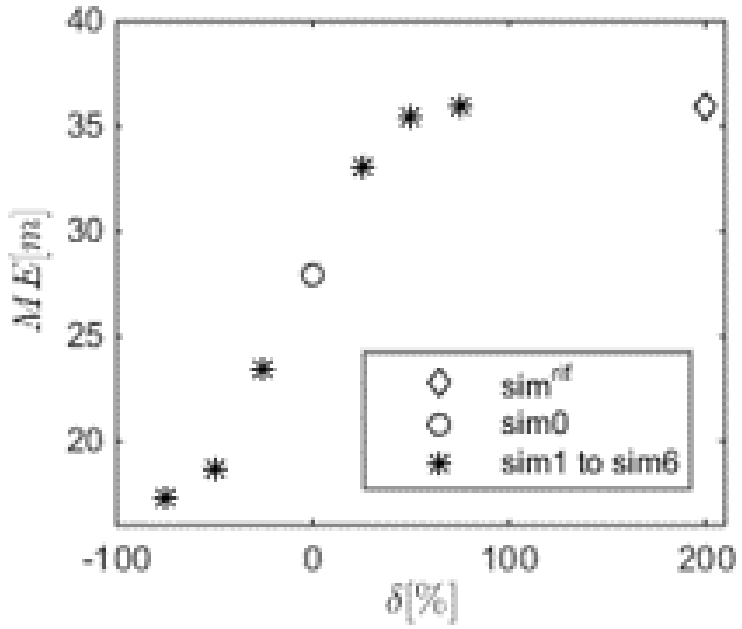

Figure 7.3: Quantitative evaluation of the effect of the obstacle on the jet cloud: ME over δ trend.

SENSITIVITY ANALYSIS

In the sensitivity analysis, substantially only the obstacle (in terms of size and shape) was varied with respect to the case study previously outlined. Hence, what described in Section *CASE STUDY* about the geometry, mesh, solver settings and simulations plan (i.e. the six simulations reported in *Table 7.1*) is still valid for the simulations that will be depicted in the following. However, a change of the obstacle clearly means a different geometry. This fact implies, therefore, two main differences among the case study and the cases analyzed in the present Section:

- As remarked in Section *CASE STUDY*, H^{rif}, ME^{rif} and D^0 are linked to the obstacle dimensions. This means that, changing the obstacle leading to new values of H and D for both sim^{rif} and sim0
- Although the mesh strategy is the same as the one described in Section *CASE STUDY*, a different obstacle causes a variation in the cells number.

As anticipated in Section *INTRODUCTION*, two are the kinds of sensitivity tested: the shape and the size of the obstacle. More in detail, for the size sensitivity a bigger horizontal cylindrical tank was considered while, for the shape sensitivity a vertical cylindrical tank which is of a size comparable to that of the case study's tank was considered. In the two following Subsections, for both the sensitivity analysis conducted, geometries are described, and the results are presented.

OBSTACLE SIZE

With respect to the case study, a bigger horizontal cylindrical tank was used to test the sensitivity of the results to the obstacle size. In particular, 2.4 m and 5.5 m (in the symmetric domain) are the diameter and the length considered, respectively, as real industrial dimensions. In this case, the height from ground of the tank axis is equal to 1.35 m. As anticipated, since the obstacle is different, new values of D and H for sim^{rif} and sim0 needs to be considered.
Table 7.2 summarizes the four geometrical key parameters' value for both sim^{rif} and sim0.

Table 7.2: Values of H, α, S and D considered in sim^{rif} and sim0, respectively.

Simulation	***H*** **(m)**	**α (°)**	***S*** **(m)**	***D*** **(m)**
sim^{rif}	1.35	0	0	42.225
sim0	1.35	0	0	14.075

With regard to the mesh cells count, placing along the jet axis this tank has led to grids with a number of elements belonging to a range of $8.61 \cdot 10^6$ and $10.2 \cdot 10^6$. To report one of the qualitative results achieved, by way of example, let consider the same simulation used in Figure 7.2 of the *CASE STUDY* Section, i.e. sim3. Therefore, Figure 7.4 shows the LFL cloud outline correspondent to the case in which δ is equal to +25 %.

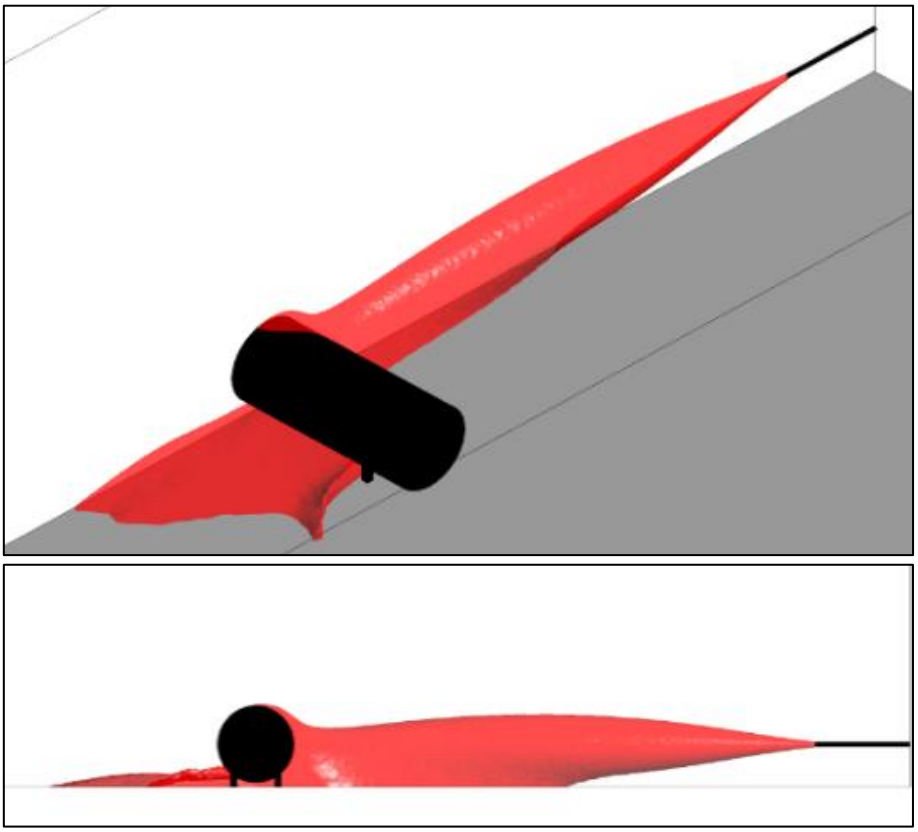

Figure 7.4: LFL cloud contour by a 3D view (a) and a side view (b) obtained from the results of sim3.

From the figure, the jet shown has a similar shape as the one in *Figure 7.2*. Therefore, the qualitative considerations done for the case study can be extended to the scenario in which a bigger-size horizontal cylindrical tank is involved. By the quantitative point of view, in *Figure 7.5* the ME of sim^{rif}, sim0 and the six simulations in which D is varied are plotted over δ. *Figure 7.5* clearly depicts that the more the obstacle is far from the orifice and the more the jet stretches, meaning that the tank acts as barrier and, therefore, its effect is in opposition to the ground one. The obstacle effect, practically, expires when δ is between +50 % and +75 %.

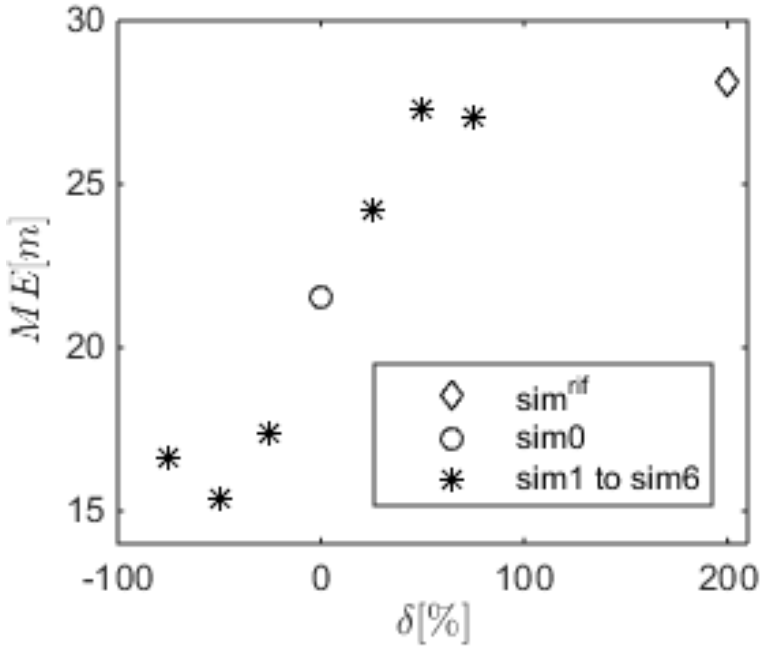

Figure 7.5: Quantitative evaluation of the effect of the big-size horizontal cylindrical tank on the jet cloud.

OBSTACLE SHAPE

The sensitivity analysis of the obstacle shape on the jet behavior was carried out considering a vertical cylindrical tank placed in front of the gas leak and varying its distance D. Comparable size with the horizontal one was considered. More precisely, the vertical tank was chosen with a diameter of 2 m and a length of 7 m, being these real industrial sizes. Notice that, in this case, the tank axis is vertically oriented. Therefore, to establish the jet height coherently to what has been done for the previous cases presented (i.e., case study and obstacle size sensitivity analysis), the nearly mid-height of the obstacle was considered, giving H = 4 m. For the scenario here investigated, *Table 7.3* reports the key parameter values for both sim^{rif} and sim0.

Table 7.3: Values of H, α, S and D considered in sim^{rif} and sim0 for the vertical cylindrical tank case.

Simulation	***H*** **(m)**	**α (°)**	***S*** **(m)**	***D*** **(m)**
sim^{rif}	4	0	0	23.34
sim0	4	0	0	7.78

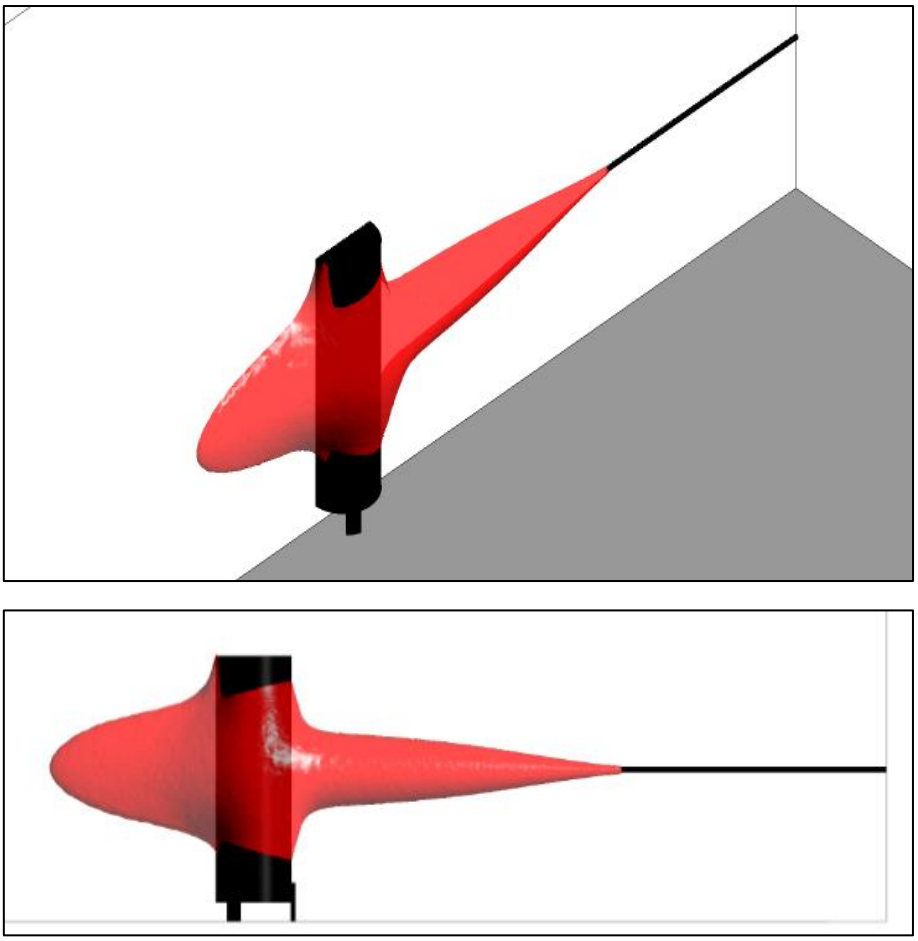

Figure 7.6: LFL outline of sim3 of the shape sensitivity analysis: 6a) in a 3D view and, 6b) in a side view.

For what concerns the mesh dimensions, the number of the elements is within $4.5 \cdot 10^6$ and $4.7 \cdot 10^6$. Looking at the results, *Figure 7.6* shows the LFL outline that is, by way of illustration, given by placing the vertical tank at a distance corresponding to δ = +25 %, while, *Figure 7.7* displays the ME over δ for sim^{rif}, sim0 and the six trials in which D was varied by a stepping δ of the 25 %, being δ ∈ [-75 %; +75 %]. In *Figure 7.6*, it is evident that the obstacle, despite the different shape with regard to the one considered in Section *CASE STUDY*, still continues to shorten the jet cloud, even thought, due to the increased jet height, in this case the LFL does not reflect against the ground surface. The latter effect is appreciable even by looking at *Figure 7.7*.

Combining the results presented in Section CASE STUDY and SENSITIVITY ANALYSIS, for different values of δ, the sensitivity of the obstacle shape and size effect on the jet evidently appears. In particular, from *Figure 7.8* (wherein ME is plotted over δ), about the size effect it is possible to point out that:

- the results related to the case study Horizontal Cylindrical Tank (HCT_{CS} in the figure) and the bigger one considered for the sensitivity analysis (HCT_{SA} in the figure) present a similar behavior

- in both cases, an approximately straight section, wherein ME increases, is followed by a plateau, meaning constant values of ME
- quantitatively, for the two sizes involved, the slope of the results changes in correspondence of δ = +50 % and the maximum value of ME is reached for δ ≥ +50 %: 35.88 m for the case of HCT_{CS} and 28.15 m for the case of HCT_{SA}
- a constant gap is present for values of δ ≥ +50 %, while a non-constant one for δ < +50 %. The former can be related to the sole ground effect (where H is constant and, in particular, equal to the height of the cylindrical tank axis from ground, therefore *H* assumes different values for HCT_{CS} and HCT_{SA}), the latter can be caused by the obstacle-ground combined effect that can differ between the two sizes (giving, substantially, two different slopes).

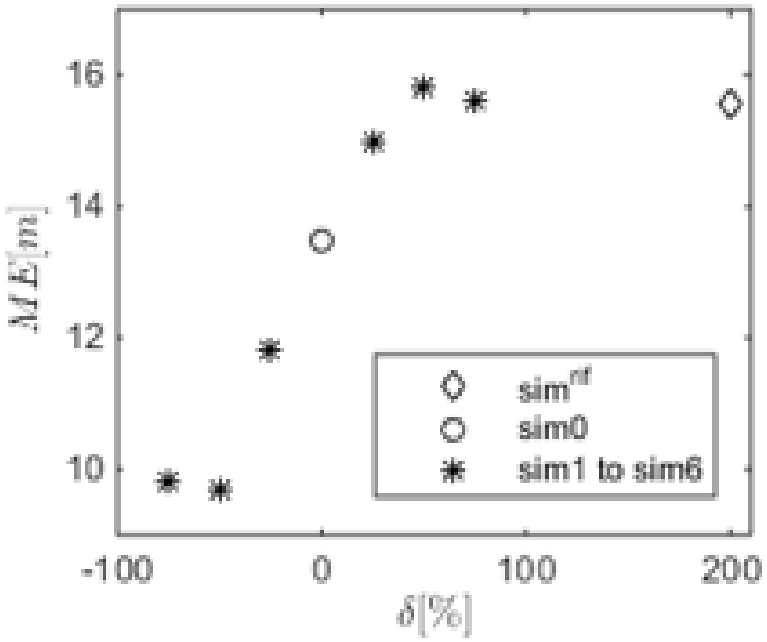

Figure 7.7: ME over δ obtained from the vertical cylindrical tank case.

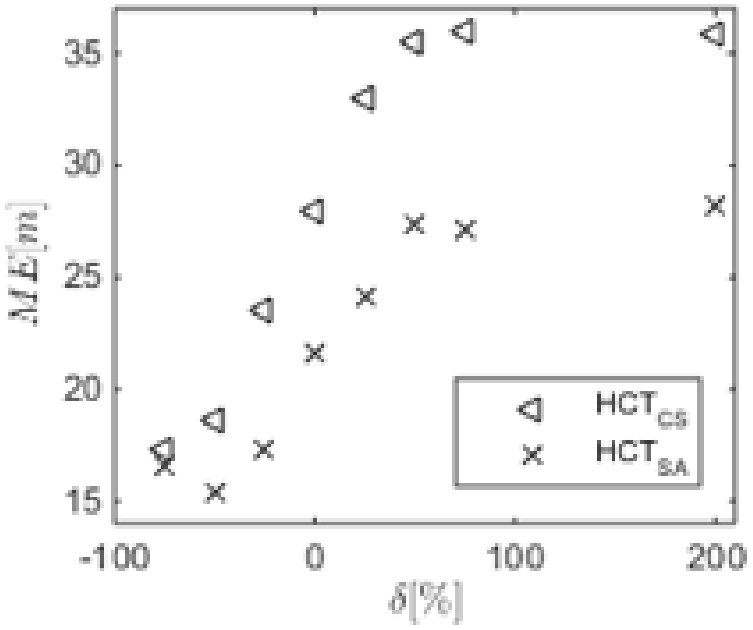

Figure 7.8: ME over δ obtained varying the obstacle size.

The same goes for the shape effect, for which, from *Figure 7.9* (wherein ME is plotted over δ), it is possible to say that:

- the results of the Vertical Cylindrical Tank used for the sensitivity analysis (VCT_{SA} in the figure) behave as the one of HCT_{CS}
- similar to the results obtained with the HCT_{SA}, an approximately straight section, wherein ME increases, is followed by a plateau even for the VCT_{SA} results where the obstacle no longer influences the jet
- quantitatively, for both shapes, the plateau of the ME is reached in correspondence of δ = +50 %. Moreover, for the same δ, there is also the maximum value of ME (which is then kept for δ > +50 %). For the VCT_{SA} case, the maximum ME is equal to 15.56 m
- a quite large constant gap is present for values of δ ≥ +50 %, while a non-constant one for δ < +50 %. The possible causes previously depicted for the size influence analysis can deemed to be still valid.

Finally, to profitably analyze the results all at once, a new graph was considered. In Figure 7.10, all the results are indeed collected and plotted in terms of ΔME over δ. While the x-axis is the same as the one used up to this point, the y-axis is here defined as $\Delta ME = (ME^{rif}-ME)/ME^{rif}$, where ME^{rif} is the cloud Maximum Extent obtained in sim^{rif} while ME is the cloud Maximum Extent obtained in each of the simulations performed. As well as the simulations results, in Figure 7.10, a dashed line is also shown corresponding to ΔME = 5 %. This set threshold can be acceptable, for all the scenarios here

addressed, since it corresponds to a little absolute jet ME variation with respect to ME^{rif}, i.e. lower than 2 m. So, concerning *Figure 7.10*, it is possible to state that:

- in a qualitatively perspective, all the results present a similar behavior
- the results compose two straight sections in which Δ*ME* decreases constantly or remains practically constant
- for all the findings, the slope change takes place at δ = +50 %
- the results of the HCT_{CS} and HCT_{SA} present a Δ*ME* that often is similar, while the ones of VCT_{SA} are, for δ < +50 %, always lower than the others. The cause can be mainly attributed to the larger *H* in the VCT_{SA} scenario with respect to the one in both HCT_{CS} and HCT_{CS} scenarios.

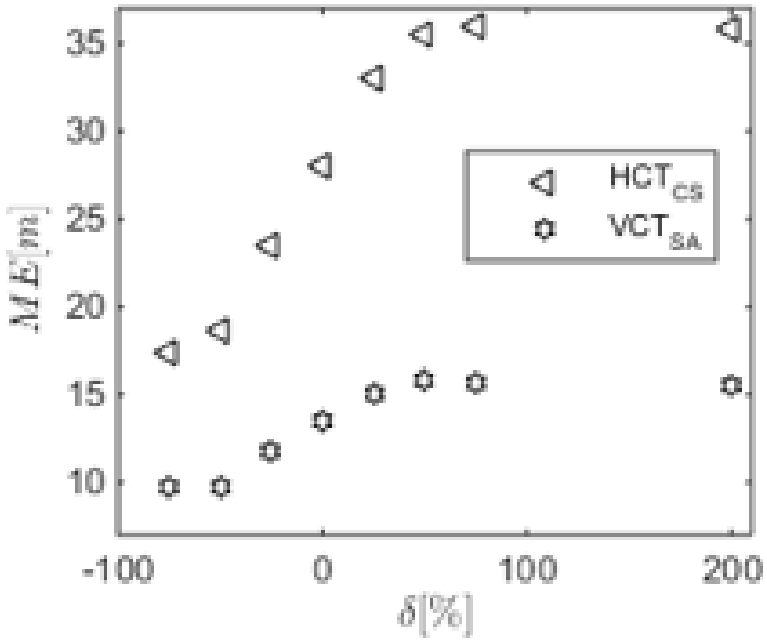

Figure 7.9: ME over δ obtained varying the obstacle shape.

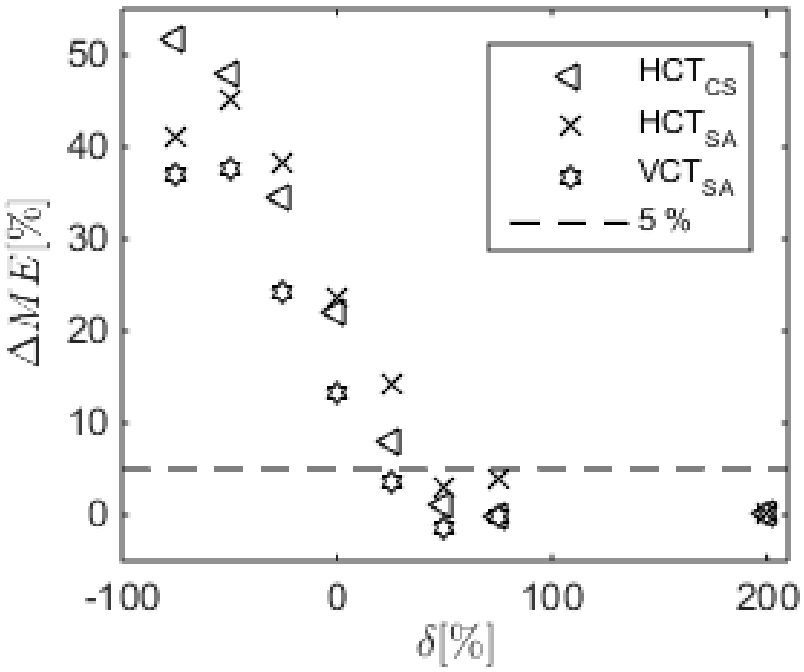

Figure 7.10: Comparison of the ME obtained varying both size and obstacle shape: ΔME over δ trend.

CONCLUSIONS

The scenario in which a 65-bara unignited methane gaseous jet that hits a realistic industrial obstacle is the focus of the present analysis. In particular, with respect to the distance between obstacle and jet orifice, the effect of a horizontal cylindrical tank of industrial use is considered on the jet LFL cloud. Moreover, with the purpose to understand how obstacle shape and size affect the jet behavior, a sensitivity analysis on these characteristics was conducted. Therefore, after validation of the CFD model with experimental data found in literature, the results of the depicted cases were obtained, and answer to the two leading questions was provided. More in detail:

- with respect to the jet orifice-obstacle distance (*D*), independently by size and shape, the obstacle acts as barrier, reducing the ME of the LFL cloud
- for all the cases investigated, the obstacle most influences the jet behaviour when it is placed as close as possible to the orifice (as shown by Figure 7.10, ΔME reaches its maximum value)
- the obstacle influence can be intended as expired when ME = ME^{rif}. Considering Δ*ME* = 5 % as an acceptable threshold, it was found that, for all the cases analyzed, the obstacle influence extinguishes for $\delta \geq +50$ %.

Finally, given that for $\delta \geq +50$ % the obstacle presence can be neglected, in those cases one can refers to simpler engineering correlations present in literature to assess the *ME* of the LFL cloud when the leak is close to plane surfaces (*e.g.*, the ground surface).

REFERENCES

Ansys Fluent User's Guide, 2017. Release 18.2. ANSYS, Inc.

Baklanov A., Barmpas P., Bartzis J., Batchvarova E., Baumann-Stanzer K., Berkowicz U., Borrego C., Britter A., Brzozowski K., Burzynski J., Costa A.M, Carissimo C., Dimitrova R., Franke J., Grawe D., Goricsan I., Hellsten A., Janour Z., Karppinen A., Ketzel M., Krajcovicova J., Leitl B., Martilli A., Moussiopoulos N., Neophytou M., Olesen H., Papachristodoulou C. Papadakis M., Piringer M., Di Sabatino S., Sandberg M., Schatzmann M., Schlünzen H., Trini-Castelli S., 2007, Cost Action 732 Quality Assurance and Improvement of Microscale Meteorological Models, Brussels, Belgium

Batt, R., Gant, S.E., Lacome, J.M., Truchot, B., 2016. Modelling of stably-stratified atmospheric boundary layers with commercial CFD software for use in risk assessment. *Chem. Eng. Trans.* 48, 61–66. https://doi.org/10.3303/CET1648011.

Bénard, P., Hourri, A., Angers, B., Tchouvelev, A., 2016. Adjacent surface effect on the flammable cloud of hydrogen and methane jets: Numerical investigation and engineering correlations. *Int. J. Hydrogen Energy* 41, 18654–18662. https://doi.org/10.1016/j.ijhydene.2016.08.173.

Birch, A.D., Brown, D.R., Dodson, M.G., Swaffield, F., 1984. The structure and concentration decay of high pressure jets of natural gas. *Combust. Sci. Technol.* 36, 249–261. https://doi.org/10.1080/00102208408923739

Busini V., Massimiliano L., Rota R., 2012, Influence of Large Obstacles and Mitigation Barriers on Heavy Gas Cloud Dispersion: A Liquefied Natural Gas Case-Study, *Industrial and Engineering Chemistry Research,* 51, 7643–50.

Busini, V. and R. Rota (2014). Influence of the shape of mitigation barriers on heavy gas dispersion. *Journal of Loss Prevention in the Process Industries 29*, 13-21.

Casal, J., Gómez-Mares, M., Muñoz, M., Palacios, A., 2012. Jet fires: A 'minor' fire hazard? *Chem. Eng. Trans.* 26, 13–20. https://doi.org/10.3303/CET1226003.

Chen, C.J., Rodi, W., 1980. Vertical Turbulent Buoyant Jets – A review of Experimental Data*,* First ed. Pergamon Press Vol. 4.

Colombini, C., Busini, V., 2019. Obstacle Influence on High-Pressure Jets based on Computational Fluid Dynamics Simulations. *Chem. Eng. Trans.* 77, 811–816. https://doi.org/10.3303/CET1977136.

Hall, J.E., Hooker, P., O'Sullivan, L., Angers, B., Hourri, A., Benard, P., 2017. Flammability profiles associated with high-pressure hydrogen jets released in close proximity to surfaces. *Int. J. Hydrogen Energy* 42, 7413–7421. https://doi.org/10.1016/j.ijhydene.2016.05.113.

Houf, W., Schefer, R., Evans, G., Merilo, E., Groethe, M., 2010. Evaluation of barrier walls for mitigation of unintended releases of hydrogen. *Int. J. Hydrogen Energy* 35, 4758–4775. https://doi.org/10.1016/j.ijhydene.2010.02.086.

Hourri, A., Angers, B., Bénard, P., 2009. Surface effects on flammable extent of hydrogen and methane jets. *Int. J. Hydrogen Energy* 34, 1569–1577. https://doi.org/10.1016/j.ijhydene.2008.11.088.

Middha, P., Hansen, O.R., Grune, J., Kotchourko, A., 2010. CFD calculations of gas leak dispersion and subsequent gas explosions: Validation against ignited impinging hydrogen jet experiments. *J. Hazard. Mater.* 179, 84–94. https://doi.org/10.1016/j.jhazmat.2010.02.061

Pontiggia, M., Busini, V., Ronzoni, M., Uguccioni, G., Rota, R., 2014. Effect of large obstacles on high momentum jets dispersion. *Chem. Eng. Trans.* 36, 523–528. https://doi.org/10.1016/j.jhazmat.2009.06.064.

Zuliani C., De Lorenzi C., Ditali S., 2016. Application of CFD Simulation to Safety Problems – Challenges and Experience Including a Comparative Analysis of Hot Plume Dispersion from a Ground Flare, Chemical Engineering Transactions, 53, 79-84. DOI: 10.3303/CET1653014.

CHAPTER 6: CONCLUSIONS

The main objective of the PhD research project was the development of simple, convenient and reliable simplified tools able to predict the influence of a realistic obstacle on the behavior of a unignited high-pressure jet. In order to tackle this goal, *ad-hoc* CFD models were developed and an extensive CFD-based analysis was carried out. Different realistic obstacles were examined, and for these interesting results were obtained.

Specifically:

- The ground interaction enhances the maximum extent of the jet; considering methane as hydrocarbon accidentally released, a quick procedure to predict the ground influence was derived (Colombini et al., 2020a); moreover, when considering compounds heavier than air accidentally released, results achieved for methane are still valid (Colombini et al., 2020b). It should be remarked that the procedure provides a reasonable, and in most of the cases conservative, estimation of the maximum jet extent only inside the parameters window investigated (*i.e.*, for upstream pressures between 2.5 and 700 bar, for upstream temperatures between 278 and 293 K, for orifice diameters between 0.0063 and 0.038 m, for methane concentration equal to 5.3 % (LFL) and for wind intensities between 1 and 20 m/s blowing parallelly the jet);
- A pipe rack presence enhances the maximum extent of the jet; considering methane as hydrocarbon accidentally released, three main characteristics parameters were defined and a quick procedure to predict the obstacle influence depicted was derived (Colombini et al., 2021a); this procedure provides a reasonable estimation, conservative in most of the cases, of the maximum jet extent for methane HP jets inside the parameters window investigated (*i.e.*, for methane only, for upstream pressures between 32.5 and 130 bar, for upstream temperature equal to 278 K, for orifice diameters between 1.2 and 5 cm, for shelves number between 2 and 6, for number of pipes per shelf between 2 and 6, for pipes diameter between 15 and 37 cm, for rack axis orientations with respect to jet axis between 90° and 135°, for methane concentrations level observed between 2.65 and 10 %, for pipe racks located far from the jet source between 25 and 100 % of the free jet length).
- A spherical obstacle presence enhances the maximum extent of the jet (however, lower than how ground and pipe rack do); considering methane as the hydrocarbon accidentally released, a quick procedure to predict the influence of a spherical obstacle was derived (Colombini et al., 2021b); this quick procedure provides a reasonable and conservative estimation of the maximum extent ME (from the point of view industrial safety), but only

inside the parameters window investigated (*i.e.*, for methane only, for upstream pressures between 65 and 650 bar, for upstream temperature equal to 278 K, for orifice diameter equal to 0.0254, for spherical obstacle diameters between 2 and 10 m, for distances of the obstacle from the source between 25 and 100 % of the free jet length and for methane concentration levels observed between 3.5 and 10 %).

- Considering the joint interaction of ground and obstacles, cylindrical tanks have the same qualitative and quantitative influence on the jet behavior. In particular, they lead to a decrease of the maximum extent of the cloud with respect to the sole ground effect (Colombini et al., 2019a; Colombini et al., 2019b). Moreover, when considering obstacles placed at a distance greater than a defined threshold, the jet results are influenced only by the ground (Colombini et al., 2019b).

As general conclusion, innovative simplified models and procedures were derived as useful alternatives to more expensive and time-consuming CFD computations, allowing the quick assessment of credible accidental scenarios of industrial interest. As stated throughout this work, these procedures are expected to provide reasonable, order of magnitude estimations only within the parameters windows investigated. Therefore, the effect of the presence of more than one obstacle, as well as the analysis of scenarios involving either heavier or lighter compounds deserve further investigations. Moreover, targeting also to consolidate the derived useful tools of practical interest, more detailed CFD computations (*e.g.*, by means of Large Eddy Simulations (LES) instead of RANS approach) or even better experimental campaigns (that may be performed at small scales and involving safer compounds of similar characteristics) may be considered.

ANNEX A

TABLE A1

Model equations and main parameters definition. In the following equations ρ is the density, v the velocity, p the pressure, $\bar{\bar{\tau}}$ the shear stress tensor, g the gravity acceleration, c_v and c_p the specific heats, T the temperature, k_T the thermal conductivity, Yi the mass fraction of species i, $\vec{J}_i$ the mass diffusion of species i (when in turbulent flows), $D_{i,m}$ the mass diffusion coefficient for species i in the mixture, μ_t the turbulent viscosity, Sc_t the turbulent Schimdt number, $D_{T,i}$ the thermal diffusion coefficient, V the volume, n the mole number, R the universal gas constant, G_k the generation of turbulent kinetic energy due to mean velocity gradients, G_ω the generation of ω, Γ_k and Γ_ω the effective diffusivity of k and ω, D_ω the cross diffusion term, Y_k and Y_ω the dissipation of k and ω (details about the definition of G_k, G_ω, Γ_k, Γ_ω, Y_k, Y_ω are reported in the work of Menter (1994) and Wilcox (1998)). The use of the following turbulence closure equations was carried out with the CFD software default value for all the model constants. Since the turbulent nature of the problem (μ_t/Sc_t is expected to overwhelm $D_{i,m}$), $D_{i,m}$ was set with the CFD software default constant value for the methane-air mixture (that is to say, using the constant dilute approximation).

Expression	**Equation**
$\frac{\delta\rho}{\delta t} + \nabla\cdot(\rho\vec{v}) = 0$	Mass conservation equation
$\frac{\delta\rho}{\delta t} + \nabla\cdot(\rho\vec{v}\vec{v}) = -\nabla p + \nabla\cdot(\bar{\bar{\tau}}) + \rho\vec{g}$	Momentum conservation equation
$\frac{\delta(\rho c_v T)}{\delta t} + \nabla\cdot\left(\rho\vec{v}c_p T\right) = \nabla\cdot(k_T\nabla T)$	Energy balance
$\frac{\delta(\rho Y_i)}{\delta t} + \nabla\cdot(\rho\vec{v}Y_i) = -\nabla\cdot\vec{J}_i$	Species transport equation
$\vec{J}_i = -\left(\rho D_{i,m} + \frac{\mu_t}{Sc_t}\right)\nabla Y_i - D_{T,i}\frac{\nabla T}{T}$	Mass diffusion in turbulent flows
$pV = nRT$	Equation of state
$\frac{\delta}{\delta t}(\rho k) + \frac{\delta}{\delta x_i}(\rho k u_i) = \frac{\delta}{\delta x_j}\left(\Gamma_k\frac{\delta k}{\delta x_j}\right) + G_k - Y_k + S_k$	k transport equation
$\frac{\delta}{\delta t}(\rho\omega) + \frac{\delta}{\delta x_i}(\rho\omega u_i) = \frac{\delta}{\delta x_j}\left(\Gamma_\omega\frac{\delta\omega}{\delta x_j}\right) + G_\omega - Y_\omega + D_\omega + S_\omega$	ω transport equation

FIGURE A1

Comparison of LFL mole fraction contours of methane in air computed within the grid sensitivity analysis, considering same heights of Figure 3 in the manuscript. Contours in Figure 1S (a) are the same of Figure 3 in the manuscript, contours in Figure 1S (b) refer to the analysis carried out with the less dense mesh, while, contours in Figure 1S (c) refer to the analysis carried out with the thicker mesh. All the contours shown are computed in correspondence of the vertical symmetry plane.

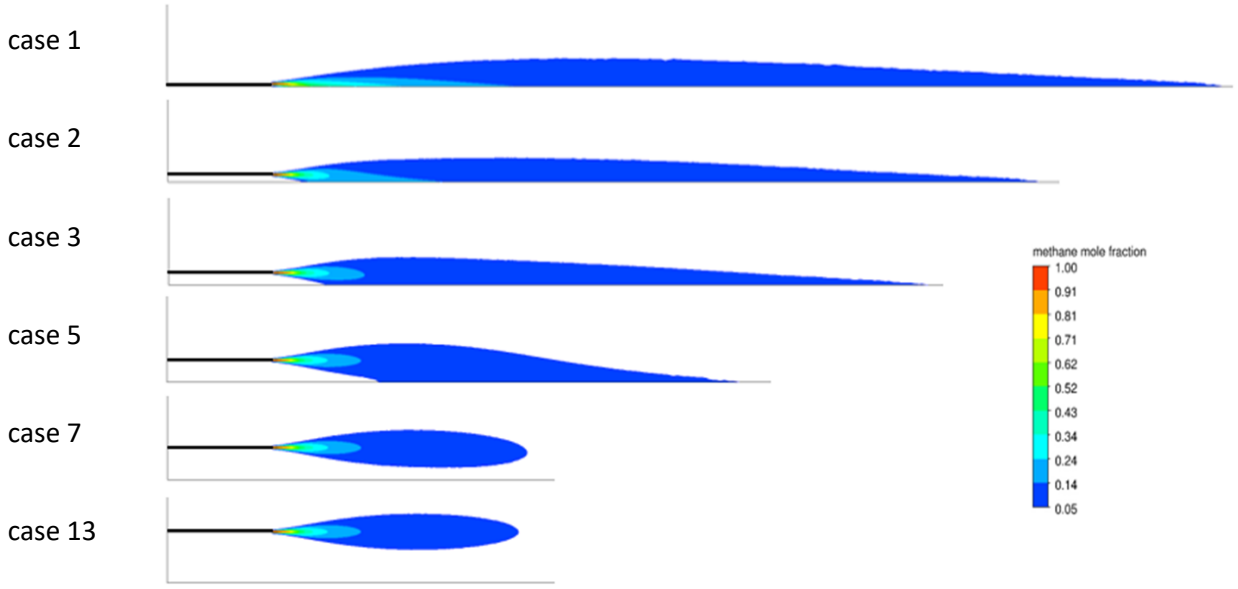

(a)

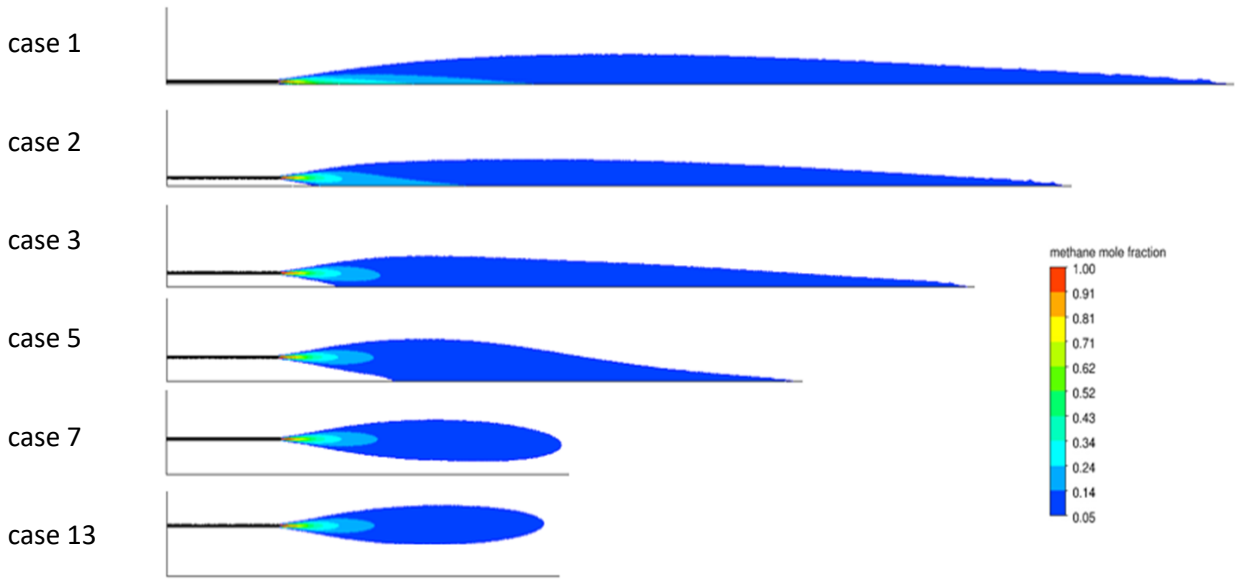

(b)

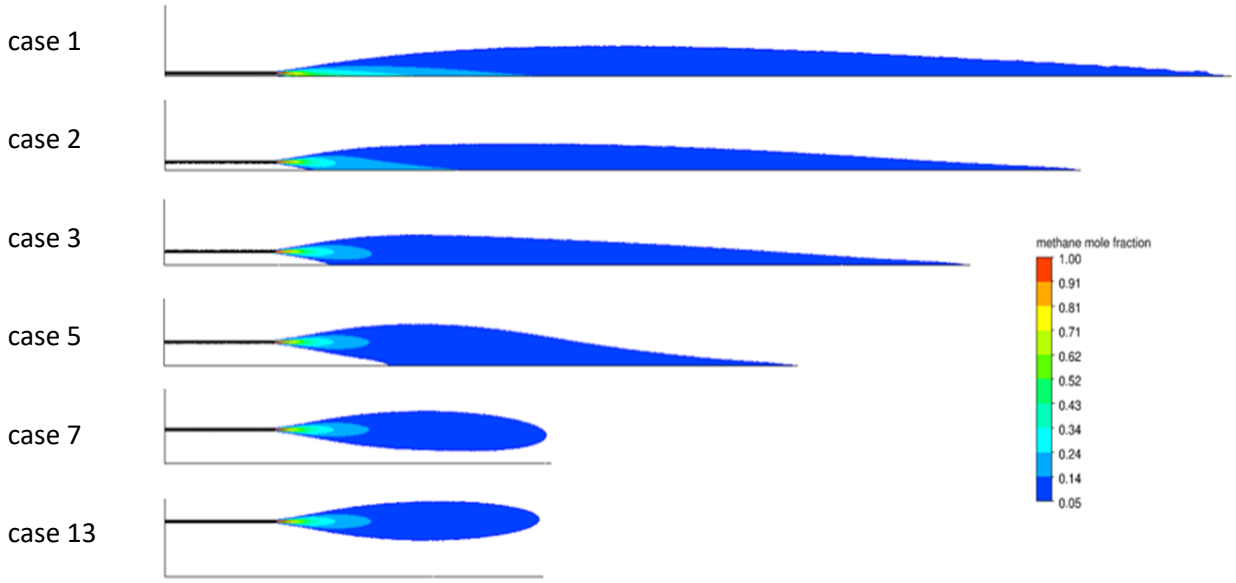
case 1
case 2
case 3
case 5
case 7
case 13
methane mole fraction
1.00
0.91
0.81
0.71
0.62
0.52
0.43
0.34
0.24
0.14
0.05

(c)

FIGURE A2

Temperature (a), velocity (b) and turbulent kinetic energy (c) fields computed in correspondence of the vertical symmetry plane for two representative cases, namely case 3 and case 13 of the base case scenario.

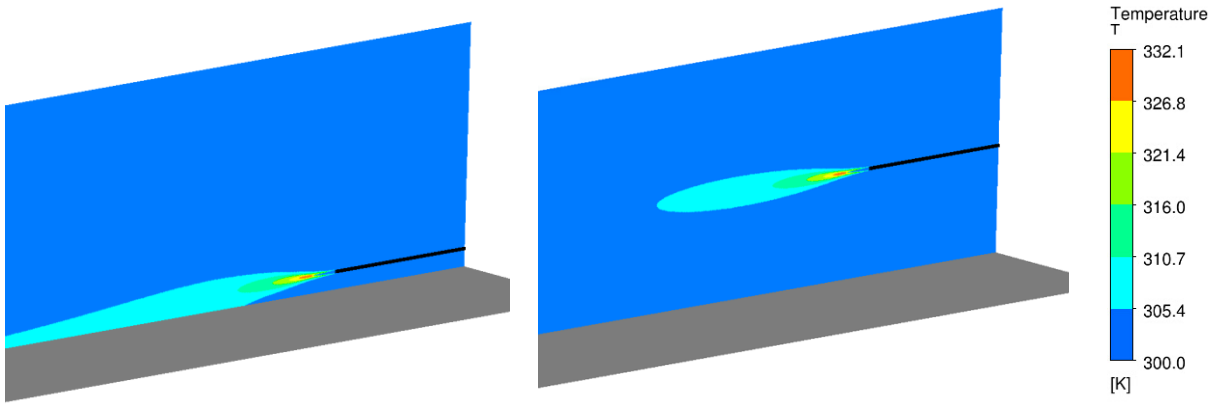

(a)

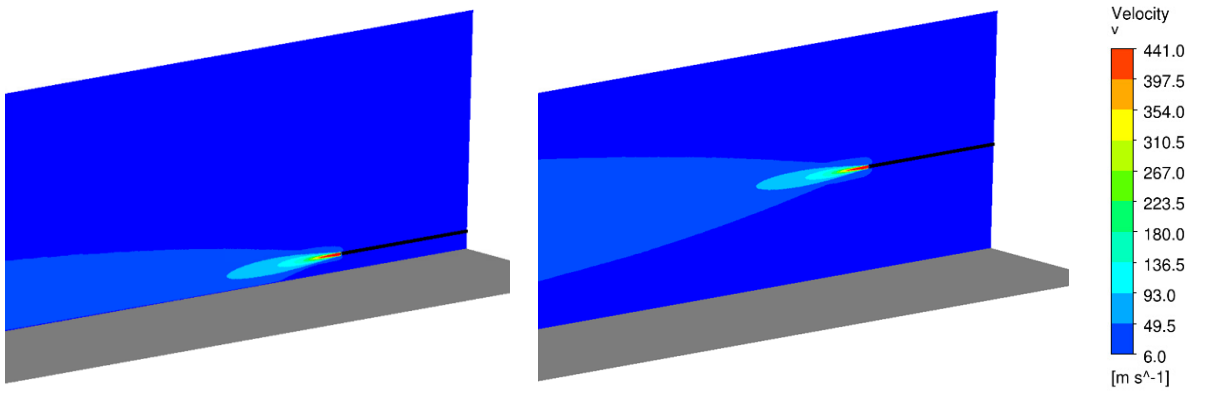

(b)

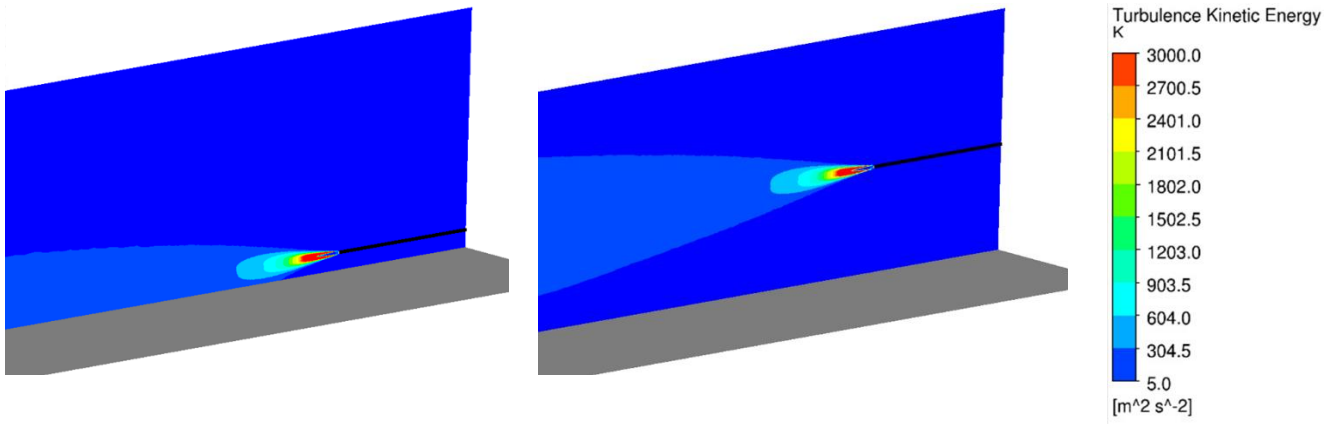

(c)

References

Wilcox, D. C., 1998, Turbulence modeling for CFD. DCW Industries, Inc. La Canada, California.

Menter, F.R., 1993. Zonal Two Equation kω Turbulence Models for Aerodynamic Flows. *24th Fluid Dynamics Conference*.

ANNEX B

TABLE B1

Model equations and main parameters definition. In the following equations ρ is the density, v the velocity, p the pressure, $\bar{\bar{\tau}}$ the shear stress tensor, g the gravity acceleration, c_v and c_p the specific heats, T the temperature, k_T the thermal conductivity, Yi the mass fraction of species i, $\vec{J}_i$ the mass diffusion of species i (when in turbulent flows), $D_{i,m}$ the mass diffusion coefficient for species i in the mixture, μ_t the turbulent viscosity, Sc_t the turbulent Schimdt number, $D_{T,i}$ the thermal diffusion coefficient, V the volume, n the mole number, R the universal gas constant, G_k the generation of turbulent kinetic energy due to mean velocity gradients, G_ω the generation of ω, Γ_k and Γ_ω the effective diffusivity of k and ω, D_ω the cross diffusion term, Y_k and Y_ω the dissipation of k and ω (details about the definition of G_k, G_ω, Γ_k, Γ_ω, Y_k, Y_ω are reported in the work of Menter (1994) and Wilcox (1998)). The use of the following turbulence closure equations was carried out with the CFD software default value for all the model constants. Since the turbulent nature of the problem (μ_t/Sc_t is expected to overwhelm $D_{i,m}$), $D_{i,m}$ was set with the CFD software default constant value for the methane-air mixture (that is to say, using the constant dilute approximation).

Expression	**Equation**
$\frac{\delta\rho}{\delta t} + \nabla\cdot(\rho\vec{v}) = 0$	Mass conservation equation
$\frac{\delta\rho}{\delta t} + \nabla\cdot(\rho\vec{v}\vec{v}) = -\nabla p + \nabla\cdot(\bar{\bar{\tau}}) + \rho\vec{g}$	Momentum conservation equation
$\frac{\delta(\rho c_v T)}{\delta t} + \nabla\cdot\left(\rho\vec{v}c_p T\right) = \nabla\cdot(k_T\nabla T)$	Energy balance
$\frac{\delta(\rho Y_i)}{\delta t} + \nabla\cdot(\rho\vec{v}Y_i) = -\nabla\cdot\vec{J}_i$	Species transport equation
$\vec{J}_i = -\left(\rho D_{i,m} + \frac{\mu_t}{Sc_t}\right)\nabla Y_i - D_{T,i}\frac{\nabla T}{T}$	Mass diffusion in turbulent flows
$pV = nRT$	Equation of state
$\frac{\delta}{\delta t}(\rho k) + \frac{\delta}{\delta x_i}(\rho k u_i) = \frac{\delta}{\delta x_j}\left(\Gamma_k\frac{\delta k}{\delta x_j}\right) + G_k - Y_k + S_k$	k transport equation
$\frac{\delta}{\delta t}(\rho\omega) + \frac{\delta}{\delta x_i}(\rho\omega u_i) = \frac{\delta}{\delta x_j}\left(\Gamma_\omega\frac{\delta\omega}{\delta x_j}\right) + G_\omega - Y_\omega + D_\omega + S_\omega$	ω transport equation

FIGURE B1

Comparison of methane mole fraction in air and velocity contours computed within the grid sensitivity analysis, considering run 12 in Table 3 of the Manuscript as testing case. Figure 1S (a) compares the concentration contours computed using the default mesh (0 %) and the two used to check the results independence from the grid (+/- 50 % the elements size of the body of influence features). Figure 1S (b) compares the velocity contours computed using the default mesh (0 %) and the two used to check the results independence from the grid (+/- 50 % the elements size of the body of influence features). All the contours shown were evaluated in correspondence of the vertical symmetry plane.

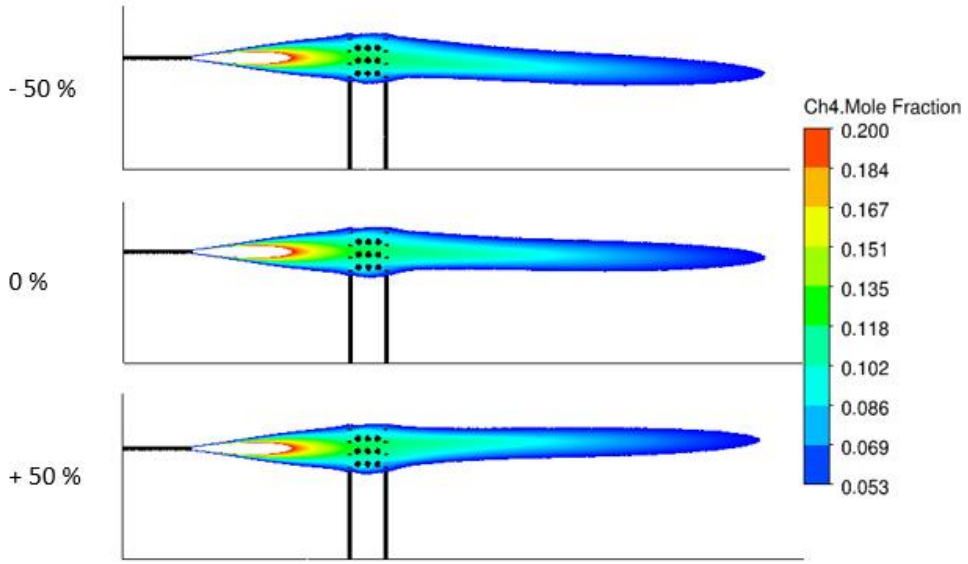

(a)

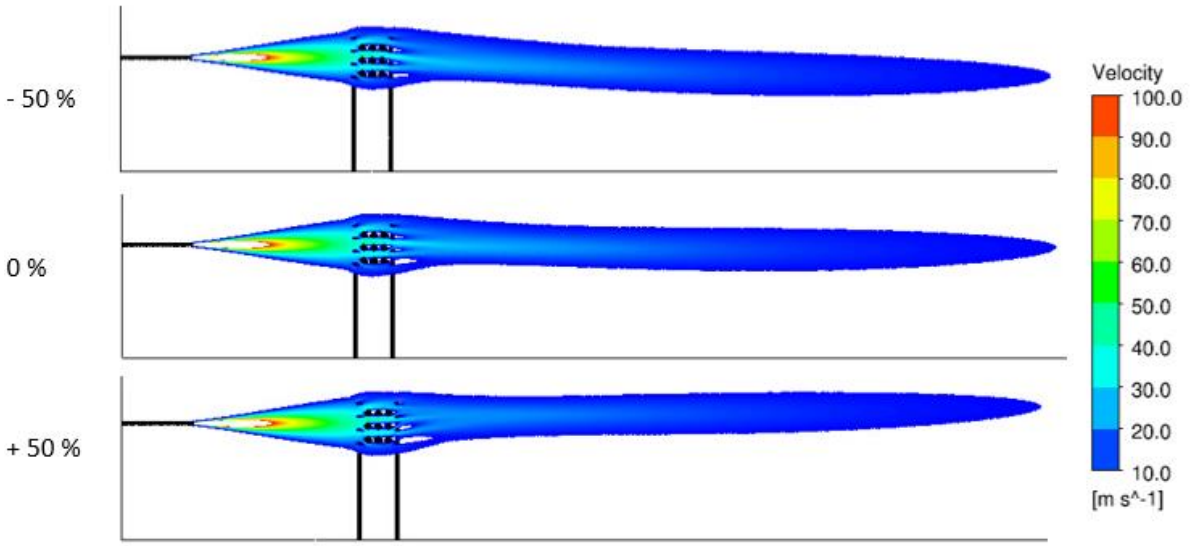

(b)

FIGURE B2

Comparison of the methane jet radial extent computed with the CFD model developed and the analytical model proposed by Cushman-Roisin (Cushman-Roisin, 2020) combined with the models of Chen and Rodi (1980) and Birch et al. (1984), for several distances from the source orifice and for a concentration level equal to LFL (5.3 %). The jet considered is the one used to define runs listed in Table 3, in this case without the presence of the pipe rack (i.e., in free jet conditions). In the Figure, x axis is the axial distance from the jet source while y axis is the half width of the free jet. X markers are the results computed with the CFD model while circle markers are the results computed with the analytical model. From the Figure, the agreement of the two predictions is satisfactory, giving a maximum relative percentage error equal to 11 %.

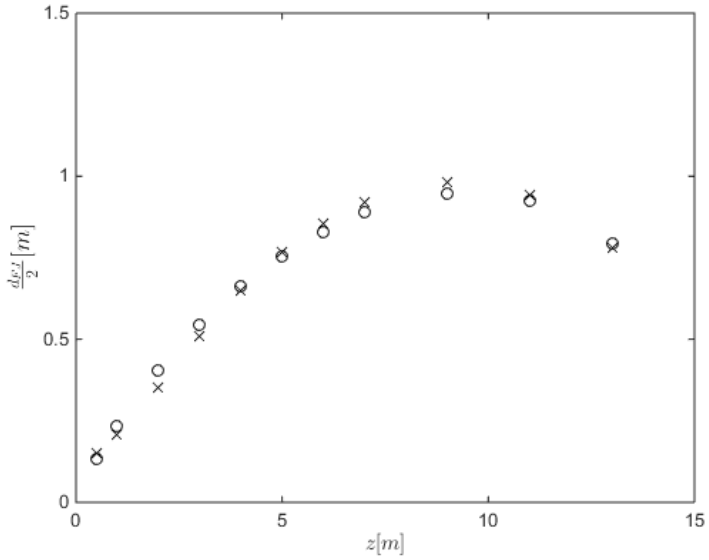

References

Birch, A.D., Brown, D.R., Dodson, M.G., Swaffield, F., 1984. The structure and concentration decay of high pressure jets of natural gas. *Combust. Sci. Technol.* 36, 249–261. https://doi.org/10.1080/00102208408923739.

Chen, C.J., Rodi, W., 1980. Vertical Turbulent Buoyant Jets – A review of Experimental Data, First ed. Pergamon Press Vol. 4.

Cushman-Roisin, B., Environmental Fluid Mechanics – John Wiley & Sons, Book in preparation. Last online access: August 2020. http://www.dartmouth.edu/~cushman/books/EFM/chap9.pdf

Menter, F.R., 1993. Zonal Two Equation kω Turbulence Models for Aerodynamic Flows. *24th Fluid Dynamics Conference*.

Wilcox, D. C., 1998, Turbulence modeling for CFD. DCW Industries, Inc. La Canada, California.

ANNEX C

TABLE C1

Parameters values defining the scenarios of methane HP jet impinging the spherical obstacle. In first column, subscript x indicates the concentration level observed; it can assume three states: x = L means c = 3.5%, x = M means c = 5.3% (LFL) and x = H means c = 10%. This way, runs 1_L-88_L are the scenarios defined as in this Table and evaluated at the jet cloud equal to 3.5% of methane in air, runs 1_M-88_M are the scenarios defined as in this Table and evaluated at the jet cloud equal to 5.3% of methane in air and runs 1_H-88_H are the scenarios defined as in this Table and evaluated at the jet cloud equal to 10% of methane in air. Notice that, in this analysis any ground effect was considered. Therefore, the results reported in this Table are referred to only scenarios of spherical obstacles influencing HP jets.

Run	p [bar]	d [m]	d_{PS} [m]	D_T [m]	D_{NT} [m]	D_L [m]	ME [m]		
							x = L	x = M	x = H
$\mathbf{1_X}$	65	0.0254	0.1458	2	1.9375	0.1	27	16.7	8.7
$\mathbf{2_X}$	65	0.0254	0.1458	2	3.875	0.1	32.8	20.5	8.4
$\mathbf{3_X}$	65	0.0254	0.1458	2	5.8125	0.1	34.8	22.2	8.3
$\mathbf{4_X}$	65	0.0254	0.1458	2	7.75	0.1	34	21.3	8.5
$\mathbf{5_X}$	65	0.0254	0.1458	2	9.6875	0.1	33.2	20.4	8.4
$\mathbf{6_X}$	65	0.0254	0.1458	2	11.625	0.1	32.6	18.8	8.4
$\mathbf{7_X}$	65	0.0254	0.1458	2	13.5625	0.1	31.7	16.8	8.4
$\mathbf{8_X}$	65	0.0254	0.1458	2	15.5	0.1	30.9	15.9	8.4
$\mathbf{9_X}$	65	0.0254	0.1458	3	1.9375	0.15	25.3	16.9	7.2
$\mathbf{10_X}$	65	0.0254	0.1458	3	3.875	0.15	28.6	17.7	6.3
$\mathbf{11_X}$	65	0.0254	0.1458	3	5.8125	0.15	32.5	18.8	6.6
$\mathbf{12_X}$	65	0.0254	0.1458	3	7.75	0.15	33.4	18.3	8.3
$\mathbf{13_X}$	65	0.0254	0.1458	3	9.6875	0.15	32.9	17.3	8.4
$\mathbf{14_X}$	65	0.0254	0.1458	3	11.625	0.15	32.2	15.8	8.4
$\mathbf{15_X}$	65	0.0254	0.1458	3	13.5625	0.15	31.1	16.0	8.4
$\mathbf{16_X}$	65	0.0254	0.1458	3	15.5	0.15	29.6	15.9	8.4
$\mathbf{17_X}$	65	0.0254	0.1458	4.5	1.9375	0.23	26	17.3	5.1
$\mathbf{18_X}$	65	0.0254	0.1458	4.5	3.875	0.23	25.6	14.1	6.4
$\mathbf{19_X}$	65	0.0254	0.1458	4.5	5.8125	0.23	24.2	12.4	7.3
$\mathbf{20_X}$	65	0.0254	0.1458	4.5	7.75	0.23	24.4	12.3	8

21$_X$	65	0.0254	0.1458	4.5	9.6875	0.23	26.5	13.8	8.4
22$_X$	65	0.0254	0.1458	4.5	11.625	0.23	26.3	14.8	8.4
23$_X$	65	0.0254	0.1458	4.5	13.5625	0.23	24.9	15.2	8.4
24$_X$	65	0.0254	0.1458	4.5	15.5	0.23	24.2	15.7	8.4
25$_X$	65	0.0254	0.1458	6	1.9375	0.23	27.6	16.0	5.2
26$_X$	65	0.0254	0.1458	6	3.875	0.23	23.3	11.1	6.0
27$_X$	65	0.0254	0.1458	6	5.8125	0.23	21.8	11	7
28$_X$	65	0.0254	0.1458	6	7.75	0.23	20	12.4	7.9
29$_X$	65	0.0254	0.1458	6	9.6875	0.23	19.4	13.5	8.4
30$_X$	65	0.0254	0.1458	6	11.625	0.23	19.1	14.3	8.4
31$_X$	65	0.0254	0.1458	6	13.5625	0.23	19.5	15	8.4
32$_X$	65	0.0254	0.1458	6	15.5	0.23	20.9	15.7	8.4
33$_X$	65	0.0254	0.1458	7.5	1.9375	0.39	24.1	10.8	5.05
34$_X$	65	0.0254	0.1458	7.5	3.875	0.39	19.7	9.87	5.76
35$_X$	65	0.0254	0.1458	7.5	5.8125	0.39	18.4	11.1	6.7
36$_X$	65	0.0254	0.1458	7.5	7.75	0.39	17.3	12.3	7.9
37$_X$	65	0.0254	0.1458	7.5	9.6875	0.39	17.2	13.3	8.4
38$_X$	65	0.0254	0.1458	7.5	11.625	0.39	18.4	14.1	8.4
39$_X$	65	0.0254	0.1458	7.5	13.5625	0.39	19.6	14.7	8.4
40$_X$	65	0.0254	0.1458	7.5	15.5	0.39	21	15.7	8.4
41$_X$	65	0.0254	0.1458	10	1.9375	0.68	20	10.8	3.7
42$_X$	65	0.0254	0.1458	10	3.875	0.68	16.6	9.5	4.2
43$_X$	65	0.0254	0.1458	10	5.8125	0.68	15.4	10	5.3
44$_X$	65	0.0254	0.1458	10	7.75	0.68	15.2	10.9	6.9
45$_X$	65	0.0254	0.1458	10	9.6875	0.68	16.3	11.6	8.6
46$_X$	65	0.0254	0.1458	10	11.625	0.68	17.6	12.6	8.4
47$_X$	65	0.0254	0.1458	10	13.5625	0.68	18.7	13.6	8.4
48$_X$	65	0.0254	0.1458	10	15.5	0.68	19.3	14.8	8.4
49$_X$	130	0.0254	0.2062	3	1.9375	0.15	36.6	23.7	12.2
50$_X$	130	0.0254	0.2062	3	3.875	0.15	42.3	25.8	11.6
51$_X$	130	0.0254	0.2062	3	5.8125	0.15	44.4	27.8	10.7

52$_X$	130	0.0254	0.2062	3	7.75	0.15	48.2	30.3	11.1
53$_X$	130	0.0254	0.2062	3	9.6875	0.15	48.6	30.7	12
54$_X$	130	0.0254	0.2062	3	11.625	0.15	48.1	29.7	12.1
55$_X$	130	0.0254	0.2062	3	13.5625	0.15	48	28.8	11.9
56$_X$	130	0.0254	0.2062	3	15.5	0.15	46.6	27.0	11.9
57$_X$	195	0.0254	0.2526	3	1.9375	0.15	-	28.3	14.7
58$_X$	195	0.0254	0.2526	3	3.875	0.15	-	32.7	16
59$_X$	195	0.0254	0.2526	3	5.8125	0.15	58.5	36.8	17.3
60$_X$	195	0.0254	0.2526	3	7.75	0.15	58.8	37.8	16.5
61$_X$	195	0.0254	0.2526	3	9.6875	0.15	59.4	38.7	16.1
62$_X$	195	0.0254	0.2526	3	11.625	0.15	59	38.3	15
63$_X$	195	0.0254	0.2526	3	13.5625	0.15	58.7	37.7	15.1
64$_X$	195	0.0254	0.2526	3	15.5	0.15	57.5	36.4	14.5
65$_X$	260	0.0254	0.2916	3	1.9375	0.15	-	-	16.4
66$_X$	260	0.0254	0.2916	3	3.875	0.15	-	38.7	18.9
67$_X$	260	0.0254	0.2916	3	5.8125	0.15	69.2	42	21.4
68$_X$	260	0.0254	0.2916	3	7.75	0.15	68	44.1	21.2
69$_X$	260	0.0254	0.2916	3	9.6875	0.15	68.2	44.6	21
70$_X$	260	0.0254	0.2916	3	11.625	0.15	67.4	44.4	19.6
71$_X$	260	0.0254	0.2916	3	13.5625	0.15	66.7	43.6	18
72$_X$	260	0.0254	0.2916	3	15.5	0.15	65.8	43	17.7
73$_X$	455	0.0254	0.3858	3	1.9375	0.15	-	-	21.6
74$_X$	455	0.0254	0.3858	3	3.875	0.15	-	-	23.7
75$_X$	455	0.0254	0.3858	3	5.8125	0.15	88.7	55	28.7
76$_X$	455	0.0254	0.3858	3	7.75	0.15	87.2	56.7	29.8
77$_X$	455	0.0254	0.3858	3	9.6875	0.15	87.8	58.3	30.9
78$_X$	455	0.0254	0.3858	3	11.625	0.15	86.5	58	30.5
79$_X$	455	0.0254	0.3858	3	13.5625	0.15	85.5	57.6	29.3
80$_X$	455	0.0254	0.3858	3	15.5	0.15	84.6	57	28.1
81$_X$	650	0.0254	0.4611	3	1.9375	0.15	-	-	25.5
82$_X$	650	0.0254	0.4611	3	3.875	0.15	-	-	27.85

83$_X$	650	0.0254	0.4611	3	5.8125	0.15	105.7	63.5	32.4
84$_X$	650	0.0254	0.4611	3	7.75	0.15	102.8	67.2	36.2
85$_X$	650	0.0254	0.4611	3	9.6875	0.15	101.7	67.9	37.2
86$_X$	650	0.0254	0.4611	3	11.625	0.15	101	68.1	37.2
87$_X$	650	0.0254	0.4611	3	13.5625	0.15	99.7	67.6	36.65
88$_X$	650	0.0254	0.4611	3	15.5	0.15	98.7	67	35.8

TABLE C2

Model equations and main parameters definition. In the following equations ρ is the density, v the velocity, p the pressure, $\bar{\bar{\tau}}$ the shear stress tensor, g the gravity acceleration, c_v and c_p the specific heats, T the temperature, k_T the thermal conductivity, Yi the mass fraction of species i, $\vec{J}_i$ the mass diffusion of species i (when in turbulent flows), $D_{i,m}$ the mass diffusion coefficient for species i in the mixture, μ_t the turbulent viscosity, Sc_t the turbulent Schimdt number, $D_{T,i}$ the thermal diffusion coefficient, V the volume, n the mole number, R the universal gas constant, G_k the generation of turbulent kinetic energy due to mean velocity gradients, G_ω the generation of ω, Γ_k and Γ_ω the effective diffusivity of k and ω, D_ω the cross diffusion term, Y_k and Y_ω the dissipation of k and ω (details about the definition of G_k, G_ω, Γ_k, Γ_ω, Y_k, Y_ω are reported in the work of Menter (1994) and Wilcox (1998)). The use of the following turbulence closure equations was carried out with the CFD software default value for all the model constants. Since the turbulent nature of the problem (μ_t/Sc_t is expected to overwhelm $D_{i,m}$), $D_{i,m}$ was set with the CFD software default constant value for the methane-air mixture (that is to say, using the constant dilute approximation).

Expression	**Equation**
$\frac{\delta\rho}{\delta t} + \nabla\cdot(\rho\vec{v}) = 0$	Mass conservation equation
$\frac{\delta\rho}{\delta t} + \nabla\cdot(\rho\vec{v}\vec{v}) = -\nabla p + \nabla\cdot(\bar{\bar{\tau}}) + \rho\vec{g}$	Momentum conservation equation
$\frac{\delta(\rho c_v T)}{\delta t} + \nabla\cdot\left(\rho\vec{v}c_p T\right) = \nabla\cdot(k_T\nabla T)$	Energy balance
$\frac{\delta(\rho Y_i)}{\delta t} + \nabla\cdot(\rho\vec{v}Y_i) = -\nabla\cdot\vec{J}_i$	Species transport equation
$\vec{J}_i = -\left(\rho D_{i,m} + \frac{\mu_t}{Sc_t}\right)\nabla Y_i - D_{T,i}\frac{\nabla T}{T}$	Mass diffusion in turbulent flows
$pV = nRT$	Equation of state
$\frac{\delta}{\delta t}(\rho k) + \frac{\delta}{\delta x_i}(\rho k u_i) = \frac{\delta}{\delta x_j}\left(\Gamma_k\frac{\delta k}{\delta x_j}\right) + G_k - Y_k + S_k$	k transport equation
$\frac{\delta}{\delta t}(\rho\omega) + \frac{\delta}{\delta x_i}(\rho\omega u_i) = \frac{\delta}{\delta x_j}\left(\Gamma_\omega\frac{\delta\omega}{\delta x_j}\right) + G_\omega - Y_\omega + D_\omega + S_\omega$	ω transport equation

FIGURE C1

Comparison of the sensitivity analysis results in terms of ME variation with respect to different mesh refinements. Run 11_M in Table 1S was taken as benchmark case to perform the grid sensitivity analysis. Considering the starting mesh (in the Figure, 0 % of refinement (5.7 million of elements)), the size of the elements discretizing the jet axis was varied of the +/-25 and +/-50 % (with cells count ranging between 3.2 and 7.1 million). The maximum percentage relative error amounted to 2 %.

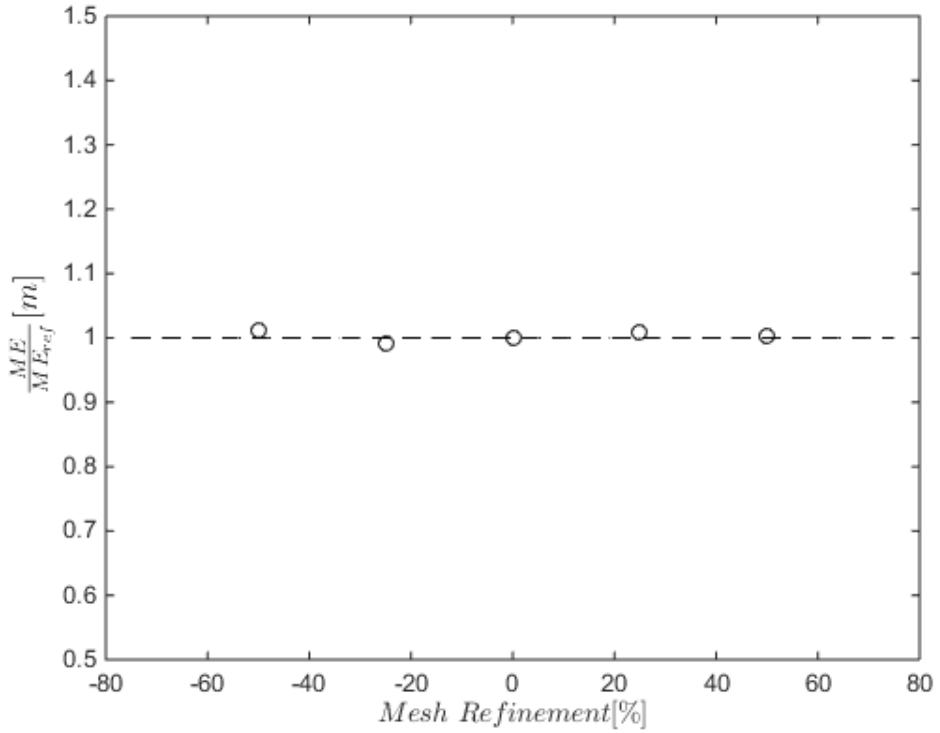

References

Menter, F.R., 1993. Zonal Two Equation kω Turbulence Models for Aerodynamic Flows. *24th Fluid Dynamics Conference*.

Wilcox, D. C., 1998, Turbulence modeling for CFD. DCW Industries, Inc. La Canada, California